System Identification and Adaptive Current Balancing ON/OFF Control of DC-DC Switch Mode Power converter

Chen Wang
B.Eng., M.Sc.

A thesis submitted for the degree of

Doctor of Philosophy

May, 2017

School of Electrical Electronic Engineering

Newcastle University
United Kingdom

Abstract

Reliability becomes more and more important in industrial application of Switch Mode Power Converters (SMPCs). A poorly performing power supply in a power system can influence its operation and potentially compromise the entire system performance in terms of efficiency. To maintain a high reliability, high performance SMPC effective control is necessary for regulating the output of the SMPC system. However, an uncertainty is a key factor in SMPC operation. For example, parameter variations can be caused by environmental effects such as temperature, pressure and humidity. Usually, fixed controllers cannot respond optimally and generate an effective signal to compensate the output error caused by time varying parameter changes. Therefore, the stability is potentially compromised in this case. To resolve this problem, increasing interest has been shown in employing online system identification techniques to estimate the parameter values in real time. Moreover, the control scheme applied after system identification is often called “adaptive control” due to the control signal self-adapting to the parameter variation by receiving the information from the system identification process. In system identification, the Recursive Least Square (RLS) algorithm has been widely used because it is well understood and easy to implement. However, despite the popularity of RLS, the high computational cost and slow convergence speed are the main restrictions for use in SMPC applications. For this reason, this research presents an alternative algorithm to RLS; Fast Affline Projection (FAP). Detailed mathematical analysis proves the superior computational efficiency of this algorithm. Moreover, simulation and experiment result verify this unique adaptive algorithm has improved performance in terms of computational cost and convergence speed compared with the conventional RLS methods. Finally, a novel adaptive control scheme is designed for optimal control of a DC-DC buck converter during transient periods. By applying the proposed adaptive algorithm, the control signal can be successfully employed to change the ON/OFF state of the power transistor in the DC-DC buck converter to improve the dynamic behaviour. Simulation and experiment result show the proposed adaptive control scheme significantly improves the transient response of the buck converter, particularly during an abrupt load change condition.

Dedication

To my loving homeland—P.R.China.

Acknowledgements

I would like to thank all people who ever helped me, encouraged me, taught me, pushed me and punished me. All those enjoys and sufferings from you make me better and stronger. I will keep embracing all challenges and happiness from you in the rest of my life.

I acknowledge with sincere gratitude towards my supervisors, Dr Matthew Armstrong and Dr Shady Gadoue for their professional support. The successful completion of this work would not have been possible without their indefatigable patience and push. I am extremely grateful for having the privilege to work with Dr Matthew Armstrong and learn from his expertise. His inspiration always shows me a path to solving the problem. With his suggestion, I always find the answer by myself. What I learned from him is beyond just solving the research problems, he taught me how to find a way to solving these problems.

I am also very thankful to my colleagues in the UG lab (Electrical Power Group). I have an excellent research period with all creative, dedicated and talented colleagues. I am more than enjoyable to discuss with all my colleagues in all four-year PhD study.

My heartfelt appreciation goes to my parents for their altruistic support and encouragement from the beginning of my life. I would like to thank my family members and relatives who have inspired and continued to motivate me when I was young. I particularly thank my girlfriend Ina Peng for her devotion and faithful love to me. Finally, I appreciate my family for their financial support and understanding in this research work and other endeavour.

Contents

Figures

Tables

Symbols

DC	Direct current
APA	Affine Projection Algorithm
PWM	Pulse Width Modulation
DSP	Digital Signal Processor
RLS	Recursive Least Square
LMS	Least Mean Square
AR	Autoregressive
ARX	Autoregressive with exogenous input
SMPCs	Switch Mode Power Converter
AC	Alternating Current
KF	Kalman Filter
CF-PR	Constant-Frequency Peak-Ripple-Based
MMC	Modular Multilevel Converter
HVDC	High-level Voltage Direct Current
FIR	Finite Impulse Response
MOSFET	Metal Oxide Field Effect Transistor
IGBT	Insulated Gate Bipolar Transistor
BBO	Biogeography-Based Optimization
BJ	Box-Jenkines
OE	Output Error
LTI	Linear Time Invariant
PRBS	Pseudo Random Binary Sequence
DCD	Dichotomous Coordinate Descent
ESR	Equivalent Series Resistance
VSC	Voltage Source Converter
PEF	prediction-error filter
PI	Proportional-Integral
ADC	Analogue to Digital Converter
FL	Fuzzy Logic
TSMC	Total Sliding Mode Control
AFNNC	Adaptive Fuzzy-Neural-Network Control
XOR	Exclusive-or gate
EMSE	Excess-Mean-Square-Error
FPGA	field programmable gates arrays
CCS	Code Composer Studio
IDE	integrated development environment
HRPWM	High-Resolution PWM
CSP	Code Support Package
NI	National Instruments
RTW	Real Time Workshop

SMD	Surface Mounted Device
FAP	Fast Affine Projection
APSA	Affine Projection Sign Algorithm
PVSSA	Practical Variable Step-Size Adaptive Algorithms
VSS-APSA	variable step-size affine projection sign algorithm
MVSS-APSA	Modified variable step-size affine projection sign algorithm
MLPRLS	Memoryless Polynomial RLS
FTRLS	Fast Transversal Recursive Least Squares algorithm
FQRD-RLS	Fast QR-decomposition Recursive Least Squares
LCVFFRLS	Low-Complexity Variable Forgetting Factor Recursive Least Squares
SST	Solid State Transformer

Chapter 1 Introduction and scope of this thesis

1.1 Introduction

As an essential power electronics component, Switch Mode Power Converters (SMPCs) are widely being used in many modern applications such as power conversion, energy transmission, energy storage, and electrical powertrains. SMPCs are gradually replacing many conventional transformer-based systems due to their superiority low cost and high flexibility. To meet the increasing demand for reliability and functionality of SMPCs, much research has been carried on the control of SMPCs. With the fast development of Digital Signal Processors (DSPs), power electronics systems are now easily integrated with digital ICs and control algorithms can be readily programmed into microprocessors. Consequently, digital control theories are rapidly overtaking analogue control solutions to meet modern specifications.

Most digital control techniques are based on a mathematical model which contains all the parameter information of the SMPC; for example the values of passive components. As a result, knowledge of the parameters is often an essential precondition to designing and delivering a particular control strategy.

Unfortunately, to complicate matters, the value of most system parameters (such as passive components) is inevitably subject to change over time. This may be due to a range of reasons, including; time varying environmental conditions, wear and tear, component failure, and unpredictable external load changes.

Therefore, an effective way to monitoring, or estimating, the value of passive components over time is desirable in many control applications. This is the basis for developing system identification, or parameter estimation, methods. In this area, many algorithms have been developed to achieve system identification and/or parameter estimation. Assisted by these technique, subsequent auto-tuning and adaptive digital controllers are also now playing an increasingly important role in SMPC systems. Moreover, with the rapid development of digital control techniques, these auto-tuning and adaptive controllers have become more and more popular and complex in nature in recent years [2-5]. Even without these adaptive control schemes, online/offline system identification has been shown to be a powerful tool for system monitoring and fault diagnosis.

In terms of system identification algorithms, many have been developed from recognised adaptive filters from the signal processing field. As a similar form of linear mathematical model is typically used in both SMPC and adaptive filtering systems, similar algorithms can be applied in both research areas. Several forms of algorithm are particularly popular, due to their computational complexity, noise immunity and convergence speed. The first is Least Mean Square (LMS). The basic Least Mean Square algorithm is a classic adaptive algorithm with reasonable convergence speed and very low computational cost, however, noise immunity is a main drawback in some specific applications. The Recursive Least Square family compensates for this drawback by introducing a more complex regression form and a forgetting factor to adapt for noise conditions. Consequently, the computational cost is increased as a compromise. Numerous variations on RLS have been developed for the purposes of system identification; all offering unique advantages in different circumstances. For example, a Dichotomous Coordinate Descent based RLS variant is developed in [1] and applied for system identification of a DC-DC buck converter system in [2]. This method significantly reduces the computational cost of conventional RLS algorithm by applying a "bit-shift" idea to eliminate several multiplications and a division in the iterative computation. As a result, the computational cost of RLS is reduced from $O(N^2)$ multiplication per sample to $O(3N)$ multiplication per sample. However, this method does not improve the convergence speed compared to the conventional RLS algorithm, and it modestly sacrifices accuracy as reported in [2]. In [3], a Biogeography-Based Optimisation method is proposed to improve the accuracy of parameter estimation. However, this method only focuses on the accuracy, but not the computational cost and convergence speed. Therefore, the method is only proposed as a component monitoring method but not a parameter estimation method for adaptive control. An

accurate system identification algorithm based on a Kalman Filter (KF) approach has also been developed to estimate the system parameters. This algorithm demonstrates excellent convergence speed and more accurate results when compared with the RLS. However, the computational cost is much heavier—from $O(N^2)$ to $O(N^3)$ [4,34]. It increases the computational burden on the DSP and requires lower sampling frequencies as a result.

All these algorithms prove that adaptive algorithms can successfully estimate parameters in SMPC systems. However, none are perfect and address all the challenges presented. Therefore, it is necessary for further research to be carried out into optimising the system identification and adaptive digital filtering approaches for SMPC systems.

Interestingly, online system identification is now often considered as a pre-process for subsequent closed loop controller design. In particular, self-tuning or auto-tuning controllers can use the parameter estimation to compensate for parameter variation caused by the aforementioned reasons. Such control methods, generally referred to as adaptive control techniques, have been applied in many research papers [2,4-7,103]. However, as discuss in last paragraph, for real time control applications, only a select few algorithms are well suited for online system identification and digital control applications in SMPCs. Limitations of candidate methods often include:

1. Numerous multiplication and division operations. Such operations result in additional computational burden on the DSP.
2. Slow convergence. A slow identification response can result in delays to the employment of the control method; particularly in systems with rapidly changing conditions.
3. Low accuracy and bad noise immunity. Clearly, this can result in incorrect parameter estimation results and sub-optimal control.

For these reasons, finding a suitable adaptive algorithm is the crucial part in the entire adaptive control process. Many advanced control schemes have been proposed in the literature [2-14], however, their purpose is usually to achieve one or more of the following:

a. To increase the stability of the SMPCs over a wide range of parameter value variation c [9,11,12].
b. To improve the transient response characteristics under parameter value variation [5,13, 14].

c. To achieve high efficiency power management of the SMPC during parameter value variation; minimise losses [3].

Many control theories have been applied to achieve the above purposes, for example; Sliding Mode control, Model Based Predictive control, and Switching Surface control. An appropriate adaptive controller can be developed by either modifying one of these existing control methodologies (combine them with a suitable adaptive algorithm), or developing a novel control method based on the estimated parameters. For example, average current control and voltage feedback control are conventional control schemes. However, instead of these, V^2 control, peak current control, and Constant-Frequency Peak-Ripple-Based (CF-PR) control have been widely used in SMPC systems.

1.2 Scope and contribution of this research

Recent technical advances in microprocessor technology now allows for advanced control algorithms to be implemented in many SMPC system, however, cost and complexity are still clearly a major concern in this price and reliability sensitive application. For this reason, the main motivation of this research is to develop a computationally efficiency and rapid adaptive algorithm for system identification of SMPC system. Then, as a second motivation, to develop an adaptive control scheme to improve the robustness of the SMPC system.

To quickly and accurately estimate the parameter of SMPC system, a Fast-Affine-Projection (FAP) algorithm is proposed for the online system identification of DC-DC buck converter system. Compared with conventional LMS and RLS algorithms, the FAP algorithm provides a faster convergence speed with similar accuracy to the RLS, but with less computational cost. The computational complexity reduction is particularly valid in an autoregressive with exogenous input model. This model exactly represents the operation of SMPC system in digital control. Therefore, the proposed FAP algorithm is ideal for online system identification of SMPC systems. By analysing the iterative formula for RLS and FAP, the convergence speed improvement is discussed in detail.

Following the implementation of the proposed FAP algorithm, an adaptive current balancing constant ON/OFF control scheme is proposed to improve the voltage transient response during an abrupt load resistance change. By analysing the operating principles of a synchronous DC-DC buck converter, it is shown that the constant ON/OFF controller has better dynamic performance

compared with conventional duty cycle control. This proposed control method is compared with a conventional PID control controller over a wide range of load conditions. The simulation and experiment results verify the proposed current balancing technique performs with superior dynamic behaviour in all cases considered (see Chapter 3 and Chapter 5).

In summary, the main objectives and contributions of this research includes:

- To propose a novel system identification algorithm. This algorithm must have better performance and overcome issues reported in previous research. Key metrics for consideration is convergence speed and computational cost.

- Optimise this algorithm for SMPC systems and evaluate the performance as a specific system identification tool for SMPC systems.

- To develop a novel adaptive control method for transient response improvement; as compared to conventional control methods.

- To combine this adaptive control scheme with the proposed system identification algorithm to successfully implement a closed loop adaptive control scheme for a DC-DC buck converter system.

- To experimentally assess the performance of proposed system identification algorithm and adaptive control use a Digital Signal Microprocessor (DSP) and a hardware synchronous DC-DC buck converter system.

1.3 Publication arising from this research

This research has resulted in several academic publications:

- **Chen Wang**; Armstrong, M.; Gadoue, S.; Missailidis, P., "System identification of a DC-DC converter system using a Fast Affine Projection algorithm," *7th IET International Conference on Power Electronics, Machines and Drives (PEMD 2014)*, vol., no., pp.1,6, 8-10 April 2014

- **Chen Wang**; Bing Ji; Xueguan Song; Pickert, V.; Wenping Cao, "IGBT condition monitoring with system identification methods," *Transportation Electrification Asia-Pacific (ITEC Asia-Pacific), 2014 IEEE Conference and Expo* , vol., no., pp.1,6, Aug. 31 2014-Sept. 3 2014
- **Chen Wang**; Armstrong, M.; Gadoue, S., "System identification and adaptive control of a DC-DC converter using a current balancing ON/OFF control technique for optimal transient performance," *in Power Electronics and Applications (EPE'15 ECCE-Europe), 2015 17th European Conference on* , vol., no., pp.1-10, 8-10 Sept. 2015
- Ruisheng, L.; Armstrong, M.; Gadoue, S.; **Chen Wang**, "On-line Parameter Estimation of Non-Minimum Phase Switch Mode Power Converters," *8th IET International Conference on Power Electronics, Machines and Drives (PEMD 2016)*
- **Chen Wang**; Armstrong, M.; Gadoue, S., "Dual feedback adaptive control for voltage regulation of cascade DC-DC converter systems," *8th IET International Conference on Power Electronics, Machines and Drives (PEMD 2016)*

1.4 Layout of this thesis.

The thesis is organised into 7 chapters as follow:

Chapter 2 presents a detailed literature review on system identification and adaptive control techniques. Many applications use system identification and adaptive control is discussed in detail. The advantages of using system identification and adaptive control are set out in these applications.

Chapter 3 provides a detail mathematical derivation of the mathematical model for a DC-DC buck converter. This derivation starts from the basic operational principle of the DC-DC buck converter system, including the effect of PWM switching. After that, the discrete time domain mathematical model for the DC-DC buck converter is presented. Then, the limitation of using this mathematical model are discussed by analysing the transient characteristics of the DC-DC buck converter system. Finally, the conventional pole-zero cancellation method for determining the parameters of PID controller is proposed.

Chapter 4 presents a detailed mathematical derivation of the RLS and FAP algorithms. Both algorithms are derived from the basic stochastic gradient descent algorithm. The key properties

and feature of both algorithms are evaluated; with respect to computational cost, convergence speed and estimation accuracy, these two algorithms are fully compared. The results shows the superiority of the FAP algorithm in terms of convergence speed and computational cost, thus making it particularly suitable for system identification of SMPC systems.

Chapter 5 presents a proposed adaptive current balancing ON/OFF control scheme. Section one of this chapter provides a transient analysis of the DC-DC converter system, by analysing the power flow through the energy storage components. The transient response of the DC-DC converter can be divided into four key sections. Each section corresponds to a particular energy flow condition within the circuit. The proposed ON/OFF control scheme aims to minimise the period of time spent in each section. A detailed mathematical analysis demonstrates the potential benefits compared with the conventional duty cycle varied control scheme. The simulation results prove the proposed ON/OFF control scheme has a superior performance on improving transient response when load changes occur.

Chapter 6 focuses on the experimental validation of the proposed adaptive algorithm applied in a synchronous DC-DC buck converter system. The algorithm is programmed into a digital signal processor (DSP) for online system identification. The structure of the synchronous buck converter prototype is initially presented. Then, experimental comparison of results or the RLS and FAP for online system identification is presented. Finally, the experiment results of the proposed adaptive current balancing ON/OFF control are presented, the verification is done by comparing the approach to a conventional PID control as done in Chapter 5.

A conclusion of this study and a possible suggestion for future research is presented in the final chapter.

1.5 Notations of symbols in this thesis

In this thesis, all matrices and vectors use bolder characters to represent. As the regression matrix is $\{\boldsymbol{R}_{du}, \boldsymbol{R}_{u}\}$. The embellishment ^ on the head of bolder characters stands for an approximation of this matrix or vector. All electrical signals and components use normal italic character to represent. The difference between capital letter and small letter is capital letter stand for those signals which

remain constantly during system operation, such as input voltage of buck converter V_g. Physical parameters of SMPC system always uses capital letters to represent.

Chapter 2 Literature Review of System Identification and adaptive control method techniques for SMPC applications

2.1 Introduction

For many years, Switch Mode Power Converters have been replacing traditional transformer-based power supplies in many electrical applications. SMPCs offer cost effective, reliable and light weight solutions. With the advent of digital control, it is also possible to implement advanced control functionality within these systems. In the field of DC-DC power conversion, conventional power converter topologies such as the buck, boost and buck-boost converter are regularly employed. Significant academic and industrial research has been carried out to achieve enhanced performance; such as ultra-high gain, faster dynamic performance, lower power loss. DC-DC power converters have become essential power electronic systems and are widely used in many applications; such as Computer Power Supplies, Battery charging circuits, EV/HEV powertrain systems, renewable energy applications, and Vehicle to Grid (V2G) systems.

In digital control, system monitoring techniques have also been studied to improve system stability. Furthermore, they have been applied to optimise the size of passive components in power converter systems [15]. Sophisticated mathematical modelling techniques have been developed to better understand the impact of environmental factors, such as temperature and humidity, on power converter semiconductor device performance. Also, many control schemes have been developed to improve the reliability of power converter systems. Some of them are responsible for improving the transient response [16-19], others focus on robustness and maintaining stability [9]. In all areas of SMPC control and condition monitoring, awareness of the system parameters is essential. To achieve this, like many other scientific fields, analytical mathematical models are often required to describe the power converter system. Determining the mathematical model of the physical

system, and then establishing the system parameters is a branch of control theory often described as "System Identification". As defined in [19, 98]: "System identification is the art and science of building mathematical models of dynamic systems from observed input and output data". It uses statistical methods to identify the mathematical model and analyse the system behaviour in real-time applications. System identification is also the foundation for more advanced control features, such as "adaptive control". Adaptive control attempts to overcome real-time variation within a system. System identification is one way to measure or predict the variation. The pre-defined control method then adapts to any deviation to minimise its impact and maintain regulation of the system. This so-called "auto-tuning" strategy has been used in many power converter control methods.

In this chapter, a detailed literature review of system identification and adaptive control methods is presented. The advantages of many of these techniques are described, and their application for power converter technology is considered. Limitations of the present research are outlined, and the potential research gaps defined. This sets the background and motivation for the research contained within this thesis.

2.2 Literature review of system identification

The objective of system identification is to use sampled data to describe the system behaviour. Usually, the system is considered as a black box. Only observable quantities can be acquired from this black box [99,101]. A predefined mathematical model is implemented to describe the system behaviour. As aforementioned, the system can be influenced by environmental variation. This is captured by the variation of the parameters in the system's mathematical model. The overall procedure is shown as Fig.2.1. Broadly speaking, all system identification algorithms can be categorised two classes; parametric system identification and non-parametric system identification. The following provides an overview of literature on these two classes.

2.2.1 *Non-parametric system identification*

A non-parametric identification for Wiener systems is presented in [20]. This research using the impulse response approach to obtain regression curves to identify the system behaviour of a specific Wiener system. In [21], a non-parametric identification technique for non-linear systems

is presented. The author uses a Kernel-based non-parametric approach and a garrotte estimator to identify each part of the non-linear system. In [22], two-nonlinear-series-connected systems are identified via observing the harmonic frequency response. The harmonic frequency response gives an accurate system model and its output fits well with the actual system output.

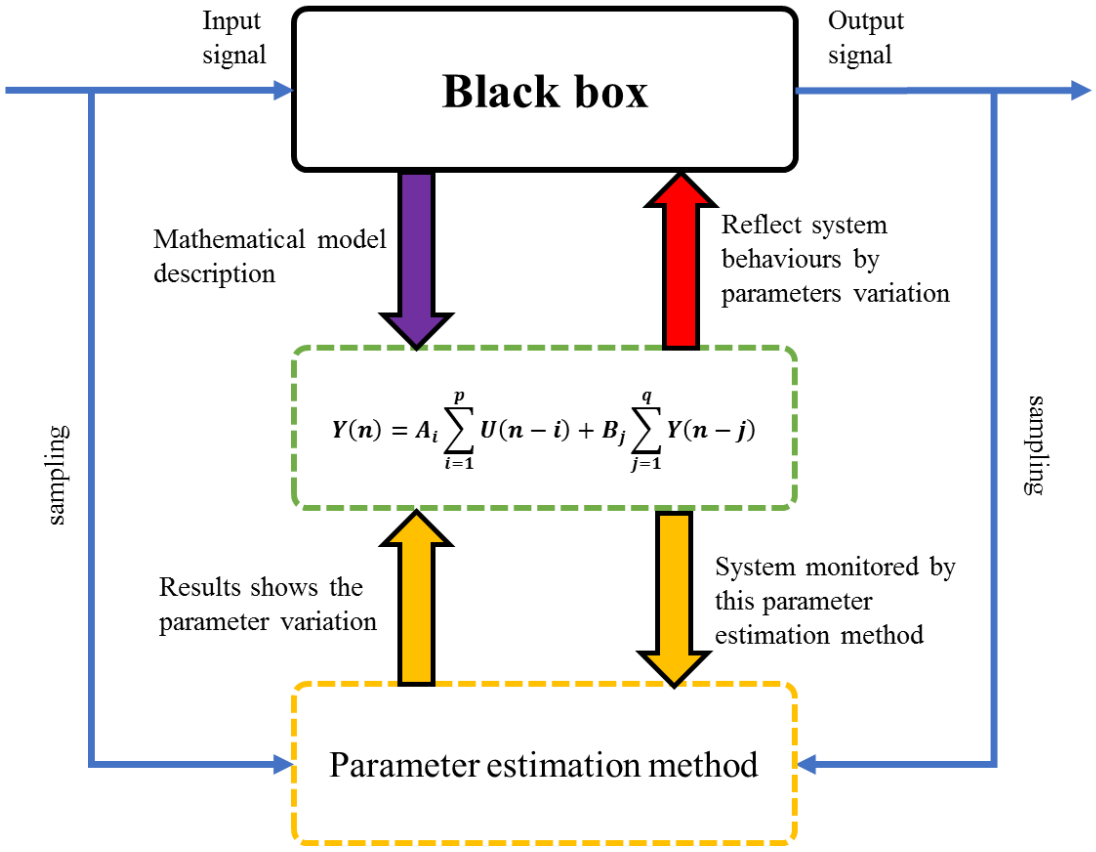

Figure 2.1 system identification of black box plant

As shown from the examples in literature, non-parametric system identification methods often use the transient response or correlation analysis to estimate the impulse response. Then, frequency analysis or spectrum analysis is applied to model the system. A key property of non-parametric system identification is that there is no a-priori knowledge about the system model due to its non-linearity and/or complexity [41]. Long-term data extraction is often necessary before the non-parametric system identification can be applied accurately. This is because many non-linear systems are sensitive to noise, and statistical measurements may need be considered. Due to the system complexity and the long-term data extraction, there is inevitably high computational cost

involved in implementing the identification algorithms. As a result, it can be difficult to implement these methods in real time applications, particularly those with significant, fast, and unpredictable parameter changes. In broader context, this also precludes many of these methods from hardware-in-loop applications, which are of growing interest in several research fields.

2.2.2 *Parametric system identification*

With certain design and empirical examination, many systems can be described using a particular, often pre-selected, mathematical model. This mathematical model describes the system dynamic or static behaviour. To pre-select a mathematical, some level of prior information about the system is necessary. Therefore, unlike the aforementioned black-box system, this kind of system is call grey-box. In a grey-box system [100], the system structure and dynamic behaviour may be partially known and thus can be simulated. As an example, a classic second order transfer function model can be used to describe the dynamic behaviour of many SMPCs and motor drives, as shown in Eq.2.1

$$G(s) = \frac{b_1 s + b_2}{s^2 + a_1 s + a_2} \tag{2.1}$$

The task of the system identification process is to estimate the mathematical system coefficients from the measurement data. In SMPC systems, the system coefficients are determined overall by the inductor, capacitor and resistor values.

Compared with non-parametric system identification, parametric system identification usually focuses on identifying a linear system with prior knowledge of its mathematical model. This mathematical model needs to be sufficiently accurate to describe the dynamic response of the plant system. In addition to estimating the SMPC system model, research has been carried out to determine the actual physical component values in the power converter system. Some studies have shown that this approach can be used for monitoring or fault detection in power converter applications [3,23,26,102].

Parametric system identification can be categorised into two types: offline system identification and online system identification. Typically, each system identification method is best suited to either online or offline system applications.

In Offline system identification, sampled data is stored in memory and is processed in a manner which is not time dependent on the operational condition of the system. As such, the system identification result is not used in real-time to update and change the system operation. Offline system identification is sometimes applied when the computational ability of a microprocessor is restricted or the mathematical model is too complicated to estimate all the parameters online.

An offline system identification method for determining the system transfer function can be found in [27]. The author uses underdamped-step-response data to identify the parameters in a second order transfer function. It presents a very simple method to estimate damping factor ζ and natural frequency ω_n. Elsewhere, alternative research uses the basic Laplace transform to evaluate the system parameter effect towards on the step response, developed a time-interval measurement method to estimate the parameter in overdamped and underdamped system [28]. Similarly, researches have been done in frequency domain [29] [30]. All these researches rely on a system response pattern to estimate parameters in mathematical model. It does not need heavy computational cost but require a specific system response pattern and the identification process can only be executed after acquired such patterns.

Online parametric system identification often utilises stochastic gradient descent algorithms to estimate mathematical model parameters. The stochastic gradient descent is a generic term of approximation methods for minimising an objective function iteratively. It uses sample data to update mathematical parameter iteratively to minimise the cost function. In most cases, stochastic gradient descent method serve linear system model looks like Eq.2.2.

$$y = \sum_{j=0}^{n} \theta_j x_j \tag{2.2}$$

Or can be written as a matrix form

$$y = \boldsymbol{\theta}^{\boldsymbol{T}} \boldsymbol{x} \tag{2.3}$$

To find the most accurate value of θ_j, the cost function of Eq.2.2 is applied

$$J(\theta) = \frac{1}{2m} \sum_{i=1}^{m} \left(y(i) - \theta_i x_i \right)^2 \tag{2.4}$$

To find minimum value of Eq.2.4, the gradient of this equation is needed to be found, therefore the problem becomes

$$\theta_j := \theta_j - \alpha \frac{1}{m} \sum_{i=1}^{m} \left(y(i) - \theta^{(i)} x_j^{(i)} \right) x_j^{(i)} \tag{2.5}$$

Where *i* stands for the iteration number and α is a small step size. A basic parameter update method is by calculating all existing data in *m* iteration and repeated in all terms of Eq.2.3 (i.e. from $j = 0,1,\cdots n$). This method called "Batch gradient descent". However, in many cases, *m* could be a very large value and only one update can be done based on above equations is too expensive in terms of computation. That is because it could be a heavy computational burden for a microprocessor to calculate all *m* derivative results. Alternatively, a better parameter update equation for Eq.2.5 can be reformed as

$$\theta_j := \theta_j - \alpha \left(y(i) - \theta^{(i)} x_j^{(i)} \right) x_j^{(i)} \tag{2.6}$$

In this case, only one iteration result is used to update the parameter value. The parameter only modified a little bit better in this iteration. By doing that step by step, the parameter gently converges to the true parameter. So, rather than store all *m* data into memory, a little bit progress can be more efficient for microprocessor converging the cost function to global minimum. This parameter update method is called stochastic gradient descent algorithm. By applying stochastic gradient descent algorithm, the converge direction maybe incorrect if the data is affect by noise as shown in Fig.2.2. Whereas the general direction should be towards to minimising $J(\theta)$.

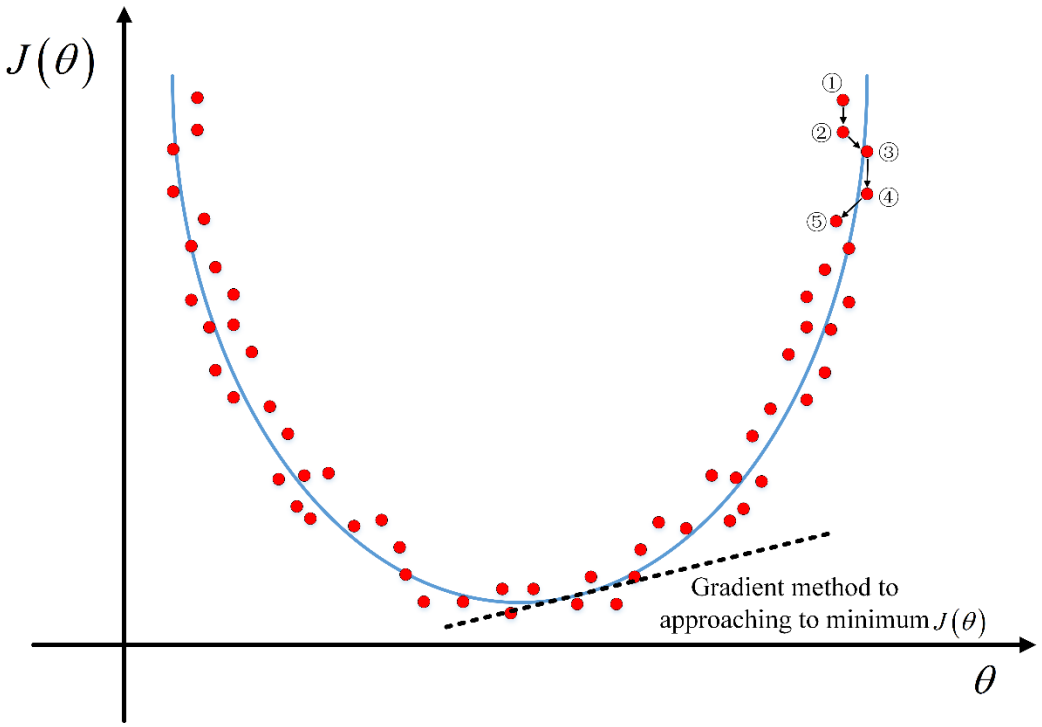

Figure 2.2 Stochastic gradient descent method

Based on stochastic gradient descent algorithm, many algorithms have been developed to solve this problem in Eq.2.4. As aforementioned, several adaptive algorithms such as RLS and LMS have been widely used in many system identification application [31-33, 42].

A brief literature review about using gradient descent algorithm and stochastic gradient descent algorithm is presented here. These literatures are only focus on the algorithm itself but not applied in any practical systems.

The first literature review is about evaluation Affine Projection (AP) algorithm. A convergence analysis study has been done in [82]. The comparative study is built by vary projection order of AP algorithm and the system parameter number. The projection order is an integer value determines the number of data point for updating the parameter matrix in AP algorithm. The results show AP algorithm has no much difference on estimation accuracy with uncorrelated input signal. The convergence speed may increase if the projection order is increased.

A variable forgetting factor mechanism for RLS algorithm is introduced in [83]. It varies the forgetting vector value by evaluating the error correlation. By applying this low-complexity

variable forgetting factor mechanism, the RLS has a faster convergence speed but only require few fix numbers of operations.

Some research articles have utilised one kind of stochastic gradient descent algorithm in system identification of SMPCs or other kind of power electronics system.

A unified hybrid model is given for power electronic circuits based on hybrid system theory has been published in [35]. This article summarises six kinds of SMPC systems including CCM and DCM mode. All parameters in that hybrid mathematical model are identified via RLS algorithm. It proves the conventional RLS can identify basic parameters including inductance, capacitance, load resistance and ESR of capacitor. Also, the experiment results prove that RLS performs a high accuracy in this hybrid mathematical model.

A recent research using gradient descent adaptive algorithm is presented in [36]. This article uses gradient descent adaptive algorithm to achieve fault prognosis. Firstly, the mathematical analysis of an interleaved DC-DC Boost converter via state space model is done. Then, a generalised gradient descent algorithm is applied to identify the state space model parameter [*A, B, C, D*]. When a fault is occurred, the system physical coefficients such as resistance, capacitance and inductance can be monitored via model parameter [*A, B, C, D*]. The experiment result has been done to prove this algorithm can identify the variation of capacitance and inductance in step perturbation and ramp perturbation condition. Both perturbations are simulated as different fault occur condition.

A real-time parameter estimation of DC-DC buck converters using a self-tuned Kalman filter has been done in [4]. In this research, a Kalman filter algorithm has firstly implemented in system identification of SMPC system. With the feature of decent convergence speed, and high estimation accuracy and good noise resistance, Kalman filter algorithm is a good candidate as adaptive algorithm for system identification of SMPC system. This article uses a Kalman gain and related innovation term to tune the diagonal matrix Q. Consequently, the tracking ability and noise immunity of Kalman filter is further improved. The only drawback of this algorithm is the heavy computational cost. It contains a $O(N3)$ calculation in each iteration, it increases the computational cost compared with RLS from $O(N2)$ to $O(N3)$.

Another Kalman-filter based system identification research has been done in [81]. This research utilises an extended Kalman filter to identify the parameter in a Luenberger state observer. This Luenberger state observer dedicated to an online estimation of the model parameters. By estimating this observer matrix, all observable system parameter can be acquired. This system identification tasks have been done in boost converter and interleaved boost converter.

Besides the stochastic gradient descent algorithm family, some other control algorithm can also be applied for online parametric system identification in SMPC system.

A FPGA-based online parametric identification algorithm for resonant power converters is presented in [37]. In this research, a phase-sensitive detector parametric identification method is applied. This method uses different sinusoidal waveform to extract different order of harmonic to reflect the capacitance and load impedance in resonant capacitor. With involving a low pass filter or finite impulse response (FIR) filter, the different dynamic response has been improved.

A biogeography-based optimization (BBO) method to improve the estimation accuracy has been developed in [3]. This method generates numerous populations of candidate estimation result. In each iteration, all estimation results are ranked to find the best and worst candidates. The worst candidate estimation result is replaced by the best estimation result in pervious iteration. Then, the current step best candidate is estimated based on the error between the best and worst in previous iteration. This article theoretically proves the BBO method has a better parameter estimation accuracy compared with RLS. However, the amount of candidate needs to be large. As it suggested, the candidate population should be set as 10 times of parameter values. In this research, a buck converter is as the SMPC system for parameter estimation. So, 40 candidate parameter group is here for update iteratively. As a result, the computational complexity is much higher than conventional RLS based on the calculation table provided by the author.

2.2.3 *Model variation for parametric system identification*

As aforementioned, the online parametric system identification focuses on linear mathematical model. Due to the variety of linear mathematical model, numerous adaptive algorithms have been developed to fit specific mathematical model. A brief introduction of linear mathematical model is presented here.

The basic form of linear system can be presented as

$$\boldsymbol{y(t) = \theta^T x(t) + \varphi^T v(t)} \tag{2.7}$$

Where the data vector is $x(t)$, θ is the parameter matrix for input data vector. $v(t)$ is a noise/disturbance vector and φ is parameter vector for noise signal. The mathematical model can be categorised as AR model, ARX model ARMAX model, OE model and BJ model, with variety type of input signal and model construction.

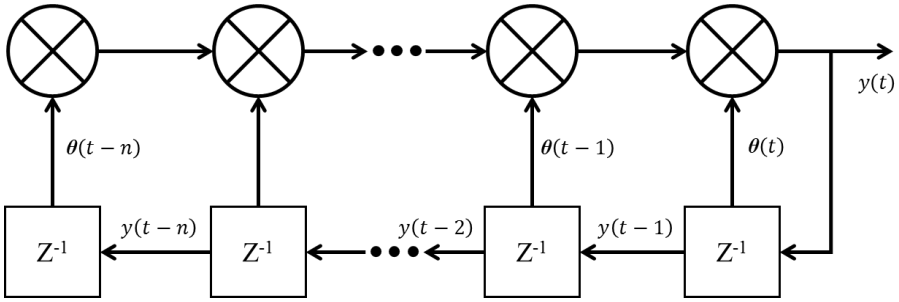

Figure 2.3 AR model structure[65]

Autoregressive model (AR) is constructed as Fig 2.3. The output sequence is only affect by the previous output sequence with certain parameter matrix involved. No system inputs or disturbances are used in the modelling. This very simple model represents limited class of systems. In this case, the data matrix is constructed by finite previous output signals.

Autoregressive with exogenous input model (ARX) model is shown in Fig.2.4. The Z^{-1} block is a unit delay block to recall the input/output data of previous step. $u(\cdot)$ and $y(\cdot)$ are stand for input and output data sequence respectively. $\theta(\bullet)$ is co-efficient value of each input/output term. This model can be summarised as "the current step output data is obtained by previous input and output data" in digital control. As the construction of transfer function of SMPC systems, most of them can be considered as an ARX model in digital control applications. A detailed mathematical derivation of SMPC system is presented in next chapter.

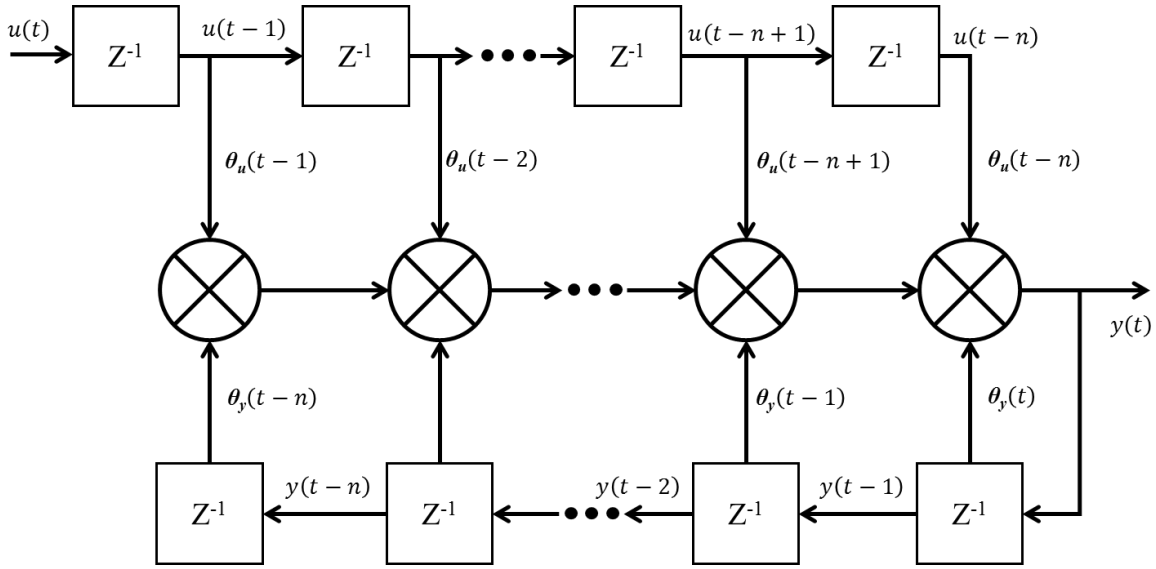

Figure 2.4 ARX model structure [93]

The above two models are an ideal condition that the disturbance signal $\boldsymbol{v(t)}$ can be neglected. However, in some cases, the disturbance signal is dominating to the dynamic response of system. An Autoregressive moving average with exogenous input model (ARMAX) can be represented the model in this case as shown in Fig.2.5.

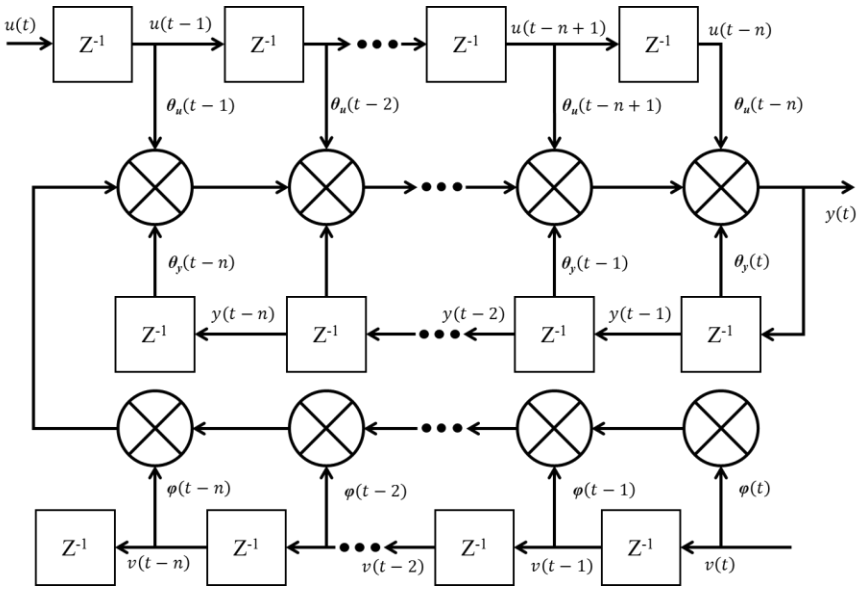

Figure 2.5 ARMAX model structure

As rest two type of model structure, Box-Jenkines (BJ) and Output Error (OE) are consider more about the disturbance effect to the system. The dynamic of the disturbance in BJ and OE models are separated from system model.

2.3 Literature review of Adaptive control

With high requirement about system reliability and robustness, many advanced control methods have been researched in power electronics field. Amount those method, most of them need a priori information about the system parameter for substituting in their control algorithm [39-40]. However, system coefficients are likely to be varied due to the environmental effect, such as temperature, humidity, pressure, etc.

Due to this practical issue, as one branch of modern control theory—parameter estimation based adaptive control has been widely researched in recent years [5, 24, 43]. This control method can be defined as a control method used by a controller which must adapt to a controlled system with parameters which vary or are initially uncertain. A control law is needed that adapts itself to such changing conditions [5]. It can be seen from the definition that adaptive control does not need the priori information about the system parameter, and able to work when system parameter is varying. To be more specific, in power electronics field, many researches focus on automatically vary the duty ratio signal to control the power converter system. As a result, so-called self-tuning/auto-tuning controller has been researched in literatures [44-47]. In this section a detailed literature review on recent publications and the motivations in system identification and adaptive/self-tuning controllers for dc-dc power converters is presented.

2.3.1 Non-parametric system identification based adaptive control methods

In terms of non-parametric system identification method, a cross-correlation system identification method has been done in [24]. The input signal is injected with a multi-period pseudo random binary signal (PRBS), the impulse response of it can be put forward to compute the frequency response. This computed frequency response has high consistency compared with the frequency response from conventional frequency analysis. After that, subsequent research has been done in

[48] to improve this non-parametric system identification method. Firstly, the accuracy of existing non-parametric cross-correlation system identification method is improved by using three different techniques: windowing the measured cross correlation, delayed sampling of the output voltage signal, and correcting for the non-ideal spectrum of the injected pseudorandom binary sequence (PRBS) signal [49]. Next, Roinila *et al*. [50] proposed to inject a different type of PRBS signal to improve the sensitivity to disturbance during the system identification process.

Jeffrey et al. [51] presented an online monitoring method to obtain the system crossover frequency and phase margin. A special cycle efficient software frequency response analyser is presented in [52], this article detailed introduces the frequency response analysis method for system identification of SMPC system. With cycle efficient feature, this analyser can be used as a tool for online system identification [52].

Costabeber *et al.* [53] presented an auto-tuning of PID controller method by using cross-correlation method. This auto-tuning method injects a disturbance in the duty cycle to measure impulse response of system. Compared with the result from frequency response, an error can be obtained for determine the parameter value of *Kp* and *Kd* in PID controller. As a result, the auto-tuning process is only performed on the proportional-derivative gains. An optimised search method is used to tune the PD coefficients; this results in minimising the estimated error.

Compared with this method, a more functional method is presented in [47], this method do not require the knowledge of power stage frequency response and do not depends on any conventional control criteria. It only depends on observing the compensated-error-signal time domain characteristics. The compensator parameters such as gains, poles and zeros are adjusted in a direction that will increase or decrease the compensated-error-signal. By finding the relationship between compensated-error-signal amplitude, trend and all record of previous measurement, with close-loop frequency response characteristic, the compensator parameter can be auto-tuned to meet the requirement from frequency response without measuring it. Several control laws between the frequency domain and compensated-error-signal has been built in this article to guide the parameter tuning direction.

In summary, as many methods presented here, the non-parametric system identification and subsequent auto-tuning method are based on the directly/indirectly acquiring of frequency response. Most of those methods have no ability for online system identification and adaptive

control are mostly under pre-defined rules, such as phase margin and gain margin requirement from frequency response. Therefore, so many pre-processing for adaptive control are needed to be done, which is unsuitable for time-varying system affected by environmental condition.

Compared with that, many online parameter estimation methods using stochastic gradient descent algorithm has been applied in adaptive control. With stochastic gradient descent algorithms, system parameter can be fast identified, and the control law is much more flexible due to many advanced control schemes have been developed based on the priori information of system parameters. From below examples, many adaptive control methods achieved online system identification and auto-tuning the controller parameter in real-time and result in a better performance in system operation.

2.3.2 Parametric system identification based adaptive control methods

A typical parameter estimation method for improving converter performance of HVDC system has been introduced in [54]. The author used recursive least square algorithm to estimate the equivalent gird impedance and equivalent grid voltage based on a RL network of HVDC system. Based on these parameters, the operation point of the controller for HVDC system can be determined. The optimised operation point can significantly improve the power distribution quality and efficiency. The author also pointed out that the computational cost of recursive least square is a main barrier for implement this technique in real time application. A hardware-in-loop experiment has been done to verify this research. Additionally, with a non-complex non-matrix form of recursive least square method, the computational cost is significantly reduced. A real-time experiment of implementing this simplified recursive least square method is carried out to verify the control theory.

Kelly *et al.* [55] proposed an adaptive dual-purpose controller. This controller uses a linear prediction-error filter (PEF) which updating the error signal to the controller. Least Mean Square (LMS) is the algorithm for the prediction calculation. This solution does not need as priori information about system parameters. However, there are several limitations appear to this system. Firstly, the function of voltage regulation is appeared over time due to the prediction-error filter is with tap-weights in this Auto-Regressive (AR) modelling. Secondly, the LMS algorithm is a basic

adaptive algorithm which cannot provide fast convergence speed for filter application. Thirdly, a PD type controller is implemented in this research, the steady state error cannot be eliminated due to lack of integral part. From this research, the basic idea of using stochastic gradient descent algorithm for adaptive control in SMPCs is cleared and many subsequent articles are applied this method to do the system identification and adaptive control.

A Self-tuning indirect adaptive control for noninverting buck-boost converter is presented in [7]. This research uses typical Recursive Least Square (RLS) algorithm to identify the parameter at beginning. Then, designed a polynomial formed compensator to achieve pole placement compensation for the best pole placement of system. With the cancellation of zeros in the system and working to select the minimum degree pole placement. Parameters in the polynomial compensator can be determined using the system parameter acquired from RLS algorithm. This method is straightforward to be implemented. However, this research utilised a conventional adaptive algorithm with a basic PID controller tuning logic in SMPC system, which cannot well fit if the system operating in a specific dynamic circumstance.

Another research has been done in [2]. The author uses a novel bit-shift idea called dichotomous coordinate descent (DCD) to significantly reduce the computational cost of conventional RLS algorithm. Then, uses the DCD-RLS algorithm replacing LMS algorithm in Predictive Error Filter (PEF) from the research done by Kelly. Moreover, an integral part is added in the controller part to form a PD+I controller in total. With this PD+I controller, the output voltage can be regulated to eliminate the steady state error. Similarly, as the work done by Kelly, the DCD-RLS algorithm used in PEF update the *Kp* and *Kd* value to auto-tuning the controller parameter when system load changed. From its experiment result, it can be concluded that the control method has good improvement of transient response compared with conventional PI controller. It flexibly tuned the *Kp* and *Kd*, but still cannot detect and improve the dynamic response in a one-off load change condition. Additionally, there are insufficient literatures/derivations that support the PID controller is the optimal controller to improving the dynamic response in this load change condition.

From above examples, a general parametric system identification based adaptive control procedure can be concluded as Fig.2.6. With an uncertainty environmental factor affect the system operation, one or many system parameter(s) is/are varied. By applying parameter estimation algorithm identify the variation of system parameter(s), a control signal is generated based on the control

algorithm. The control signal is auto-tuned depends on the parameter variation. All above literatures are only consider one parameter changed per condition. However, parametric system identification for many parameters changed condition can often be found for determining State of Charge of Li-ion battery [114].

In the research of [105], an autotuning method based on parameter estimation is presented. This work applied a novel type of Kalman filter to estimate the parameter first. Then, a discrete PID gain tuning law called Bányász/Keviczky method is applied to tuning K_p, K_i and K_d in each switching time interval. The updated duty ratio is calculated by the three PID parameter and previous step duty ratio. The simulation result and experiment result show this proposed autotuning method has a superior transient response compared with conventional pole placement method.

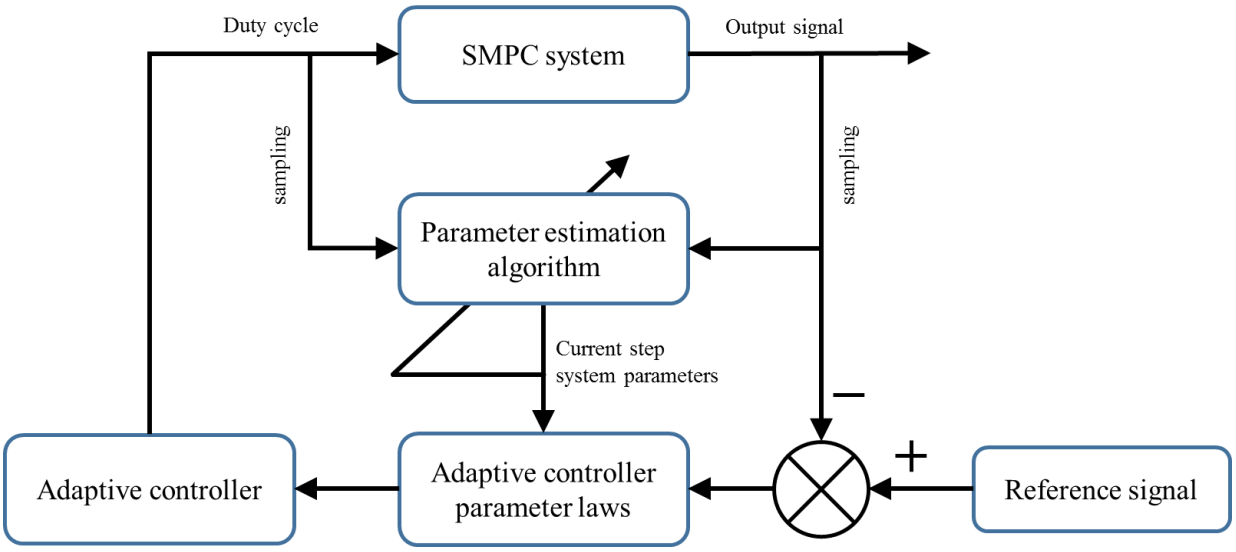

Figure 2.6 schematic diagram of parametric system identification based adaptive control

2.3.3 Other type of adaptive control method

Besides of parametric and non-parametric system identification based adaptive control method, many other adaptive control rules have been developed in power electronics systems.

An adaptive control for improve the transient response in high step-up DC-DC converter is presented in [56]. This technique combines the conventional existing current-mode control law

and an adaptive law that generates the inverse of the load resistance. The load resistance is estimated by sampling the load voltage and find the derivative of the error voltage which is bounded by a threshold. The controller gain is then varied based on this estimation of load resistance.

In [57], an adaptive on-time control is presented for eliminating serious electronic–magnetic interface noise when the converter operation is based on a ripple-based control scheme. An adaptive voltage positioning method is built by finding the relationship between output voltage and inductor current. Based on that, the adaptive on-time period can be determined when the output voltage is varied. The experiment shows the power conversion efficiency can reach 88.2% by applying this method.

An adaptive control is presented in [58] for three-phase voltage source converter (VSC) acting as a static power factor compensator. This method approximates third-order nonlinear model of VSC that accounts for uncertainty in three system parameters. These three system parameters are estimated by using quadratic Lyapunov function. The controller parameters update law is derived from the estimated system parameter. Compared with traditional vector control scheme, this proposed adaptive control performs a good tracking ability and transient response.

Neural-network and Fuzzy logic (FL) are widely used in identify nonlinear system due to its special tracking and learning ability. Some researchers are also developed them into adaptive schemes for effectively control the SMPCs system using fast developed digital control technique. An adaptive fuzzy-neural-network control (AFNNC) scheme is designed in [59] for the voltage tracking control of a conventional dc–dc boost converter. This AFNNC method tuning the controller parameter to meet the stability criteria derived from Lyapunov law. Based on sensing the output voltage and applied this AFNNC method, the proposed total sliding mode control (TSMC) method significantly improves voltage tracking performance of this boost converter.

A novel DC-DC control scheme has been introduced in [60]. This proposed method in this article is varying the switching frequency of converter while tracking the converter minimum input power (maximum efficiency) point under variable operation conditions of the power converter. An adaptive control scheme is applied to find the optimum switching frequency which can minimise the power loss while the converter parameter and conditions are vary. First, the relationship between switching frequency and two types of loss (conduction loss and switching loss) is

analysed in both CCM and DCM condition. Then, a minimum input power point is tracked based on the loss analysis and the power loss caused by current variation is also discussed. This research points out that in parameter varying condition, the current variation is the main result for power loss. The proposed adaptive frequency optimisation method tracks the minimum input power point and tuning the frequency based on the current variation.

From above literature review, only few stochastics-gradient-decent type algorithms have been applied in adaptive control of SMPCs. Many adaptive control/auto-tuning control schemes are based on directly signal measurement and a predefined tuning law to tune the controller parameter. The reason for seldom usage of adaptive algorithm can be summarised as caused by two problems [2]. First problem restricting the implementation of adaptive algorithms for SMPCs is the parameter convergence speed. Many stochastic gradient descent algorithms are too slow to apply in real time. It is not fast enough to help tuning controller parameter. The second problem is high computational burden caused by adaptive algorithm restrict the consequent control algorithm implemented in microprocessor. Matrix computations require significant resources of microprocessors, this usually results no spaces for implementing control algorithm. Therefore, it can be concluded that an adaptive algorithm with fast convergence speed and low computational cost is necessary for online system identification and adaptive control of SMPC system.

2.4 Chapter summary

This chapter has presented an overview of the principles and techniques used in system identification and adaptive control. It has provided an overview of the system identification techniques that have been applied across a broad range of research. Several examples of non-parametric and parametric system identification have been described. It can be concluded that non-parametric system identification is well suited to complex systems which can only be presented as a black-box, and as such no priori information can be acquired. In contrast, parametric system identification focuses on systems that can be represented by a recognised mathematical model before the identification process is applied. Based on this, several popular mathematical model structures have been introduced. A popular online system identification method, the stochastic gradient descent algorithm has been presented and its key advantages discussed.

Finally, several adaptive control applications based on non-parametric and parametric system identification are introduced. Furthermore, adaptive control without system identification is also presented as a new perspective on adaptive control. It is worth to investigate a proper mathematical model for SMPC and find a fast and effective adaptive algorithm for system identification process. In next chapter, a mathematical model derivation for DC-DC buck converter is presented.

Chapter 3. Mathematical model and operation principle of DC-DC buck converter

3.1 Introduction

As discussed in Chapter 2, a viable mathematical model is a prior information in parametric system identification. It is essential to determine this mathematical model before system identification. This chapter develops a mathematical model of a DC-DC buck converter for the purpose of system identification. In parametric system identification field, especially for stochastic gradient decent algorithm family, three criteria for this mathematical model must be obtained. Firstly, the mathematical model must represent the dynamic or static behaviour of the DC-DC buck converter. Secondly, all physical coefficients value can be calculated via the mathematical model. Thirdly, the mathematical model can be transferred to a discrete linear equation for parameter estimation via adaptive algorithm.

In this case, an averaging state space model of DC-DC buck converter is derived as a linearization example for SMPCs. Consequently, the well-recognised control to output transfer function is used as the mathematical model for the buck converter. Its discrete form can be represented as an Autoregressive with exogenous (ARX) output model, which is used in many adaptive control schemes. Following the determination of the mathematical model, several widely-used digital feedback control schemes for SMPC system are presented. Finally, the limitation and drawbacks of using control-to-output transfer function or averaging state space model as the mathematical model for SMPC in system identification is also analysed.

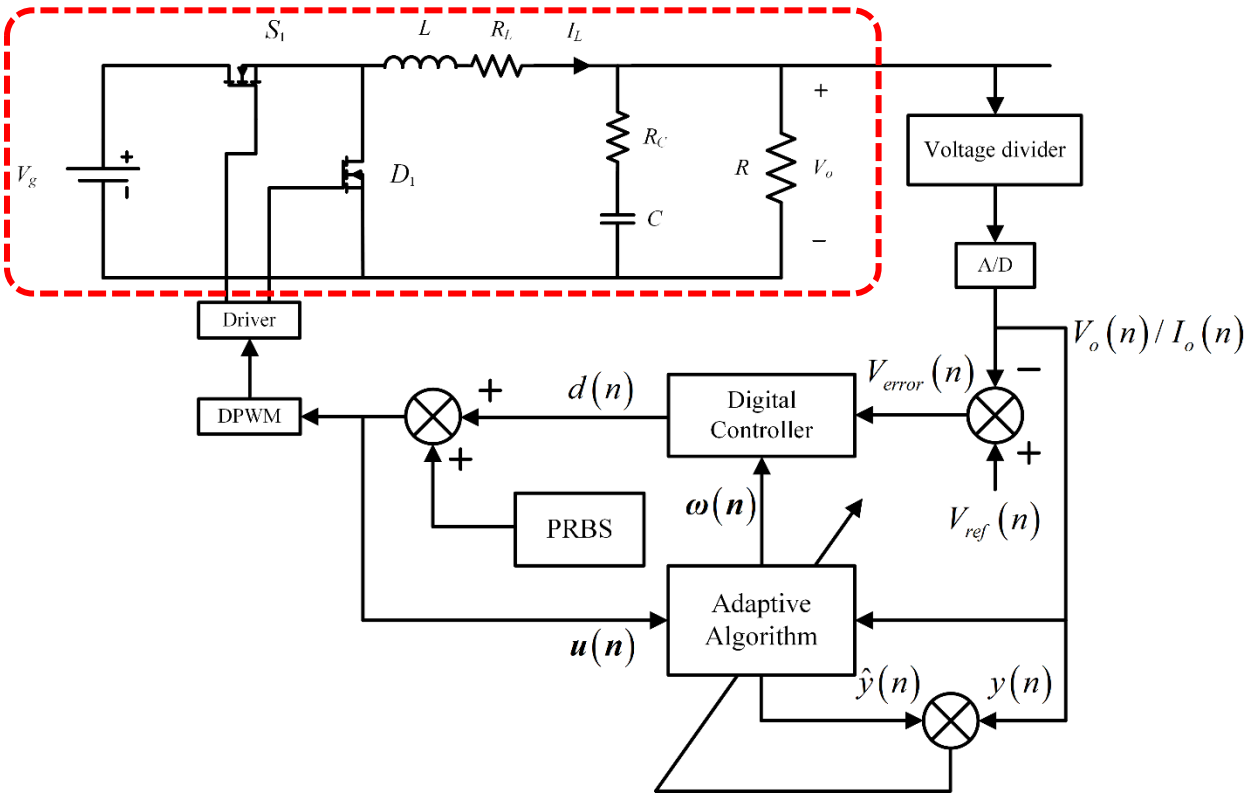

Figure 3.1 system identification and adaptive control of DC-DC buck converter—mathematical model part

3.2 Basic principle of operation of DC-DC buck converter

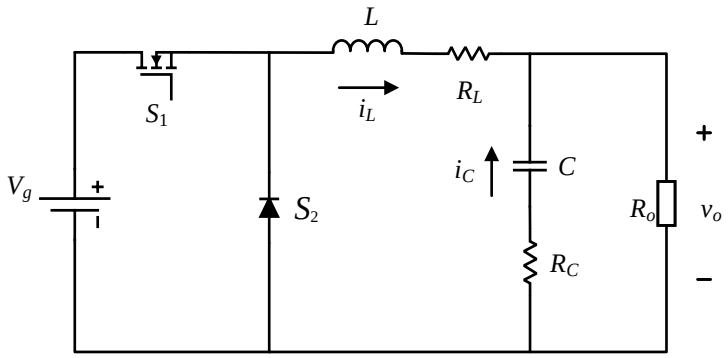

Figure 3.2 DC-DC Buck Converter

Consider Fig. 3.2. The function of the DC-DC buck converter is to step down the input voltage V_g to a lower output voltage V_o .By controlling the semiconductor device, (e.g. MOSFET), the output

voltage and inductor current can be regulated to achieve a set point condition. As aforementioned, many PWM switching methods have been studied to control the system. However, fundamentally the ratio of the "ON" period to the whole switching period is defined as the duty ratio and determines the step-down gain of the DC-DC buck converter. Here, a differential equation-based DC-DC buck converter model is derived to express the relationship between the gain and the duty ratio [78].

Consider Fig. 3.3. When the semiconductor device is on ("Switch ON" state), the buck converter circuit configuration.

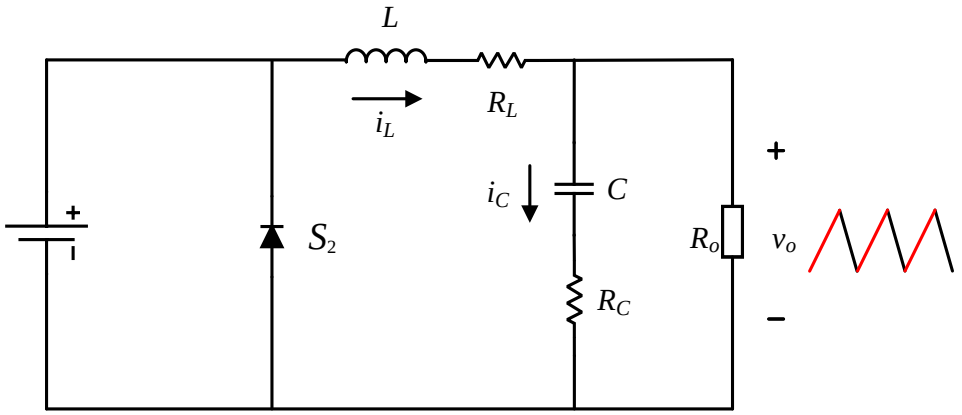

Figure 3.3 Buck converter "ON" state

According to Kirchhoff's circuit laws, the differential equations for inductor current and capacitor voltage can be described as

$$L\frac{di_L}{dt}\bigg|_{ON} = V_g - i_L\left(R_L + R_C\right) - v_C + \frac{v_o}{R_o}R_C \tag{3.1}$$

$$C\frac{dv_c}{dt} = i_L - \frac{v_o}{R_o} \tag{3.2}$$

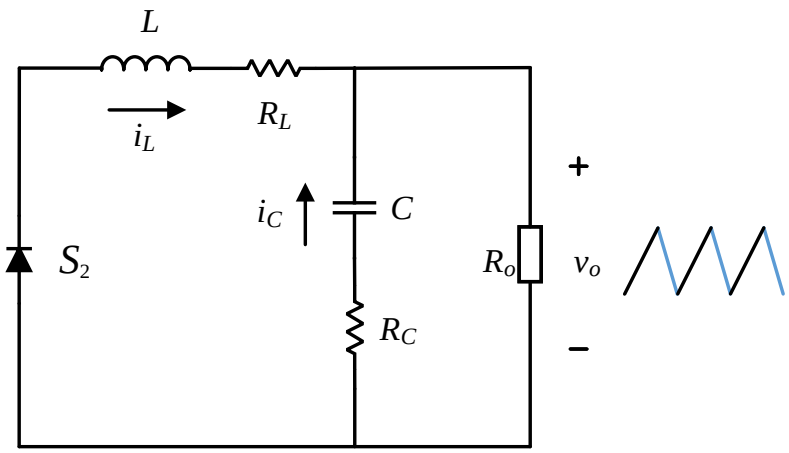

Figure 3.4 Buck converter "OFF" state

Similarly, when the semiconductor device is open ("Switch OFF" state), the following two differential equations can be obtained from Fig.3.4

$$L\frac{di_L}{dt}\bigg|_{OFF} = \frac{v_o}{R_o}R_C - i_L\left(R_L + R_C\right) - v_C \tag{3.3}$$

$$C\frac{dv_c}{dt} = i_L - \frac{v_o}{R_o} \tag{3.4}$$

Note that the differential term for v_c is the same regardless of whether the semiconductor switch is in the "ON" or "OFF" state. However, in practice the capacitor voltage waveform rises when the switch is "ON" and falls when the switch is "OFF". This is because of the unbalance between the load current and the inductor current during these 2 states. During the "ON" state, the capacitor discharges to supply power to the load resistor and the inductor receives energy from the power source. As a result, the capacitor voltage drops and the inductor current increases during this period - until the inductor current is greater than the load current. At the same time, capacitor voltage slope ($\frac{dv_c}{dt}$) changes from negative to positive. During the "OFF" state, the inductor delivers power to the capacitor and load resistor. As a result, the inductor current drops and capacitor voltage rises during this period. The capacitor keeps charging due to the unbalanced current caused during the "ON" state. This charging ceases once the load current is greater than the inductor

current. It can be seen that the capacitor voltage $\frac{dv_c}{dt}$ slope is affected by two continuous-varying currents. As a consequence, the capacitor voltage behaviour differs compared to the inductor current; there is no sharp change at the point of a switching event. In contrast, the output voltage follows the inductor current as shown in Fig.3.5. This performance determines the shape of the carrier waveform in many control schemes.

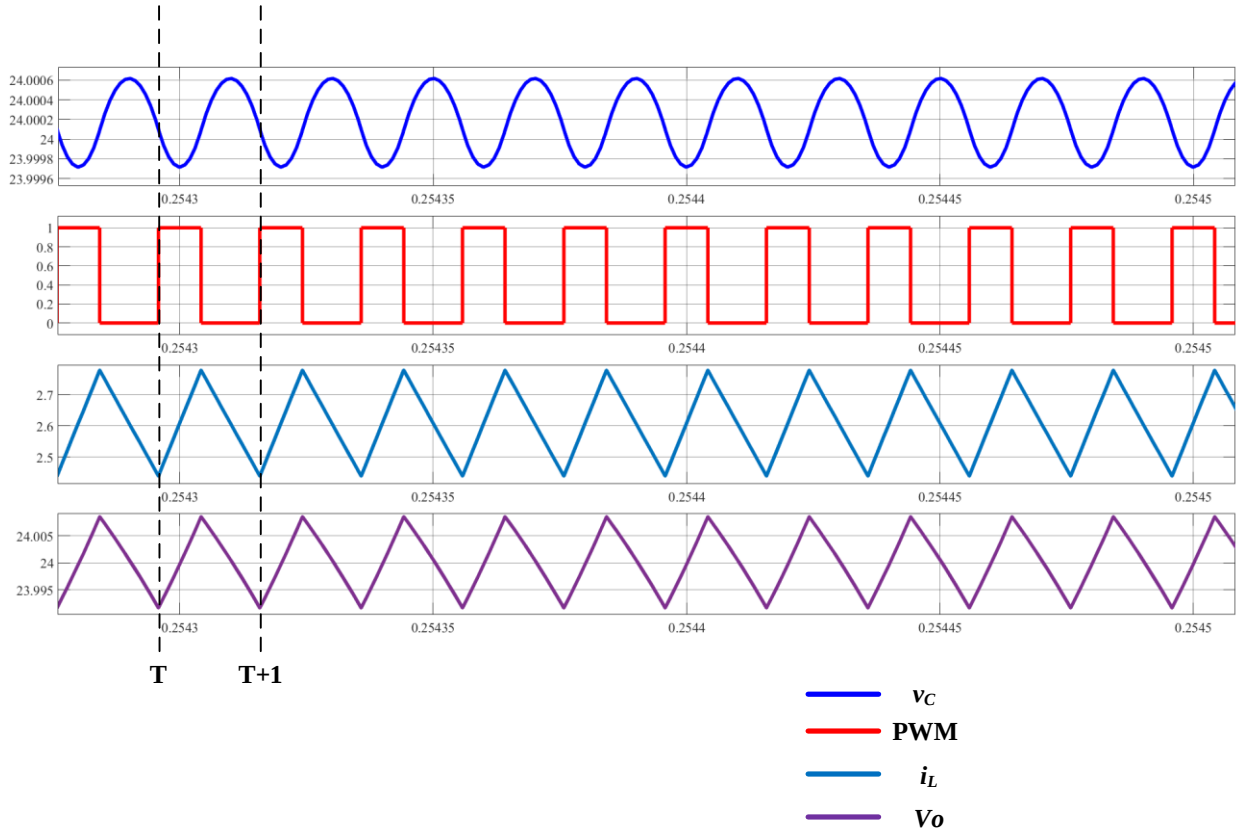

Figure 3.5 steady state waveforms of DC-DC buck converter

When the DC-DC buck converter operates in CCM (Continuous Conduction Mode) and the system operates at a steady state condition, the net variation of inductor current across a complete switching period should equal zero. So, Eq.3.5 can be obtained as

$$\left.\frac{di_L}{dt}\right|_{ON} T_{on} + \left.\frac{di_L}{dt}\right|_{OFF} \left(T - T_{on}\right) = 0 \qquad (3.5)$$

Where T stands for a complete switching period, and T_{on} is the switching ON period.

By substituting Eq.3.1 and Eq.3.3, one can obtain the following:

$$V_g T_{on} + \frac{v_o}{R_o} R_C T - i_L R_L T - i_L R_C T - v_C T = 0 \tag{3.6}$$

By dividing by T and defining $D = \frac{T_{on}}{T}$, one can obtain

$$V_g D + \frac{V_o}{R_o} R_C - i_L R_L - i_L R_C - v_C = 0 \tag{3.7}$$

Rearrange Eq.3.7

$$V_g D = v_C + \left(i_L - \frac{V_o}{R_o} \right) R_C - i_L R_L \tag{3.8}$$

However;

$$v_o = v_C + \left(i_L - \frac{v_o}{R_o} \right) R_C \tag{3.9}$$

Therefore

$$\frac{v_o}{V_g} = D + \frac{i_L R_L}{V_g} \tag{3.10}$$

If all the Equivalent Series Resistance (ESR) and other inherent parasitic can be neglected, then

$$v_C = v_o \tag{3.11}$$

and

$$V_g D - v_C = 0 \tag{3.12}$$

Thus, we obtain the relationship between input and output voltage as

$$\frac{v_c}{V_g} = D \tag{3.13}$$

Therefore, semiconductor device is the key controllable component to vary the duty ratio to control the output voltage. With a certain input voltage, the duty ratio is considered as the input of SMPC

system and the output voltage is the output. The switch swap between each switching condition corresponding with two differential equation series to obtain the desire output voltage level. Compared with traditional transformer. The SMPCs have a more flexible voltage ratio range and less cost. However, an inevitable nonlinear behaviour is involved into the system due to the ON/OFF switching of semiconductor device.

It is needed to be noticed that the duty ratio is relative with the inductor ESR R_L , if this ESR cannot be neglected. The duty ratio can be presented as

$$D = \frac{v_o - i_L R_L}{V_g} \tag{3.14}$$

Here, the output voltage stands for the stepped down voltage minus the voltage across the voltage between inductor ESR. Because of this, the duty ratio in open loop condition need to be carefully determined if the inductor ESR cannot be neglected.

3.3 Basic digital feedback control scheme

Due to the feature that programmable control in digital signal processor (DSP), easily-integration features and fast development of DSP, digital control is more widely used in control of SMPCs recently. A basic schematic diagram of digital control of SMPCs is shown in Fig.3.6. After sensing and transducing the current/voltage signal in each switching period, the analogue signal is converted to digital signal by ADC and compared with reference signal before or after signal processing. Then, following the control algorithm to calculate the duty ratio of next switching period, feed into the DPWM model and acquire the corresponding PWM waveform. After the PWM waveform is amplified by gate drive ICs, the gate signal control the semiconductor switching ON and OFF to achieve the certain duty ratio as the input signal of the system. Then, the output voltage can be maintained in a lower voltage compared with input voltage. There are many different control schemes by sensing different analogue signals and following different control scheme to generate PWM waveform for controlling the SMPCs. Here, several commonly used control schemes is introduced as a general review of digital control of SMPCs.

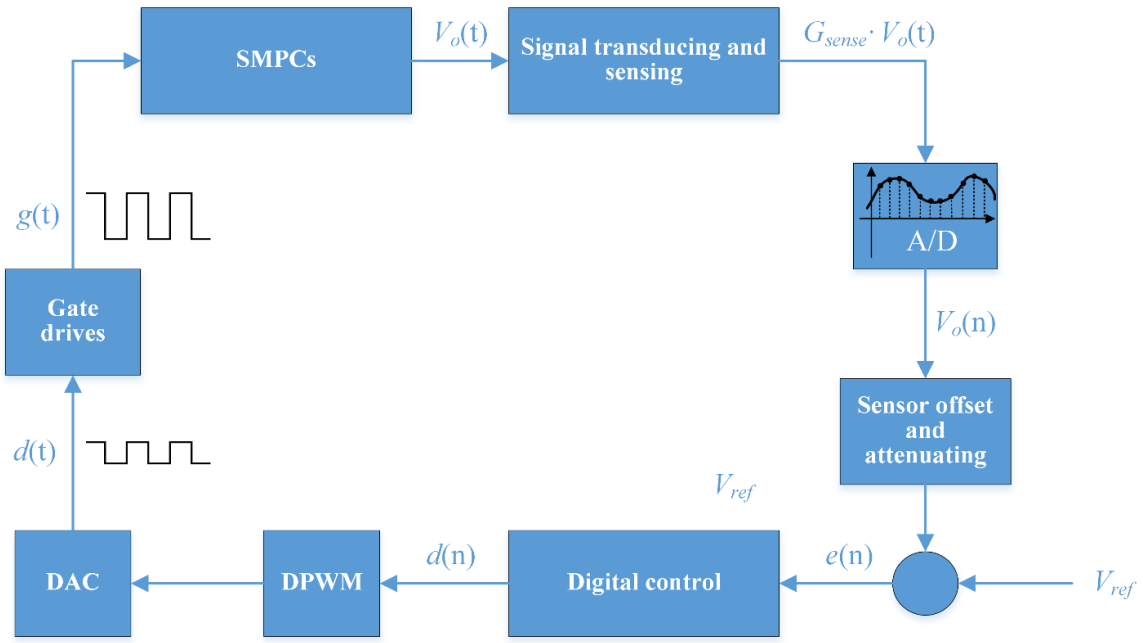

Figure 3.6 Digital control of SMPCs

3.3.1 *Voltage feedback control*

The voltage feedback control is a commonly used feedback control scheme due to its simplicity. As shown in Fig.3.7, the output voltage is sampled every switching period and compared with the reference value to determine the duty ratio, a Proportional-Integral-Derivative (PID) controller is usually applied before the error signal compared with carrier waveform. This PID controller can improve the transient response and achieve voltage regulation purpose. Also, the integral part can regulate the duty ratio to maintain the stability when a transient response occurred. The duty ratio converted to a certain value in DSP to meet the specified symmetric model in EPWM model, as a result that the carrier waveform is different corresponding with each symmetric model in simulation. Also, the comparator rule is different and consequents a leading-edge PWM and trailing-edge PWM. The transfer function of SMPCs might be varied based on two PWM structure [61]. As shown in Fig.3.8, the trailing-edge PWM keeps transistor switching ON at the beginning of each switching cycle, turn OFF when the carrier is greater than duty ratio. As contrary, the leading-edge mode keeps transistor switch OFF at start and turn it ON when the carrier value is greater than duty ratio. In EPWM submodules, trailing-edge corresponding with the step-down mode and leading-edge corresponding with the step-up mode. Also, a third type of PWM generation rule can be found in many researches called double-edges modulation, as shown in

Fig.3.9. It keeps transistor OFF at beginning of each switching cycle, turn it ON when the duty ratio is less than carrier waveform and turn it OFF when duty ratio greater than carrier waveform value. As in EPWM submodules, an UP-DOWN count mode is corresponding with this leading-triangle-edge modulation. The trailing-triangle-edge modulation is also existed and applied UP-DOWM count mode in DSP.

In this research, a voltage feedback control with leading-triangle-edge modulation method is applied. With simply voltage feedback control method, the control signal is only dependent with output voltage. The dynamic behaviours of inductor and capacitor can be easily analysed and illustrated in this case. The mathematical model of DC-DC buck converter can be easily derived based on the leading-triangle-edge modulation method. Due to its simplicity and effectiveness, voltage feedback control method is also usually used in industry.

It needs to be noticed that the mathematical model varied depends on the PWM mode. A detailed comparative study of mathematical model for different PWM mode can be found in [61].

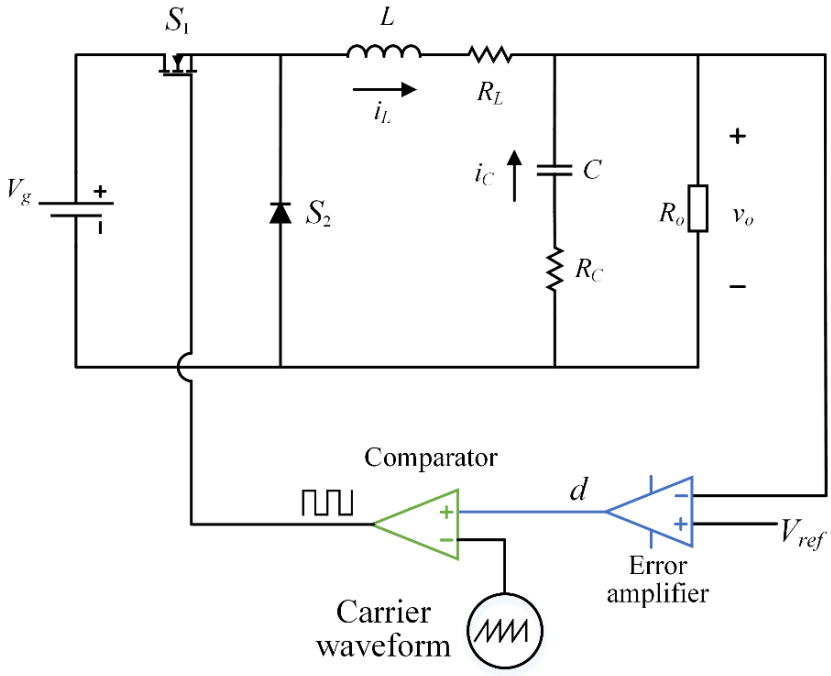

Figure 3.7 voltage feedback control of DC-DC buck converter

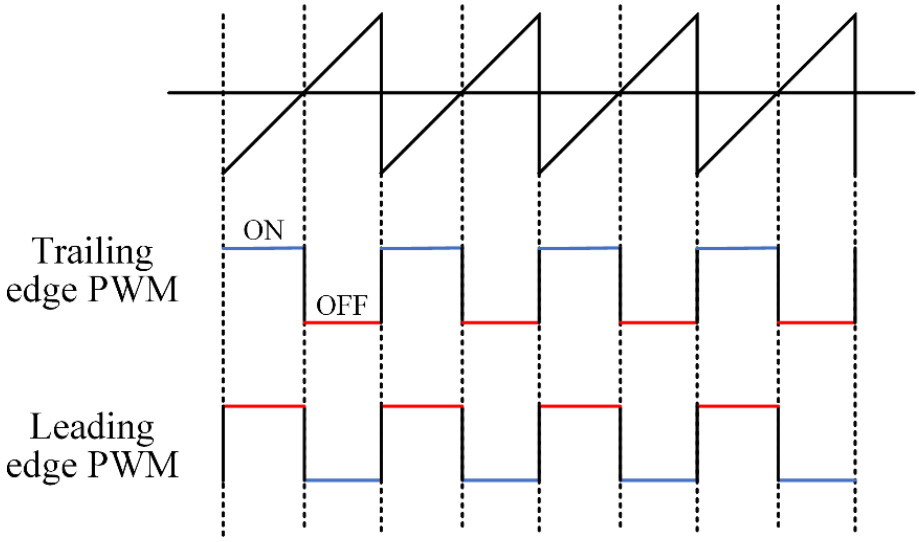

Figure 3.8 Trailing edge and Leading edge modulation

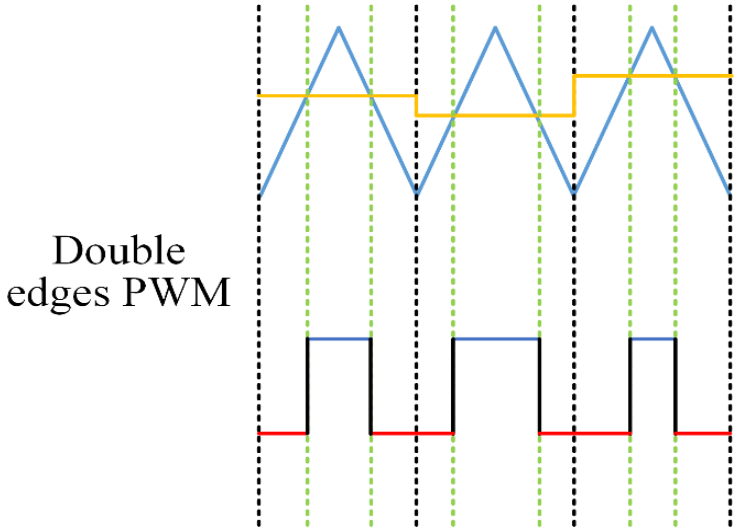

Figure 3.9 Leading triangle edge modulation

3.3.2 *Averaging current control*

Besides the voltage feedback scheme, many PWM control methods are derived from the current signal and it is more popular in recent research than the basic voltage feedback control. The technique of averaging current control is compared desired current level with averaged current level to calculate the duty ratio for next switching cycle [64]. In Fig. 3.10, the desired inductor

current value is calculated by measuring the voltage error. The voltage error feed into the comparator with the sampled inductor current to compute the desired duty ratio of minimising the current error between these two current signals. A saw-tooth carrier waveform compared with this duty ratio value and generate the PWM signal for next switching cycle. This technique uses current as a reference signal to control the SMPC system and often combine with voltage feedback control scheme to form a dual feedback control scheme in some application.

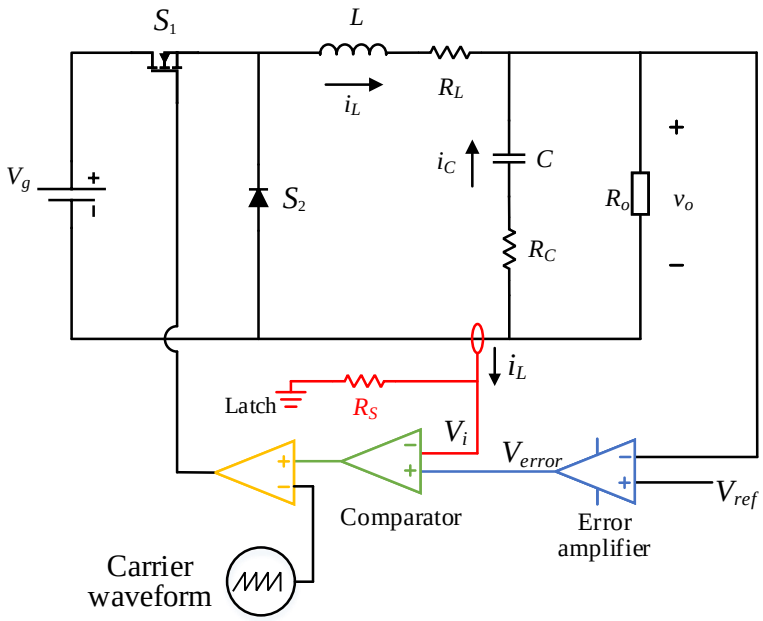

Figure 3.10 average current control

3.3.3 *Peak current control*

Peak current control is one of commonly used Constant-Frequency Peak-Ripple-Based (CF-PR) control method for SMPCs [79]. It samples the inductor current and output. At beginning of each switching cycle, the transistor is turned ON when a clock signal is received. The transistor keeps as ON until the sampled inductor current reach the desired maximum current level. This current level is calculated by the voltage error. One of the drawbacks of this technique is a slope compensation is required to overcome the instability caused by the sub-harmonic oscillation when the duty ratio is exceeding 0.5. As presented in Fig.3.14, the slope compensation results as a saw-tooth ramp signal feed into the V_{error} in Fig.3.13 to generally reduce the initially current error.

Some stability analysis has been done to generate a proper slope signal to maintain the stability of SMPCs [9, 112, 113]. Same control method as using ripple signal are V^2 control, enhanced- V^2 control [79].

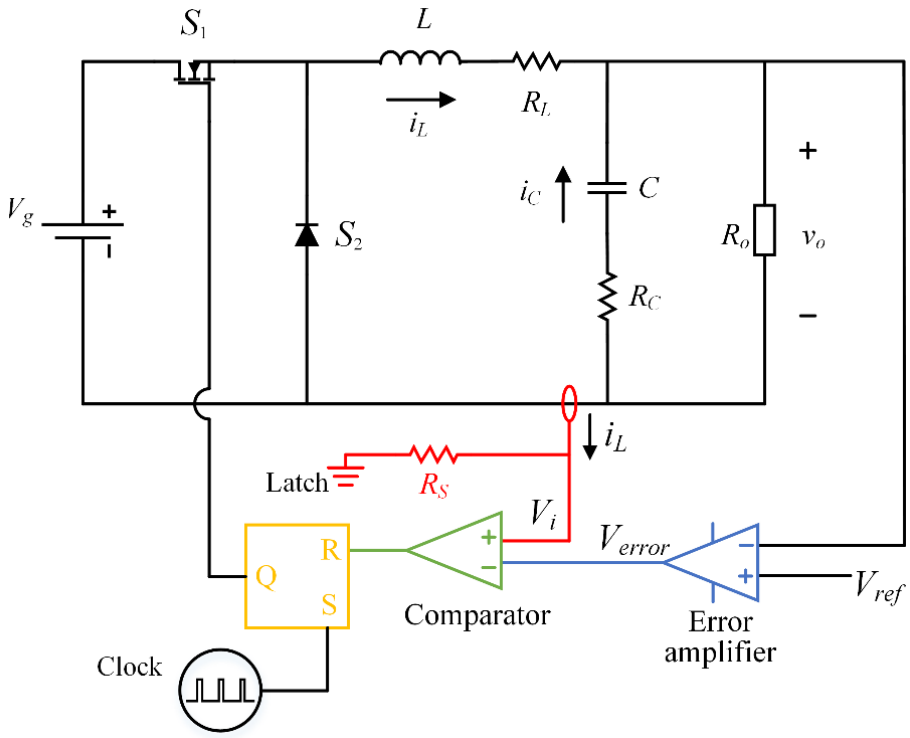

Figure 3.11 peak current control

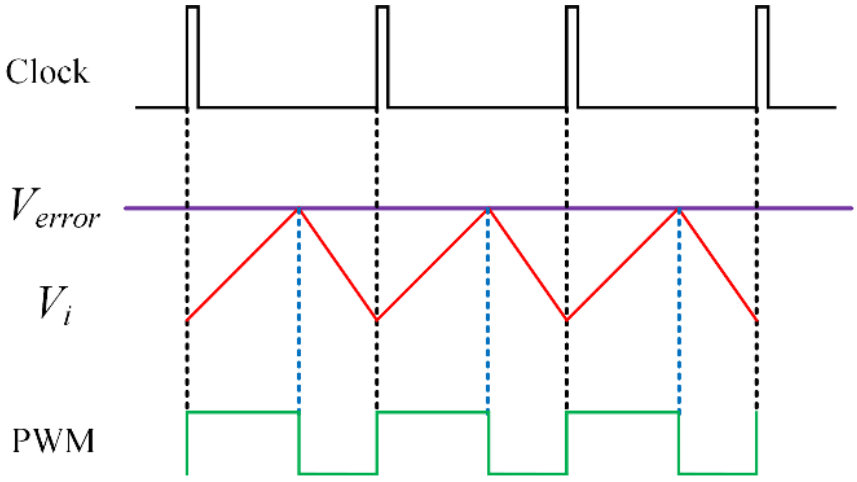

Figure 3.12 peak current control PWM generation

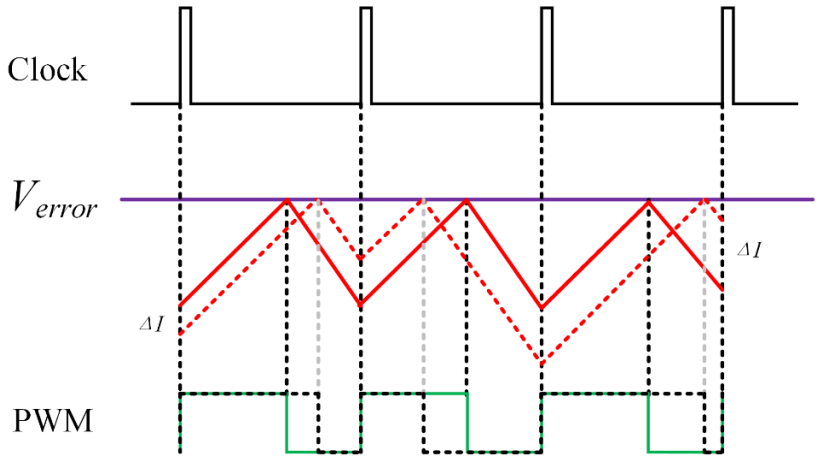

Figure 3.13 sub-harmonic caused instability when d>0.5

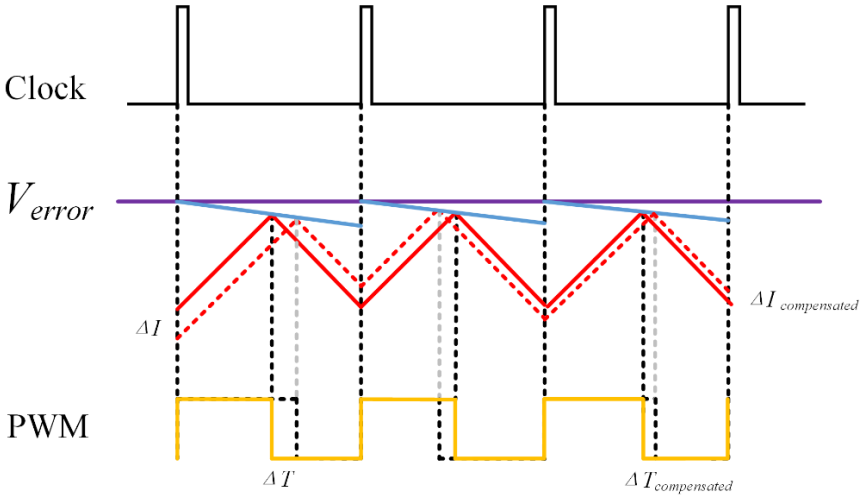

Figure 3.14 slope compensation for peak current control

3.4 Averaging state space model for DC-DC buck converter

The state space average model is one of the most commonly used modelling methods to linearize the SMPC system and obtain a Linear Time Invariant (LTI) system.

$$\begin{cases} \dot{X} = AX + BU \\ Y = CX + DU \end{cases} \tag{3.15}$$

If we consider i_L and v_C are two variables in this system, V_g is the input and v_o is the output, by substituted Eq.3.1-Eq.3.4, each parameter in Eq.3.14 can be presented as

$$\boldsymbol{A}_{on} = \boldsymbol{A}_{off} = \begin{bmatrix} \dfrac{-1}{(R_o + R_C)C} & \dfrac{R_o}{(R_o + R_C)C} \\ \dfrac{-R_o}{(R_o + R_C)L} & \dfrac{-(R_L + R_o \,||\, R_C)}{L} \end{bmatrix}$$

$$\boldsymbol{B}_{on} = \begin{bmatrix} 0 \\ \dfrac{1}{L} \end{bmatrix} \qquad \boldsymbol{B}_{off} = 0$$

$$\boldsymbol{C}_{on} = C_{off} = \begin{bmatrix} \dfrac{R_o}{R_o + R_C} & R_o \,||\, R_C \end{bmatrix} \tag{3.16}$$

$$\boldsymbol{D} = \boldsymbol{O}$$

$$\boldsymbol{x} = \begin{pmatrix} v_C \\ i_L \end{pmatrix}$$

Then by involving the duty ratio d into Eq.3.16, the averaged state space model of DC-DC buck converter can be obtained as

$$\begin{cases} \begin{pmatrix} \dot{v}_c \\ \dot{i}_L \end{pmatrix} = \begin{bmatrix} \dfrac{-1}{(R_o + R_C)C} & \dfrac{R_o}{(R_o + R_C)C} \\ \dfrac{-R_o}{(R_o + R_C)L} & \dfrac{-(R_L + R_o \,||\, R_C)}{L} \end{bmatrix} \begin{bmatrix} v_c \\ i_L \end{bmatrix} + d \begin{bmatrix} 0 \\ \dfrac{1}{L} \end{bmatrix} V_g \\ v_o = \begin{bmatrix} \dfrac{R_o}{R_o + R_C} & R_o \,||\, R_C \end{bmatrix} \begin{bmatrix} v_c \\ i_L \end{bmatrix} + \boldsymbol{o} \end{cases} \tag{3.17}$$

By applying

$$\boldsymbol{C}\left(s\boldsymbol{I} - \boldsymbol{A}\right)^{-1}\boldsymbol{B} + D \tag{3.18}$$

The voltage-to-voltage transfer function can be easily obtained.

$$G_{gv}(s)=\frac{v_{out}(s)}{V_g(s)}=\frac{D\left(CR_c s+1\right)}{s^2 LC\left(\frac{R_o+R_c}{R_o+R_L}\right)+s\left(R_c C+C\left(\frac{R_o R_L}{R_o+R_L}\right)+\frac{L}{R_o+R_L}\right)+1} \quad (3.19)$$

However, as mentioned before, the duty ratio is the controllable input signal for SMPCs. So, a control-to-output voltage transfer function is more important than a voltage to voltage transfer function, in system identification application. The duty ratio to output transfer function is derived from Laplace transform to the small signal average equivalent circuit [62],

A general form of control to output SMPCs transfer function is presented as

$$G_{dv}(s)=G_o\frac{1+\frac{s}{w_{zesr}}}{1+\frac{s}{Qw_o}+\left(\frac{s}{w_o}\right)^2} \quad (3.20)$$

Where, the w_o is the corner frequency of buck converter, Q is the quality factor, w_{zesr} is zero-frequency of responding of equivalent series resistance and the G_o is the DC gain. All those parameters can be obtained as:

$$\begin{aligned} w_o &= \sqrt{\frac{R_o+R_L}{LC\left(R_o+R_C\right)}} \\ Q &= \frac{1}{w_o\left(R_C C+\frac{L}{R_o+R_L}+\frac{R_o R_L C}{R_o+R_L}\right)} \\ G_o &= V_g=\frac{v_o}{D} \\ w_{zesr} &= \frac{1}{CR_C} \end{aligned} \quad (3.21)$$

It needs to be noticed that the DC gain G_o is varied if the R_L cannot be neglected as the derivation of duty ratio. In this case, if the inductor current is quite high, the transfer function is looks different. In that case the inductor current is involved as a parameter to adjust the duty ratio. However, in many applications, the R_L is much smaller compared with R_o . The voltage drop on inductor can be neglected. Therefore, the mathematical model of buck converter can be presented as a typical transfer function

$$G_{dv}(s)=\frac{v_{out}(s)}{d^{'}(s)}=\frac{V_g\left(CR_cs+1\right)}{s^2LC\left(\frac{R_o+R_c}{R_o+R_L}\right)+s\left(R_cC+C\left(\frac{R_oR_L}{R_o+R_L}\right)+\frac{L}{R_o+R_L}\right)+1} \quad (3.22)$$

The next step is converting the continuous transfer function to discrete transfer function. In digital control system, the above transfer function can be presented via z-form transfer function.

$$G_{z,dv}=\frac{b_1z^{-1}+b_2z^{-2}}{1+a_1z^{-1}+a_2z^{-2}} \quad (3.23)$$

This continuous to discrete conversion can be directly uses Matlab function "c2d" based on variety kinds of discretisation methods. Otherwise, it can be done by applying a small signal conversion method based on [61]. In [61], Dragan *et al*. has considered the sampling delay existed in digital controller, a short duration t_d is then involved in discrete transfer function as Eq.3.24.

$$G_{dv}(s)=\frac{v_{out}(s)}{d^{'}(s)}=\frac{\frac{V_gT_s}{LC}\left(T_s-t_d+CR_C\right)\left(z+\frac{T_s}{T_s-t_d+CR_C}\left(\frac{R_C}{R}-\frac{CR_C}{T_s}-\frac{\left(T_s-t_d\right)R_C}{L}+\frac{t_d}{T_s}\right)\right)}{z^2-z\left(2-\frac{T_s}{RC}\right)+\left(1-\frac{T_s}{RC}+\frac{T_s^2}{LC}\right)} \quad (3.24)$$

In Eq.3.24, T_s represents the sampling period of ADC. This value matters the number of sampling point and performance of parameter estimation. Details can be found in section 3.5. In this research the sampling period is chose as 20μs for the sake of number of sampling points and parameter accuracy. To simplify the discrete transfer function, the term R_L and R_C are neglected. The discrete transfer function of buck converter derived from Eq.3.22 can be presented as [61]

$$G_{z,dv}=\frac{V_gT_s^2\left(z^{-1}+\frac{1}{T_s}z^{-2}\right)}{1-\left(2-\frac{T_s}{R_oC}\right)z^{-1}+\left(1-\frac{T_s}{R_oC}+\frac{T_s^2}{LC}\right)z^{-2}} \quad (3.25)$$

The operator z^{-n} is represented as a unit delay of *n* step in discrete domain, the discrete transfer function can be converted to an Auto-Regressive with exogenous input (ARX) model as shows in Fig. 3.15.

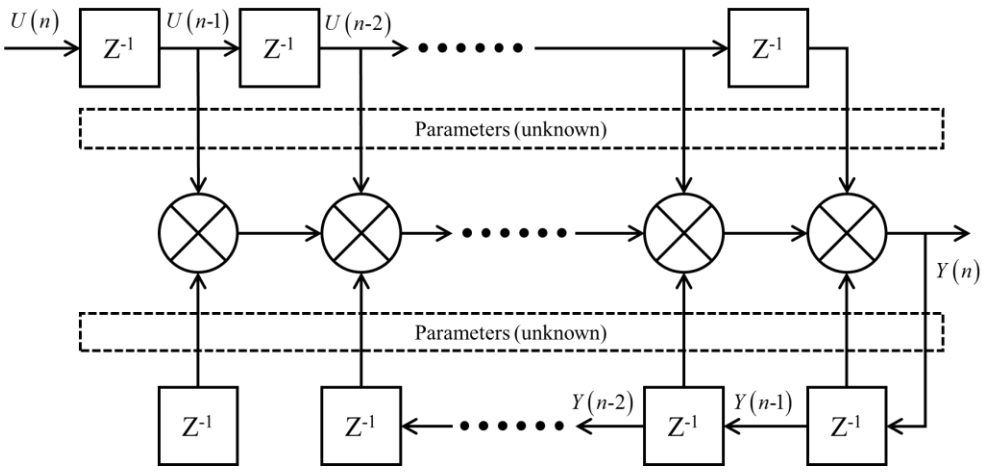

Figure 3.15 ARX model for system identification

The mathematical model for ARX model is shown as Eq.3.25

$$Y(n) = A_i \sum_{i=1}^{p} U(n-i) + B_j \sum_{j=1}^{q} Y(n-j) \tag{3.26}$$

In Eq. 3.25, the p and q stands for the regressive order, which is determined by the system order. The parameters A_i and B_i contains all the information of components coefficients in Eq. 3.21. The proposed system identification technique in this paper uses per sampled $Y(n)$ and $U(n)$ data to estimate the parameters of A_i and B_i iteratively, and then coefficients in Eq.3.22 can be obtained.

Specifically, in DC-DC buck converter system,

$$\frac{V(z)}{d(z)} = \frac{V_g T_s^2 \left(z^{-1} + \frac{1}{T_s} z^{-2} \right)}{1 - \left(2 - \frac{T_s}{R_o C} \right) z^{-1} + \left(1 - \frac{T_s}{R_o C} + \frac{T_s^2}{LC} \right) z^{-2}} \tag{3.27}$$

$$\Rightarrow V(n) - \left(2 - \frac{T_s}{R_o C} \right) V(n-1) + \left(1 - \frac{T_s}{R_o C} + \frac{T_s^2}{LC} \right) V(n-2) = V_g T_s d(n-2) + V_g T_s^2 d(n-1) \tag{3.28}$$

re-allocate Eq.3.28, we can obtain

$$V(n)=\left(2-\frac{T_s}{R_oC}\right)V(n-1)-\left(1-\frac{T_s}{R_oC}+\frac{T_s^2}{LC}\right)V(n-2)+V_gT_sd(n-2)+V_gT_s^2d(n-1) \quad (3.29)$$

The Eq. 3.29 will be used in next few chapters as a difference equation format for parameter estimation. The system input data is the duty ratio in each switching period, the output data is the sampled output voltage or inductor current. Due to the system is a second order system, the regressive order p and q are equal to 2, the Eq. 3.26 can be re-written as

$$Y(n)=A_1U(n-1)+A_2U(n-2)+B_1Y(n-1)+B_2Y(n-2) \quad (3.30)$$

Where $A_1=\left(2-\frac{T_s}{R_oC}\right)$, $A_2=-\left(1-\frac{T_s}{R_oC}+\frac{T_s^2}{LC}\right)$, $B_1=V_gT_s$ and $B_2=V_gT_s^2$, respectively. These 4 parameters are the parameter actually estimated in Chapter 4. In this case, the current step (*n*) output data is calculated by using the input and output sampled data of previous (*n*-1) step and (*n*-2) step.

3.5 Limitation of using transfer function/averaged state space model as mathematical model in system identification technique

In this section, the limitation of using averaged state space model or transfer function as the mathematical model for system identification is analysed. These limitations restrict a good adaptive controller design based on the parameter estimation result. However, the averaged state space model and transfer function are still good candidates for system identification when the system is working in a steady state condition. Here, a detailed analysis of strictly sampling point and limited number of sampling points is done based on Fig. 3.16 and Fig. 3.17 is presented.

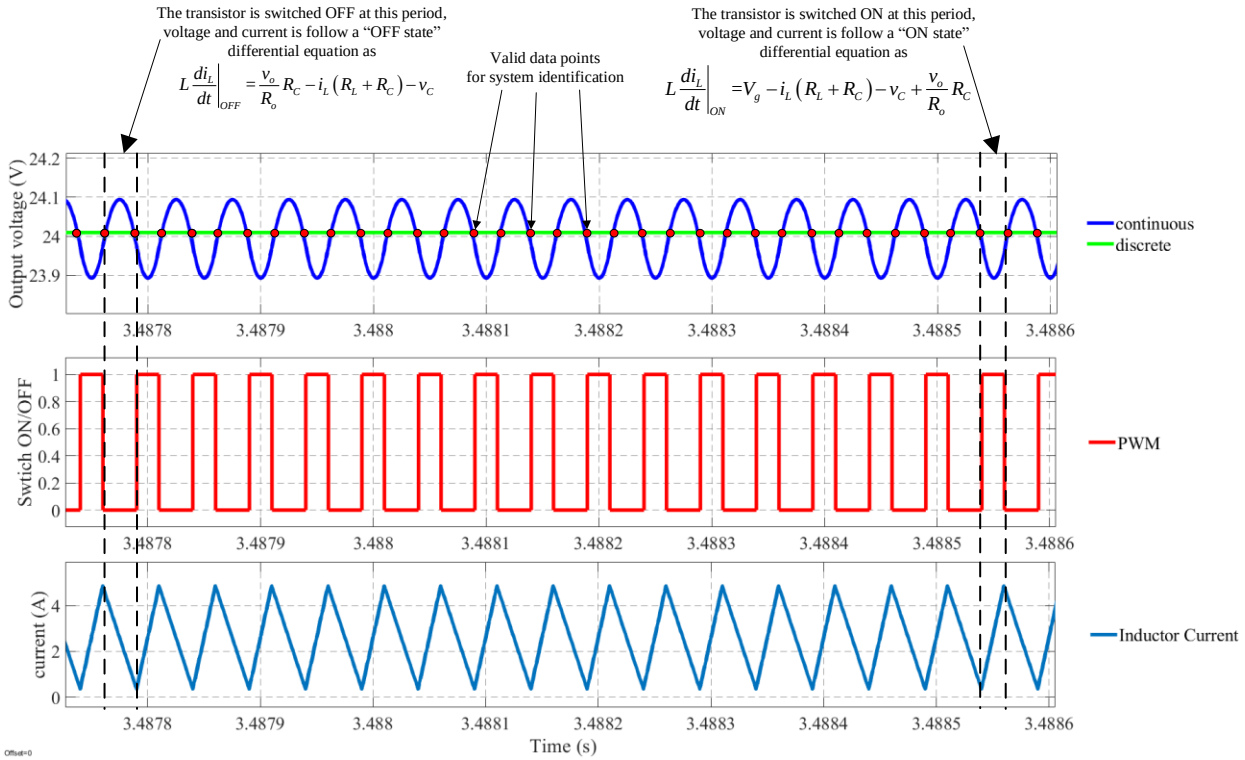

Figure 3.16 the sampling rule when using averaged state space model

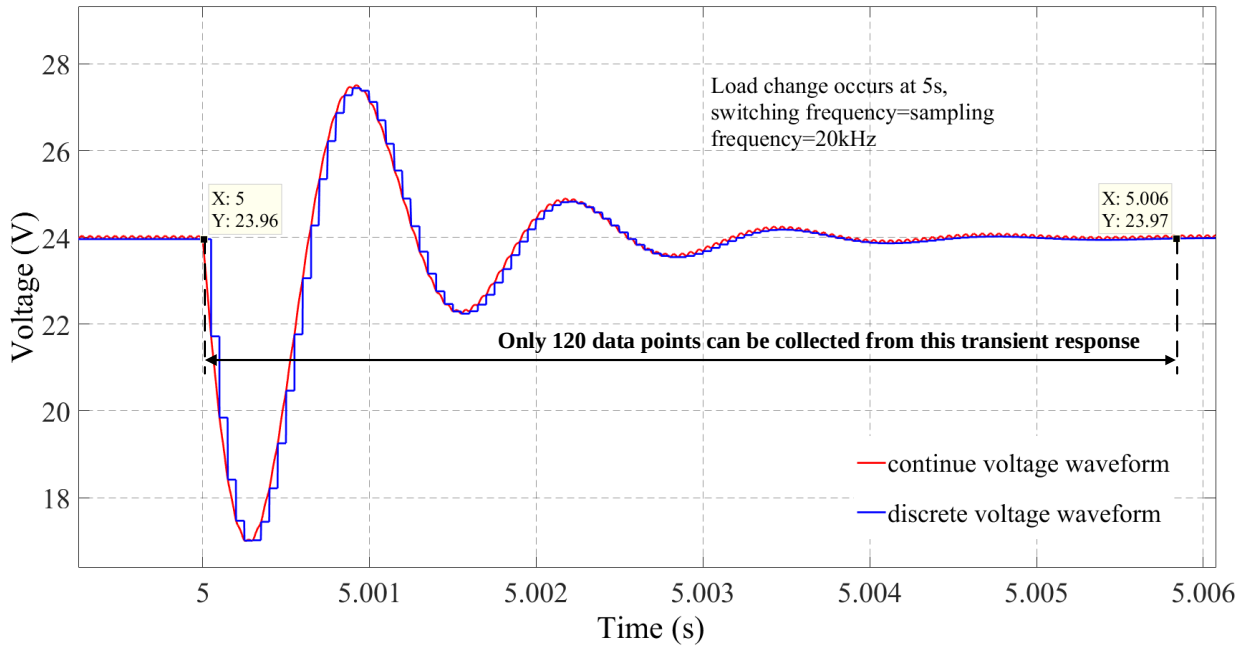

Figure 3.17 Limitation of sampling amount in dynamic response

3.5.1 *Limited sampling frequency and strict sampling point requirement*

From Eq. 3.1 to Eq. 3.5, it can be seen that DC-DC buck converter is a nonlinear system with two differential equation series to describe the dynamic behaviours when the transistor in a "ON" and "OFF" condition. To linearize this system, the averaged state space model combines two switching conditions together using the duty ratio in Eq. 3.16. Therefore, it cannot present the voltage dynamic behaviours in either ON state or OFF state as shown in Fig. 3.16. So, only data sampled at the switching instant—ON to OFF or OFF to ON can be utilised as the sampling data for parameter estimation. Based on that, the maximum sampling frequency can be set to twice of switching frequency. However, the switching action may occur at different moment in each switch period when the duty ratio is changing. In this case, the sampling action is difficult to follow the time-variant switching action. Also, the extreme duty ratio value and sampling delay may significantly affect the accuracy of the data. Therefore, the best way is to set the sampling frequency equal to the switching frequency. This strict sampling rule causes the first limitation of applying average state space model—number of sampling data is restrained by the switching frequency. Limited number of data points can be acquired if the switching frequency is low. This is especially can be found in the application of improving dynamic response (see Fig.3.17). When parameter variation occurs, the output voltage probably recovered fast due to the close loop effect and only few switching periods occurred in transient period. From Fig.3.17, only 120 data points can be collected during the transient period, but most adaptive algorithms need at least 200 data points to estimate the parameter [4]. As a conclusion, the averaged state space model is easy to be implemented as the mathematical model for system identification, but it is not always suitable for parameter estimation, especially in dynamic response. Sometimes, the varied parameter has not been estimated yet whereas the transient response has already passed.

Even the strictly sample point and limited number of sample point restricts the usage of averaged state space model. Some researches [2-5] have used it and no reports are given to pursue a better mathematical model. That is because the averaged state space model is commonly used as a mathematical model to describe the dynamic behaviour of SMPCs due to its simplicity and well accuracy on describing the dynamic behaviours of SMPCs. Also, the applications in [2-5] do not require pre-system identification step before the adaptive control is applied in a one-off load

change event. Since they always assume the load change is periodically and execute the adaptive control after identify the parameters from previous load change event.

3.5.2 *Inevitable delay on inaccuracy increment of transfer function*

In [61], a small-time variable t_d is defined to compensate the sampling delay affected to the system transfer function. This delay caused by the A/D sampling, the computational period in DSP and the period that duty ratio delivers to the actual PWM signal. In practical adaptive control process, a high accurate parameter estimation is a pre-process step for control part. If selecting an adaptive algorithm with complicated matrix multiplication and division, the algorithm consumes much time for the parameter estimation in the DSP process. This heavy computation probably significantly delays the duty ratio calculation step, which followed by the control rules. This computational time have to count in the switching frequency determination, which may heavily affect the operation of SMPCs. After the DAC step, the semiconductor driver has a delay when it received a rising/falling edge to generate PWM signal. Also, the semiconductor itself has a delay to switch ON and OFF. This time delay has been evaluated on the effect towards transfer function. However, it is difficult to measure this time delay in practice, only we can do is finding a low computational cost adaptive algorithm for system identification purpose.

It has been concluded two prior drawbacks using averaged state space model and its derivation consequence—transfer function as the mathematical model for system identification and adaptive control. Whereas, as the commonly used mathematical model to describe the system response and it has been widely used in many applications both industry and academia, it is necessary to achieve the parameter estimation in transfer function as it is a fundamental part of system identification. Also, many researches have already proved that transfer function can be utilised as the system mathematical model in fault detection and conditional monitoring applications.

3.6 Typical PID controller for SMPC system

In digital control system, the Proportional-Integral-Derivative (PID) controller is easy to be implemented in many close feedback loop control. Many studies have been done to help tuning the gains of PID controller in close loop feedback systems [115-121]. In this section, a typical pole-zero cancellation method for determination of the gains of PID controller is presented. The

simulation results for close loop control a typical DC-DC buck converter is shown in this section as a reference control scheme comparing with the proposed adaptive control scheme in chapter 5.

In digital control system, the PID controller can be written as a discrete form as:

$$G_c(z) = \frac{D(z)}{E(z)} = K_P + K_I \frac{1}{1-z^{-1}} + K_D\left(1-z^{-1}\right) \tag{3.31}$$

If we write it as a difference equation form, it can be presented as

$$d(n) = K_P e(n) + K_I e(n) + K_I \sum_{1}^{n-1} e(i) + K_D\left[e(n) - e(n-1)\right] \tag{3.32}$$

Where $e(n) = V_{ref}(n) - v_o(n)$, is the error between reference voltage and measured voltage in current step. The $d(n)$ is the duty ratio of current step.

Since the PID controller mathematically add poles and zeros to the close loop system, the performance such as loop bandwidth, phase margin and close loop gain are much determined by the parameter of PID controller. So, it need much attention to tuning the parameter when designing the controller for SMPC system. There are three parts of PID controller, if we consider the PID controller as a feedback controller in continuous domain, this controller can be presented as a transfer function as

$$G_{PID}(s) = K_P + K_I \frac{1}{s} + K_D s \tag{3.33}$$

The three parts of PID controller has different effect to the dynamic response of the open loop system. The proportional gain gives a proportion gain of the error between reference value and measured value. It can speed up the close loop effect but also can result the instability of the system since it is a gain in the denominator part. The integral part sum instantaneous error over time and gives the accumulated offset that should have been corrected previously. This part is the key function to eliminate the steady state error of the feedback loop. The derivative part calculates the slop rate of the error and multiply the derivative gain. Derivative action predicts system behaviour and thus improves settling time and stability of the system. However, the parameter may impact the stability in some applications.

There are many parameterisation methods have been developed for PID controller, such as Ziegler–Nichols method [122], Tyreus Luyben method [123] etc. In this research, a pole-zero cancellation method is applied for determination of the gains of PID controller.

3.6.1 *Pole & Zero cancellation method*

In this research, a voltage close loop feedback control scheme is applied. Therefore, the system can be presented as

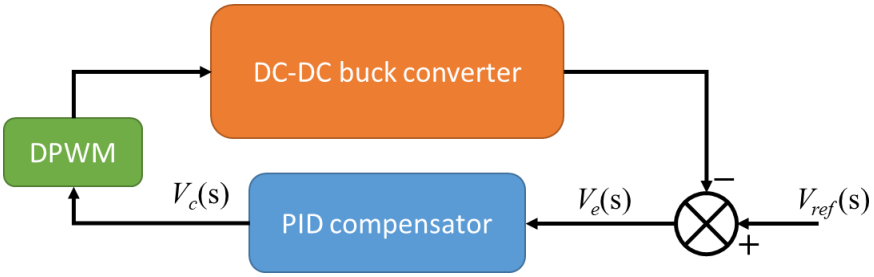

Figure 3.18 schematic diagram of voltage feedback loop control

If we name the transfer function of DC-DC buck converter is $G(s)$ and the transfer function of PID compensator is $G_c(s)$, the overall transfer function of close loop system shown in Fig.3.18 can be presented as

$$G_{CL}(s)=\frac{V_{ref}}{V_{out}}=\frac{G(s)G_c(s)}{1+G(s)G_c(s)} \tag{3.34}$$

In Eq.3.34, the PID controller $G_c(s)$ is also can be presented as a continuous transfer function form.

This ideal controller can be obtained from open loop transfer function *G*(s) and close loop transfer function G_{cl}(s)

$$G_{c,ideal}(s)=\frac{G_{cl}(s)}{1-G_{cl}(s)}\frac{1}{G(s)} \tag{3.35}$$

and the discrete form

$$G_{c,ideal}(z)=\frac{G_{cl}(z)}{1-G_{cl}(z)}\frac{1}{G(z)} \tag{3.36}$$

If all terms of PID controller are considered (proportion, integral and derivative), the continuous template of PID compensator can be presented as the same as Eq. 3.33

$$G_c(s)=\frac{V_c(s)}{V_e(s)}=K_p+K_i\frac{1}{s}+K_d s \tag{3.37}$$

And it can be reformed as

$$G_c(s)=\frac{V_c(s)}{V_e(s)}=\frac{K_p s+K_i+K_d s^2}{s}=\frac{\left(s^2/\omega_c^2\right)+\left(s/\omega_c Q_c\right)+1}{s} \tag{3.38}$$

Where the $V_c(s)$ is the voltage error signal after the controller and $V_e(s)$ is the voltage error before the controller. On the other side, the buck converter can be presented as (same as Eq. 3.20)

$$G_{dv}(s)=G_o\frac{1+\dfrac{s}{\omega_{zesr}}}{1+\dfrac{s}{Q\omega_o}+\left(\dfrac{s}{\omega_o}\right)^2} \tag{3.39}$$

Where Q is the quality factor and ω_o is the resonant frequency of converter, both are determined by the passive components of the converter system as shown in Eq. 3.40.

$$\begin{aligned}
\omega_o &= \sqrt{\frac{R_o+R_L}{LC\left(R_o+R_C\right)}} \\
Q &= \frac{1}{\omega_o\left(R_C C+\dfrac{L}{R_o+R_L}+\dfrac{R_o R_L C}{R_o+R_L}\right)} \\
G_o &= V_g=\frac{v_o}{D} \\
\omega_{zesr} &= \frac{1}{CR_C}
\end{aligned} \tag{3.40}$$

The controller should be designed to compensate the open loop system to meet the specific transient requirement.

From the control theory, the system transient response is determined by the characteristic equation of the transfer function, which is the denominator of the transfer function. Usually, ξ (damping ratio) and ω_n (angular resonant frequency) are used to quantify the dynamic response. Therefore, in this research, the system transient response is determined by the characteristic equation from the denominator part of Eq.3.34. The characteristic equation can be defined as

$$CE(s) = \frac{s^2}{\omega_n^2} + \frac{s}{\omega_n Q} + 1 \tag{3.41}$$

The ω_n is the parameter determining the rising time t_r and Q determines the overshot M_p [115]

$$t_r \approx \frac{1.8}{\omega_n} \tag{3.42}$$

$$M_p = e^{-(\pi/2Q)/\sqrt{1-4Q^2}} \tag{3.43}$$

Thus, the required ω_n and Q can be defined as

$$\omega_n \approx \frac{1.8}{t_r} \tag{3.44}$$

$$Q = -\frac{\sqrt{1+\left(\ln\left(M_p\right)/\pi\right)^2}}{2\left(\ln\left(M_p\right)/\pi\right)} \tag{3.45}$$

Therefore, the controller parameter can be deduced from the specific transient requirement by substitute them to Eq. 3.44 and Eq.3.45 and then obtained from Eq.3.34.

3.6.2 *Example of PID Controller design based on Pole & Zero cancellation method*

Here, an example of determination of PID controller parameter is illustrated in this section. A DC-DC buck converter has the parameters: $V_g = 60$ V , $V_o = 24$ V , $C = 940\ \mu$F , $L = 860\ \mu$H , $R = 9.2\ \Omega$, $f_{sample} = f_{switch} = 50$ kHz , $R_L = 0.475\ \Omega$, $R_C = 0.05\ \Omega$. The MOSFET ON state Drain to Source resistance is 0.01Ω . The transfer function of this buck converter can be deduced based on Eq.3.39 and Eq.3.40, and it is:

$$G(s) = \frac{0.00282s + 60}{8.128\times10^{-7}s^2 + 0.0001405s + 1} \tag{3.46}$$

And it can be written as a discrete form:

$$G(z) = \frac{0.08505z^{-1} - 0.05557z^{-2}}{1 - 1.996z^{-1} + 0.9965z^{-2}} \tag{3.47}$$

If a close-loop performance requirement is

$$t_r \le 100\mu s \quad \text{and} \quad M_p \le 10\% \tag{3.48}$$

Substitute Eq.3.48 to Eq.3.42 and Eq.3.43, we obtain

$$\omega_n \geq 18000, \quad Q \leq 0.8458 \tag{3.49}$$

Bring the result from Eq.3.49 to Eq.3.41, then characteristic equation of close loop transfer function can be obtained as

$$CE(s) = 3.0864\times10^{-9}s^2 + 6.7593\times10^{-5}s + 1 \tag{3.50}$$

It can be written as a discrete form by applying "Zero-pole matching method":

$$CE(z) = 9.924z^2 - 14.93z + 6.002 \tag{3.51}$$

the close loop transfer function then can be obtained as

$$G_{cl}(z) = \frac{n_0 z^2 + n_1 z + n_2}{9.924z^2 - 14.93z + 6.002} \tag{3.52}$$

By applying "Truxal-rules"[116], which is

$$G_{cl}(z)_{|z=\infty} = 0, \quad G_{cl}(z)_{|z=1} = 1 \quad \text{and} \quad \frac{dG_{cl}(z)}{dz}_{|z=1} = \frac{1}{K_v} \tag{3.53}$$

Where K_v is the constant error of the ramp signal. n_2 n_1 and n_0 can be obtained by applying this constraint,

$$n_2 = 0; \quad n_1 = \text{-}6.002 \qquad n_2 = 6.998; \tag{3.54}$$

This resulting the close loop transfer function is

$$G_{cl}(z) = \frac{0.1044z + 0.6534}{z^2 - 1.549z + 0.6534} \tag{3.55}$$

From Eq.3.57, Eq.3.47 and substitute into Eq.3.36, the transfer function of ideal controller can be obtained as

$$G_{c,ideal}(z) = \frac{0.1044z^5 + 0.2844z^4 - 1.1817z^3 + 2.785z^2 - 1.778z + 0.4207}{0.0836z^5 - 0.3219z^4 + 0.04423z^3 - 0.2645z^2 + 0.05855z} \tag{3.56}$$

The step response of close loop system with ideal compensator is presented in Fig.3.19.

So far, this is the typical pole-zero cancellation method to determine the transfer function of the controller. Apparently, conventional PID controller cannot form the transfer function of Eq.3.58. A method to approximate the result from the optimal result is proposed in [115] to determine the parameters of PID controller to partially satisfy the dynamic requirement.

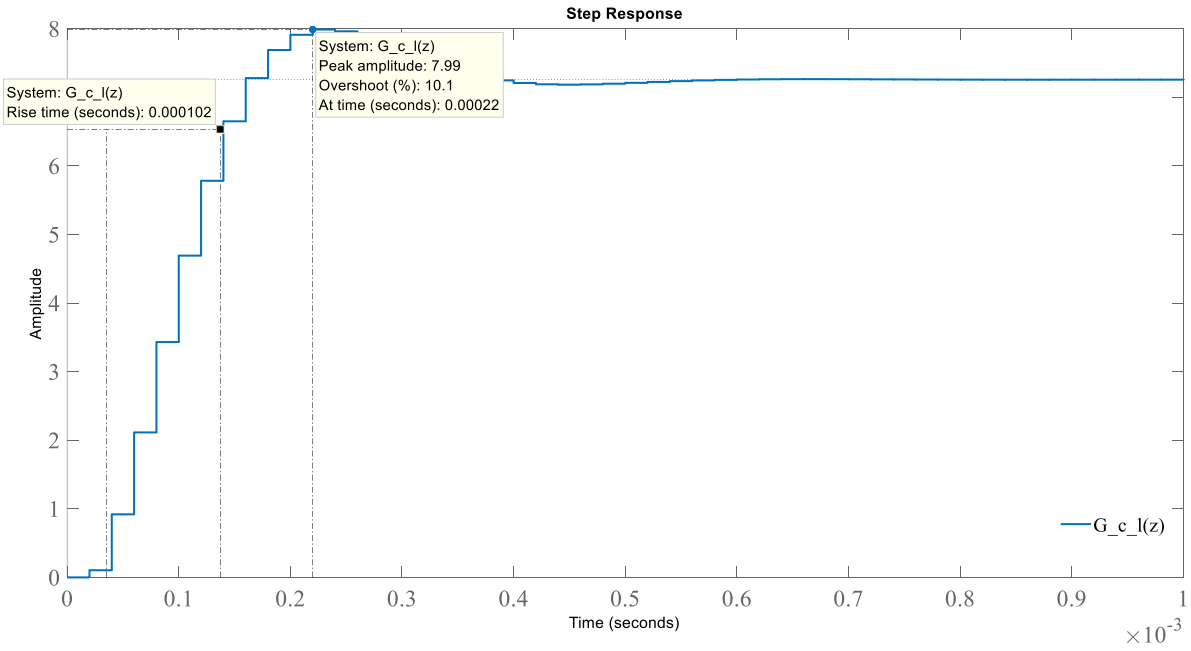

Figure 3.19 step response of close loop system with idea compensator

The input and output relationship of PID controller in Eq.3.31 can be rewritten as

$$\frac{V_c(s)}{V_e(s)} = \frac{as^2 + bs + c}{s} \tag{3.57}$$

Where $a = K_P + K_I + K_D$, $b = -(K_P - 2K_D)$ and $c = K_D$. This PID controller is a close loop compensator in Fig.3.18. This compensator can be written as a transfer function way as [120]

$$G_{comp}(s) = K_{comp} \frac{1 + \frac{s}{Q_{comp}\omega_z} + \left(\frac{s}{\omega_z}\right)^2}{s} \tag{3.58}$$

The ω_z is approximated to be at the same value of power converter corner frequency. As a result, the compensator zeros are assigned close to the converter poles; this will ensure system robustness. With this approximation, the compensator zeros cancel the poles of power converters, as a result the overall loop gain $\left[G_c(s)G(s)\right]$ is reduced as simple transfer function. In this specific application, if the R_C can be neglected, the continues transfer function of power converter can be derived from Eq.3.39 and Eq.3.40 as

$$G(s) = \frac{60}{8.084\times10^{-7}s^2 + 9.348\times10^{-5}s + 1} \tag{3.59}$$

The overall loop gain can be acquired as

$$L(s) = \frac{60K_{comp}}{s} \tag{3.60}$$

The K_{comp} is determined by satisfying design requirements such as phase margin and gain margin. The root-locus method can be used to calculate K_{comp}. From [121, 122], the K_{comp} can be determined directly based on the desired loop bandwidth. In practice, the bandwidth chosen will be $f_b = f_s/10$ [121, 122]. Where $f_s = 1/\omega_z$ and K_{comp} is calculated as

$$K_{comp} = \frac{2\pi f_b}{60} \tag{3.61}$$

Based on the pole-zero cancellation method the transfer function of PID controller can be

$$G_{PID}(s) = \frac{116.5 \cdot \left(8.084 \times 10^{-7} s^2 + 9.348 \times 10^{-5} s + 1\right)}{s} \tag{3.62}$$

From Eq. 3.57 and $a = K_P + K_I + K_D$, $b = -\left(K_P - 2K_D\right)$, $c = K_D$, the K_P, K_I and K_D can be acquired as 233, -349.5, 233 respectively.

The comparison of PID compensator and ideal compensator is shown in Fig.3.20.

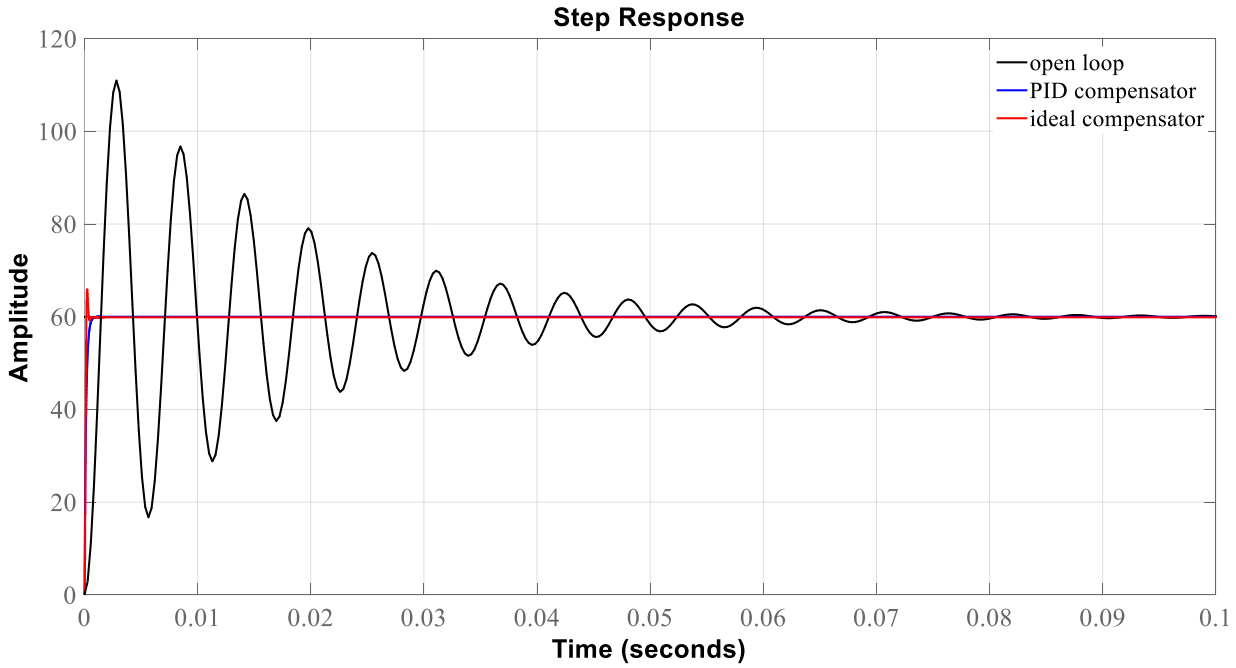

Figure 3.20 step response comparisons between PID controller, open loop system and ideal compensator

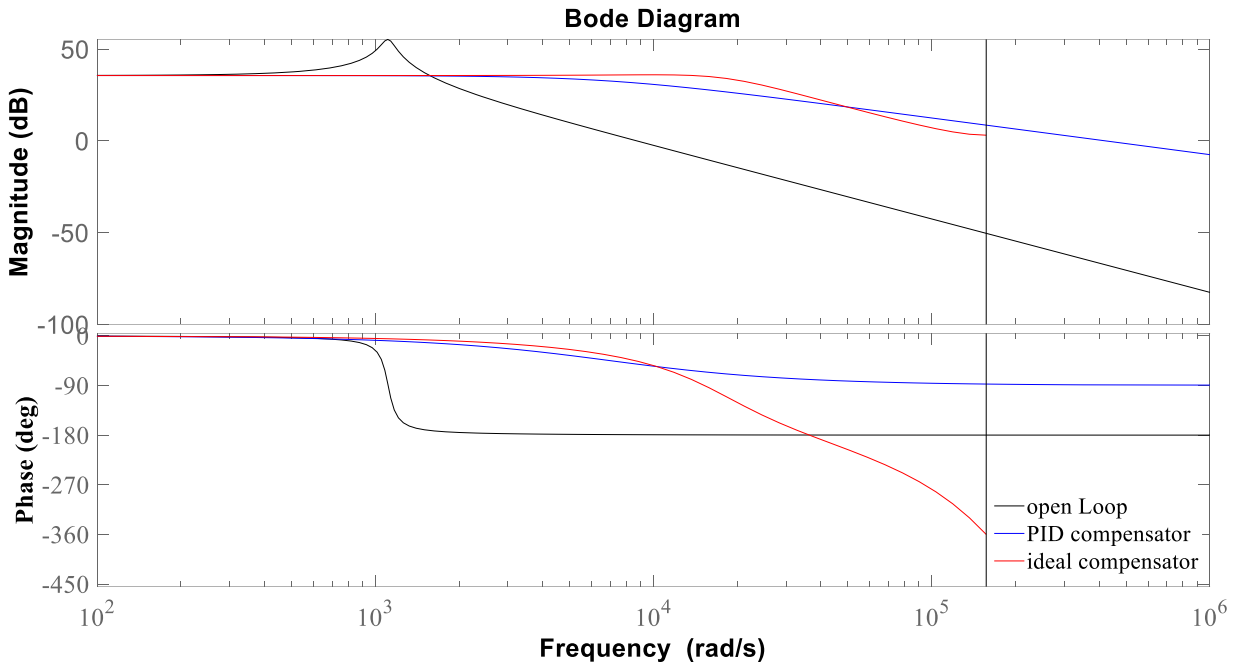

Figure 3.21 frequency response comparisons between PID controller, open loop system and ideal compensator

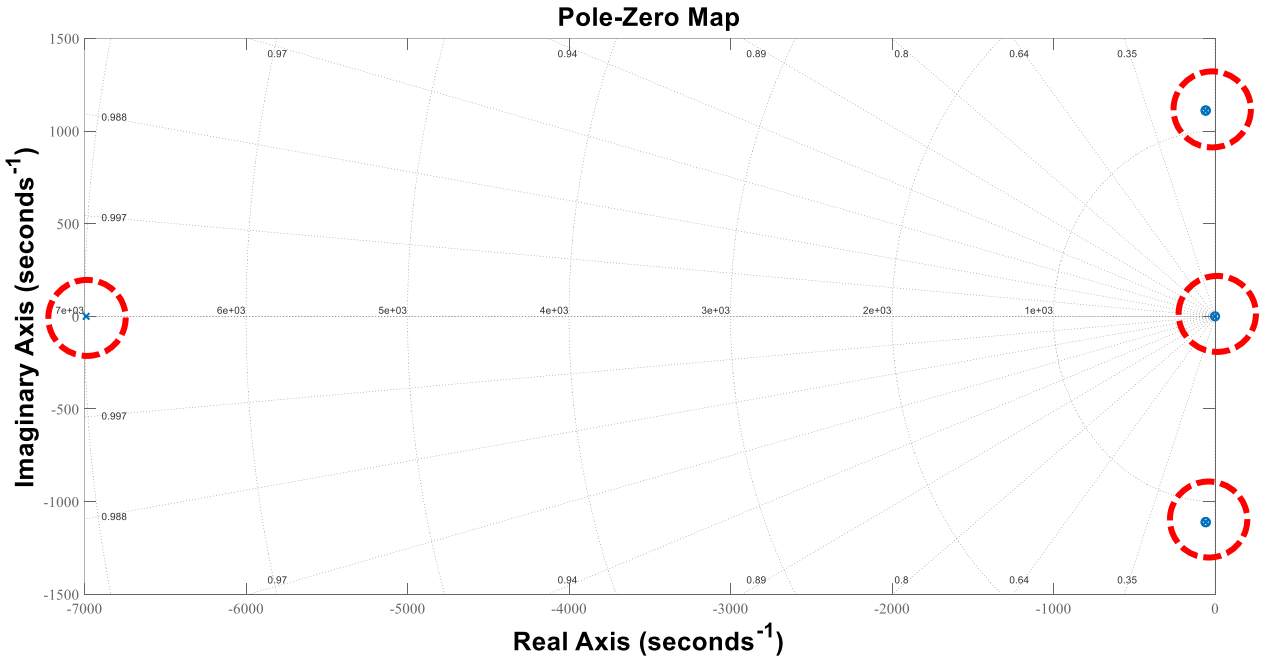

Figure 3.22 poles and zeros placement of close loop system with PID controller

Here, the procedure of designing the PID controller for voltage feedback loop is introduced. The parameters of section 3.62 are extracted based on the real buck converter system that developed

for this research. Therefore, the parameters of PID controller deduced from here are directly used in chapter 5 and chapter 6.

3.7 Chapter summary

This chapter presented a detailed analysis of modelling DC-DC buck converter in continuous and discrete time domain. This mathematical model is derived from basic differential equation series when the transistor in switching ON condition and OFF condition. Several commonly used feedback control schemes are introduced here as a reference for further system identification application. As the switching action are existing during the DC-DC converter operation. A linearization process is needed for parametric system identification. In this case, the system is linearized by applying averaging state space model. This model can used to derive a voltage to voltage transfer function. A control to output transfer function is derived based on a small signal model. With the sampling action during the system operation, a discrete transfer function and subsequent difference equation for ARX model are introduced. This difference equation is an overview structure for system identification of DC-DC buck converter. Finally, the limitation of using this mathematical model in system identification application is analysed.

After determining the mathematical model of SMPCs, the next step is finding an effective adaptive algorithm. This adaptive algorithm must have a fast convergence speed, a low computational cost and a descent noise immunity capability.

Chapter 4. Comparative study of adaptive algorithm in system identification technique for DC-DC buck converter system

4.1 Introduction

Adaptive algorithms have been applied in many fields including digital signal processing, echo-cancellation and adaptive filtering. Accurate performance is a basic requirement which must be guaranteed. Additionally, many researchers have focused on improving the computational efficiency and convergence speed of the algorithm. For the purposes of system identification in SMPCs, low computational cost and fast convergence speed are two crucial criteria when developing an adaptive control scheme. One of the most popular and well-recognised adaptive algorithms, Recursive Least Squares (RLS), has been applied in many fields due to its convergence speed and good noise immunity. It has also been applied for the purposes of system identification of SMPCs [2][4][67]. However, it imposes a relatively heavy computational burden on the microprocessor, which can restrict its use in low cost SMPC applications. For this reason, several researchers have considered variants of the RLS to meet the requirement of low computational cost. Unfortunately, achieving this often comes at the expense of parameter estimation convergence speed. Likewise, a review of the literature show that most research focuses on improving a single key metric. It is uncommon to observe a method that can improve both convergence speed and computational cost simultaneously.

For this reason, this chapter introduce a novel approach, based on the Fast Affine Projection (FAP) algorithm, and is applied for on-line system identification of an SMPC.

Firstly, to benchmark the proposed FAP algorithm, a detailed mathematical derivation of the classic RLS is presented. This is followed by a similar derivation for the proposed FAP algorithm. Secondly, the computational cost for both RLS and FAP algorithms is analysed. Using a data

regression model for the SMPC, the proposed FAP algorithm is proven to have a significantly lower computational cost than the classic RLS. Thirdly, the convergence speed is evaluated for both RLS and FAP algorithms. Again, the result proves that the proposed FAP algorithm has superior dynamic performance compared to the RLS. Finally, simulation verification of system identification for DC-DC buck converter is presented.

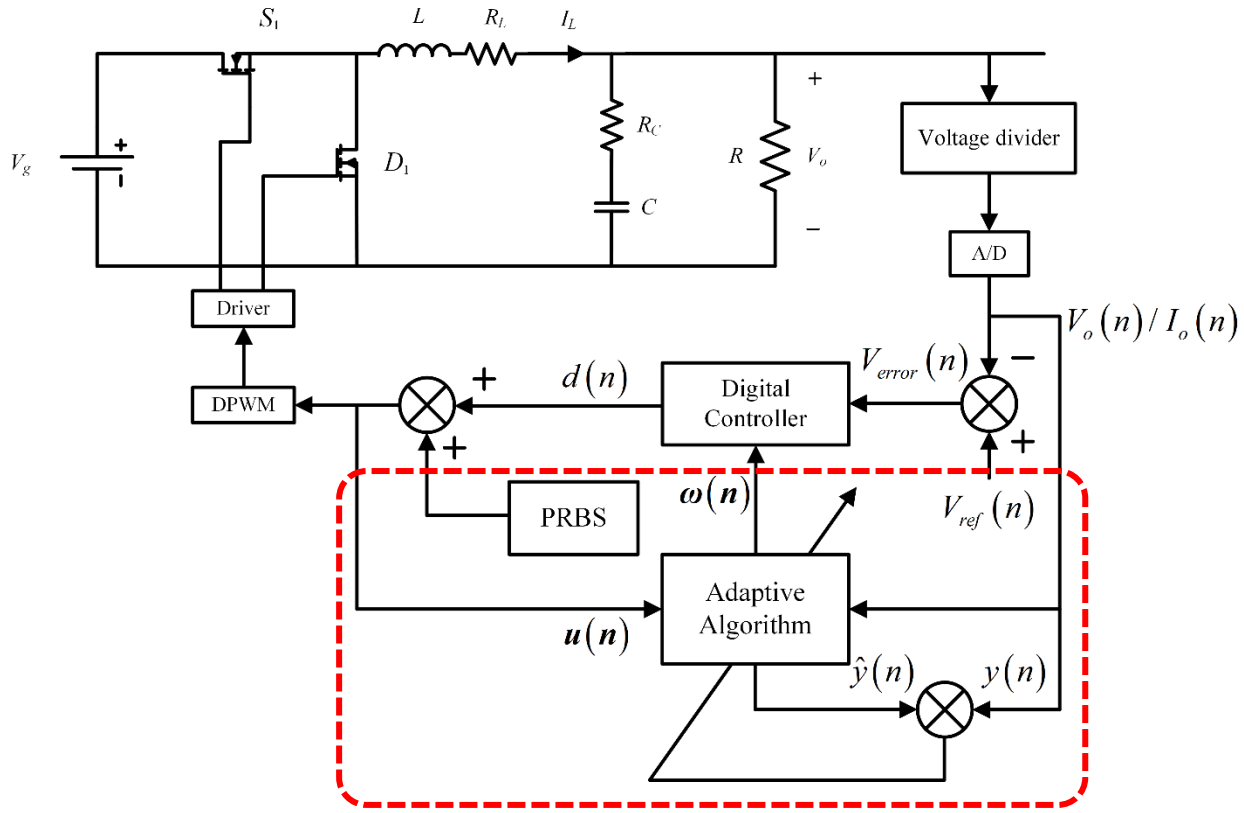

Figure 4.1 system identification and adaptive control of DC-DC buck converter—system identification part

4.2 Adaptive algorithm procedures for system identification of SMPC system

Although many adaptive algorithms are developed based on the concept of stochastic gradient descent algorithms, most adaptive algorithms for system identification can be summarised as by the generic flow chart in Fig. 4.2. As shown, all parameters and key metrics in the adaptive algorithms are initialised. Then, once the system identification signal is active, the sampled input and output data is applied to form a regression matrix and the parameter update calculation is commenced. The estimated output of the current iteration is then calculated using the previously

calculated parameter matrix and current regression matrix. Following this, the error between the estimated output and the sampled output is calculated. Finally, this error is substituted into an algorithm specific regressive formula to update the parameter matrix for the current iteration. Given many adaptive algorithms have been developed on the concept of a stochastic gradient descent algorithm, a detailed derivation of the RLS and FAP based on the stochastic gradient descent algorithm is presented in the next section.

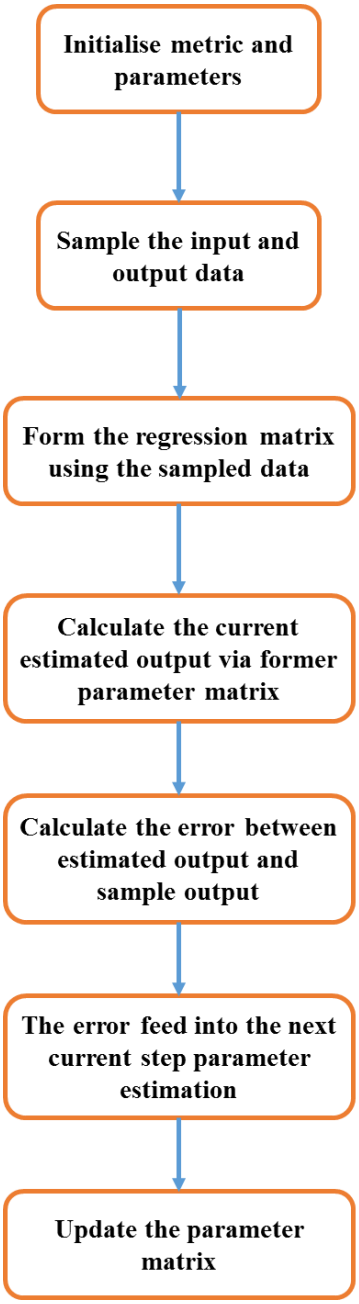

Figure 4.2 flow diagram of adaptive algorithm operation

4.3 Introduction of stochastic gradient descent algorithm

As previously mentioned, many adaptive algorithms are developed from the stochastic gradient descent algorithm. This type of algorithm may be used to solve a time-invariant parameter system. Consider a system that can be presented as:

$$d(i) = \boldsymbol{\omega}_i \boldsymbol{A}_i + \boldsymbol{\nu}_i \tag{4.1}$$

Where $d(i)$ is the discrete output data from the system, $\boldsymbol{\omega}_i$ is the parameter matrix, $\boldsymbol{A}_i$ is the discrete input data and $\boldsymbol{\nu}_i$ is a stochastic noise sequence matrix. The main aim of the adaptive algorithm is to minimise the following cost function:

$$J_{\min}(n) = \sum_{i=1}^{n} e_p^2(i) = \sum_{i=1}^{n} \left[d(i) - \hat{\boldsymbol{\omega}}_i \boldsymbol{A}_i \right]^2 \tag{4.2}$$

To minimise this cost function, a recursion formula is derived. In this thesis, both the RLS algorithm and proposed Fast Affine Projection algorithm are considered for this purpose by approximating the cross-correlation of this stochastic-gradient recursion:

$$\boldsymbol{\omega}_i = \boldsymbol{\omega}_{i\text{-}1} + \boldsymbol{\mu}\left[\boldsymbol{R}_{du} - \boldsymbol{R}_u \boldsymbol{\omega}_{i\text{-}1} \right] \tag{4.3}$$

In Eq. 4.3, $\boldsymbol{\omega}_i$ is the parameter matrix, i is the iteration number, $\boldsymbol{\mu}$ is the step size, and $\{\boldsymbol{R}_{du}, \boldsymbol{R}_u\}$ is the regression matrix which is determined by the input and output data. This expression, can also be written as a regularized Newton's recursion [65]

$$\boldsymbol{\omega}_i = \boldsymbol{\omega}_{i-1} + \boldsymbol{\mu}\left[\boldsymbol{\varepsilon}' \boldsymbol{I} + \boldsymbol{R}_u \right]^{-1} \left[\boldsymbol{R}_{du} - \boldsymbol{R}_u \boldsymbol{\omega}_{i-1} \right] \tag{4.4}$$

The algorithm uses the priori parameter value of $\boldsymbol{\omega}_{i-1}$, determined from the previous iteration and current data $\{\boldsymbol{R}_{du}, \boldsymbol{R}_u\}$ to calculate the parameter matrix $\boldsymbol{\omega}_i$ for the present iteration. All the adaptive algorithms are developed by approximating the regression matrix $\{\boldsymbol{R}_{du}, \boldsymbol{R}_u\}$ to meet the specific target requirements [65].

4.4 Recursive Least Squares and Fast Affine Projection algorithm

This section presents the derivation of the RLS and FAP from the basic regularized Newton's recursion by applying different stochastic gradient approximation for the regression matrix $\{\boldsymbol{R}_{du}, \boldsymbol{R}_{u}\}$. From the derivation of both algorithms, it is possible to compare the mathematical complexity of both algorithms and evaluate their appropriateness for low cost SMPC applications.

4.4.1 *Recursive Least Squares algorithm*

The RLS algorithm sums the input data from all previous steps and uses a factor λ to evaluate the weight, or current importance, of each previous step. It approximates $\boldsymbol{R}_u$ as

$$\hat{\boldsymbol{R}}_u = \frac{1}{i+1}\sum_{j=0}^{i}\lambda^{i-j}\boldsymbol{u}_j^*\boldsymbol{u}_j \tag{4.5}$$

and $\left(\boldsymbol{R}_{du} - \boldsymbol{R}_u\boldsymbol{\omega}_{i-1}\right)$ replaced by the instantaneous approximation

$$\left(\boldsymbol{R}_{du} - \hat{\boldsymbol{R}}_u\boldsymbol{\omega}_{i-1}\right) = \boldsymbol{u}_i^*\left[d(i) - \boldsymbol{u}_i\boldsymbol{\omega}_{i-1}\right] \tag{4.6}$$

In Eq.4.5 and Eq.4.6, $\boldsymbol{u}_i$ is the regression matrix which contains input sampling data in step i. $d(i)$ is the output data in step i.

The step-size μ and regularisation factor ε are defined as

$$\mu(i) = 1/(i+1) \tag{4.7}$$

$$\varepsilon(i) = \lambda^{i+1}\varepsilon/(i+1) \tag{4.8}$$

From this, the regularized Newton's recursion (Eq.4.4) becomes

$$\boldsymbol{\omega}_i = \boldsymbol{\omega}_{i-1} + \left[\lambda^{i+1}\varepsilon\boldsymbol{I} + \sum_{j=0}^{i}\lambda^{i-j}\boldsymbol{u}_j^*\boldsymbol{u}_j\right]^{-1}\boldsymbol{u}_i^*\left[d(i) - \boldsymbol{u}_i\boldsymbol{\omega}_{i-1}\right] \tag{4.9}$$

We define

$$\boldsymbol{\Phi}_i \triangleq \left[\lambda^{i+1}\varepsilon \boldsymbol{I} + \sum_{j=0}^{i} \lambda^{i-j} \boldsymbol{u}_j^* \boldsymbol{u}_j \right] \tag{4.10}$$

Where $\boldsymbol{\Phi}_i$ satisfies the recursion

$$\boldsymbol{\Phi}_i = \lambda \boldsymbol{\Phi}_{i-1} + \boldsymbol{u}_i^* \boldsymbol{u}_i \tag{4.11}$$

Now, let $\boldsymbol{P}_i = \boldsymbol{\Phi}_i^{-1}$, and then apply the matrix inversion formula. P_i can then be written in recursive form:

$$\boldsymbol{P}_i = \lambda^{-1} \left[\boldsymbol{P}_{i-1} - \frac{\lambda^{-1} \boldsymbol{P}_{i-1} \boldsymbol{u}_i^* \boldsymbol{u}_i \boldsymbol{P}_{i-1}}{1 + \lambda^{-1} \boldsymbol{u}_i \boldsymbol{P}_{i-1} \boldsymbol{u}_i^*} \right] \tag{4.12}$$

As a result, the RLS algorithm can be defined as

$$\boldsymbol{P}_i = \lambda^{-1} \left[\boldsymbol{P}_{i-1} - \frac{\lambda^{-1} \boldsymbol{P}_{i-1} \boldsymbol{u}_i^* \boldsymbol{u}_i \boldsymbol{P}_{i-1}}{1 + \lambda^{-1} \boldsymbol{u}_i \boldsymbol{P}_{i-1} \boldsymbol{u}_i^*} \right] \tag{4.13}$$

$$\boldsymbol{\omega}_i = \boldsymbol{\omega}_{i-1} + \boldsymbol{P}_i \boldsymbol{u}_i^* \left[d(i) - \boldsymbol{u}_i \boldsymbol{\omega}_{i-1} \right] \tag{4.14}$$

From Eq.4.14, the RLS algorithm uses all the previous data construct regression matrix and exponentially weight the importance of all previous data by adding a "forgetting factor" λ. Then, the regression matrix reformed as a recursive form to update the data iteratively.

4.4.1 *Fast Affine Projection Algorithm*

The FAP algorithm is developed from the conventional Affine Projection algorithm (APA). Both use the most recent sampling data as an approximation of the regression matrix $\{\boldsymbol{R}_{du}, \boldsymbol{R}_u\}$. A positive integer call projection order, K, is used to define how many step values are to be used in the approximation. The regression matrix is obtained as follows:

$$\hat{\boldsymbol{R}}_u = \frac{1}{K} \left(\sum_{j=i-K+1}^{i} \boldsymbol{u}_j^* \boldsymbol{u}_j \right) \tag{4.15}$$

$$\hat{\boldsymbol{R}}_{du} = \frac{1}{K} \left(\sum_{j=i-K+1}^{i} d(i) \boldsymbol{u}_j^* \right) \tag{4.16}$$

We define:

$$\boldsymbol{U}_i = \begin{bmatrix} \boldsymbol{u}_i \\ \boldsymbol{u}_{i-1} \\ \vdots \\ \boldsymbol{u}_{i-K+1} \end{bmatrix} \qquad (K \times M) \tag{4.17}$$

$$\boldsymbol{d}_i = \begin{bmatrix} d(i) \\ d(i-1) \\ \vdots \\ d(i-K+1) \end{bmatrix} \qquad (K \times 1) \tag{4.18}$$

And the regularisation matrix

$$\varepsilon(i) = \varepsilon / K \tag{4.19}$$

From this, the regression matrix $\{\boldsymbol{R}_{du}, \boldsymbol{R}_u\}$ becomes

$$\hat{\boldsymbol{R}}_u = \frac{1}{K}\boldsymbol{U}_i^* \boldsymbol{U}_i, \quad \hat{\boldsymbol{R}}_{du} = \frac{1}{K}\boldsymbol{U}_i^* \boldsymbol{d}_i \tag{4.20}$$

So, the regularized Newton recursion Eq.4.4 becomes

$$\boldsymbol{\omega}_i = \boldsymbol{\omega}_{i-1} + \mu\left(\varepsilon \boldsymbol{I} + \boldsymbol{U}_i^* \boldsymbol{U}_i\right)^{-1} \boldsymbol{U}_i^* \left[\boldsymbol{d}_i - \boldsymbol{U}_i \boldsymbol{\omega}_{i-1}\right] \tag{4.21}$$

By applying the matrix inversion formula, the term $\mu\left(\varepsilon \boldsymbol{I} + \boldsymbol{U}_i^* \boldsymbol{U}_i\right)^{-1} \boldsymbol{U}_i^*$ becomes

$$\left(\varepsilon \boldsymbol{I} + \boldsymbol{U}_i^* \boldsymbol{U}_i\right)^{-1} \boldsymbol{U}_i^* = \boldsymbol{U}_i^* \left(\varepsilon \boldsymbol{I} + \boldsymbol{U}_i \boldsymbol{U}_i^*\right)^{-1} \tag{4.22}$$

As a result, the Affine Projection algorithm (APA) can be defined as

$$\boldsymbol{\omega}_i = \boldsymbol{\omega}_{i-1} + \mu \boldsymbol{U}_i^* \left(\varepsilon \boldsymbol{I} + \boldsymbol{U}_i \boldsymbol{U}_i^*\right)^{-1} \left[\boldsymbol{d}_i - \boldsymbol{U}_i \boldsymbol{\omega}_{i-1}\right] \tag{4.23}$$

Where $\boldsymbol{U}_i$ and $\boldsymbol{d}_i$ are defined by Eq. 4.17 and Eq.4.18 as $K \times M$ and $K \times 1$ matrix respectively. M is the total number of parameters and K is the projection order of the AP algorithm. The computational cost of AP per iteration can be presented as Table 4.1

Term	×	+
$\boldsymbol{u}_i\boldsymbol{\omega}_{i-1}$	KM	$K(M-1)$
$\boldsymbol{d}_i-\boldsymbol{U}_i\boldsymbol{\omega}_{i-1}$		K
$\boldsymbol{U}_i\boldsymbol{U}_i^*$	K^2M	$K^2(M-1)$
$\varepsilon\boldsymbol{I}+\boldsymbol{U}_i\boldsymbol{U}_i^*$		K
$\left(\varepsilon\boldsymbol{I}+\boldsymbol{U}_i\boldsymbol{U}_i^*\right)^{-1}$	K^3	K^3
$\left(\varepsilon\boldsymbol{I}+\boldsymbol{U}_i\boldsymbol{U}_i^*\right)^{-1}\left[\boldsymbol{d}_i-\boldsymbol{U}_i\boldsymbol{\omega}_{i-1}\right]$	K^2	$K(K-1)$
$\mu\boldsymbol{U}_i^*\left(\varepsilon\boldsymbol{I}+\boldsymbol{U}_i\boldsymbol{U}_i^*\right)^{-1}\left[\boldsymbol{d}_i-\boldsymbol{U}_i\boldsymbol{\omega}_{i-1}\right]$	KM	$(K-1)M$
$\boldsymbol{\omega}_i$		M
Total per iteration	$K^3+K^2(M+1)+2MK$	$K^3+K^2(M+1)+2KM$

Table 4.1 computational cost of AP per iteration

The computational cost of the classic AP algorithm can be further improved if the plant system is modelled using an ARX model. |Fortunately, as aforementioned in chapter 2, the ARX model is nominally the mathematical model for a classic DC-DC SMPC system.

The Fast Affine Projection is developed as follows. At step *i-1*, both sides of Eq. 4.23 are multiplied by $\boldsymbol{U}_i$. From this, we can get

$$\boldsymbol{U}_i\boldsymbol{\omega}_{i-1}=\boldsymbol{U}_i\left(\boldsymbol{\omega}_{i-2}+\mu\boldsymbol{U}_{i-1}^*\left(\varepsilon\boldsymbol{I}+\boldsymbol{U}_{i-1}\boldsymbol{U}_{i-1}^*\right)^{-1}\left[\boldsymbol{d}_{i-1}-\boldsymbol{U}_{i-1}\boldsymbol{\omega}_{i-2}\right]\right) \tag{4.24}$$

$$\boldsymbol{U}_i\boldsymbol{\omega}_{i-1}=\boldsymbol{U}_i\boldsymbol{\omega}_{i-2}+\mu\boldsymbol{U}_i\boldsymbol{U}_{i-1}^*\left(\varepsilon\boldsymbol{I}+\boldsymbol{U}_{i-1}\boldsymbol{U}_{i-1}^*\right)^{-1}\left[\boldsymbol{d}_{i-1}-\boldsymbol{U}_{i-1}\boldsymbol{\omega}_{i-2}\right] \tag{4.25}$$

In Eq. 4.25, $\boldsymbol{U}_i\boldsymbol{\omega}_{i-2}$ can be written as

$$\boldsymbol{U}_i\boldsymbol{\omega}_{i-2}=\begin{bmatrix}\boldsymbol{u}_i & \boldsymbol{u}_{i-1} & \dots & \boldsymbol{u}_{i-K+1}\end{bmatrix}^*\boldsymbol{\omega}_{i-2}=\begin{bmatrix}\boldsymbol{u}_i\boldsymbol{\omega}_{i-2} & \boldsymbol{u}_{i-1}\boldsymbol{\omega}_{i-2} & \cdots & \boldsymbol{u}_{i-K+1}\boldsymbol{\omega}_{i-2}\end{bmatrix} \tag{4.26}$$

$$\boldsymbol{U}_{i\text{-}1}\boldsymbol{\omega}_{i-2}=\begin{bmatrix}\boldsymbol{u}_{i\text{-}1}\boldsymbol{\omega}_{i-2} & \boldsymbol{u}_{i-2}\boldsymbol{\omega}_{i-2} & \cdots & \boldsymbol{u}_{i-K}\boldsymbol{\omega}_{i-2}\end{bmatrix} \tag{4.27}$$

In Eq.4.26, $\begin{bmatrix} \boldsymbol{u}_{i-1}\boldsymbol{\omega}_{i-2} & \cdots & \boldsymbol{u}_{i-K+1}\boldsymbol{\omega}_{i-2} \end{bmatrix}$ can be obtained from $\boldsymbol{U}_{i-1}\boldsymbol{\omega}_{i-2}$ in previous step. Therefore, to get $\boldsymbol{U}_i\boldsymbol{\omega}_{i-2}$ the only term needs to be calculated is $\boldsymbol{u}_i\boldsymbol{\omega}_{i-2}$.

In Eq.4.25, $\boldsymbol{U}_i\boldsymbol{U}_{i-1}^*$ term can be written as follows.

$$\boldsymbol{U}_i\boldsymbol{U}_{i-1}^* = \begin{bmatrix} \boldsymbol{u}_i\boldsymbol{u}_{i-1}^* & \boldsymbol{u}_i\boldsymbol{u}_{i-2}^* & \cdots & \boldsymbol{u}_i\boldsymbol{u}_{i-K}^* \\ \boldsymbol{u}_{i-1}\boldsymbol{u}_{i-1}^* & \boldsymbol{u}_{i-1}\boldsymbol{u}_{i-2}^* & \cdots & \boldsymbol{u}_{i-1}\boldsymbol{u}_{i-K}^* \\ \vdots & \vdots & \ddots & \vdots \\ \boldsymbol{u}_{i-K+1}\boldsymbol{u}_{i-1}^* & \boldsymbol{u}_{i-K+1}\boldsymbol{u}_{i-2}^* & \cdots & \boldsymbol{u}_{i-K+1}\boldsymbol{u}_{i-K}^* \end{bmatrix} \tag{4.28}$$

Because

$$\boldsymbol{U}_{i-1}\boldsymbol{U}_{i-1}^* = \begin{bmatrix} \boldsymbol{u}_{i-1}\boldsymbol{u}_{i-1}^* & \boldsymbol{u}_{i-1}\boldsymbol{u}_{i-2}^* & \cdots & \boldsymbol{u}_{i-1}\boldsymbol{u}_{i-K}^* \\ \boldsymbol{u}_{i-2}\boldsymbol{u}_{i-1}^* & \boldsymbol{u}_{i-2}\boldsymbol{u}_{i-2}^* & \cdots & \boldsymbol{u}_{i-2}\boldsymbol{u}_{i-K}^* \\ \vdots & \vdots & \ddots & \vdots \\ \boldsymbol{u}_{i-K}\boldsymbol{u}_{i-1}^* & \boldsymbol{u}_{i-K}\boldsymbol{u}_{i-2}^* & \cdots & \boldsymbol{u}_{i-K}\boldsymbol{u}_{i-K}^* \end{bmatrix} \tag{4.29}$$

Therefore, with the exception of $\begin{bmatrix} \boldsymbol{u}_i\boldsymbol{u}_{i-1}^* & \boldsymbol{u}_i\boldsymbol{u}_{i-2}^* & \cdots & \boldsymbol{u}_i\boldsymbol{u}_{i-K}^* \end{bmatrix}$, the remaining $K-1$ rows in $\boldsymbol{U}_i\boldsymbol{U}_{i-1}^*$ can be obtained from the previous $\boldsymbol{U}_{i-1}\boldsymbol{U}_{i-1}^*$. The remaining term of Eq.4.25 is

$$\left(\varepsilon\boldsymbol{I} + \boldsymbol{U}_{i-1}\boldsymbol{U}_{i-1}^*\right)^{-1}\left[\boldsymbol{d}_{i-1} - \boldsymbol{U}_{i-1}\boldsymbol{\omega}_{i-2}\right] \tag{4.30}$$

Which can be obtained from the last iteration. Moreover, after obtaining the term $\boldsymbol{U}_i\boldsymbol{U}_{i-1}^*$, the only terms in $\boldsymbol{U}_i\boldsymbol{U}_i^*$ that needs be calculated is $\boldsymbol{u}_i\boldsymbol{u}_i^*$ since

$$\boldsymbol{U}_i\boldsymbol{U}_i^* = \begin{bmatrix} \boldsymbol{u}_i\boldsymbol{u}_i^* & \boldsymbol{u}_i\boldsymbol{u}_{i-1}^* & \cdots & \boldsymbol{u}_i\boldsymbol{u}_{i-K+1}^* \\ \boldsymbol{u}_{i-1}\boldsymbol{u}_i^* & \boldsymbol{u}_{i-1}\boldsymbol{u}_{i-1}^* & \cdots & \boldsymbol{u}_{i-1}\boldsymbol{u}_{i-K+1}^* \\ \vdots & \vdots & \ddots & \vdots \\ \boldsymbol{u}_{i-K+1}\boldsymbol{u}_i^* & \boldsymbol{u}_{i-K+1}\boldsymbol{u}_{i-1}^* & \cdots & \boldsymbol{u}_{i-K+1}\boldsymbol{u}_{i-K+1}^* \end{bmatrix} \tag{4.31}$$

From Eq. 4.31, the red terms can be obtained from previous data in $\boldsymbol{U}_{i-1}\boldsymbol{U}_{i-1}^*$, (see Eq. 4.29), and the blue terms can be obtained from the 1st row of $\boldsymbol{U}_i\boldsymbol{U}_{i-1}^*$. Therefore, the computational cost is

dramatically reduced if the aforementioned method is applied. Therefore, the computational cost can be reduced as shown in Tab. 4.2.

	×	+
AP	$K^3+K^2\left(M+1\right)+2MK$	$K^3+K^2\left(M+1\right)+2KM$
FAP	$K^3+K^2+\left(2K+2\right)M$	$K^3+K^2+\left(2M+1\right)K+2M+2$

Table 4.2 computational cost comparison between FAP and AP

A detailed computational cost summary of the FAP algorithm is presented in the next section.

4.5 Comparative study of RLS and FAP

In this section we evaluate RLS and FAP by mathematical deduction in terms of computational cost, convergence speed and noise immunity. Simulation results are presented to verify the mathematical deduction results.

4.5.1 *Computational cost analysis of RLS and FAP*

Considering the derivation of the RLS and FAP algorithm presented in this Chapter, the iterative computational cost of each algorithm can be described in terms of the number of multiplications, addition and division processes carried out. Tab. 4.3 summarises the RLS computational cost per iteration, where *M* is the parameter number.

Term	×	+	/
$\boldsymbol{u}_i\boldsymbol{\omega}_{i-1}$	$\boldsymbol{M}$	$M-1$	
$d(i)-\boldsymbol{u}_i\boldsymbol{\omega}_{i-1}$		1	
$\lambda^{-1}\boldsymbol{u}_i^*$	$\boldsymbol{M}$		
$\boldsymbol{P}_{i-1}\left(\lambda^{-1}\boldsymbol{u}_i^*\right)$	M^2	$M(M-1)$	
$\boldsymbol{u}_i\boldsymbol{P}_{i-1}\left(\lambda^{-1}\boldsymbol{u}_i^*\right)$	$\boldsymbol{M}$	$M-1$	
$1+\boldsymbol{u}_i\boldsymbol{P}_{i-1}\left(\lambda^{-1}\boldsymbol{u}_i^*\right)$		1	
$1/\left[1+\boldsymbol{u}_i\boldsymbol{P}_{i-1}\left(\lambda^{-1}\boldsymbol{u}_i^*\right)\right]$			1
$\left(\lambda^{-1}\boldsymbol{u}_i\boldsymbol{P}_{i-1}\boldsymbol{u}_i^*\right)\cdot\frac{1}{1+\boldsymbol{u}_i\boldsymbol{P}_{i-1}\left(\lambda^{-1}\boldsymbol{u}_i^*\right)}$	1		
$\left(\lambda^{-1}\boldsymbol{P}_{i-1}\boldsymbol{u}_i^*\right)\cdot\frac{\lambda^{-1}\boldsymbol{u}_i\boldsymbol{P}_{i-1}\boldsymbol{u}_i^*}{1+\boldsymbol{u}_i\boldsymbol{P}_{i-1}\left(\lambda^{-1}\boldsymbol{u}_i^*\right)}$	$\boldsymbol{M}$		
$\boldsymbol{P}_i\boldsymbol{u}_i^*$		$\boldsymbol{M}$	
$\boldsymbol{P}_i\boldsymbol{u}_i^*\left[d(i)-\boldsymbol{u}_i\boldsymbol{\omega}_{i-1}\right]$	$\boldsymbol{M}$		
$\boldsymbol{\omega}_i$		$\boldsymbol{M}$	
TOTAL per iteration	M^2+5M+1	M^2+3M	1

Table 4.3 Computational cost of RLS per iteration

For the Fast Affine Projection algorithm, $\boldsymbol{U}_i\boldsymbol{\omega}_{i-1}$, $\boldsymbol{U}_i\boldsymbol{\omega}_{i-2}$ and $\boldsymbol{U}_i\boldsymbol{U}_{i-1}^*$ are required. However, as previously discussed only need to calculate $\boldsymbol{u}_i\boldsymbol{\omega}_{i-2}$ and $\left[\boldsymbol{u}_i\boldsymbol{u}_{i-1}^* \quad \boldsymbol{u}_i\boldsymbol{u}_{i-2}^* \quad \cdots \quad \boldsymbol{u}_i\boldsymbol{u}_{i-K}^*\right]$, $\boldsymbol{U}_i\boldsymbol{U}_i^*$ can be simply obtained as the only terms in $\boldsymbol{U}_i\boldsymbol{U}_i^*$ that needs be calculated is $\boldsymbol{u}_i\boldsymbol{u}_i^*$. From this, the computational cost of the Fast Affine Projection algorithm is summarised as in Tab.4.4.

Term	$\times$	$+$
$\boldsymbol{u}_i\boldsymbol{\omega}_{i-2}$	M	$M-1$
$\left[\boldsymbol{u}_i\boldsymbol{u}_{i-1}^* \quad \boldsymbol{u}_i\boldsymbol{u}_{i-2}^* \quad \cdots \quad \boldsymbol{u}_i\boldsymbol{u}_{i-K}^*\right]$	KM	$K(M-1)$
$\boldsymbol{U}_i\boldsymbol{\omega}_{i-2}+\mu\boldsymbol{U}_i\boldsymbol{U}_{i-1}^*\left(\varepsilon\boldsymbol{I}+\boldsymbol{U}_{i-1}\boldsymbol{U}_{i-1}^*\right)^{-1}\left[\boldsymbol{d}_{i-1}-\boldsymbol{U}_{i-1}\boldsymbol{\omega}_{i-2}\right]$	K^2	K^2
$\boldsymbol{d}_i-\boldsymbol{U}_i\boldsymbol{\omega}_{i-1}$		K
$\boldsymbol{U}_i\boldsymbol{U}_i^*$	M	$M-1$
$\varepsilon\boldsymbol{I}+\boldsymbol{U}_i\boldsymbol{U}_i^*$		K
$\left(\varepsilon\boldsymbol{I}+\boldsymbol{U}_i\boldsymbol{U}_i^*\right)^{-1}$	K^3	K^3
$\mu\boldsymbol{U}_i^*\left(\varepsilon\boldsymbol{I}+\boldsymbol{U}_i\boldsymbol{U}_i^*\right)^{-1}\left[\boldsymbol{d}_i-\boldsymbol{U}_i\boldsymbol{\omega}_{i-1}\right]$	KM	$(K-1)M$
$\boldsymbol{\omega}_i$		M
Total per iteration	K^3+K^2 $+(2K+2)M$	K^3+K^2+ $(2M+1)K+2M+2$

Table 4.4 Computational cost of FAP per iteration

As aforementioned, the computational cost can be further reduced due to the mathematical model of DC-DC buck converter. With close inspection of $\boldsymbol{u}_i$, and because the SMPC system is represented by an ARX model, the elements in $\boldsymbol{u}_i$ can be presented as

$$\boldsymbol{u}_i\boldsymbol{u}_{i-1}^*=\begin{bmatrix}u(i-1) & u(i-2) & y(i-1) & y(i-2)\end{bmatrix}\bullet\begin{bmatrix}u(i-2)\\ u(i-3)\\ y(i-2)\\ y(i-3)\end{bmatrix} \quad (4.32)$$

$$\begin{bmatrix} u(i-1) & u(i-2) & y(i-1) & y(i-2) \end{bmatrix} \bullet \begin{bmatrix} u(i-2) \\ u(i-3) \\ y(i-2) \\ y(i-3) \end{bmatrix}$$
$$= u(i-1)u(i-2) + u(i-2)u(i-3) + y(i-1)y(i-2) + y(i-2)y(i-3) \tag{4.33}$$

In Eq.4.33, $u(i-2)u(i-3)$ and $y(i-2)y(i-3)$ can be obtained from $\boldsymbol{u}_{i-1}\boldsymbol{u}_{i-2}^{*}$, therefore, the computational cost of this step can be further reduced. The $\boldsymbol{u}_i\boldsymbol{u}_{i-1}^{*}$ term reduces to 2 multiplications and 2 additions. The $\begin{bmatrix} \boldsymbol{u}_i\boldsymbol{u}_{i-1}^{*} & \boldsymbol{u}_i\boldsymbol{u}_{i-2}^{*} & \cdots & \boldsymbol{u}_i\boldsymbol{u}_{i-K}^{*} \end{bmatrix}$ term reduced to $2K$. Additionally, the $\boldsymbol{u}_i\boldsymbol{u}_i^{*}$ term for calculating $\boldsymbol{U}_i\boldsymbol{U}_i^{*}$ only need 2 additions and 2 multiplications.

Total per iteration	$K^3 + K^2 + 3K + (K+1)M + 2$	$K^3 + K^2 + 3K + (K+1)M + 1$

Table 4.5 computation summary of FAP under ARX model

From Tab.4.5, FAP has no division compared with RLS. Also, the computational cost of FAP is highly dependent on the integer K, he choice of which is more flexible compared to RLS. In the specific case of system identification of a DC-DC buck converter system, where the parameter number $M = 4$, the computational cost is summarised in Tab.4.6.

Algorithms	RLS		FAP	
Computational operation	×	M^2+5M+1	×	$K^3+K^2+3K+(K+1)M+2$
	+	M^2+3M	+	$K^3+K^2+3K+(K+1)M+1$
	/	1	/	0
algorithm parameter	M=4		M=4, $K=2$	
Total computational cost per iteration	×	37	×	32
	+	28	+	33
	/	1	/	0

Table 4.6 computational cost comparison between RLS and FAP in DC-DC buck converter system

By comparing the computational cost between RLS and FAP, even FAP has a greater number of addition operations, but more importantly from a microprocessor implementation point of view has a lower number of multiplications and no division operations.

4.5.2 *Convergence speed analysis of RLS and FAP algorithm*

Like many other electrical systems, dynamic performance of an SMPC can suffer if the system is subjected to long periods of parameter variation; unless a robust control scheme is implemented and applied to regulate the output.

For this reason, online system identification is an extremely powerful tool, because it can be used to quickly estimate the parameters of the system. The estimation results can then be used as the basis for robust self-tuning or adaptive control.

The main criteria when applying a candidate system identification algorithm is the accuracy of the parameter estimation and the estimation convergence speed which directly affects the speed of response of the adaptive control follow a change in parameter(s).

Normally, the controller is only updated once the parameter estimation reaches a steady state value. If we define the true parameter matrix is $\hat{\boldsymbol{\omega}}$, the convergence speed can be define as a certain elapsed iteration amount *i* in $\Theta_i = \|\boldsymbol{\omega}_i - \hat{\boldsymbol{\omega}}\| < \sigma$, where σ is a defined error threshold between the estimated parameters and the true parameters. Using a regularised Newton's recursion, $\boldsymbol{\omega}_i - \hat{\boldsymbol{\omega}}$ can be represented as:

$$\Theta_i = \boldsymbol{\omega}_i - \hat{\boldsymbol{\omega}} = \boldsymbol{\omega}_{i-1} - \hat{\boldsymbol{\omega}} + \mu\left[\varepsilon' \boldsymbol{I} + \boldsymbol{R}_u\right]^{-1}\left[\boldsymbol{R}_{du} - \boldsymbol{R}_u \omega_{i-1}\right] \tag{4.34}$$

It can also be written as

$$\Theta_i = \Theta_{i-1} + \mu\left[\varepsilon' \boldsymbol{I} + \boldsymbol{R}_u\right]^{-1}\left[\boldsymbol{R}_{du} - \boldsymbol{R}_u \omega_{i-1}\right] \tag{4.35}$$

We substitute Eq.4.5, Eq.4.6, Eq.4.15 and Eq.4.16, the approximation term of $\{\boldsymbol{R}_{du}, \boldsymbol{R}_u\}$ into Eq.4.34 we obtain;

$$\Theta_{RLS,i} = \Theta_{RLS,i\text{-}1} + \left[\lambda^{i+1}\varepsilon \boldsymbol{I} + \sum_{j=0}^{i} \lambda^{i-j} \boldsymbol{u}_j^* \boldsymbol{u}_j\right]^{-1}\left[d(i)\boldsymbol{u}_i^* - \boldsymbol{u}_i^* \boldsymbol{u}_i \boldsymbol{\omega}_{i-1}\right] \tag{4.36}$$

and

$$\Theta_{FAP,i} = \Theta_{FAP,i\text{-}1} + \mu\left[\varepsilon \boldsymbol{I} + \sum_{j=i-K+1}^{i} \boldsymbol{u}_j^* \boldsymbol{u}_j\right]^{-1}\left[\sum_{j=i-K+1}^{i} d(i)\boldsymbol{u}_j^* - \sum_{j=i-K+1}^{i} \boldsymbol{u}_j^* \boldsymbol{u}_j \boldsymbol{\omega}_{i-1}\right] \tag{4.37}$$

In Eq. 4.35 and Eq.4.36, Θ_{RLS} and Θ_{FAP} are the parameter estimation errors for RLS and FAP respectively. To analyse the convergence speed, each term in Eq.4.35 and Eq.4.36 is compared to one and another to estimate Θ_i at every iteration.

In Eq.4.36, $\left[\sum_{j=i-K+1}^{i} d(i)\boldsymbol{u}_j^* - \sum_{j=i-K+1}^{i} \boldsymbol{u}_j^* \boldsymbol{u}_j \boldsymbol{\omega}_{i-1}\right]$ contains all *K* step errors that contribute towards the current step parameter estimation update. In contrast, for RLS in Eq.4.35, $\left[d(i)\boldsymbol{u}_i^* - \boldsymbol{u}_i^* \boldsymbol{u}_i \boldsymbol{\omega}_{i-1}\right]$ is only concerned with the current step error.

The term $\left[\lambda^{i+1}\varepsilon \boldsymbol{I} + \sum_{j=0}^{i}\lambda^{i-j}\boldsymbol{u}_j^*\boldsymbol{u}_j\right]^{-1}$ is highly dependent on the value of the forgetting factor λ, so it is difficult to compare with $\mu\left[\varepsilon \boldsymbol{I} + \sum_{j=i-K+1}^{i}\boldsymbol{u}_j^*\boldsymbol{u}_j\right]^{-1}$, whereas, the term $\left[\lambda^{i+1}\varepsilon \boldsymbol{I} + \sum_{j=0}^{i}\lambda^{i-j}\boldsymbol{u}_j^*\boldsymbol{u}_j\right]^{-1}$ is constructed by a summation of all previous regression matrices $\boldsymbol{u}_0 \cdots \boldsymbol{u}_i$. With $\lambda \geq 0.9$, which is the case under most normal conditions, $\left[\lambda^{i+1}\varepsilon \boldsymbol{I} + \sum_{j=0}^{i}\lambda^{i-j}\boldsymbol{u}_j^*\boldsymbol{u}_j\right]$ is greater than $\left[\varepsilon \boldsymbol{I} + \sum_{j=i-K+1}^{i}\boldsymbol{u}_j^*\boldsymbol{u}_j\right]$ [96]. Considering the matrix inversion involved, $\Theta_{FAP,i}$ is therefore typically greater than $\Theta_{RLS,i}$.

4.5.3 *Application of the FAP and RLS methods on a DC-DC buck converter system*

To confirm this mathematical lemma, a voltage controlled synchronous DC-DC buck converter system is simulation in Matlab and Simulink (see Appendix B). The configuration of this buck converter is $V_g = 60$ V, $V_o = 24$ V, $C = 940$ μF, $L = 860$ μH, $R = 9.2$ Ω, $f_{sample} = f_{switch} = 50$ kHz, $R_L = 0.475$ Ω, $R_C = 0.05$ Ω. The MOSFET ON state Drain to Source resistance is 0.01Ω. The sampling frequency of the load voltage is equal to the switching frequency. To start the system identification process, an activation signal is injected at 0.25 seconds when the DC-DC buck converter is stable.

Based on this parameter information, the control to output transfer function Eq. 3.27 can be calculated as

$$\frac{0.0836z^{-1} - 0.0542z^{-2}}{1 - 1.985z^{-1} + 0.9856z^{-2}} \tag{4.38}$$

The simulation results are shown in Fig. 4.3, Fig.4.4, Fig.4.5, Fig.4.6, Fig.4.7 and Fig.4.11. Fig.4.3 and Fig.4.4 prove this mathematical lemma and the superiority of the FAP in terms of convergence speed.

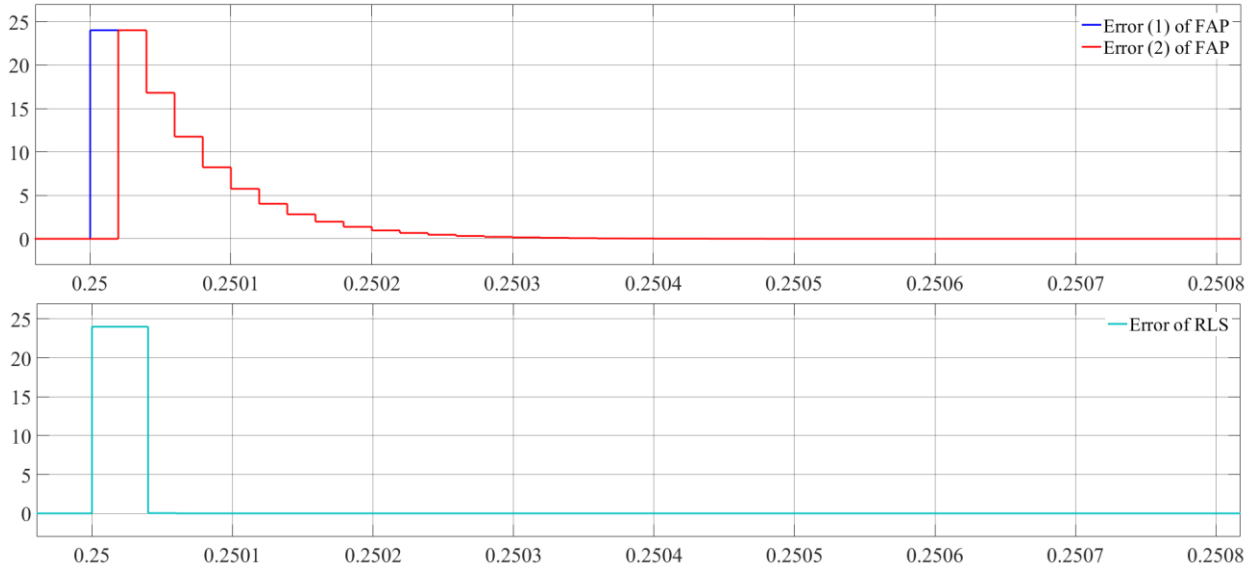

Figure 4.3 simulation result of error regression, when K=2

In Fig.4.3, the red and blue curves show the error convergences of the FAP from the term $\left[\sum_{j=i-K+1}^{i} d(i) - \sum_{j=i-K+1}^{i} \boldsymbol{u}_j \boldsymbol{\omega}_{i-1}\right]$. As the regression number K is set to two, the two curves represent the difference between the estimated output and the real output for the current step (*n*) and the difference between estimated output and the real output from the previous step (*n-1)*. Both slowly decay with time which means the error between the estimated and real output data reduces, confirming the parameter convergence during the system identification process. The light blue curve shows the error term of $\left[d(i) - \boldsymbol{u}_i \boldsymbol{\omega}_{i-1}\right]$ from the RLS. As shown, it is only effective at the beginning of the process before rapidly dropping to a near zero value. After several iterations, the two-term error can be found in Fig 4.4.

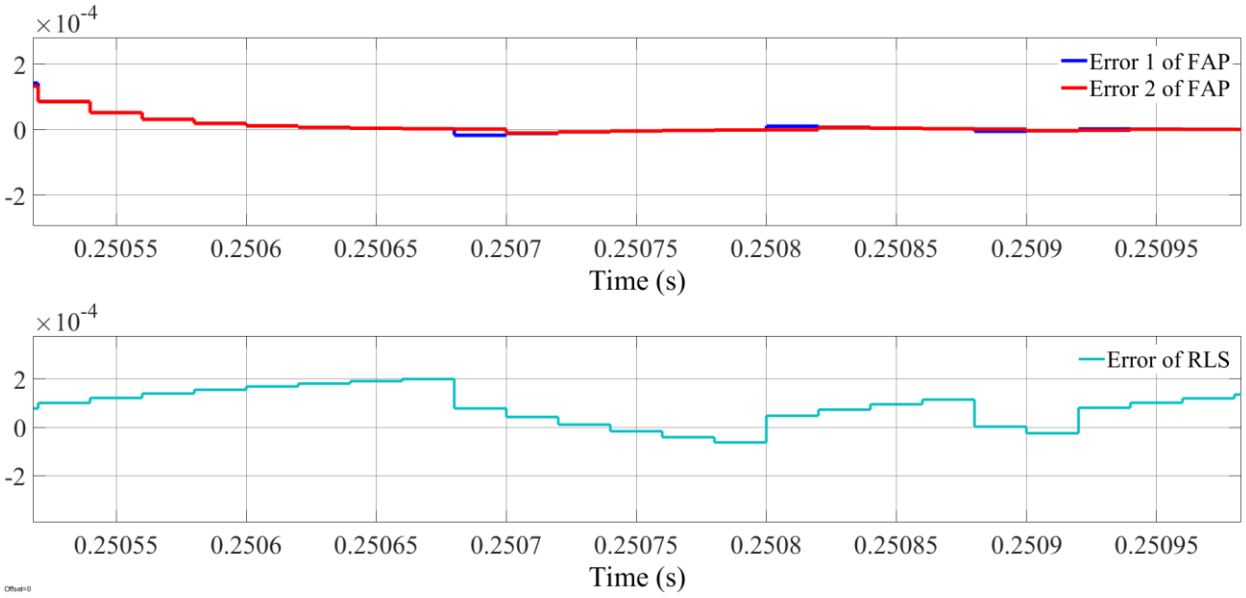

Figure 4.4 simulation result of error regression (zoom in), when K=2

From Fig 4.4, the RLS error does not readily stabilise due to the forgetting factor which takes account of the effect of the previous steps. In contrast, the two errors from the FAP are well maintained near zero as the parameters converge to the actual real values.

To illustrate the impact of sampling frequency on the parameter estimation, consider Fig. 4.5 and Fig. 4.6. The sampling frequencies in Fig. 4.5 and Fig. 4.6 are 10kHz (100μs) and 50kHz (20μs) respectively. In Fig 4.5, four parameters converge to steady value after 0.27s, whereas this time is 0.2525s in Fig. 4.6. This implies more time is needed to converge to a steady state value if the sampling frequency is low. Also, note that parameter 1 and parameter 2 values change if different sampling frequency is applied. That is because these two parameters, which appear in the numerator of the transfer function, are directly affected by the sampling period; as shown mathematically by Eq.3.27.

Here we list the correct parameters from Eq.4.38 when sampling frequency equal to 50 kHz and 10 kHz respectively. When f_{sample}=50kHz, $P_1 = 0.0836$, $P_2 = -0.0542$, $P_3 = 1.985$, $P_4 = 0.9856$. When f_{sample}=10kHz, $P_1 = 0.649$, $P_2 = 0.025$, $P_3 = 1.985$, $P_4 = 0.9856$.

To verify the superiority of the FAP in terms of convergence speed, four scenarios with different forgetting factor value and step size are simulated to facilitate further comparison between the FAP and RLS algorithms. Two forgetting factors are considered; 0.8 and 0.98 and similarly two step size scenarios are considered; 0.8 and 0.3. It should be noted that the forgetting factor and step size are usually chosen based on the system specific requirement, but the forgetting factor is usually chosen larger than 0.8 for the sake of noise immunity. As seen from Fig 4.6 to Fig 4.9, the simulation results verify the enhanced convergence speed of the FAP algorithm. This is because the small error correction value must be updated in the RLS method, and this results in a longer period to converge upon the correct parameter values. Furthermore, in FAP two or more errors are used to update the parameter which helps to speed up the convergence process.

From Fig.4.6-Fig.4.9, it is clear to see that both FAP and RLS can converge to the correct parameter values as the z^{-1} and z^{-2} terms in Eq. 4.38, which implies both can successfully estimate the parameters in the DC-DC buck converter system. With closer inspection, FAP has faster convergence speed compared with the RLS under all four conditions. More specifically, the RLS convergence speed is initially slow and heavily influenced by the forgetting factor, which places weight on the effect of all previous data towards the current parameter estimation step. The initial values in the parameter matrix are zero, which means the RLS updates future parameter matrices based on this incorrect evaluation of zero, which inevitably slows the convergence speed of the estimation process. In contrast, the FAP uses a projection order to define the data for the current step parameter estimation. It is more flexible and is not affected by potentially large signal fluctuations from previous steps. It only focuses on the current step and limited previous step result.

In Fig.4.6 and Fig.4.7, the chosen forgetting factor value is a low value, hence the parameter update cannot respond quickly to changes due to the impact of the initial values. It does not significantly change until recent and valid data dominates the regression matrix. However, FAP algorithm uses finite valid data, and thus converges quickly and smoothly to a true parameter estimation.

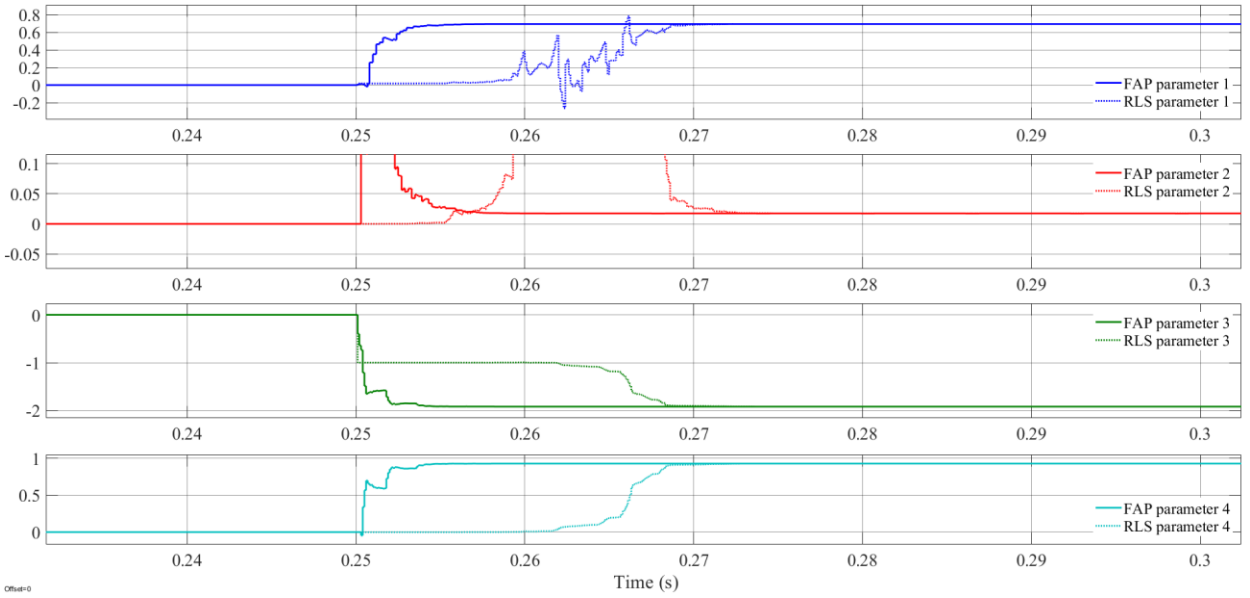

Figure 4.5 simulation result of parameter estimation comparison between RLS and FAP, μ=0.3 and λ=0.8, $T_{sample}=T_{switch}$=100µs (f_{sample}=10 kHz)

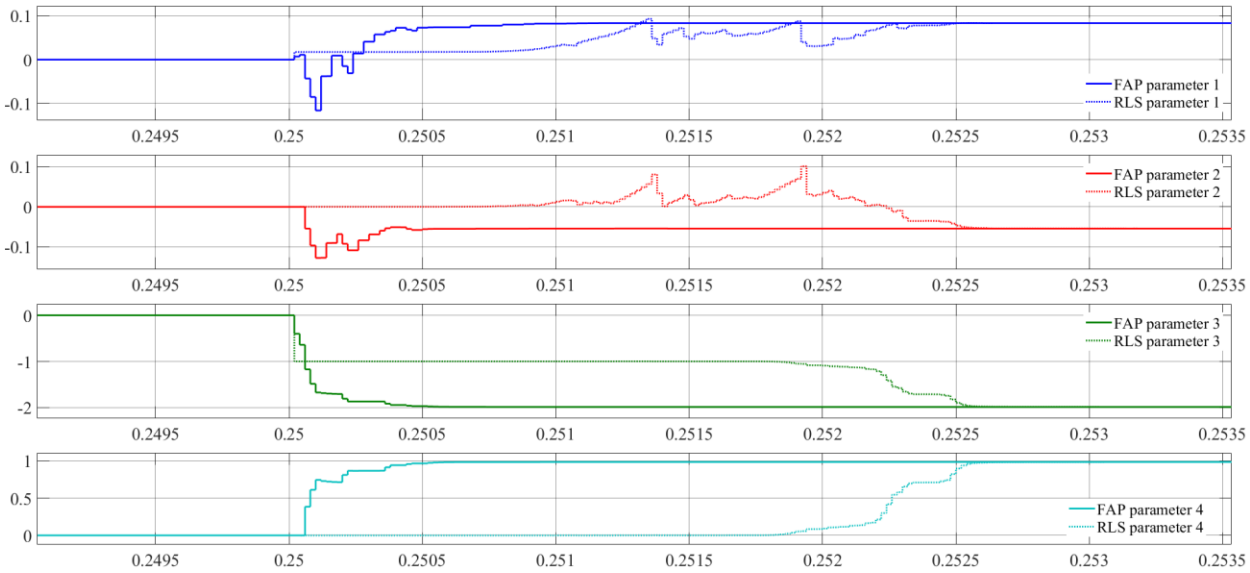

Figure 4.6 simulation result of parameter estimation comparison between RLS and FAP, μ=0.3 and λ=0.8, $T_{sample}=T_{switch}$=20µs (f_{sample}=50 kHz)

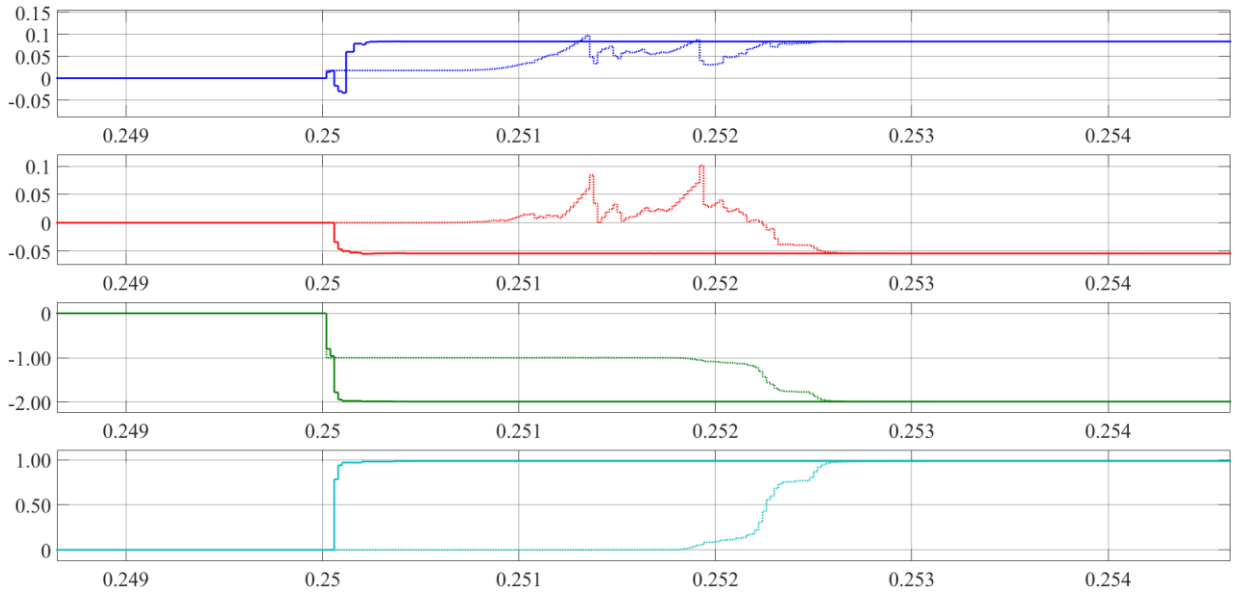

Figure 4.7 simulation result of parameter estimation comparison between RLS and FAP, μ=0.8 and λ=0.8

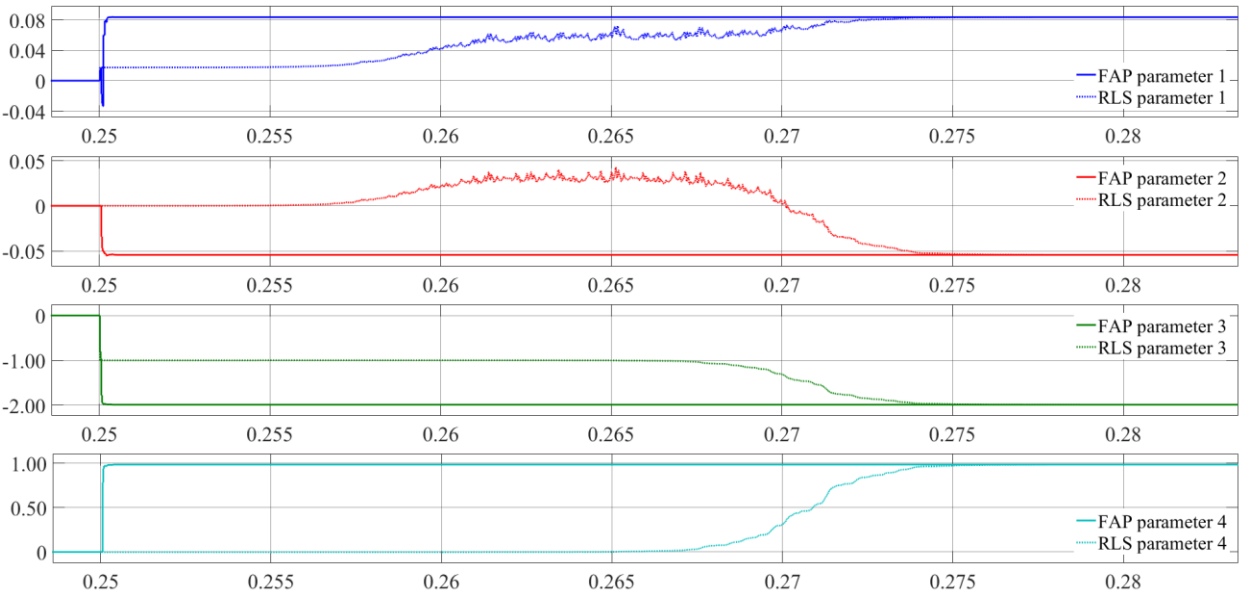

Figure 4.8 simulation result of parameter estimation comparison between RLS and FAP, μ=0.8 and λ=0.98

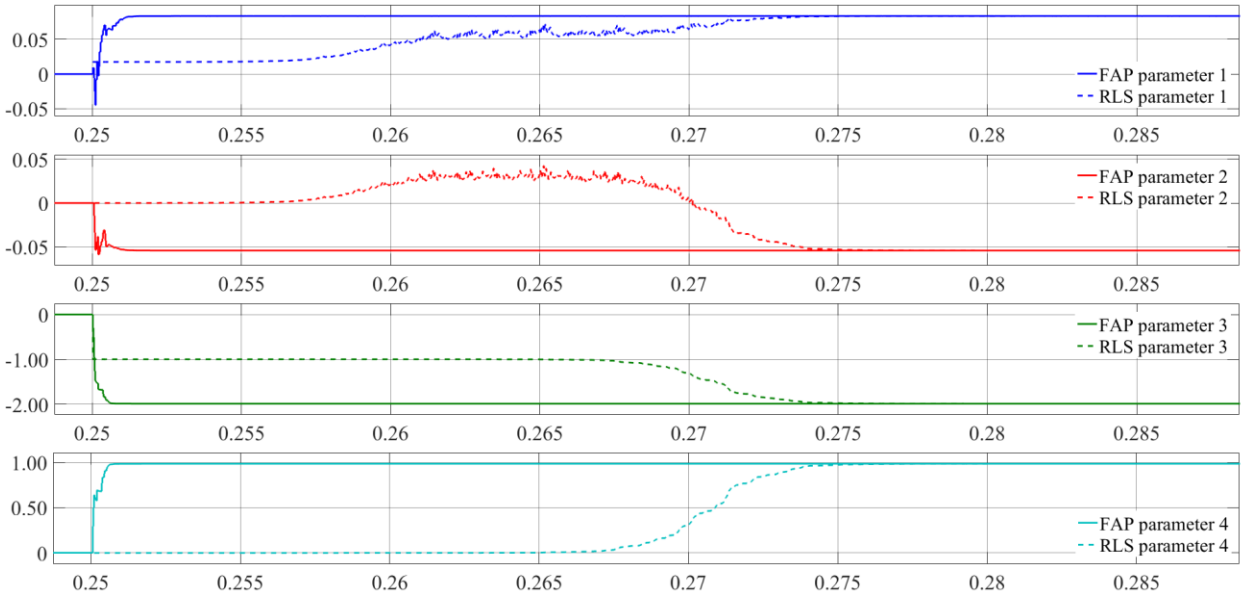

Figure 4.9 simulation result of parameter estimation comparison between RLS and FAP, μ=0.3 and λ=0.98

4.5.4 *EMSE analysis of RLS and FAP*

As aforementioned, the stochastic-gradient descent approximation method differs between the RLS and FAP, which results in differing accuracy in noisy environments. Therefore, in this section the noise immunity of the RLS and FAP for SMPC system applications is evaluated. It is difficult to evaluate the steady state error caused by the noise due to the variety type of noise or different orders or harmonic consist in practice. A typical measurement criterion is applying an Excess Mean-Square Error (EMSE) approach is considered [65]. It should be observed that this result can only be considered as a reference result due to the practical uncertainty.

Initially, we define mean square error as [65] ;

$$MSE \triangleq \lim_{i\to\infty} E\left|\boldsymbol{e}(\boldsymbol{i})\right|^2 \tag{4.39}$$

Where $\boldsymbol{e}(\boldsymbol{i})$ denotes a priori output estimation error between the current step output and the estimated output using previous step parameters, i.e.

$$\boldsymbol{e}(\boldsymbol{i}) \triangleq \boldsymbol{d}(\boldsymbol{i}) - \boldsymbol{u}_i\boldsymbol{\omega}_{i-1} \tag{4.40}$$

If ω_{i-1} is replaced by the genuine parameter matrix (optimal solution) ω_o the difference between Eq.4.38 and Eq.4.2 is defined as the excess-mean-square-error (EMSE) of the adaptive algorithm

$$EMSE \triangleq MSE - J_{\min} \tag{4.41}$$

The difference between the output error from the specific estimation algorithm and the output error from the general form of the stochastic gradient descent algorithm defines the accuracy of the estimation algorithm, because the ideal MSE result is $J_{\min}$. Since the regression matrix cannot be determined, both EMSE of RLS and FAP are approximated by specific criteria.

The EMSE of RLS, ζ^{RLS}, is derived in [65]. In [65], it is shown that:

$$\zeta^{RLS} = \frac{\sigma_v^2 (1-\lambda) M}{2-(1-\lambda) M} \tag{4.42}$$

Likewise, the EMSE of FAP, ζ^{FAP}, can be approximated by:

$$\zeta^{FAP} = \frac{\mu \sigma_v^2}{2-\mu} \tag{4.43}$$

where σ_v^2 is the variance of the input signal and M is system order.

It can be seen that ζ^{RLS} is again heavily dependent upon the forgetting factor. The EMSE of RLS increases as the forgetting factor is reduced. However, the EMSE of the FAP is relative function of the step size only. A comparison plot of EMSE for both algorithms is presented in Fig.4.8. The step size is varied from 0.1 to 1 and forgetting factor is varied from 0.8 to 0.98, the system parameter *M* here is selected as 4 which is determined by mathematical model of DC-DC buck converter system.

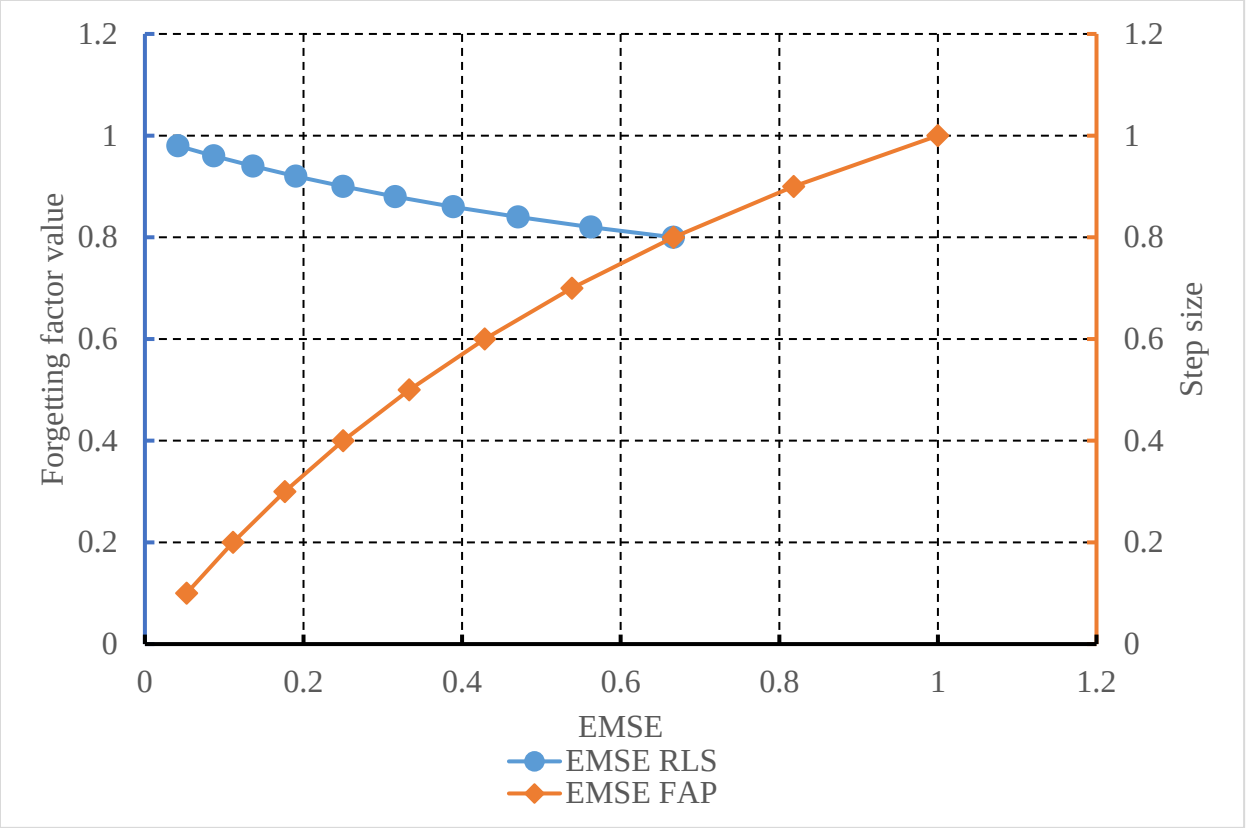

Figure 4.10 EMSE curves for RLS and FAP

From Fig.4.8, it is possible to conclude that to maintain a low ζ^{RLS} against a noisy input signal, the forgetting factor must be over 0.8. In contrast, the step size for the FAP algorithm must be selected to be a small value.

Overall, it can be concluded that FAP has a superior performance in terms of computational cost, convergence speed and noise immunity compared with RLS. It is a promising candidate algorithm for system identification in SMPC systems.

4.6 Pseudo Random Binary Sequence

Literature suggests that the input signal for system identification should be a frequency-rich signal to ensure parameter estimation accuracy [2]. Such a signal can fully excite the system and cause a small, but measurable, dynamic disturbance in the system output. In theory, a white noise-like signal is ideal as the input signal for this purpose since it contain a wide variety of frequency

components and the variance is adjustable. It also has equal intensity across the frequency spectrum and has a mean value of zero. Using this signal as the input signal, system identification algorithms can readily estimate the parameters in a few iterations.

In SMPC system identification, the input signal is typically the duty cycle, which is calculated via the control algorithm and PWM unit in the DSP. True white noise cannot readily be injected into the control loop to generate the duty ratio. Therefore, in many practical system identification applications the input signal is usually an artificially-generated frequency-rich signal.

Much research has been carried out to generate an artificial random signal with similar properties to white noise in signal processing applications. The Pseudo Random Binary Sequence (PRBS) is such a signal which is commonly used in signal processing [2]. A major attraction of the PRBS is that it is very easy to implement on a DSP and requires little computational effort. Consequently, it lends itself well to system identification of digital controlled SMPCs.

The PRBS is a rectangular pulse sequence with a "random" modulation pattern, as shown in Fig.4.9. This sequence is generated by a fixed number of digital bits, shift registers, and an exclusive-or gate (XOR) in the feedback loop [69]. As an example, shown in Fig.4.9, a nine-bit PRBS signal is generated. At each iteration, the data bits are shifted right by one bit. The value which exits bit 9 is the PRBS output and is used as the excitation signal within the digital control loop. The XOR operator is applied to bits 5 and 9 and the output of this operation is used to refresh the value of bit 1 in the register following the shift.

In theory, the maximum length of the PRBS sequence before repetition is $L = 2^m - 1$, where m is the number of bits. The register bit number should be long enough to provide a sufficiently frequency rich signal for the intended application. A good way to determine the competence of the PRBS is to follow these steps: 1. perform a frequency response test, based on the nominal transfer function of the SMPC system. 2. From the frequency response of SMPC, establish the bandwidth of the system. 3. Select a PRBS sequence length which covers the frequency band and has enough data points for system identification (usually >200 data points). By following these basic steps, an 11-bits PRBS sequence is selected for this research. In a SMPC application, the duty ratio can only be changed at each switching interval. That means the input update frequency is limited by the switching frequency. Therefore, the maximum frequency component of PRBS perturbation signal

is intrinsically bound to the switching frequency, it cannot update and have an impact between normal duty ratio updates.

For completeness, Table 4.7 shows the maximum sequence length for different size PRBS. This table also shows which register bits should be XOR to ensure the maximum sequence. Due to the algorithmic generation of the PRBS signal, it cannot be considered as a pure random signal just like Gaussian white noise. A detailed test should be done before applying specific PRBS signal in practice.

In terms of the PRBS perturbation signal, this very much depends on the mathematical model, system sensitivity to disturbance, and the effectiveness of the control loop feedback. If a robust system control loop is applied, the PRBS amplitude can be selected as a higher value to increase the accuracy of parameters estimation, and vice versa.

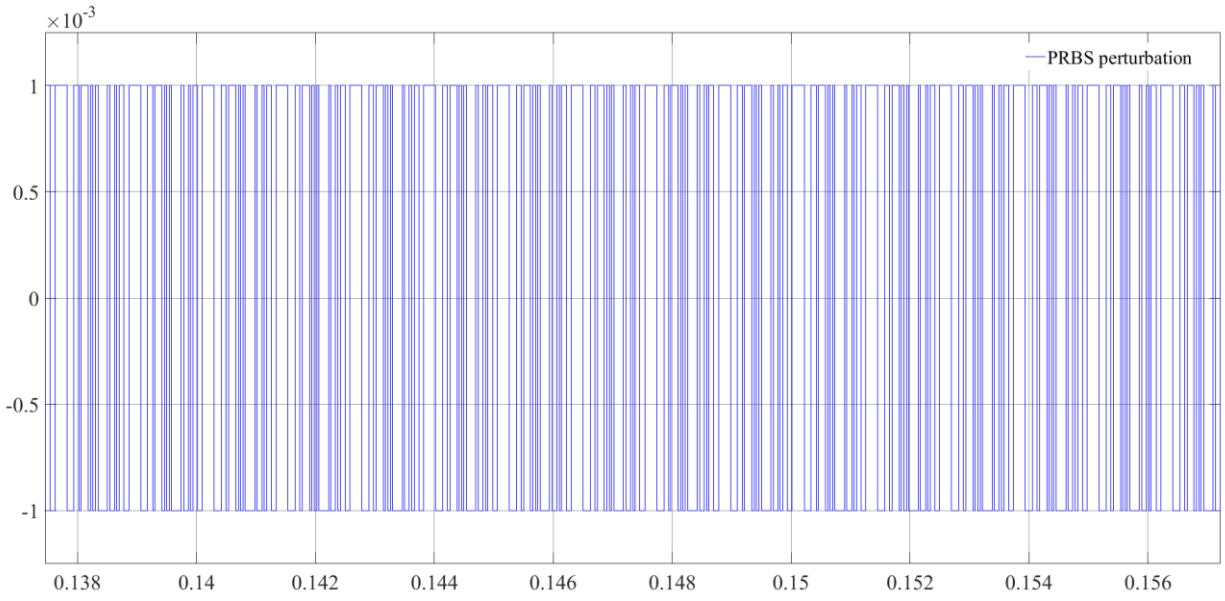

Figure 4.11 PRBS perturbation waveform

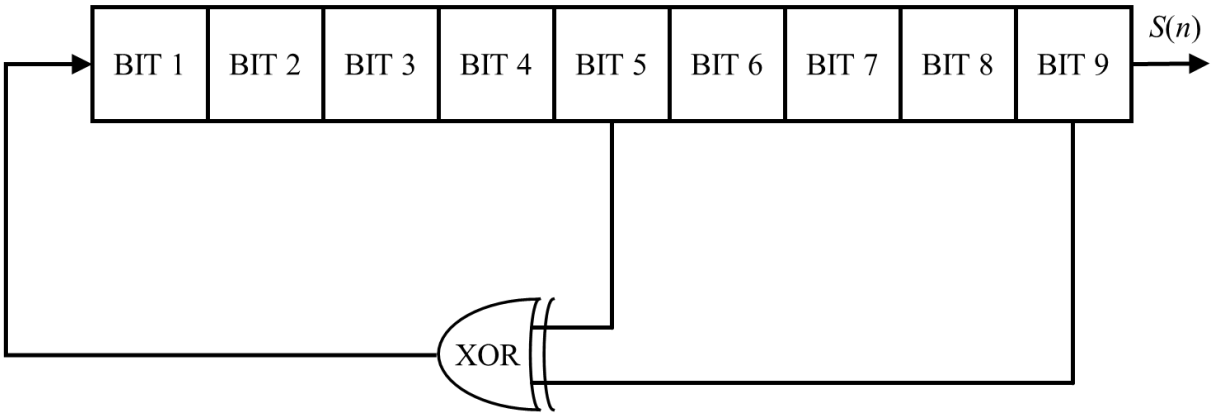

Figure 4.12 PRBS bit generation method

Number of bits (*m*)	***L* = 2^m - 1**	**Bits in XOR operation**
2	3	1 and 2
3	7	1 and 3
4	15	3 and 4
5	31	3 and 5
6	63	5 and 6
7	127	6 and 7
8	255	2, 3, 4 and 8
9	511	5 and 9
10	1023	7 and 10
11	2047	9 and 11
12	4095	4, 10, 11 and 12
13	8191	8, 11,12 and 13
14	16383	2, 12, 13 and 14
15	32767	14 and 15

Table 4.7 length of PRBS in different number of bits

To verify the impact of the PRBS signal with respect to the DC-DC buck converter operation and system identification results, simulation studies have been performed. The variation of duty ratio and output voltage is presented in Fig. 4.13. It can be observed that the duty ratio is perturbed when the PRBS sequence is injected into the control loop. This is also the same time that the system identification process is enabled. The output voltage begins to slightly fluctuate when the PRBS signal is injected. This level of disturbance may be greater in practice due to resonance and the effect of parasitic inductance or capacitance within the circuit. The amplitude of the injected PRBS signal must be kept small to minimise the impact on the output voltage in SMPC systems.

It can be seen that there is a voltage oscillation after 0.3s where is the end of PRBS injection. It is caused by a feedback loop which contains a typical PID controller. Fig.4.12 shows the parameter estimation result without PRBS perturbation signal.

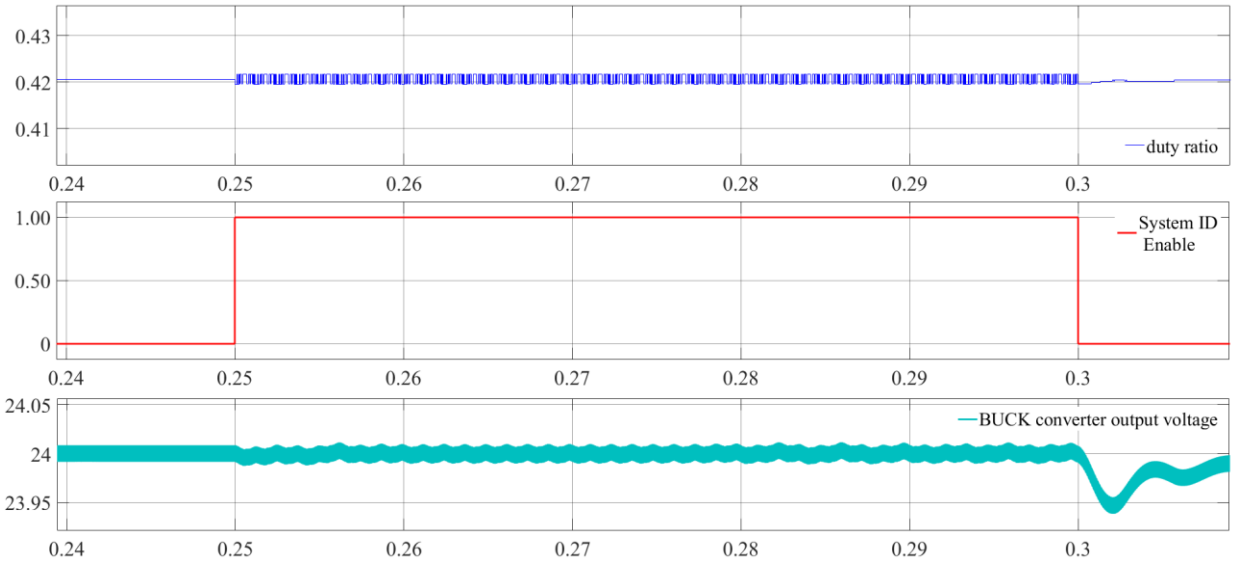

Figure 4.13 PRBS effect on duty cycle, and output voltage signal

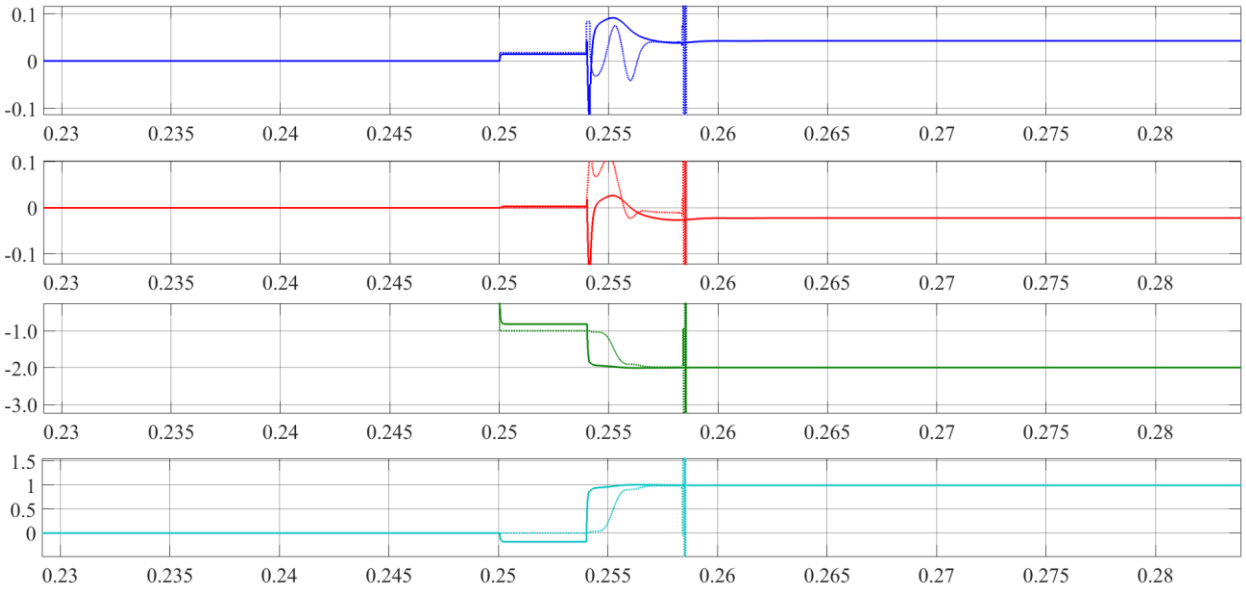

Figure 4.14 system identification result without PRBS, comparison between RLS and FAP, μ=0.3 and λ=0.98

It can be seen in Fig.4.14 that, without the PRBS signal, both FAP and RLS cannot estimate the correct value for parameter 2 (red curve, see correct result in Fig.4.7). Also, the RLS output exhibits significant oscillations around 0.285s and ultimately does not converge to the correct value. In terms of convergence speed, it is much slower in the absence of the PRBS injection. This confirms that injecting the PRBS signal is essential in the system identification process and is necessary to establish an accurate transfer function model of the SMPC.

4.7 Chapter summary

In this chapter, a detailed study of the proposed Fast Affine Projection (FAP) algorithm is presented. A detailed mathematical analysis demonstrates that the proposed FAP algorithm is computationally simpler than conventional Recursive Least Squares (RLS) algorithm due to the special data regression model of SMPCs. Importantly, there is no division operation involved in FAP algorithm, which significantly reduces the computational cost compared to RLS. The mathematical derivation and simulation results also show that the FAP algorithm has a faster convergence speed compared with the RLS. Overall, the FAP algorithm is proven to be a viable candidate algorithm for system identification and adaptive control.

Chapter 5. Adaptive Control of a DC-DC Converter using a Current Balancing ON/OFF Control Technique for Optimal Transient Performance

5.1 Introduction

Due to the essential need for high efficiency and reliability in power electronic systems, there is increasing demand for research into the optimisation of SMPCs and their respective digital controllers. Furthermore, mitigation of undesirable transient behaviour due to known, and unknown, disturbances is a key research topic at present. Output voltage spikes caused by abrupt load changes, or variation of circuit parameters, have widely been recognised as having a detrimental effect on the power dissipation of energy storage components and shortening the lifetime of semiconductor devices [70-72].

With the development of digital control devices, such as microprocessors, digital signal processors (DSP), and field programmable gates arrays (FPGAs), a plethora of advanced adaptive control schemes have been developed and widely applied to achieve exceptional output voltage regulation [88], robust performance over a wide range of operating conditions [86,106, 107], and low sensitivity to parameter variation within the system [89,90,91]. Several solutions have been proposed in literature, ranging from model based predictive control (MPC) schemes [8, 73,87], sliding mode control (SMC) [74], nonlinear control [75,92] and indeed conventional linear control [40]. Until recently, most research was based on the hypothesis that the controller had prior information about the power converter system parameters. However, this typically conflicts with the situation in reality, where the parameters of the system often cannot be determined in advance.

To overcome this, new on-line system identification and adaptive control techniques have recently been developed and shown to facilitate more robust control solutions [1,2,26,66]. Many efficient adaptive algorithms have been developed to speed up the system identification process and acquire

accurate steady state results [105]. However, just like the adaptive control law developed in [2], many researches regarding on adaptive control methods in SMPCs are only based on the parameter autotuning method of PID controller and strictly follow the transfer function/average state space model for system identification process. Despite these advances of auto-tuning, non-linear phenomena caused by switching behaviour of the semiconductor devices and the time sensitive nature of the system identification process restricts the direct adaptive control optimisation of the transient characteristics of the system.

For this reason, this chapter proposes a new adaptive control scheme for the digital control of a DC-DC SMPC system (shown in Fig.5.1). By analysing the transient behaviour of DC-DC buck converter and the dynamic response of energy storage components during the load change condition, the proposed control scheme discards the conventional PI controller method (as been used in [2, 26, 66, 105]) but employs an optimal Current Balancing ON/OFF (CBOO) technique to achieve superior transient behaviour in a dc-dc converter application. Furthermore, it applied a difference equation method as the mathematical model which overcomes the limitations of the conventional linear transfer function modelling approach illustrated in chapter 3. Also, it creates an improved operating conditions for real time system identification to be carried out at the point of parameter variation. Based on the evidence provided in Chapter 4, the Fast Affine Projection algorithm is applied for parameter estimation in this new mathematical model.

In this chapter, the transient behaviour of a DC-DC buck converter following an abrupt load change is considered in detail and linked to the behaviour of the energy storage components in the circuit. Based on the power transmission between each energy storage component, the proposed current balancing ON/OFF control technique is presented to minimise the transient periods. Mathematical analysis is presented to determine the optimal ON and OFF time for the semiconductor switch. From this, a distinct mathematical model for system identification in this control scheme is developed. Finally, the proposed control scheme is verified via simulation. This method has been theoretically proved as the optimal control method for improving the voltage transient response compared with conventional varying duty ratio method. The simulation results confirm the validity of the proposed CBOO controller and demonstrate the superiority dynamic performance compared to a conventional voltage feedback controller with PID compensation scheme.

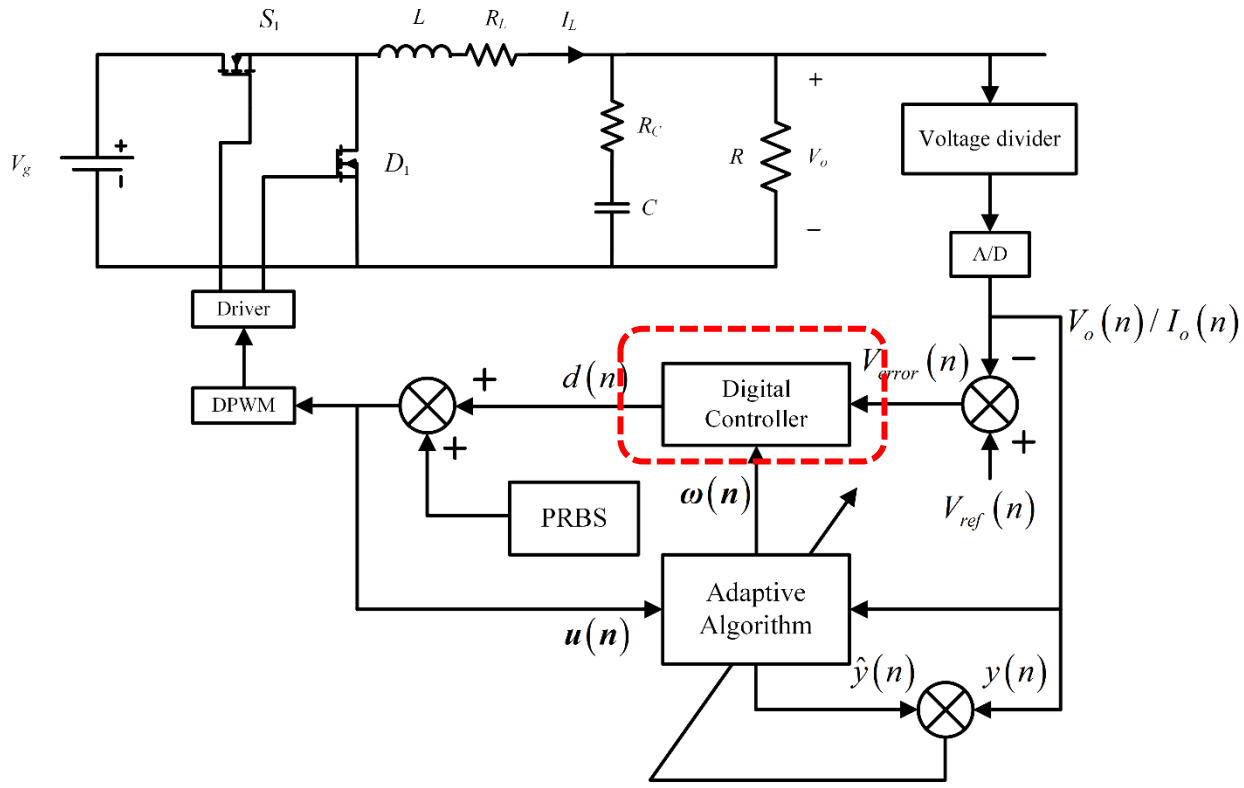

Figure 5.1 system identification and adaptive control of DC-DC buck converter—digital control part

5.2 Conventional converter transient operation analysis

The transient response of a DC-DC buck converter can be explained through analysis the power transmission between the two energy storage components in the circuit. The inductor and the output capacitor. Essentially, the voltage/current oscillation is a dynamic performance of power transmission between these energy storage components.

A simulation result with close voltage feedback loop control is shown in Fig. 5.2. The parameters are chosen as the same as in Section 3.6. The red curve is the inductor current and the blue one is the load resistor current. A load-step change occurred at 0.4s, the load resistance is reduced to 20% of the original value. Such a disturbance to the system is a common event in many applications; for example, Switched Mode Power Supplies. Closer inspection of the transient response shows that the characteristic can be divided into four key sections. These are indicated by the four time periods, T1 to T4, in Fig. 5.2.

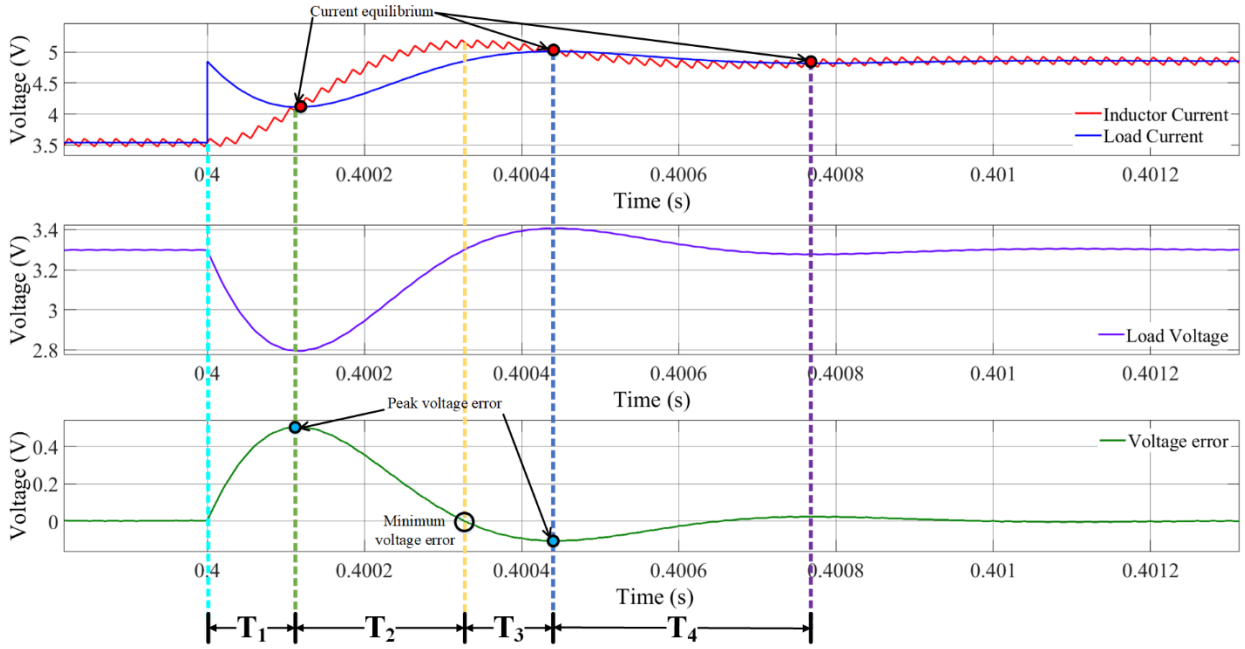

Figure 5.2 inductor current and load current transient response when applying conventional control scheme

(a) T1: capacitor discharging and inductor charging

(b) T2: capacitor charging and inductor charging

(c) T3: capacitor charging and inductor discharging

(d) T4: capacitor discharging and inductor discharging

Time period T1: At the point when the load change occurs, the load current rapidly rises, causing the power consumption at the load to increase. Consequently, the converter output capacitor starts to discharge and the load voltage, and consequently load current, begins to drop. At this point, the closed loop controller will respond by increasing the duty ratio of the dc-dc converter to counteract the voltage drop and ensure good quality voltage regulation where possible. As a result, the semiconductor switch is in the "ON" state for an increasingly dominant proportion of the PWM switching period. This in turn leads to the inductor current, i_L increasing. When the inductor current and load current are equal to each other, current balance is said to have been reached. At this point, interval T1 is complete. In summary, during the T1 period, the inductor is dominated

by charging and the capacitor is dominated by discharging in conventional control scheme. This situation is reflected in Fig.5.3(a).

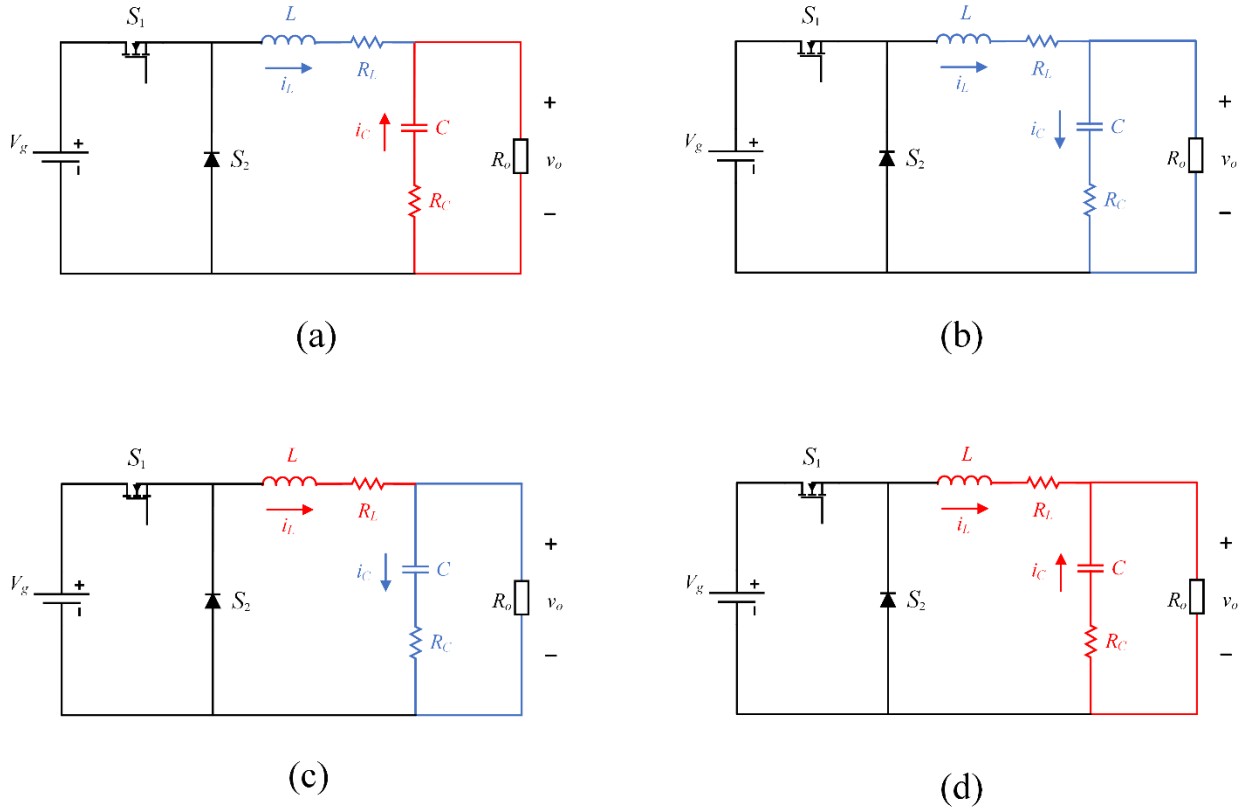

Figure 5.3 four power transmission conditions after the load abrupt change occurs

Time period T2: At the end of T1, current balance between inductor and load is established. However, a difference between load voltage and controller reference voltage will still typically exist. Therefore, a period of voltage control balance is necessary; the impact of this on the converter current is highlighted as T2 in Fig.5.2. At the beginning of T2, the controller output voltage error causes the duty ratio to still be greater than its initial value. As a result, the inductor current generally increases until the voltage balance is met. The inductor current simultaneously supplies the load and charges the capacitor to achieve voltage balance. In this period, both capacitor and inductor are dominated by charging; refer as Fig.5.3(b). Once the load voltage is equal to the reference voltage, the PWM duty ratio stops incrementing. The T2 period ends when the inductor current reaches the peak, which is normally greater than the load current.

Time period T3: In period T3, current balancing between the inductor current and output current commences again. In this period, the duty ratio is decreased because the inductor current continues to charge the output capacitor. At this point, the load voltage is greater than the controller reference voltage. This process stops when current balance is reached for a second time. In T3, the inductor is dominated by discharging and capacitor is dominated by charging; refer to Fig.5.3(c).

Time period T4: In the final period T4, the second period of voltage control imbalance compels the duty ratio to increase gradually to the steady state value. Following this, given the example shown in Fig.5.3, both the voltage and current converge to the steady state value. In T4, the second voltage balance is met by discharging both capacitor and inductor; refer to Fig.5.3(d). In some practical situations, the output response may exhibit several repeated oscillations in order to reach current and voltage balance (i.e. further repetition of T3 and T4), to establish a stable steady state response.

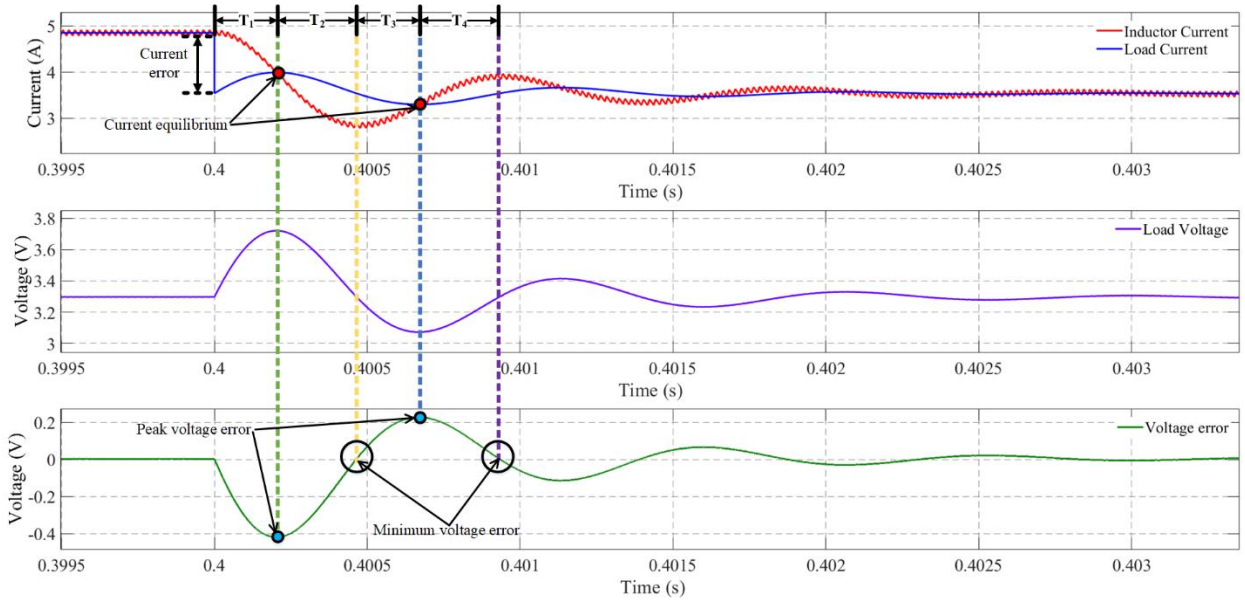

Figure 5.4 inductor current and load current transient response when applying conventional control scheme

Same charge/discharge analysis can also be done for the load increment condition as shown in Fig.5.4. The load current suddenly drops due to the abrupt load increment. Then, as the difference between load and inductor current, the capacitor charges the energy from the discharging inductor. When current reaches equilibrium, the voltage difference between reference voltage and load

voltage force the capacitor discharge to drop its voltage. As a result, the load current keeps decreasing and inductor keeps discharge as well. When the load voltage reaches the reference value, the inductor current ceases to reduce. Whilst the current difference exists, the load current keeps reducing and the inductor current begins to rise in an attempt to reach a current balance equilibrium. Such unbalance of voltages and currents occurs several times, but when both reach equilibrium simultaneously steady state conditions result. In summary the oscillatory voltage and current behaviour is due to the mismatch between current and voltage in the circuit. For voltage regulation purposes, the control scheme can be developed to speed up the process of reducing the voltage equilibrium process.

Here, we only develop the control scheme for an abrupt load reduction scenario, however, an increase in load can be analysed using the same method.

5.3 Current Balancing ON/OFF Control Technique

5.3.1 Basic control scheme of current balancing ON/OFF control

One way to potentially eliminate undershoot and overshoot during the transient period is to carefully control the duty ratio of the semiconductor switch to reduce the charging/discharging time of the energy storage components. Therefore, in this section, a current balancing, constant switching state (ON/OFF) method is proposed to significantly improve the transient response characteristics of the dc-dc converter. By minimising the 4 transient periods T1—T4 previously described, this method can reduce the transient undershoot and settling time in the Fig. 5.2. In doing so, the over/undershoot caused by the imbalance of currents and voltages in the control loop are significantly reduced. Consider Fig.5.5, this shows the basic concept of the constant switching action. The waveform is compared to the conventional PWM switching methodology.

For a dc-dc buck converter, the characteristic differential equations which describe the two possible switching states are:

$$\text{Switch ON: } \begin{cases} i_L = \dfrac{1}{L}\int\left(V_g - i_L\left(R_L + R_C\right) - v_C + \dfrac{v_o}{R_o}R_C\right)dt \\ v_o = \dfrac{1}{C}\int\left(i_L - \dfrac{v_o}{R}\right)dt \end{cases} \tag{5.1}$$

$$\text{Switch OFF: } \begin{cases} i_L = \dfrac{1}{L}\int\left(-i_L\left(R_L + R_C\right) - v_C + \dfrac{v_o}{R_o}R_C\right)dt \\ v_o = \dfrac{1}{C}\int\left(i_L - \dfrac{v_o}{R}\right)dt \end{cases} \tag{5.2}$$

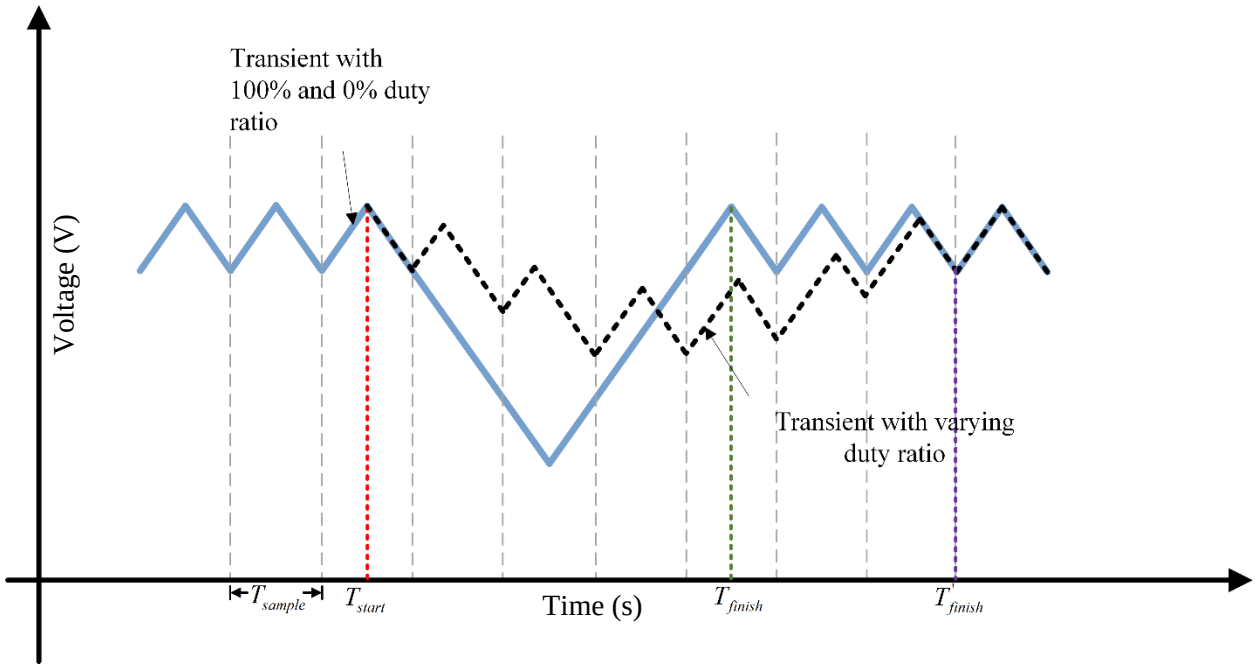

Figure 5.5 concept diagram of switching action in improvement of transient response

Here, i_L, v_o, i_0, R, C and L are the inductor current, load voltage, load current, load resistance, filter capacitance and inductance respectively. In T1, the voltage drop is caused when i_L is less than i_0. However, if the semiconductor switch is kept ON constantly, i_L will continuously increase and prevent i_0 from dropping too fast. Therefore, during T1, optimal control action can be achieved by simply holding the semiconductor switch ON (one could consider this as 100% PWM Duty Cycle during T1). In T2, the output voltage starts to recover to the steady state value. In both "ON" and "OFF" switching states, the rate of voltage rise/fall can be described as:

$$\frac{dv_C}{dt} = \frac{i_L - i_o}{C} \tag{5.3}$$

In practice, continuously triggering the ON and OFF action can be achieved by detecting when the sampled output voltage drops/increases beyond pre-set threshold. A Timer within the digital signal processor can be programmed to start recording the elapsed time following a switching action event.

Assuming good quality control and the ESRs of components can be neglected, the steady state value of the output voltage should be the same as before any transient disturbance. The current will change depending upon the output resistance. The steady state value of the inductor current, and load current, at equilibrium is given by:

$$i_o^{"} = i_L^{"} = \frac{v_o}{R^*} \tag{5.4}$$

Here, $i_L^{"}$ and $i_0^{"}$ represent the inductor current and load current after the transient period respectively, and R^* is the new resistance value following a load change (defined system disturbance). The initial current is:

$$i_o^{'} = i_L^{'} = \frac{v_o}{R} \tag{5.5}$$

The load current can be presented as:

$$\frac{di_o}{dt} = \frac{i_L - i_o}{RC} \tag{5.6}$$

Since the load suddenly changed at the start, and the inductor current cannot increase that fast to reach the current equilibrium, the load current starts drop at this moment, as shown in Eq. 5.6. However, this drop eventually would be stopped by the close loop effect, and the load current re-rise to the value at the load change point. Therefore, a positive $\frac{di_o}{dt}$ is needed. The inductor current is inevitable over the final equilibrium current to "drag" the output current as the T2 and T3 period in Fig. 5.2.

The differential equation of inductor current can be presented as:

$$\left.\frac{di_L}{dt}\right|_{OFF} = -\frac{v_C}{L} \tag{5.7}$$

As the capacitor voltage is always positive, the rate of change of inductor current is always negative during the switch at "OFF" condition. Therefore, before it reaches the equilibrium current, the switch should maintain the ON state to ride through the T1 period as soon as possible. After the inductor current exceeds the equilibrium current, the transistor can keep as "ON" state to keep increasing the inductor current, which can drag load current to approach to equilibrium current. Less worry put towards the inductor current for its recovering since when switch turns OFF, the inductor current drops fast based on the capacitor voltage. To demonstrate this, a simple simulation based on this ON/OFF method is carried out, the results of which are shown in Fig.5.6. Here, the input voltage is 60V and output voltage is 24V, and the load is changed from 100% to 20% at 0.3s. For the DC-DC buck converter, a 940μF capacitor and 860μH inductor are used in the simulation. The switching frequency is equal to the sampling frequency as 50kHz. From Fig 5.6, It shows if keep applying this ON/OFF control, the inductor current can reach its maximum value after several switching period. When the inductor current reaches its maximum value, the output voltage almost recovers to the steady state value. It means after this maximum point, the variance of load voltage can be neglected. With this approximation, the inductor current can be analysed independently with load current.

Apparently, the optimal control scheme needs a constantly ON before the inductor current reaches the equilibrium current. However, after currents reach equilibrium, either keep using constant ON/OFF control or change to conventional control scheme (duty cycle varied control) is an option for further control. It is needed to be analysed to find an optimal way to minimise the recovering time of load voltage.

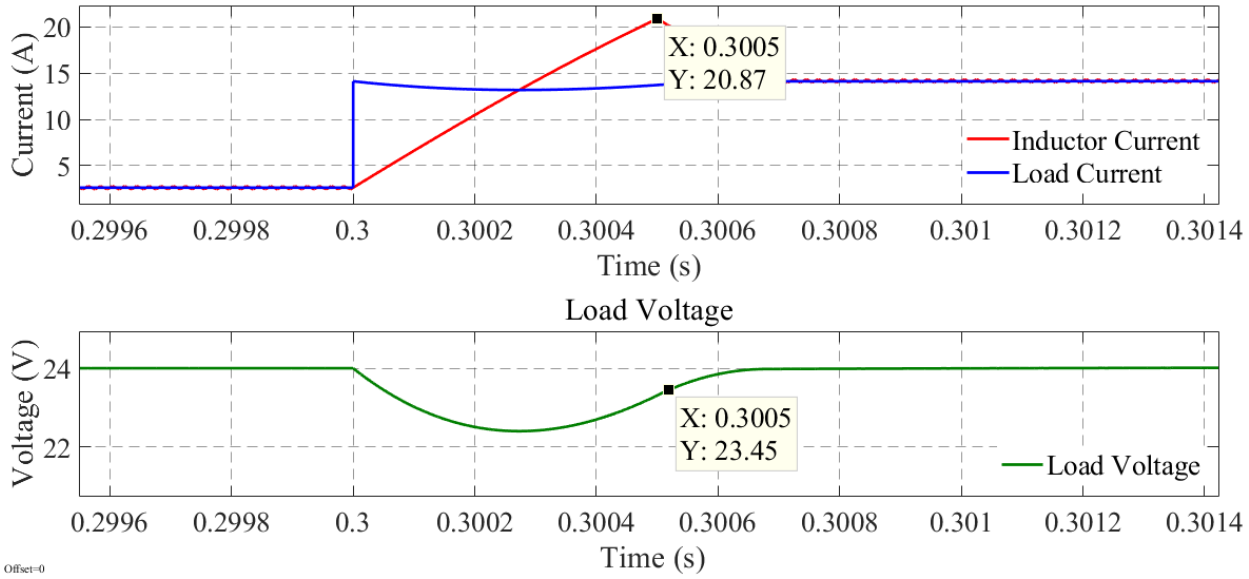

Figure 5.6 voltage recovery when ON state terminated

Whether choosing the conventional control or constant ON/OFF control, a certain rule here must be followed: When the inductor current reaches the final steady state current, assuming an optimal switching sequences to rising and dropping the inductor current as the fastest way converge load current and inductor current to the equilibrium current is applied. Then, the totally ON time define as T_{on} and totally OFF time define as T_{off} must follow:

$$\left(\frac{di_L}{dt}\right)_{on}\cdot T_{on}+\left(\frac{di_L}{dt}\right)_{off}\cdot T_{off}=\frac{V_g-v_C}{L}\cdot T_{on}-\frac{v_C}{L}\cdot T_{off}=0 \qquad (5.8)$$

To illustrate the superiority of ON/OFF control, a comparison between PID control and ON/OFF control is shown in Fig.5.7. This figure illustrates the condition after the load current suddenly increased, which is from the beginning of T1. If applying constant ON/OFF control scheme, the two currents converge like the red and blue solid lines. In contrary, the load current certain has a much slower increasing speed if applied the varied duty ratio control method (PID controller), as the load current differential equation can be presented as in Eq. 5.6. The load current increasing speed depends on the difference between inductor current and load current itself. From Eq.5.7, the inductor current is dropping when transistor is in OFF state, but load current keeps increasing in

this period due to the load current still less than inductor current. Consequently, the difference between load and inductor current is less than the difference if constant ON is applied, which decrease the slope rate of load current in next time interval. Therefore, if applying same T_{on}, the varied switching cycle method must not reach the steady state value eventually, as the green and yellow dash line in Fig.5.7. So, applying a typical duty ratio method prolongs the transient period compared with the constant ON/OFF control.

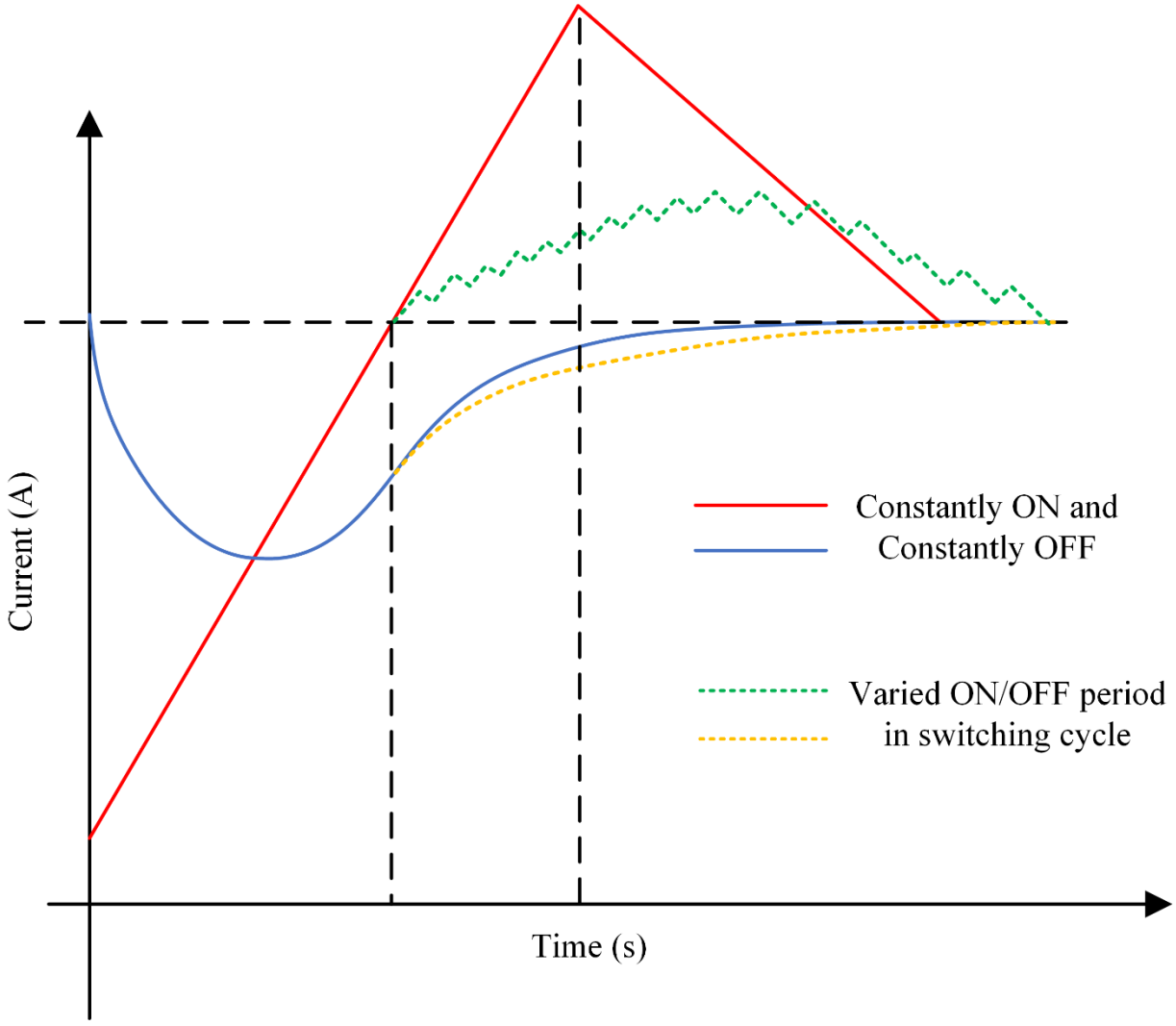

Figure 5.7 transient response between constantly ON/OFF method and conventional duty ratio method

As a conclusion, if the semiconductor switch is kept constantly ON to increase the difference between inductor current and load current, the slope rate of load voltage can be maximised. This

is a good start to minimise the recovery. However, there is a need to carefully determine the termination point of the ON period, because if the difference between the inductor and output current becomes too large, there is the potential risk of prolonging period T3 as shown in Fig. 5.2. An analysis of when to switch the transistor "OFF" is shown in Fig. 5.8. Similar as Fig.5.7, it illustrates the condition after the load current suddenly increased, which is from the beginning of T1. In Fig.5.8, three possibilities are considered to highlight the significance of the ON period termination point: Case 1: The ON period is terminated at the specific point when both inductor current and load current can converge to steady state value in OFF period. Case 2: ON period is terminated earlier than Case 1. Case 3: ON period is terminated later than Case 1. From Fig.5.8, Case 1 is the optimal solution; the second and third Cases need significantly more time to reach the steady state value. To be more specific, Case 2 reduces the crossover point between load and inductor current to below the steady state value; this causes the controller to implement an additional increment of inductor current to pull the load current up to the desired value. Likewise, if the ON period is terminated late, the current crossover point is greater than the steady state value; this causes an overshoot of load current and a further decrement of current is necessary, which will prolong the transient response further. Therefore, the optimal control scenario is to find the exact switching instant when both inductor current and load current will reach final steady state value rapidly and simultaneously. To achieve this, the exact time for constant ON and constant OFF should be established. These times can be determined through the real-time parameter estimation values of the system.

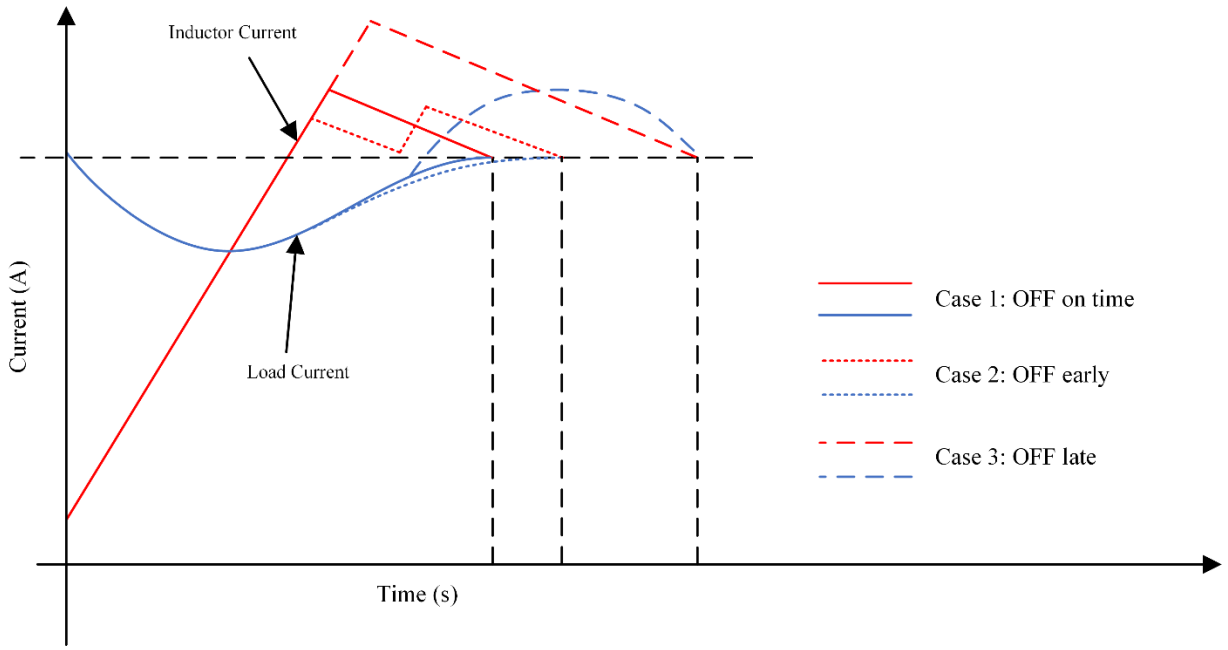

Figure 5.8 transient response analysis for inductor current

As a summary, the propose ON/OFF control method is to keep the transistor at a "ON" condition when load change occurs and switch it "OFF" and keep it "OFF" from a specific time until the current reaches balance. The next section derives this specific "OFF" time.

5.3.2 Switching ON and OFF period determination

The goal of this control scheme is finding a fastest way to converge both current to this equilibrium current using proposed ON/OFF control scheme.

To maximise the recovery speed of output voltage, the slope rate of output current must remain at least not reducing, i.e.

$$\frac{di_{o,n}}{dt} \leq \frac{di_{o,n+1}}{dt} \tag{5.9}$$

Where n stands for time interval, from the differential equation derived in chapter 3, we obtain

$$\frac{di_o}{dt} = \frac{dv_o}{R \cdot dt} = \frac{i_L - i_o}{RC} \tag{5.10}$$

Rewritten Eq.5.7 by substituting Eq.5.8, we get

$$\frac{di_{o,n}}{dt} \le \frac{di_{o,n+1}}{dt} \Leftrightarrow \frac{\left(i_{L,n+1} - i_{L,n}\right) - \left(i_{o,n+1} - i_{o,n}\right)}{RC} \ge 0 \tag{5.11}$$

The term $\left(i_{L,n+1} - i_{L,n}\right) - \left(i_{o,n+1} - i_{o,n}\right)$ means Eq.5.11 must satisfy

$$\frac{di_{o,n}}{dt} \le \frac{di_{L,n}}{dt} \tag{5.12}$$

That means inductor current increment speed must greater than load current increment speed, as the inductor current differential equation when switching on is

$$\left.\frac{di_{L,n}}{dt}\right|_{ON} = \frac{V_g}{L} - \frac{v_{C,n+1}}{L} \tag{5.13}$$

and the load current differential equation in both on and off state are shown in Eq.5.8. Substituting them into Eq.5.10 we obtain

$$i_{L,n}L - i_{o,n}\left(L - R^2C\right) \le V_g RC \tag{5.14}$$

This criterion is needed to be followed at the beginning of transient (the difference between load current and final equilibrium current is significant). It is broken after several switching cycle since this criterion is increasing the difference between $i_{L,n}$ and $i_{o,n}$, which against the final goal of both currents converge to equilibrium current. It is not worthy to maintain this criterion if the load voltage is almost recovered and inductor current is dramatic high. Converging both currents to equilibrium current value is the dominant in this moment.

The rate of change of inductor current and load current during the ON state can be presented as:

$$\begin{cases} \dfrac{dv_C}{dt} = \dfrac{i_L}{C} - \dfrac{v_C}{RC} \\ \dfrac{di_L}{dt} = \dfrac{v_g - v_C}{L} \end{cases} \Rightarrow \begin{cases} \dfrac{di_o}{dt} = \dfrac{i_L}{RC} - \dfrac{i_o}{RC} \\ \dfrac{di_L}{dt} = \dfrac{v_g}{L} - \dfrac{R}{L} i_o \end{cases} \tag{5.15}$$

From this, the discrete equivalent can be determined as:

$$\begin{cases} \dfrac{i_o(m) - i_o(m-1)}{T} = \dfrac{i_L(m)}{RC} - \dfrac{i_o(m)}{RC} \\ \dfrac{i_L(m) - i_L(m-1)}{T} = \dfrac{v_g}{L} - \dfrac{R}{L} i_o(m) \end{cases} \quad m > 0 \tag{5.16}$$

Where the *T* is the sampling period.

Likewise, the rate of change inductor current and load current in the OFF state is:

$$\begin{cases} \dfrac{dv_C}{dt} = \dfrac{i_L}{C} - \dfrac{v_C}{RC} \\ \dfrac{di_L}{dt} = -\dfrac{v_C}{L} \end{cases} \Rightarrow \begin{cases} \dfrac{di_o}{dt} = \dfrac{i_L}{RC} - \dfrac{i_o}{RC} \\ \dfrac{di_L}{dt} = -\dfrac{R}{L} i_o \end{cases} \tag{5.17}$$

From this, the discrete equivalent is:

$$\begin{cases} \dfrac{i_o(n) - i_o(n-1)}{T} = \dfrac{i_L(n)}{RC} - \dfrac{i_o(n)}{RC} \\ \dfrac{i_L(n) - i_L(n-1)}{T} = -\dfrac{R}{L} i_o(n) \end{cases} \quad n > m \tag{5.18}$$

Here the *m* and *n* stand for the number of discrete time interval steps, *m* is the switching ON number of steps and *n* is totally number of steps since the ON/OFF control applied. All inductor current and load current can be measured directly via a typical current sensor, or in low cost applications estimated by the new load value. Also, with estimated parameter in system identification process, the equilibrium current value can be determined easily. Therefore, the final value of $i_o(n)$ and $i_L(n)$ is equal to this equilibrium current, substitute them into Eq.5.18 can form to two number series equations. Similarly, the initial value of $i_o(m)$ and $i_L(m)$ can be obtained when the voltage drop is sensed. Another two number series equations can be formed. Based on these two number series equations, *m* and *n* can be found when

$$\begin{aligned} & i_o(m) = i_o(n) \\ & \textit{or} \\ & i_L(m) = i_L(n) \end{aligned} \tag{5.19}$$

Therefore, the number of time intervals *m* and *n* can be calculated via R (resistance before load changed), R^* (resistance after load changed), C, L, $i_o(m)$, $i_o(n)$, $i_L(n)$ and $i_L(m)$. Except current signal, all parameter values must be estimated by the system identification process before the switch OFF period commences.

Here, a detailed derivation for *m* and *n* calculation is presented. Eq.5.20 can be obtained from Eq.5.16 as

$$\frac{RCL+LT+RT}{RCLT} i_o(m) = \frac{1}{T} i_o(m-1) + \frac{v_g T}{RCL} + \frac{1}{RC} i_L(m-1) \qquad (5.20)$$

Similarly, the $i_L(m)$ can be presented as Eq.5.21 by rearrange Eq.5.16

$$\left(1+\frac{RT^2}{RCL+LT}\right) i_L(m) = \frac{v_g T}{L} - \frac{R^2 CT}{RCL+LT} i_o(m-1) + i_L(m-1) \qquad (5.21)$$

With the knowledge of $i_L(0)$ and $i_o(0)$, two sequences of $i_L(0,1,\cdots m)$ and $i_o(0,1,\cdots m)$ can be obtained from Eq.5.20 and Eq.5.21.

From Eq.5.18, with the knowledge of $i_L(n) = i_o(n) = i_{equilibrium}$, two sequences of $i_L(n, n-1, \cdots, n-n_0)$ and $i_o(n, n-1, \cdots, n-n_0)$ can be obtained. When $i_o(n-n_0) = i_o(m)$ or $i_L(n-n_0) = i_L(m)$, the number of each sequence therefore can be obtained, which the *m* and *n* is determined. The equation $T_{on} = T \cdot m$ and $T_{off} = T \cdot n$ can be used to calculate the on-state period and off-state period.

5.4 Mathematical model for the system identification in current balancing constant ON/OFF control

As illustrated in chapter 2, the conventional mathematical model for system identification is derived from the control to output transfer function of SMPCs. It suffers several problems caused by limited sampling point. Also, a PRBS signal must be injected to the duty ratio to artificially create a frequency-rich input signal for system identification. To be more specific, due to the limited sampling point as shown in Fig. 5.9, less than hundred data points are sampled. This number of sampling points cannot be used to estimate a correct parameter value by adaptive algorithm. Therefore, the conventional mathematical model cannot be applied into this control scheme for system identification. In this section, a new mathematical model is developed to resolve this problem. This mathematical model does not suffer those restrictions and much simpler than conventional mathematical model.

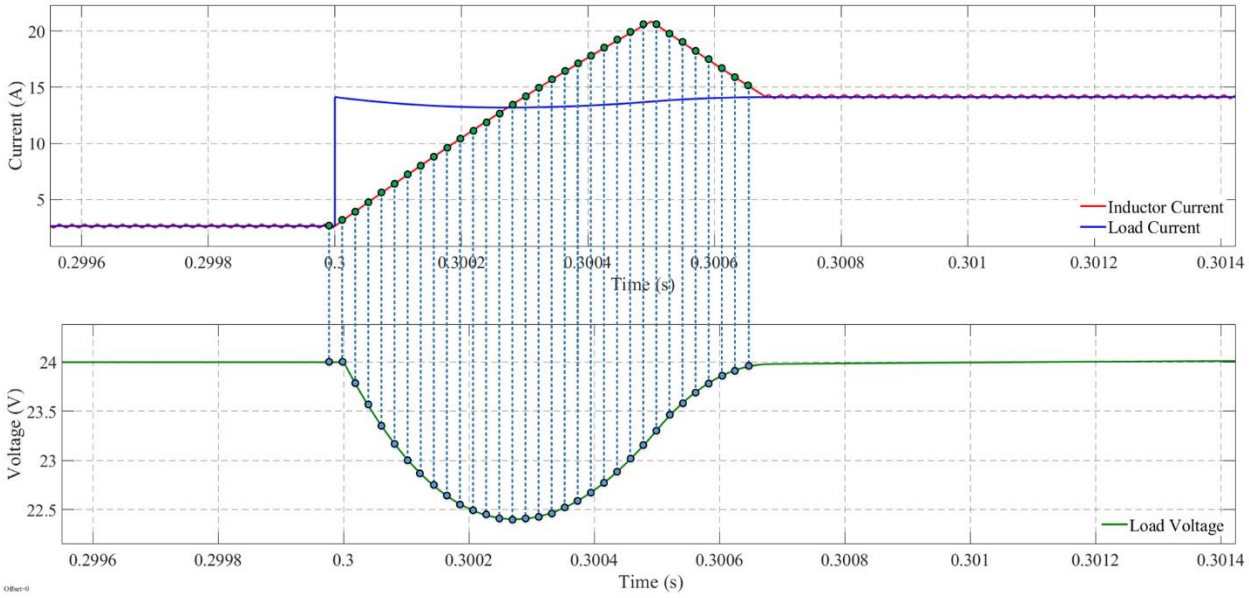

Figure 5.9 Limited sampling points if applying conventional sampling and mathematical method (50kHz sampling frequency)

Consider the differential equation series when the load abrupt change happens and a constant ON action is applied. Differential equation to describe current relationship can be presented as

$$i_L = \frac{v_o}{R} + C\frac{dv_C}{dt} \tag{5.22}$$

Where $\frac{dv_C}{dt}$ can be represented as

$$\frac{dv_C}{dt} = \frac{d\left(v_o - \left(i_L - \frac{v_o}{R}\right)R_C\right)}{dt} = \frac{dv_o}{dt} - R_C\frac{di_L}{dt} + \frac{R_C}{R}\frac{dv_o}{dt} \tag{5.23}$$

Rearrange Eq.5.23, we obtain

$$i_L = \frac{v_o}{R} + C\left(\frac{dv_o}{dt} - R_C\frac{di_L}{dt} + \frac{R_C}{R}\cdot\frac{dv_o}{dt}\right) \tag{5.24}$$

If the i_L is considered as input and v_o is output, the difference equation can be written if applied Euler's method as

$$v_o(n) = \underbrace{\left(\frac{RCR_C + RT}{T + R_C C + RC}\right) i_L(n)}_{\text{(a)}} - \underbrace{\left(\frac{RCR_C}{T + R_C C + RC}\right) i_L(n-1)}_{\text{(b)}} + \underbrace{\left(\frac{R_C C + RC}{T + R_C C + RC}\right) v_o(n-1)}_{\text{(c)}} \quad (5.25)$$

Uses term (b) divided by term (c) we obtain

$$\frac{\left(\frac{RCR_C}{T + R_C C + RC}\right)}{\left(\frac{RC + R_C C}{T + R_C C + RC}\right)} = \frac{RR_C}{R + R_C} = R \,||\, R_C \quad (5.26)$$

The R_C can be obtained from datasheet of load capacitor, in dc condition, R_C usually remain a steady value.

If the dc-dc buck converter has several load capacitors connecting in parallel to minimising the R_C and increasing capacitance, the R_C can be neglected. In this case, $v_o = v_c$, the Eq.5.24 can be reformed to

$$i_L(n) = \underbrace{\left(\frac{1}{R} + \frac{C}{T}\right) v_o(n)}_{\text{(a)}} + \underbrace{\left(-\frac{C}{T}\right) v_o(n-1)}_{\text{(b)}} \quad (5.27)$$

In this case, R can be obtained using term (a) plus term (b) and do the inversion.

Eq.5.25 and Eq.5.27 are followed the standard ARX model as Eq.3.23. It has the certain numbers of output(s) from previous steps and may have the input(s) from previous input, which satisfy the description of Eq.3.23. This means the FAP or RLS algorithm can be applied if sensing the i_L and v_o as the sampling data. Due to the constant ON action, Eq.5.25 or Eq.5.27 are not obtained from averaged state space model. These two equations can describe the waveform behaviour any time during the constant ON period. The sampling frequency is not limited by the switching frequency. Additionally, due to the sampled signal is physical signal as voltage/current waveform, the inevitable system noise is counted to increase the variance of the signal. As illustrate in Chapter 3, the noise can be considered as an injected signal to enrich the frequency response. Therefore, the PRBS signal is unnecessary to inject for system identification purpose. Moreover, the system order is reduced from 4 (2 inputs and 2 outputs) to 3 (2 inputs and 1 output—$i_L(n)$, $i_L(n-1)$ and

$v_o(n-1)$) or 2 (2 outputs—$v_o(n-1)$ and $v_o(n)$). This will dramatically reduce the computational cost in system identification process.

5.5 Simulation verification of system identification and current balancing ON/OFF control

An example dc-dc buck converter system is built in MATLAB, the system parameters are as follows: $V_g = 60\text{V}$, $V_o = 24\text{V}$, $C = 780\mu\text{F}$, $L = 860\mu\text{H}$, $R = 9.2\Omega$, $f_s = 50\text{kHz}$. All ESRs are neglected in this case. A conventional output voltage feedback control loop is applied in this system. To test the dynamic performance, an instantaneous load change is applied to the system at 0.3 seconds; the resistive load drops from 9.2 Ω to 1.7 Ω. A certain voltage threshold is set in output point to trigger the system identification process. After the voltage exceed the threshold, the system identification technique is applied. The result shows in Fig.5.8 and Fig.5.9. From Fig.5.8 and Fig.5.9, the estimation curve converges to steady state value in less than 0.1ms. This is an important metric, because the parameter estimation must be less than the smallest ON/OFF switching period likely to be determined by the proposed controller. Fortunately, as shown by the results in Fig.5.8 and Fig.5.9, this is shown to be the case by a significant margin. To be more specific, it spends around 0.1ms for FAP algorithm to estimate the parameter value of Eq.5.25. When operating in real time, the proposed controller must receive the parameter estimation values rapidly to allow enough time for "ON" and "OFF" period determination. Because of optimal determination of ON and OFF time, the controlled voltage waveforms comparison and current waveforms are shown as Fig.5.12 and Fig.5.13 respectively.

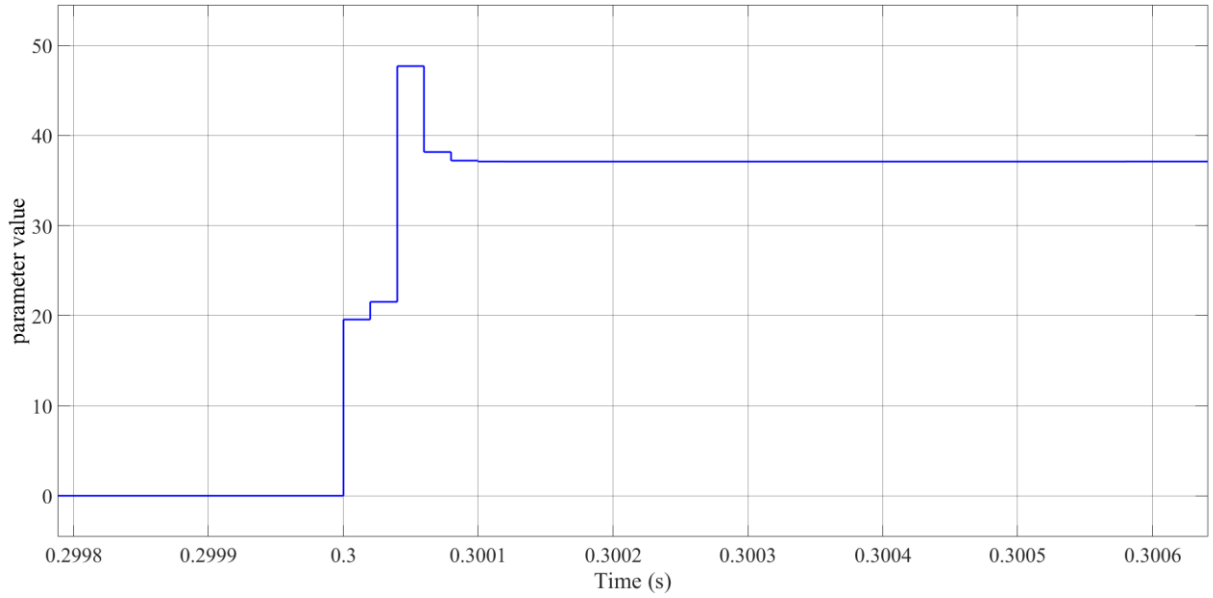

Figure 5.10 first parameter convergence curve

Fig.5.12 and Fig.5.13 show the influence of an abrupt load change on the voltage and current waveform. In Fig.5.12, the red curve is obtained by applying a conventional PID controller as a voltage feedback compensator in the system. All the parameter of PID controller is derived based on the example shown in Section 3.6 in Chapter 3. The blue curve is obtained by applying the proposed Constant ON/OFF control method.

From Fig.5.13, after the converter goes through the constant "ON" and constant "OFF" period, the two current waveforms simultaneously converge to the steady state value. The red curve, inductor current, is increased during the constant ON period; which is the charge period, and the curve dropped in constant OFF period; which shows the inductor is discharging. This confirms the theory presented above. From Fig.5.11, several overshoots and undershoots arise from the PID controller result. Closer inspection shows that the system experiences repeated oscillations to reach current and voltage balance. In comparison to this, the proposed method eliminates the subsequent oscillation after the constant ON and OFF period; a single overshoot event arises, and the controller significantly minimises the transient period. To be more specific, the valley point from 17.71 volts to 22.41 volts and the steady state reach faster—from 0.3131s to 0.3007s.

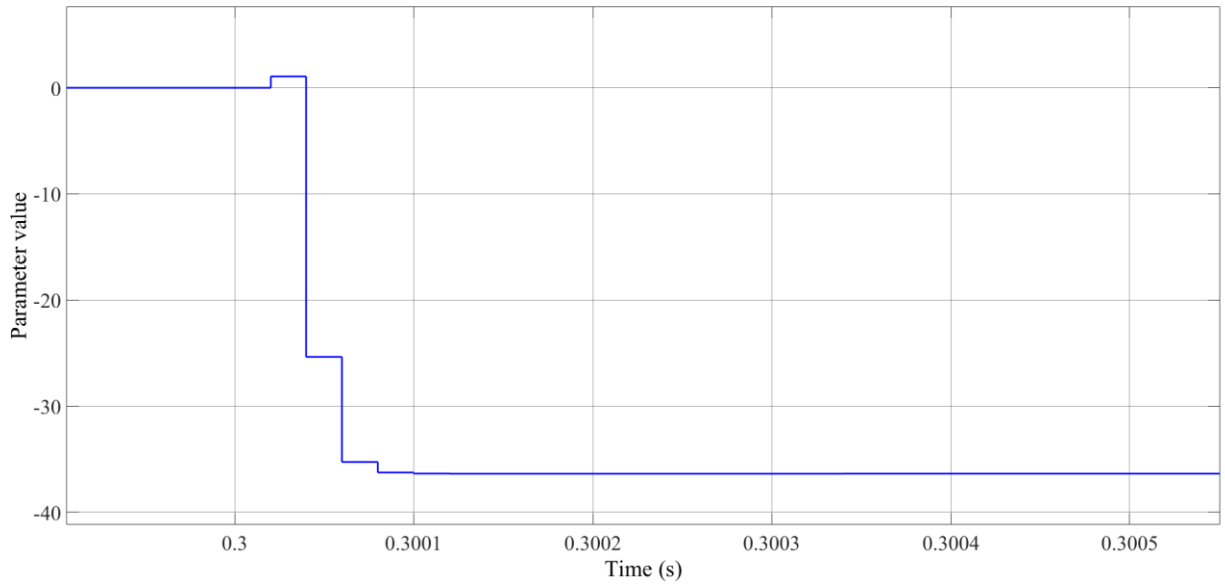

Figure 5.11 second parameter convergence curve

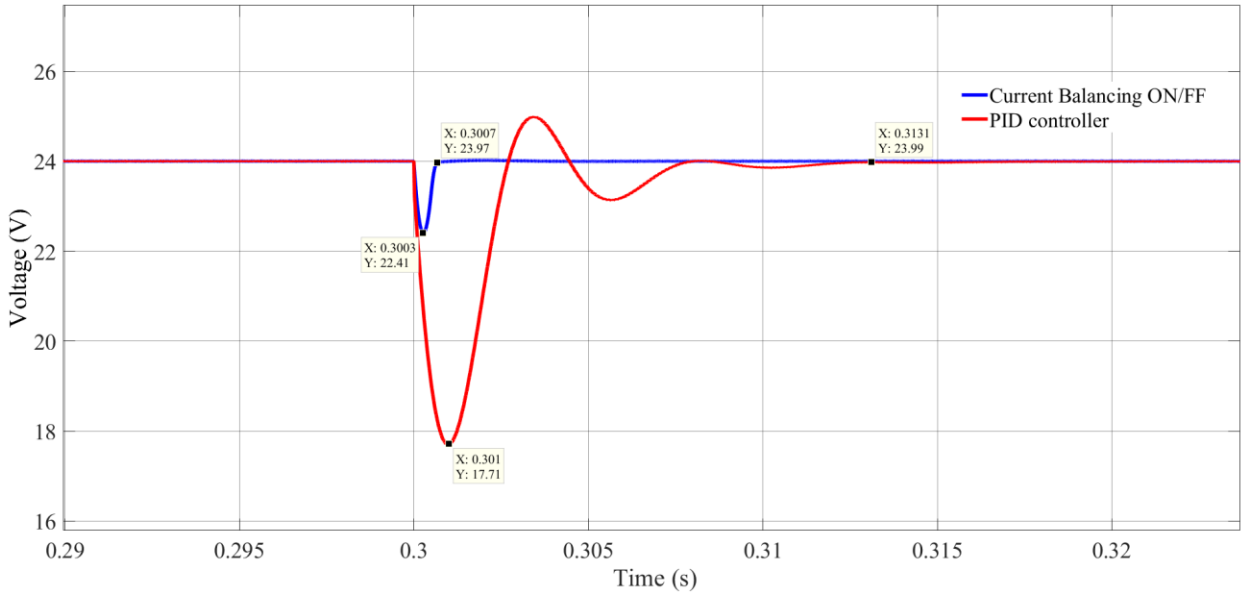

Figure 5.12 voltage transient response comparison between two control schemes

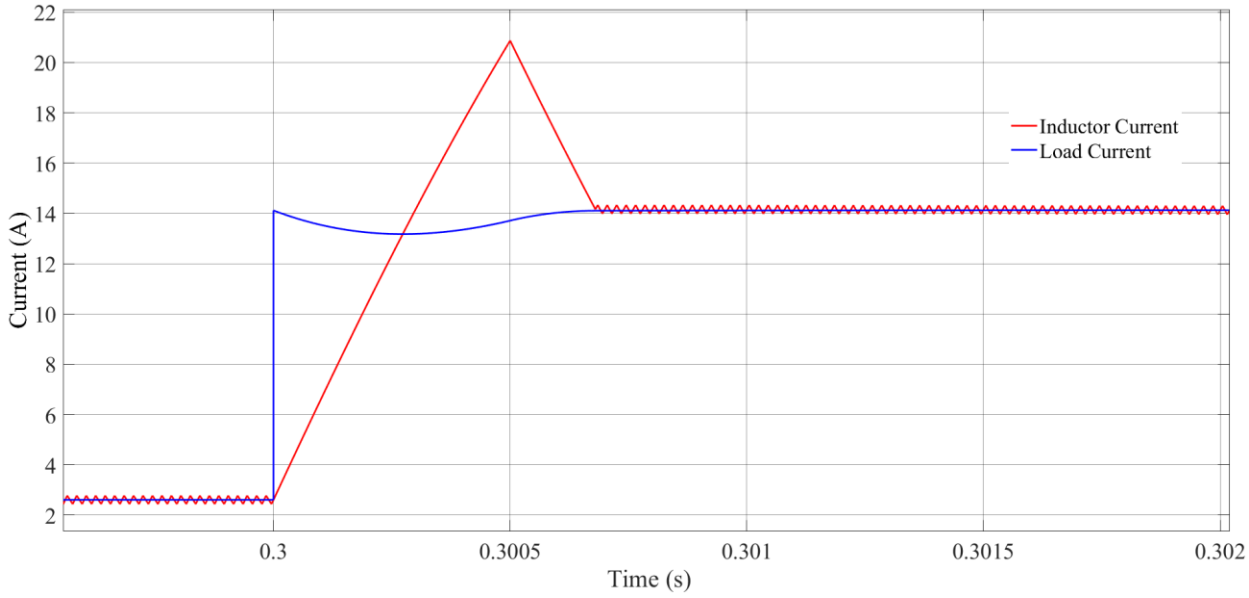

Figure 5.13 current transient curves of inductor current and load current

Another simulation test has been done to validate this Current Balancing ON/OFF control in a small load change condition. In this case, the resistive load drops from 10.9 Ω to 7.5 Ω. The simulation result of voltage comparison and the current balancing result is shown in Fig. 5.14 and Fig. 5.15 respectively.

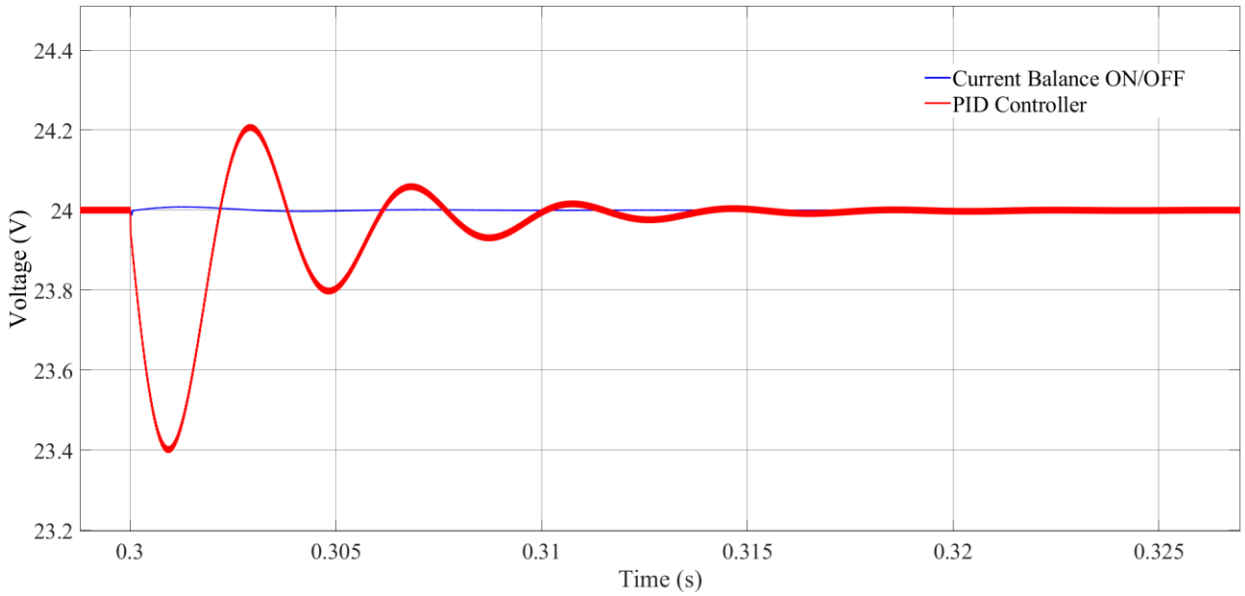

Figure 5.14 voltage transient response comparison between two control schemes in a small load change condition

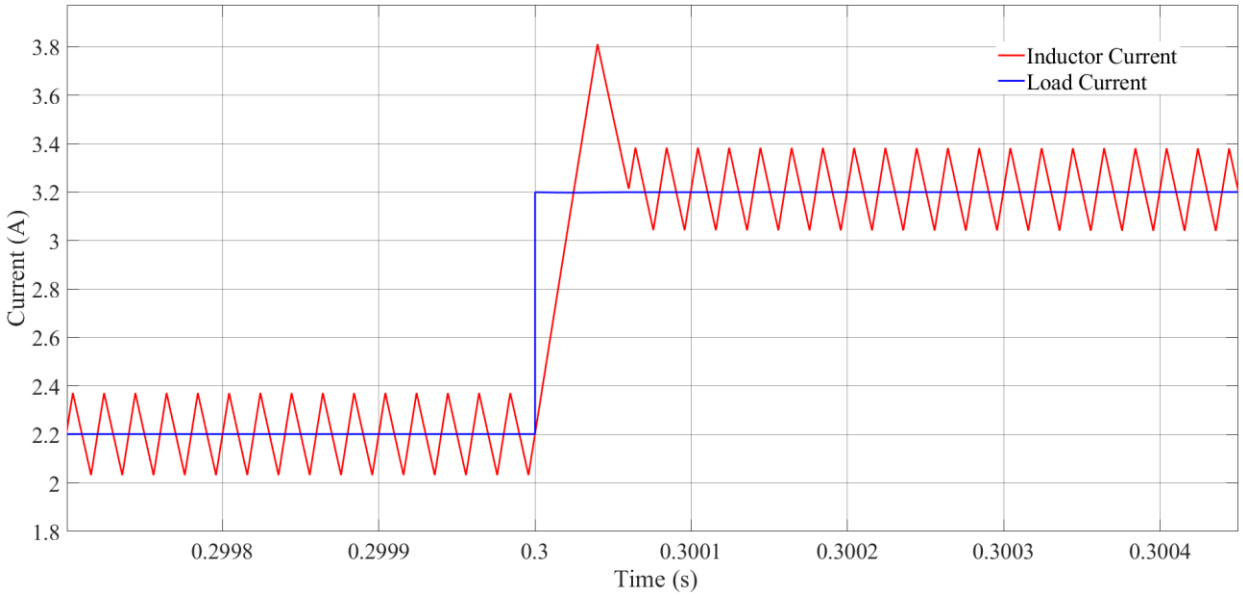

Figure 5.15 current transient curves of inductor current and load current in a small load change condition

From Fig.5.14, the excellent voltage dynamic response can be seen when applying the Current balancing ON/OFF control. However, from Fig.5.15, the ON and OFF period is quite short which less than 100μs. It is impossible to identify the parameter in such short period. In this case, the ON and OFF time are calculated with the prior knowledge of the load change. Therefore, even the current balancing ON/OFF method can provide a very good dynamic response. The requirement of awareness the resistance variation is a significant restriction for applying this method in practice. Also, this method requires a very high-speed microprocessor and ADC unit to sample and calculate the load variation value and ON/OFF time. This is another limitation of this method.

5.6 Chapter summary

This chapter presents a new system identification technique and adaptive control scheme for dc-dc converter control. The proposed adaptive controller considers an inductor/load Current Balancing ON-OFF (CBOO) control strategy to improve the transient performance of the power converter system during abrupt load changes. Such events are typical in many power electronic systems, particularly Switched Mode Power Supply applications. In these systems, a fast-dynamic response is essential to preserve the dynamic performance and efficiency of the system. The results presented demonstrate the robustness of the proposed CBOO and highlight the superior performance of the controller compared to solutions such as the conventional PID controller.

Chapter 6. Experiment verification of system identification and adaptive control in DC-DC buck converter system

6.1 Introduction

With the rapid development of microprocessor and microcontroller technologies, many digital signal processors (DSP) are now widely using in electrical and electronics engineering applications. Such devices offer fast computational speed, integrated features, and increasingly cost-effective solutions. As a result, digital control platforms have been widely used in power electronics system and being an alternative of analogue control method [108-111]. To fully validate the proposed system identification technique and adaptive control method described in previous chapters an experimental synchronous DC-DC buck converter, controlled via a Spectrum Digital eZdsp™ Texas Instruments™ F28335 development board, is considered. This chapter describes the experiment hardware and the implementation process. Finally, experiment result is presented to verify the proposed adaptive algorithm and adaptive control scheme.

6.2 TMS320F28335 Digital Signal Processor platform

A DSP is a dedicated type of microprocessor that can be programmed by general-purpose programming language such as C, C++ and C#. The implemented DSP—TMS320F28335 is a member of the TMS320C28x/ Delfino™ DSC/MCU generation release in 2007. Due to its highly integrated, high-performance solutions features, many advanced control applications have been used it as the platform for digital control [9-13].

The main clock frequency is up to 150MHz (6.67ns per cycle time). With Harvard Bus Architecture and Unified Memory Programming Model, the chip can be easily programmed and integrated. Up to 512KB flash memory and 68KB RAM is sufficient to store sampled data.

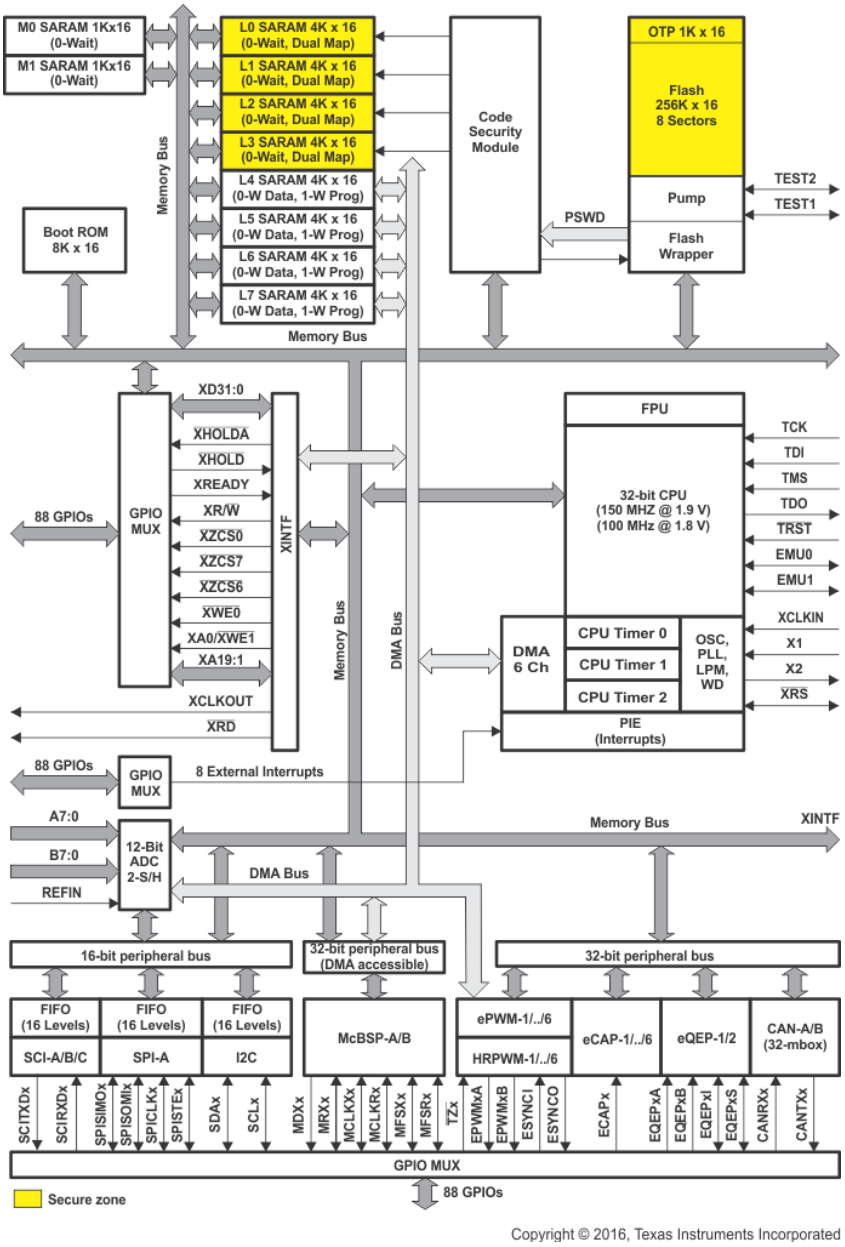

Figure 6.1 function diagram of TMS320F28335[76]

With 16-off 12-bit ADC channels with single/simultaneous conversion and 80 ns conversion rate, it can fast enough to receive and process analogue signals from a typical power converter system. Additionally, 3 CPU-timers is in this chip, which can be implemented in different asynchronous control schemes to vary the different outputs via EPWM blocks. Up to 18 PWM outputs and 6 High-Resolution PWM (HRPWM) outputs are sufficient to control most conventional power

electronic converter systems. Each EPWM channel can be independently programmed to generate symmetric or asymmetric PWM waveforms. Each EPWM module has its own programmable sub-modules to achieve event-trigger and dead-band generation.

6.3 Microprocessor programming and communication platform

The adaptive algorithm and adaptive control scheme are implemented via real time software which is downloaded to the DSP. An integrated development environment (IDE) package used to program and compile the code for the DSP. Here, TI's Code Composer Studio (CCS) is used, which supports C, C++ and C# programming languages. Additionally, to easily monitor the SMPC system operation and output dataflow, a graphical control platform is necessary. National Instrument (NI) Labview is used for this purpose (see Fig.6.2.). Sampled data is directly sent to a host PC via a USB port for use by Labview. Labview presents the data in real time whilst the SMPC is operating. Conveniently, the DSP register bits can also be modified in Labview allowing for greater flexibility to control the system operation. Similarly, Matlab & Simulink developed embedded Code Support Package (CSP) and Real Time Workshop (RTW) toolbox [94] to achieve the same visual communication and online monitoring. Compared with Labview, CSP do not need any coding to build the connection between the visual platform and DSP. Additionally, CSP provide more user-friendly platform to vary the register value without any coding. Each register's function is tagged by a label as a function description. As shown in Fig.6.3, user do not need to find the register address but easily understand the functionally of each bit in registers. Both CSP and Labview are dependent with the programme compiling in CCS.

Figure 6.2 Labview control panel

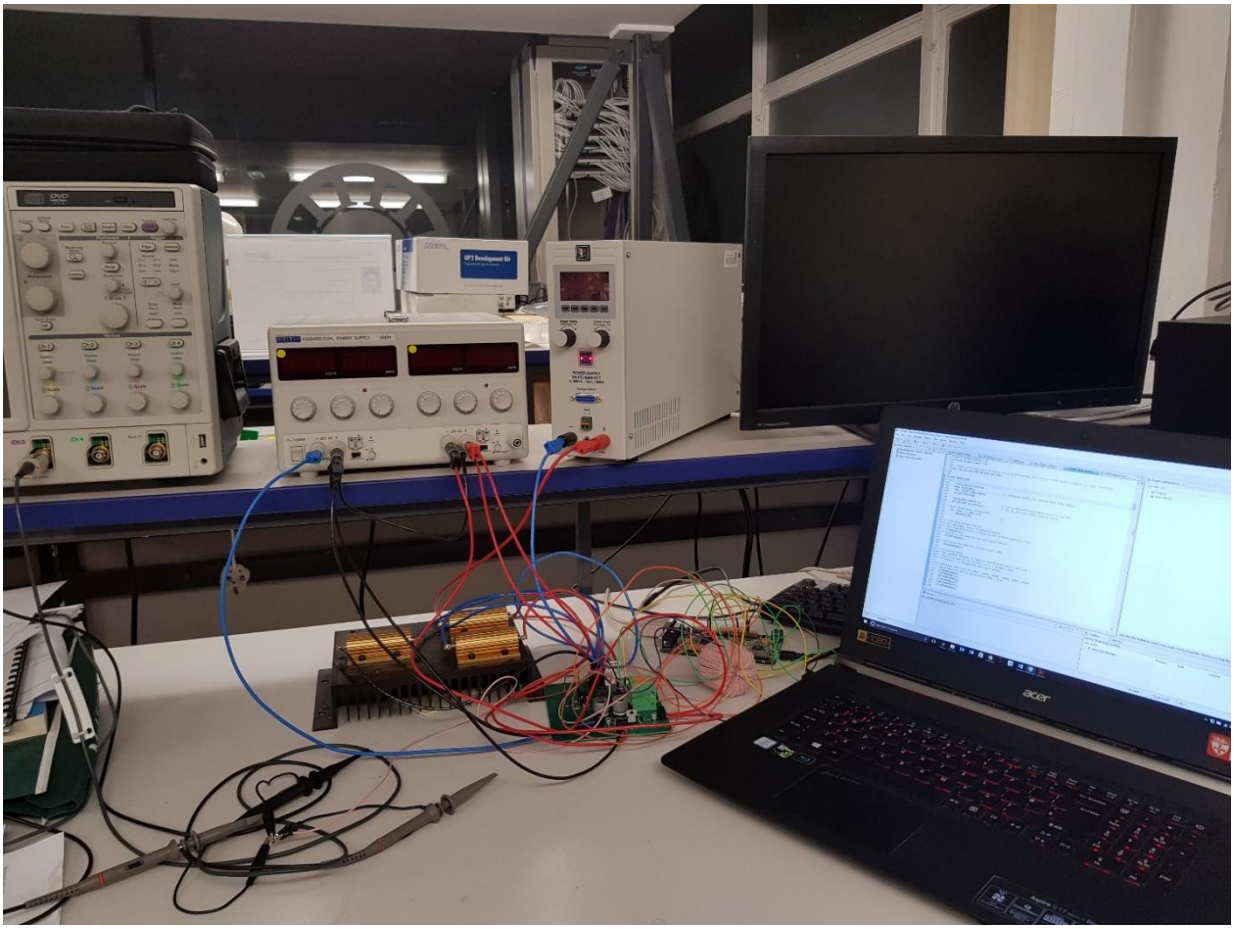

Figure 6.3 experiment platform setup

6.4 Hardware description and DSP setup

The whole experiment hardware platform is shown as Fig.6.4, six/three power resistors are connected to build an adjustable system load for the synchronous DC-DC buck power converter (in Fig. 6.4, three resistors are connected to the converter system). Totally, two branches of load resistors can be connected as load resistor, each branch has three resistors, one of them is 15Ω and other two (6.8 Ω) are connected in parallel. All resistors are selected as power resistors and mounted on a heatsink, both of them can suffer a high-power emission. In full load condition, the total resistance is 9.2Ω ([(6.8Ω//6.8Ω)+15Ω]//[(6.8Ω//6.8Ω)+15Ω]). There are two 6 pins pluggable sockets are mount on the PCB, each socket can connect with one load branch. By switching the MOSFETs connected with resistors, the load can be varied from 9.2Ω to 1.7Ω or from 18.4Ω to 3.4Ω (One branch is disconnected). Both conditions are simulating the extreme load changing condition (100% to around 20%). Two Surface Mounted Device (SMD) aluminium electrolytic capacitors are connected in parallel as the load capacitor. As a result, the capacitance is increased and ESR is halved. A silk-covered litz-wire wind into magnetic coil constructing an inductor are connect with the socket outside the PCB. It is flexible to add or reduce the round number to increase/decrease the inductance. Two DC power supplies are responsible empower the ICs and the input voltage of synchronous buck converter (See Appendix A for the schematic diagram of DC-DC buck converter circuit).

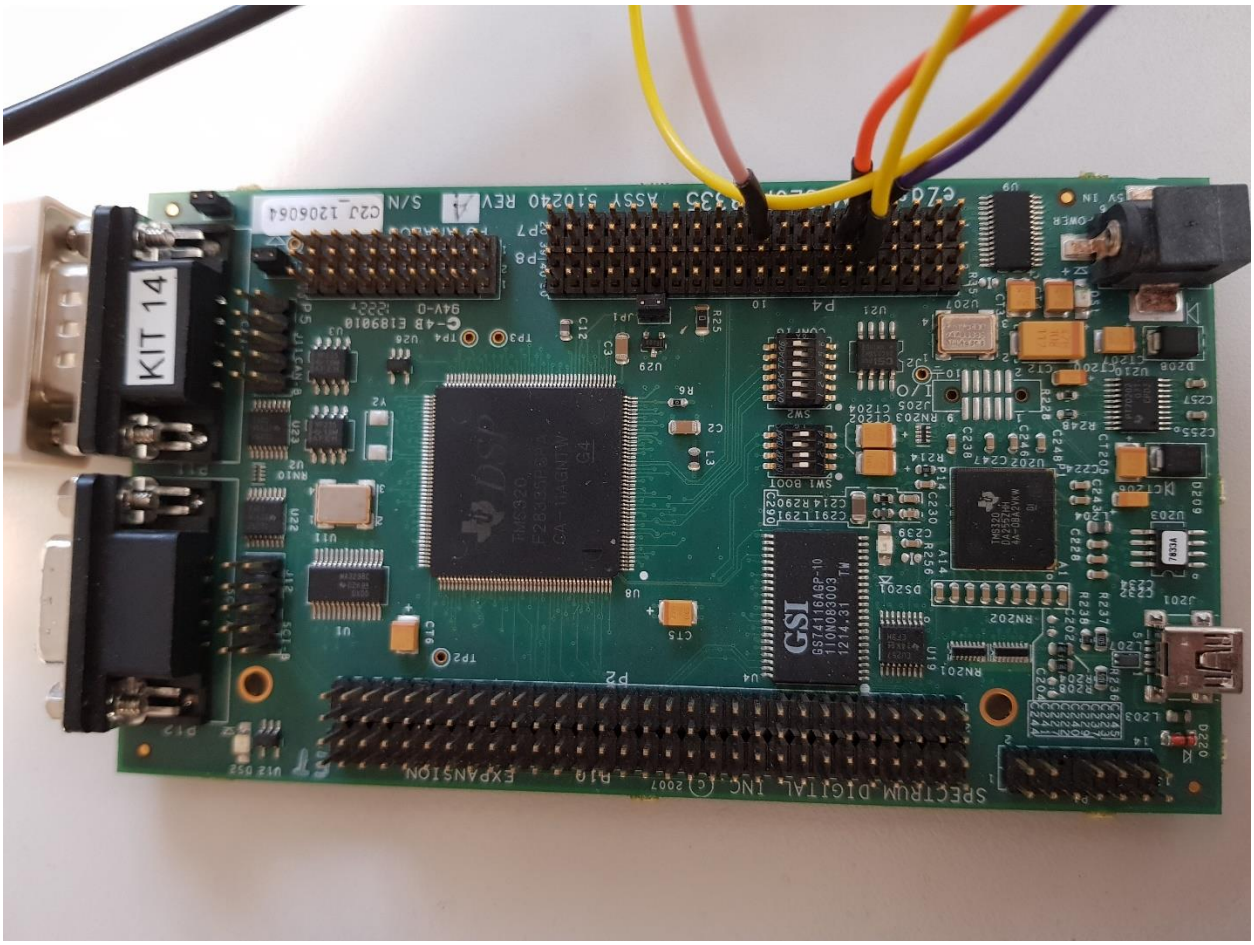

Figure 6.4 Spectrum Digital eZdsp™ Texas Instruments™ F28335 board platform

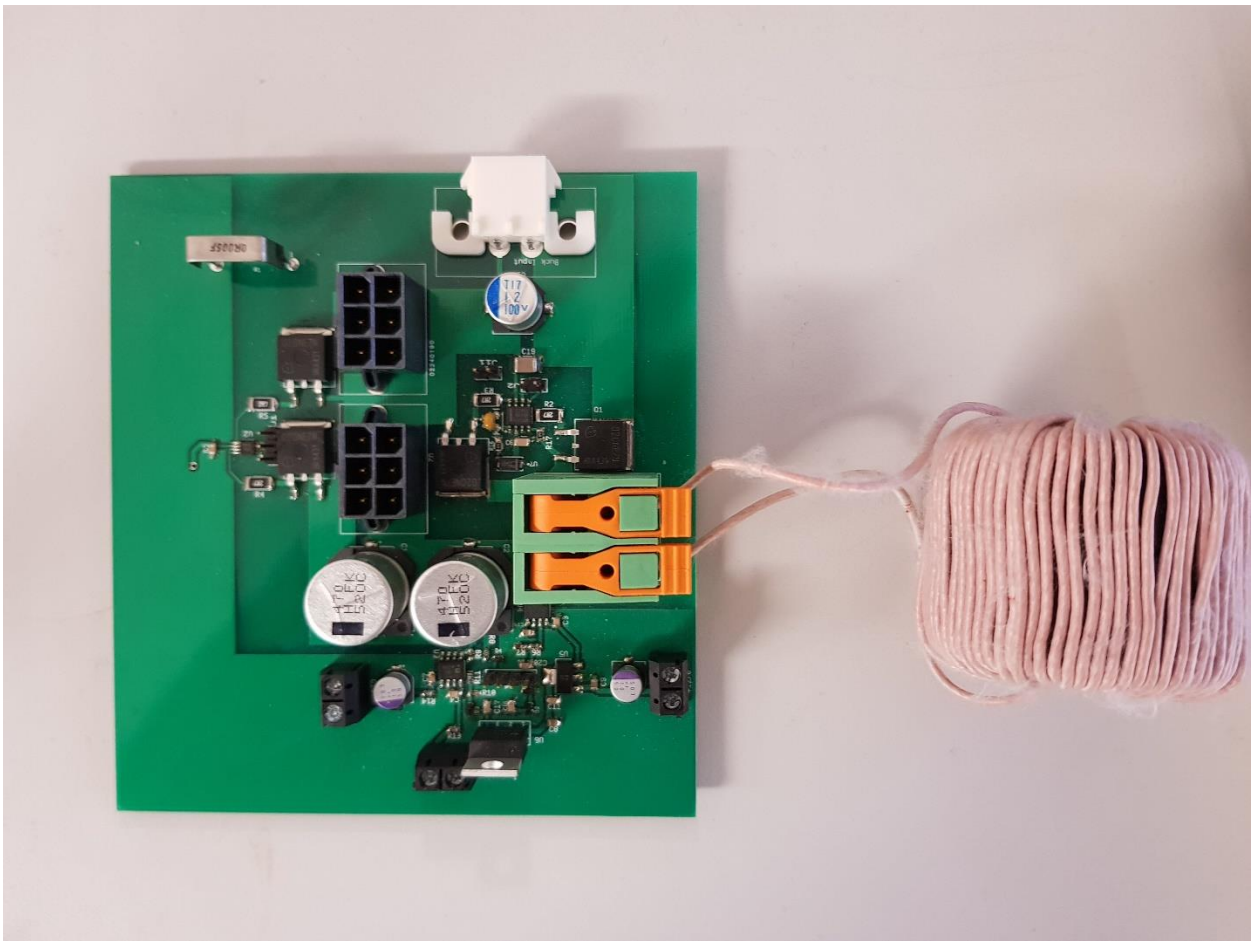

Figure 6.5 DC-DC buck converter circuit (without load)

With closer inspection, the synchronous buck DC-DC converter controlled by four power MOSFETs. Two MOSFETs are responsible for the operation of buck converter and the other two are responsible for load changing. All four MOSFETs are N-Channel with very low ON-resistance, which can significantly eliminate parameter estimation error caused by inaccurate resistance. Also, the turn ON/OFF action is achieved rapidly; in the order of several nanoseconds only. The two buck converter control MOSFETs are connected to a bootstrap MOSFET driver, by charging/discharging the bootstrap capacitor and making use of an ultrafast bootstrap diode, the high side MOSFET can rapidly transition between the ON and OFF states. Such fast switching behaviour helps facilitates the implementation of the proposed Current Balancing ON/OFF control scheme. With respect to the output voltage measurement, a high-precision voltage divider comprising of 100k (0.1%) Ω resistors are connected in parallel with the load power resistors. The

output of the potential divider circuit is fed into an instrumentation amplifier (AD8421BRZ) for further signal conditioning; mainly voltage level shifting to facilitate the interface to the DSP.

With ultra-low DC offset, low drift, high input impedance and much wider bandwidth compared to a conventional isolation amplifier, the chosen instrumentation amplifier is an ideal an isolation device between the power and digital circuits. Following this, a diode clamp circuit is incorporated to provide overvoltage protection for DSP. This comprises of two series connected Schottky diodes strapped across a 3V voltage source, with the midpoint connection going to the DSP. For the current measurement a Hall-effect current sensor is connected in series with the inductor. The Hall Effect current sensor offers galvanic isolation and produces a highly linear output voltage which is proportional to the current flowing in the circuit. Again, a diode clamp protection circuit is implemented prior to the interface to the DSP.

The key parameters of the prototyped synchronous buck converter are listed in Table.6.1. A closer view of Spectrum Digital eZdsp™ Texas Instruments™ F28335 board platform and synchronous buck converter is shown as Fig.6.5 and Fig. 6.6. Corresponding with Fig.6.4, the schematic system communication platform is presented in Fig.6.7.

Symbols	Parameter description	Parameter value
V_g	Input voltage	60V
V_o	Output voltage	24V
$I_{o\max}$	Maximum current	14A
L	Inductor	760μH
C	Capacitor	940μF
R_C	Capacitor ESR	25mΩ
R_L	Inductor ESR	0.475Ω
R_o	Load resistor	18.4Ω to 3.4Ω
		9.2Ω to 1.7Ω
f_{switch}	Switching frequency	50kHz

Table 6.1 Synchronous DC-DC buck converter parameters

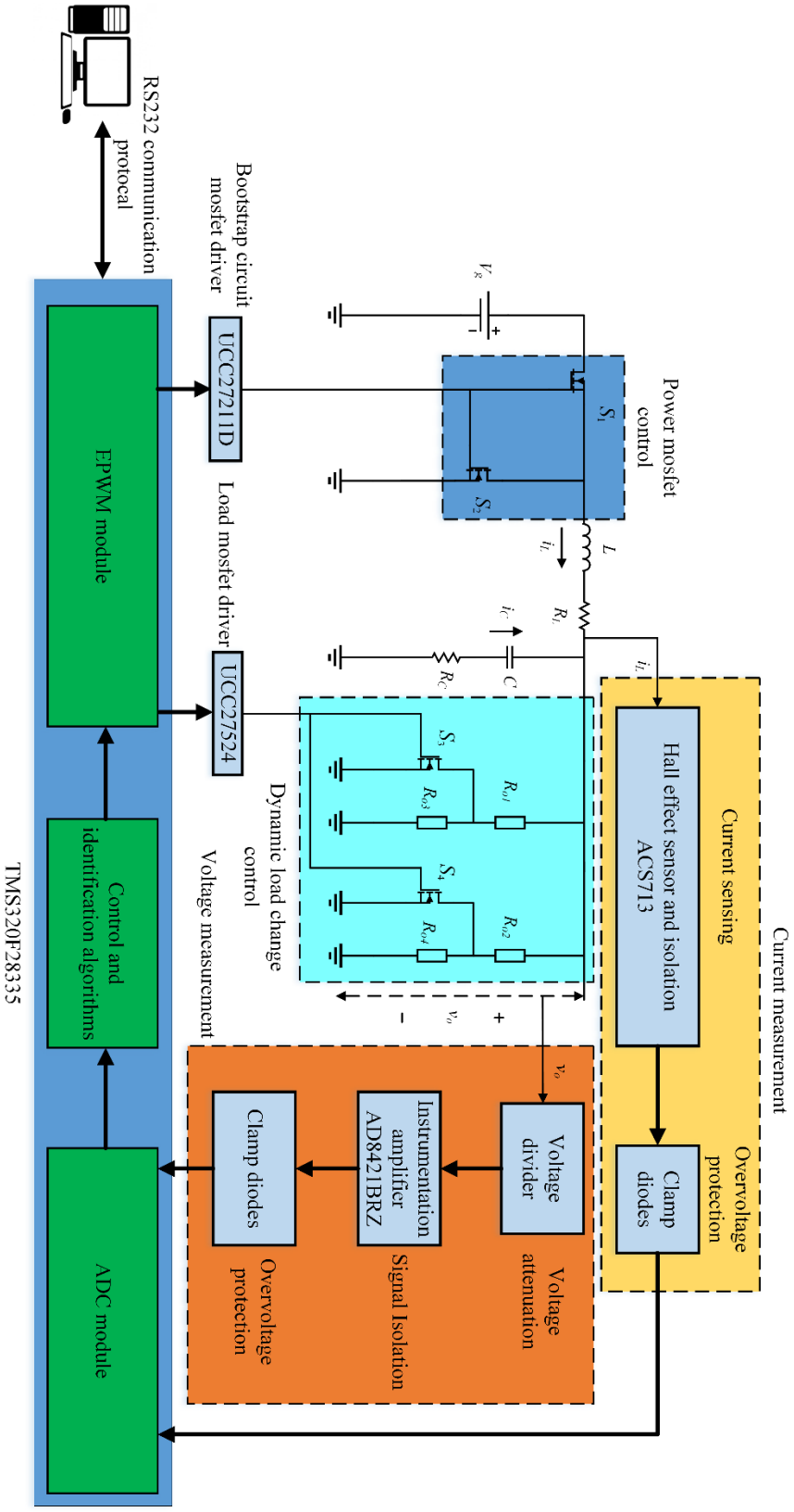

Figure 6.6 schematic system communication platform

Initially, basic PWM waveform generation is confirmed. From Fig.6.8, three PWM waveforms are generated by the DSP – two are required to control the buck converter operation and one to enable abrupt load variation. This is achieved via the EPWM modules EPWM1A, EPWM1B and EPWM2A in the TMS320F28335. In open loop conditions, two synchronous but opposite polarity 50 kHz PWM waveforms are generated from EPWM1A and EPWM1B (shown as yellow and azure traces). These two PWM waveform control the switching condition of two N-channel MOSFETs for buck converter operation [97]. In open loop, a 50% duty cycle and 25% duty cycle are presented in Fig.6.9 and Fig.6.10 respectively. The third PWM signal, shown in green, is generated by EPWM2A and controls the MOSFET connected to the load resistors. By switching from low side to high side, the load resistance is changed from 18.4 Ω to 3.4 Ω or 9.2 Ω to 1.7 Ω dependent upon how many resistor series are connected at the terminal. For testing, the frequency of signal for enable the abrupt load variation is 50 Hz, which means the load change occurs every 20ms. This 20ms is enough time for dynamic response and regulating the voltage to a new steady state value.

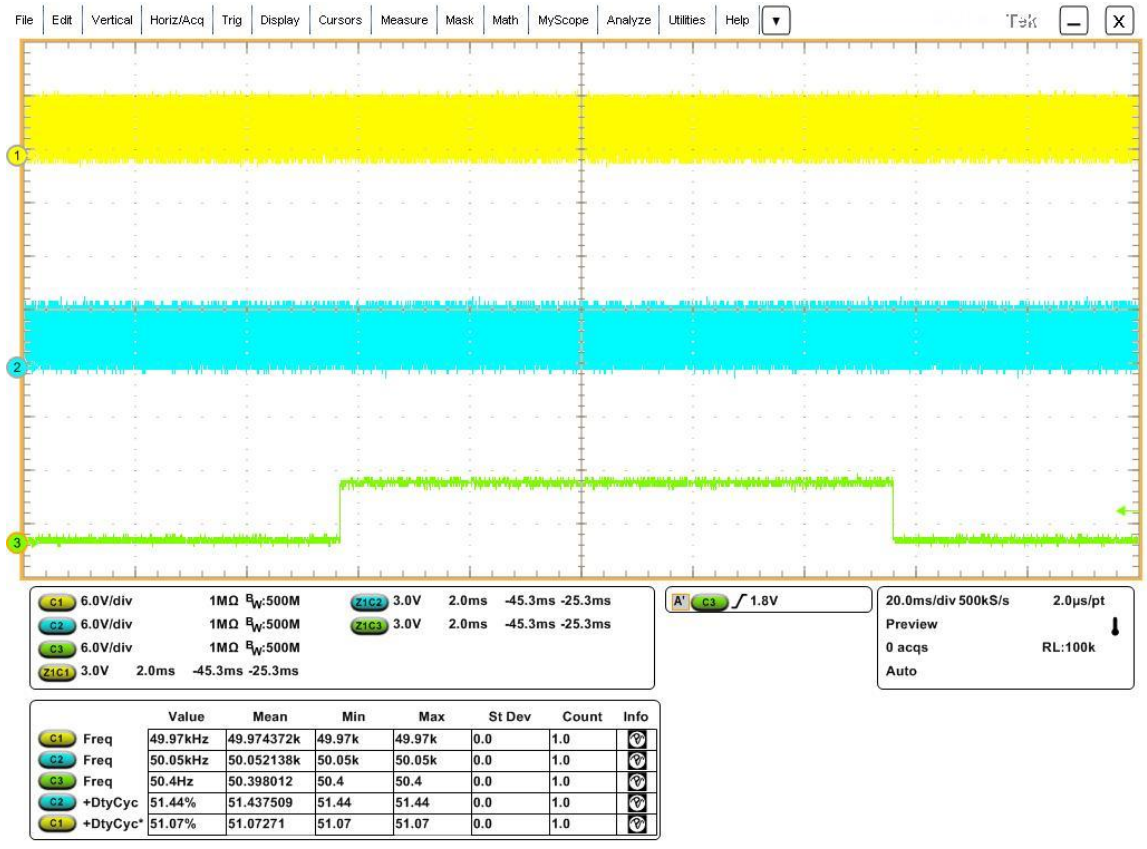

Figure 6.7 PWM waveforms for buck converter operation and load change

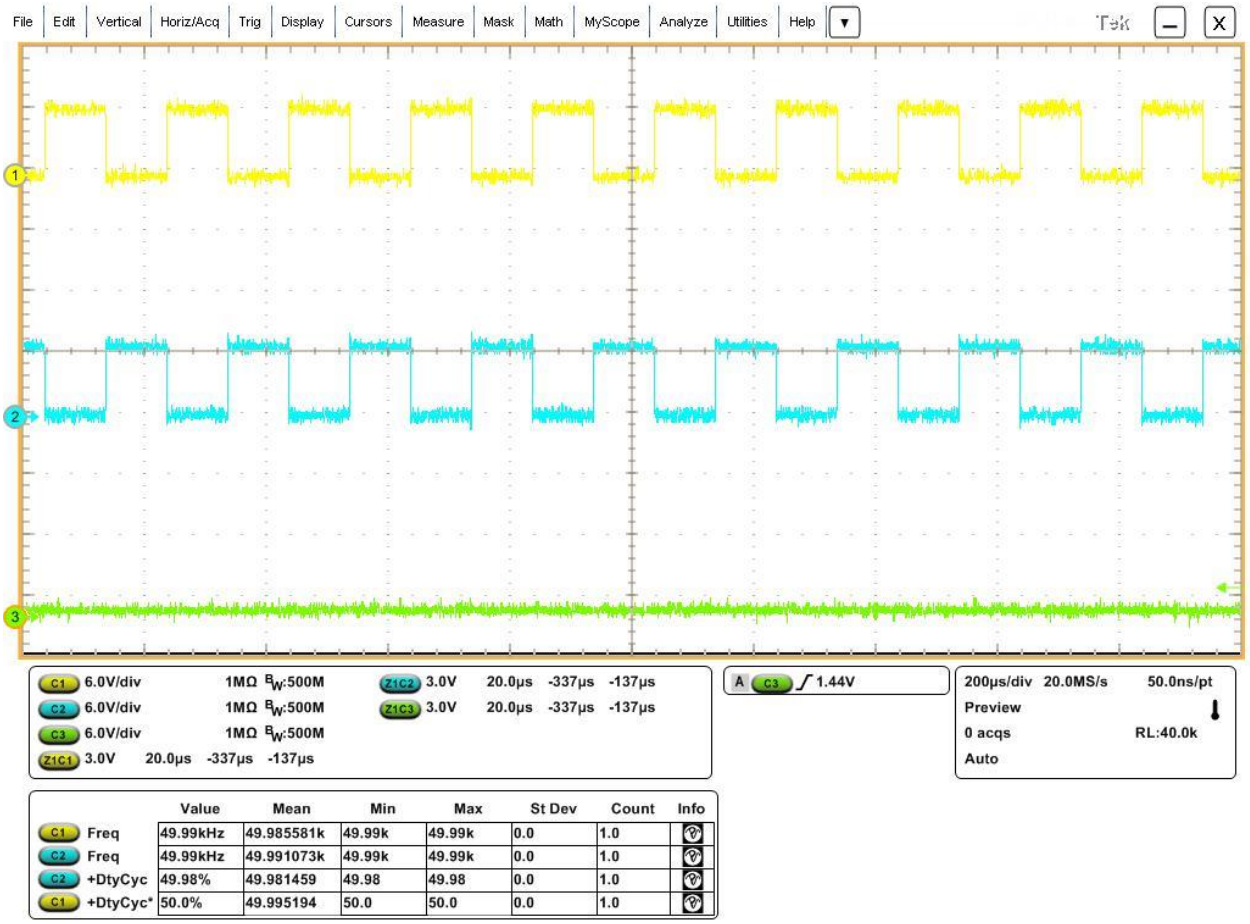

Figure 6.8 PWM waveform in open loop circuit test, 50% duty cycle

By sampling the voltage and current signal via ADC module, the close loop control applying PID controller can be applied for buck converter system. In this experiment, ADCINA0 and ADCINA1 is used to acquire voltage and current signal from instrumentation amplifier and current sensor. A voltage close loop control with PID controller is applied. An 11-bit PRBS is generated by programming and implemented in the DSP. The amplitude of PRBS, $\Delta PRBS = \pm 0.008$ and total length is 2047. Therefore, a complete system identification injection time length is $L / f_s = 0.04094s \cong 40ms$.

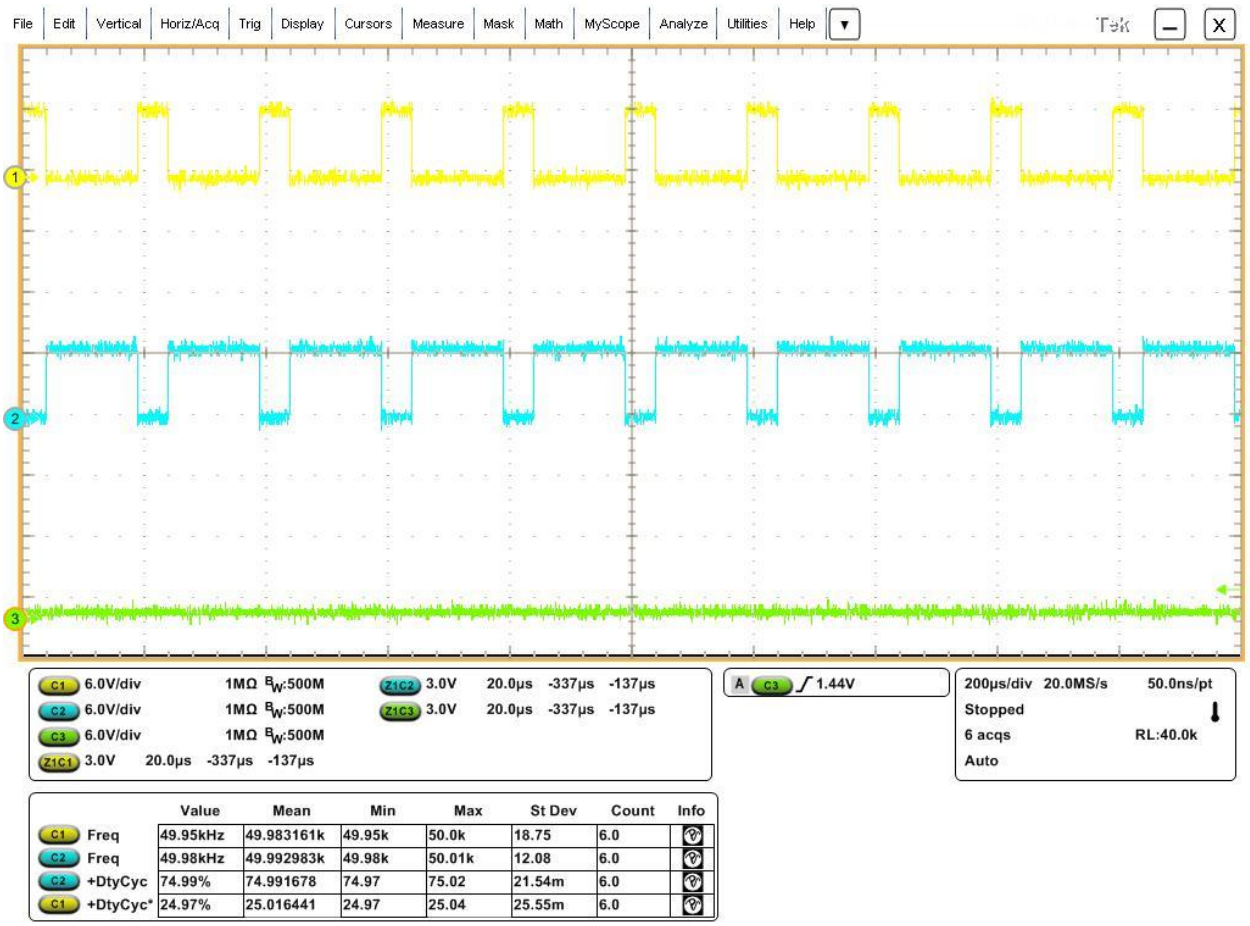

Figure 6.9 PWM waveform in open loop circuit test, 25% duty cycle

6.5 System identification using FAP and RLS experimental validation

This section presents the practical system identification results using the RLS and proposed FAP algorithms. The basic flow chart for the system identification procedure is shown in Fig.6.11. Two hundred samples of the duty cycle with injected PRBS signal are plotted in Fig.6.12. Likewise, two hundred samples of the load voltage are presented in Fig.6.13.

To eliminate the noise effect, several kinds of filter has been applied in the system identification progress. As a result, a four-tap moving average filter is finally applied for RLS and FAP algorithm. This filter is designed to smooth the output voltage noise caused by the stray capacitance/inductance or any other kinds of inevitable reasons. As a compromise, this moving average filter has an extent slowing down the convergence speed of both algorithms.

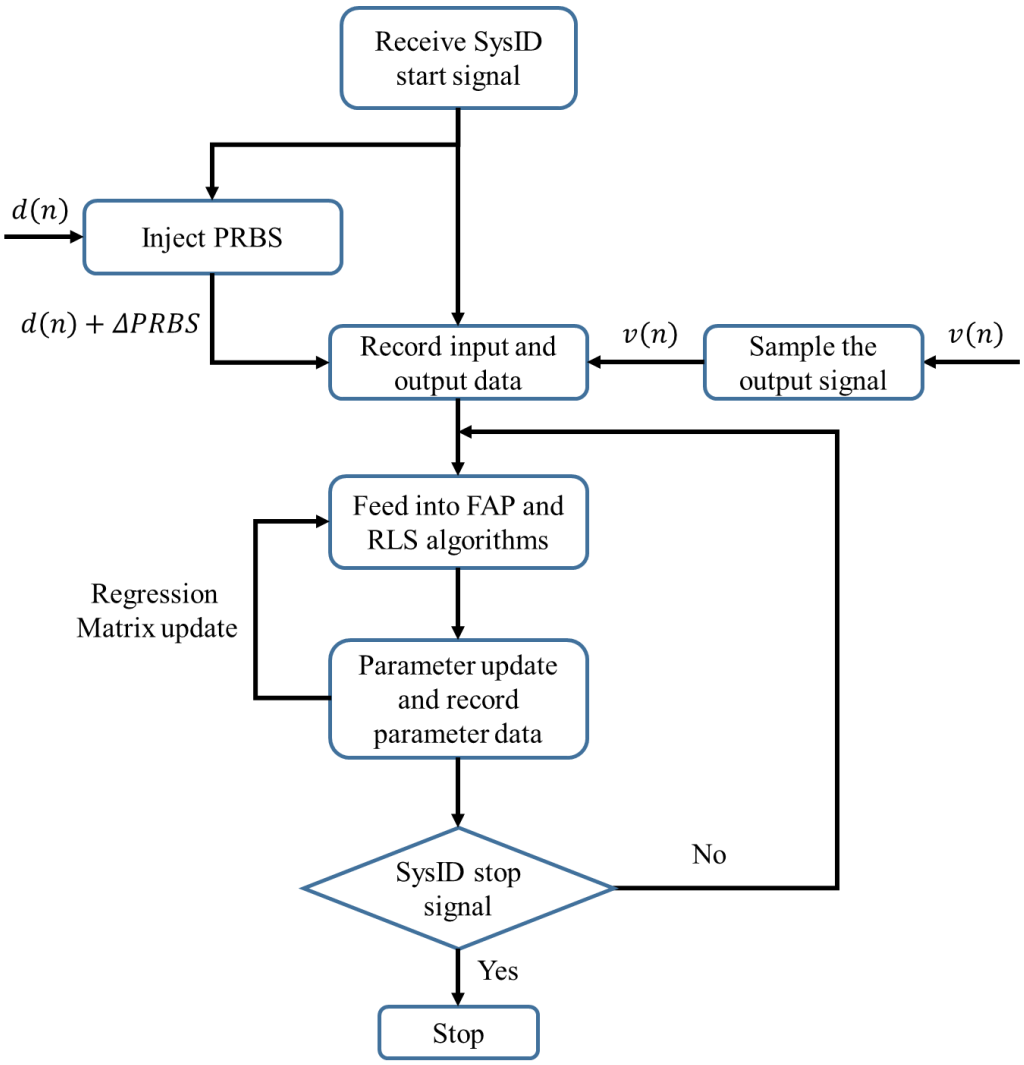

Figure 6.10 Flow chart of system identification in experimental validation

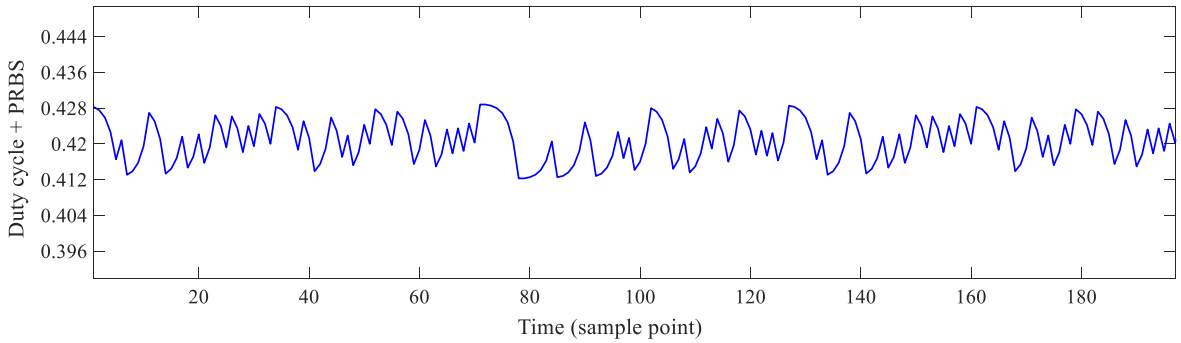

Figure 6.11 two hundred data point of PRBS + duty cycle

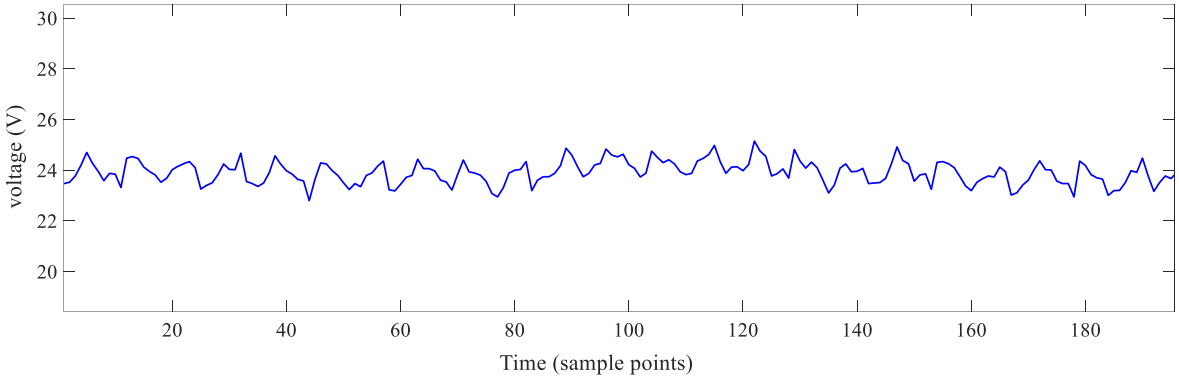

Figure 6.12 two hundred data point of load voltage

A clear and visible load voltage disturbance is caused by injecting the PRBS signal into the duty cycle, as shown in Fig.6.14. This disturbance only appears when the system identification is enabled and the PRBS is injected into the duty cycle. After this perturbation, lasting 36ms, the disturbance is gradually eliminated because of the closed loop controller. The amplitude and length of the PRBS has an impact on the accuracy of the parameter estimation, and ultimately the performance of any adaptive control mechanism dependent upon system identification. In this research, the PRBS amplitude is varied to maintain the stability of the buck converter, yet also achieve high accuracy parameter estimation result.

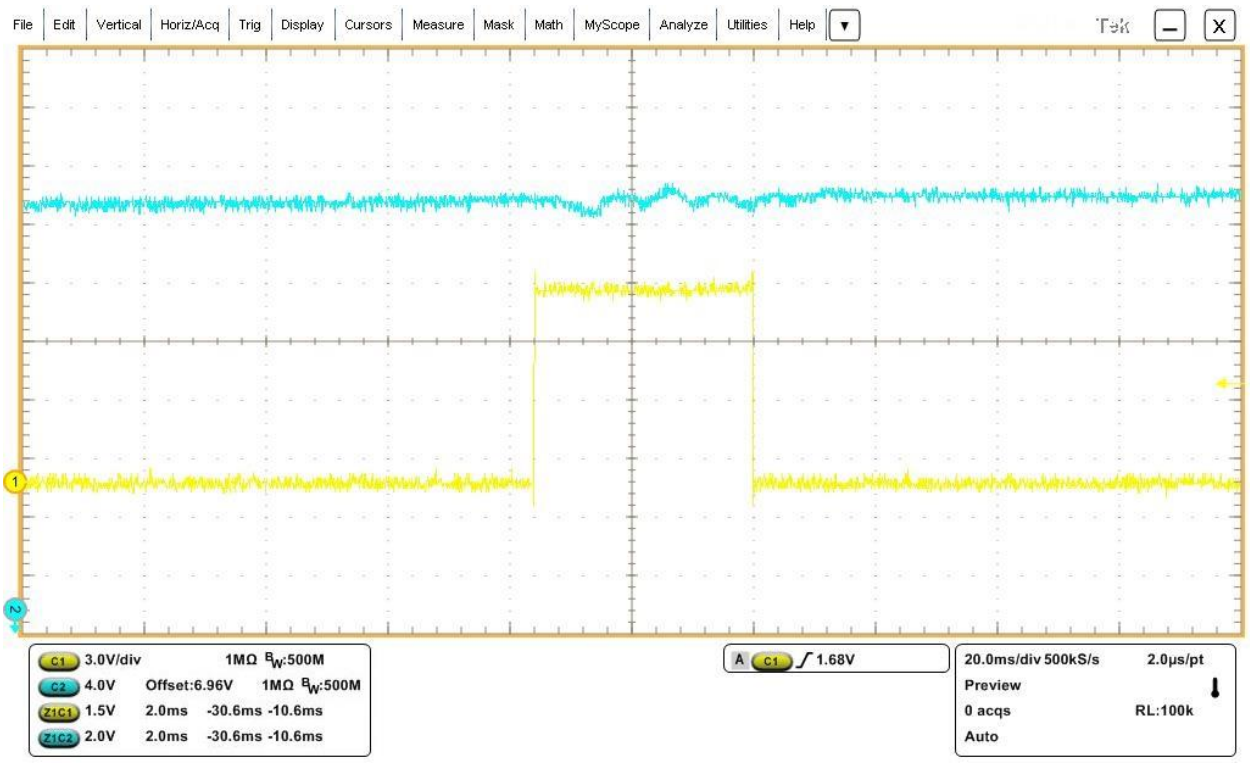

Figure 6.13 Experimental load voltage waveform when identification enabled

The parameter estimation convergence curves for the four parameters of the DC-DC synchronous buck converter's second order discrete transfer function is shown in Fig.6.15. The system identification is performed before any load abrupt change has occurred. The dotted lines represent the parameter estimation of the FAP algorithm and the dashed lines represent the RLS. The four solid lines represent the parameter data calculated from the mathematical model. As shown, both adaptive algorithms converge to a successful solution, correctly estimating the parameters to a good level of accuracy. Importantly though, the FAP has much faster convergence speed compared to the RLS for all four parameters. In this result, the forgetting factor λ of the RLS is selected as 0.9 and the projection order of the FAP is chosen as 0.6

In Fig.6.15, it can be noticed that four parameters do not converge to the ideal model parameters at the same rate. Parameter converges to a steady state value before the other three parameters. Some fluctuations happen when parameters converge to a relatively stable period. This might be caused by noise from circuity or measurement noise during signal transmission.

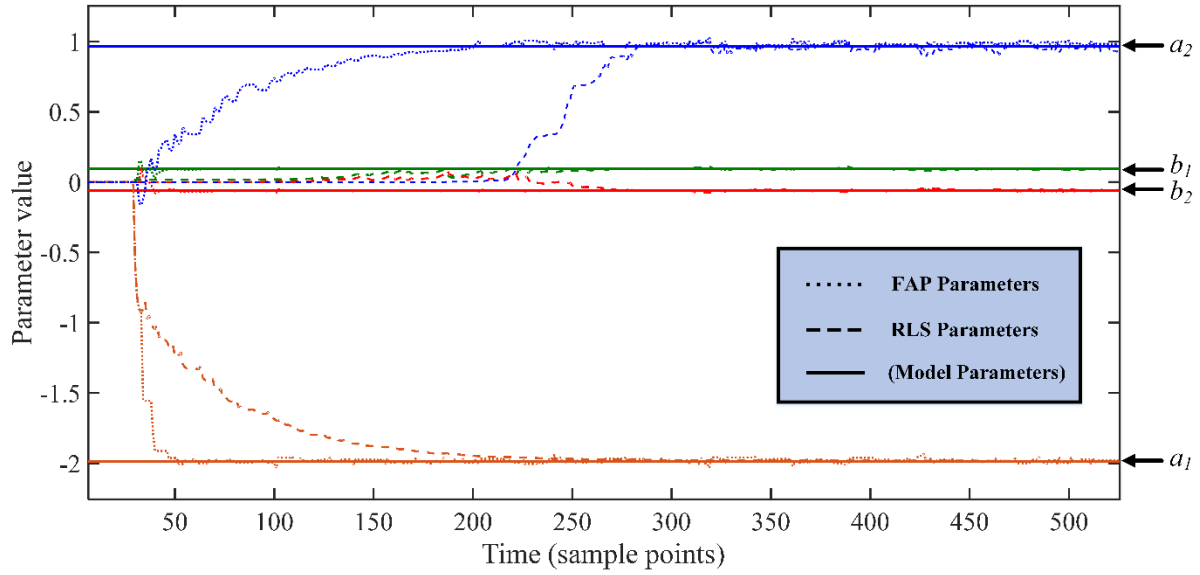

Figure 6.14 experimental parameter estimation convergence curves for comparison between RLS and FAP algorithm

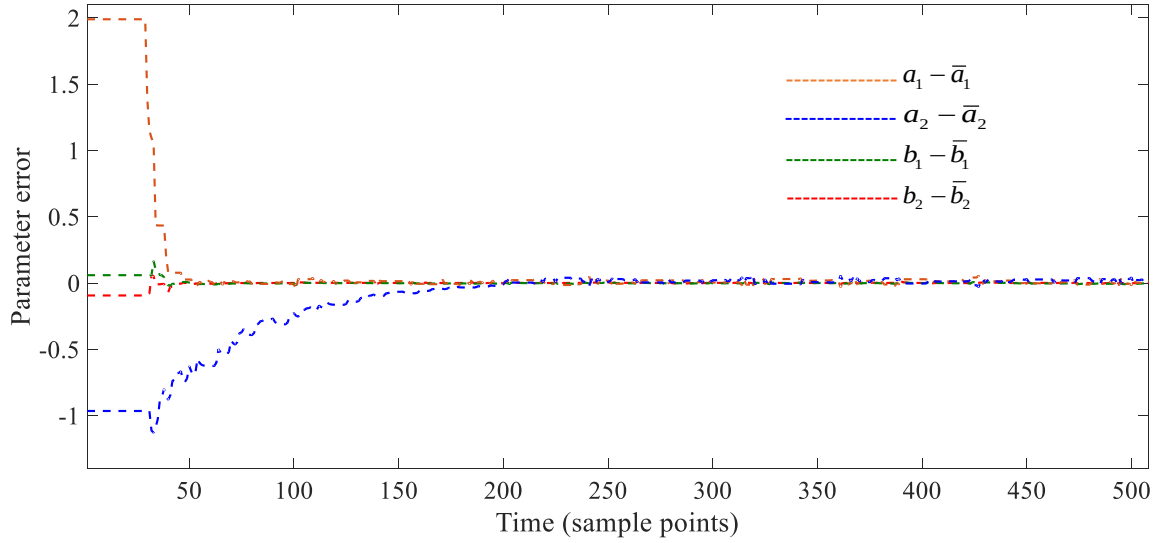

Figure 6.15 experimental parameter error, FAP (K=2)

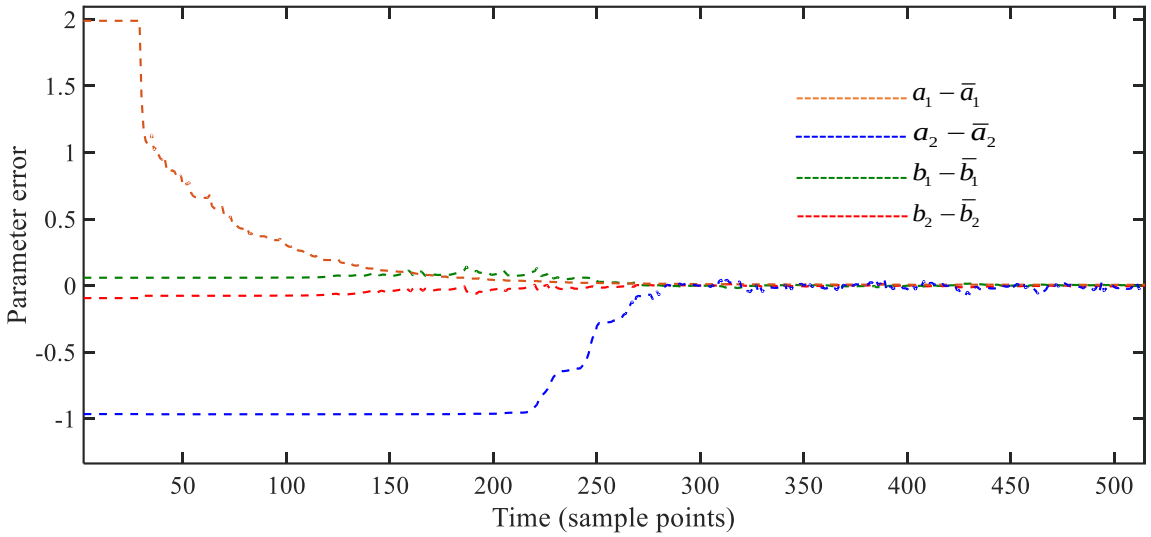

Figure 6.16 experimental parameter error, RLS

The parameter estimation error for both RLS and FAP are presented in Fig.6.16 and Fig.6.17. It can be seen both RLS and FAP algorithm rapidly estimate the parameters, 300 sampling points (6ms) for RLS, and 200 sampling points (4ms) for FAP. In Fig.6.18, the effect of the FAP projection order (*K*) is investigated. Using the same input and output data as the previous parameter estimation test, the projection order is set as 2, 3 and 4. The computational cost of changing the projection order can be obtained from Table.6.2. The computational cost heavily increases when the projection order K is increased.

Calculation operator	FAP		
X	$K^3+K^2+3K+(K+1)M+2$		
+	$K^3+K^2+3K+(K+1)M+1$		
/	0		
	M=4, $K=2$	M=4, $K=3$	M=4, $K=4$
X	32	62	113
+	33	63	114
/	0	0	0

Table 6.2 computational cost of FAP in K=2, 3, 4

However, as clearly shown in Fig 6.18, the greatest impact is on the convergence speed of a2. For the other three parameters, the impact of increasing K is not as marked.

The estimation accuracy can be obtained by acquiring the Mean Square Error (MSE) in the practical experiment. The MSE plots for parameter a2 for RLS and FAPs for different projection orders are presented as Fig.6.19.

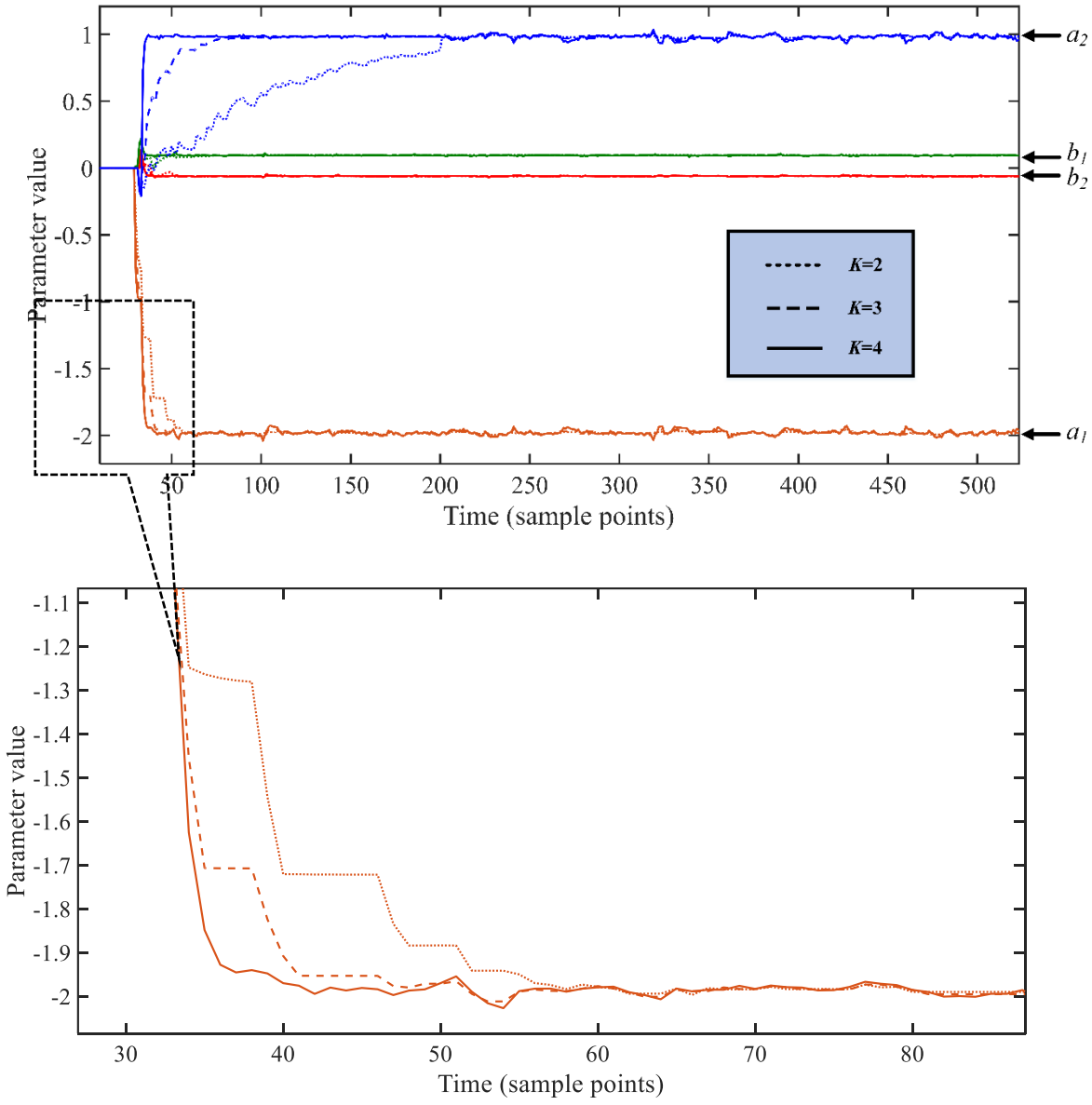

Figure 6.17 Parameter convergence curves when projection order K=2, 3 and 4

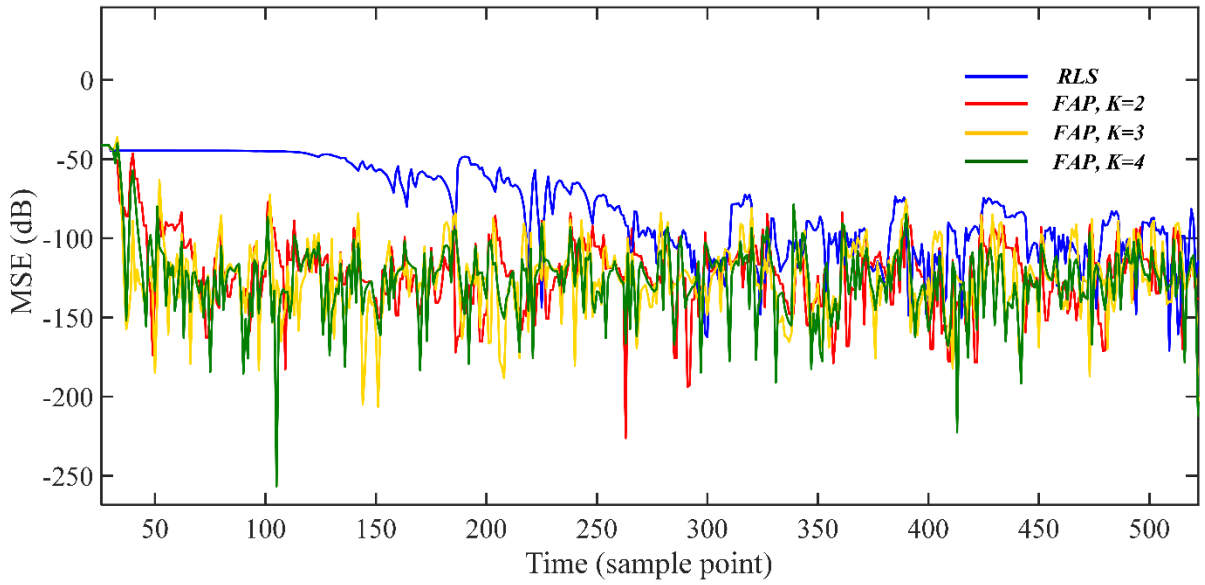

Figure 6.18 Mean Square error curves of FAP and RLS (parameter a_2)

All adaptive algorithms ultimately achieve very low values of MSE, but still vary to some extent due to the impact of system noise. After 250 sample points, all algorithm can maintain the MSE value below -100dB. Compared to the FAP algorithm, the conventional RLS appears to exhibit slightly greater fluctuation.

Comparing the FAP for different projection orders, there is no significant improvement on the estimation accuracy; in each case accurate results are achieved, and the level of fluctuation is the same. Therefore, it is concluded the projection order only affects computational burden and convergence speed. Therefore, the projection order is selected as 2; this still provides fast convergence speed and whilst it is not optimal, the reduction in computational complexity warrants this decision.

6.6 Adaptive current balancing ON/OFF control experimental validation

This section presents the practical validation of the proposed adaptive current balancing ON/OFF control method. To compare with traditional PID controller, a basic PID voltage feedback controller is implemented on the experimental hardware. The output voltage is regulated as 24V. A MOSFET switching signal triggers a repetitive load resistance change between 18.4Ω and 3.4Ω. As Fig.6.8 shows, the step load change frequency is 50Hz, resulting in a load current change

between 1.34A and 7.06A at 20ms intervals and significant load voltage transients. All other system parameter remains unchanged, as presented in Table. 6.1.

6.6.1 *Transient response of conventional PID control*

The transient response of the conventional PID controller is shown in Fig.6.20 and Fig.6.21. It can be seen that significant undershoot and overshoot arise when the load change signal is enabled. The transient period lasts about 8.68ms and the voltage drop is 2.56V during this period. The PID controller parameters are calculated using a pole placement method [2,4,5]. This calculation uses all system coefficients listed in Table.6.1 and the load resistance used is the value before the transient arises. All PID controller parameters are fixed during this transient period.

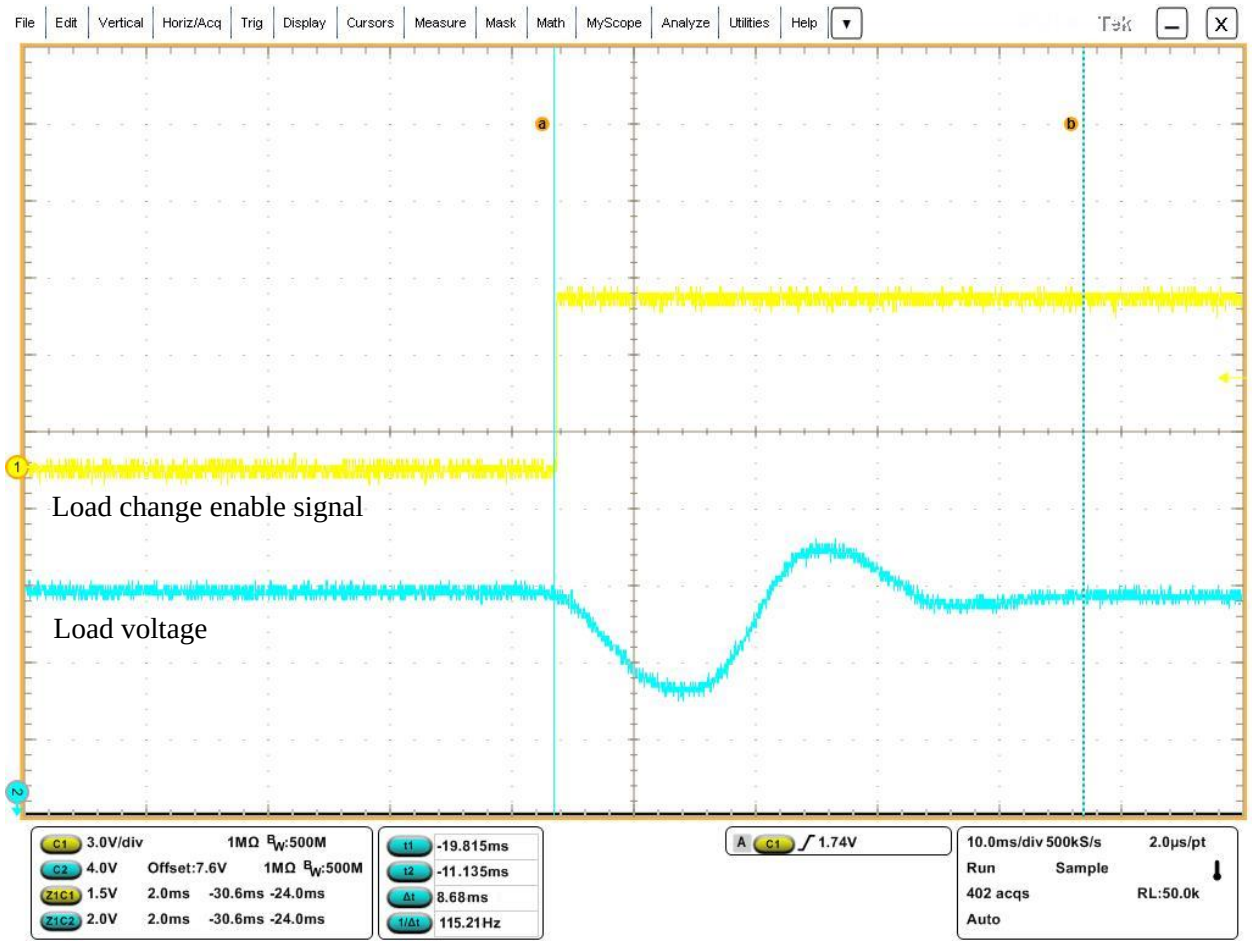

Figure 6.19 transient response of PID controller with abrupt load change between 18.4Ω to 3.4Ω, transient period measurement

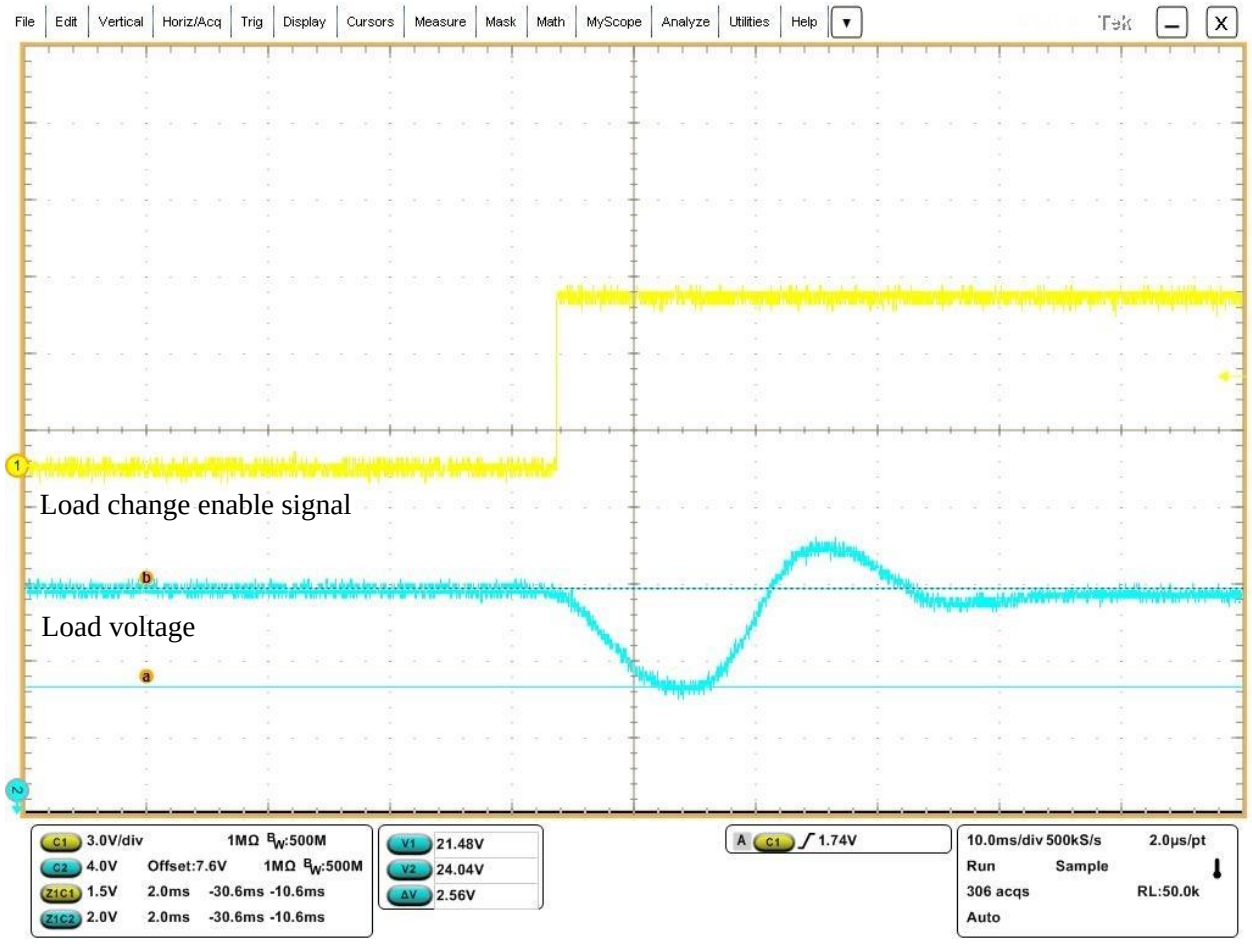

Figure 6.20 Transient response of PID controller with abrupt load change between 18.4Ω to 3.4Ω, transient magnitude measurement

With fixed PID controller parameters the duty cycle cannot optimally adapt to counteract the impact of the load change, largely due to the integral component. The duty cycle is updated with a fixed sampling frequency and only depends on the output voltage signal. These conditions lead to the unwanted voltage oscillation in the transient response.

6.6.2 *Transient response of Current Balancing ON/OFF control*

When applying the current balancing ON/OFF control, the power MOSFET remains constantly ON when the voltage is detected below a certain threshold, as may be the case when an abrupt load change occurs. A CPU timer in the DSP is set to control the ON and OFF period in the software. When load change occurs, the ADC channels (voltage and current measurement) are activated to double the sampling frequency from 50kHz to 100kHz as a method to gathering more data for system identification. However, there is a compromise between sampling frequency and estimation accuracy due to the sampling period is a component in the mathematical model (see Eq.5.23). The sampled inductor current and load voltage are shown in Fig. 6.22 and Fig.6.23 respectively.

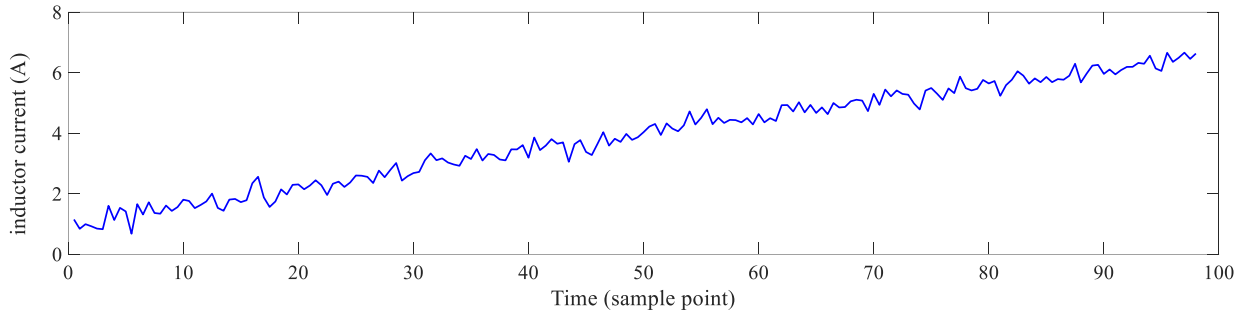

Figure 6.21 sampled inductor current data in constant switching ON condition

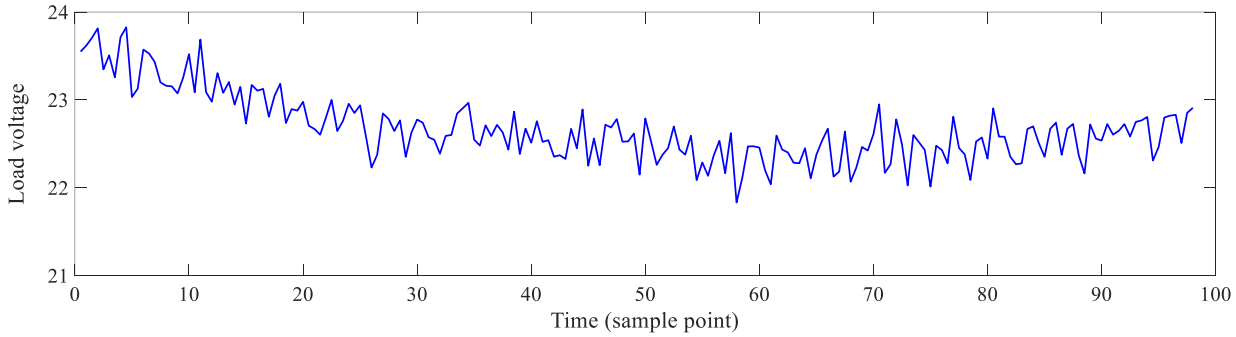

Figure 6.22 sampled load voltage data in constant switching ON condition

The variation of load resistance can be estimated using the inductor current data and load voltage data, which can help to determine the ON and OFF period as illustrated in section 5.3 in Chapter 5.

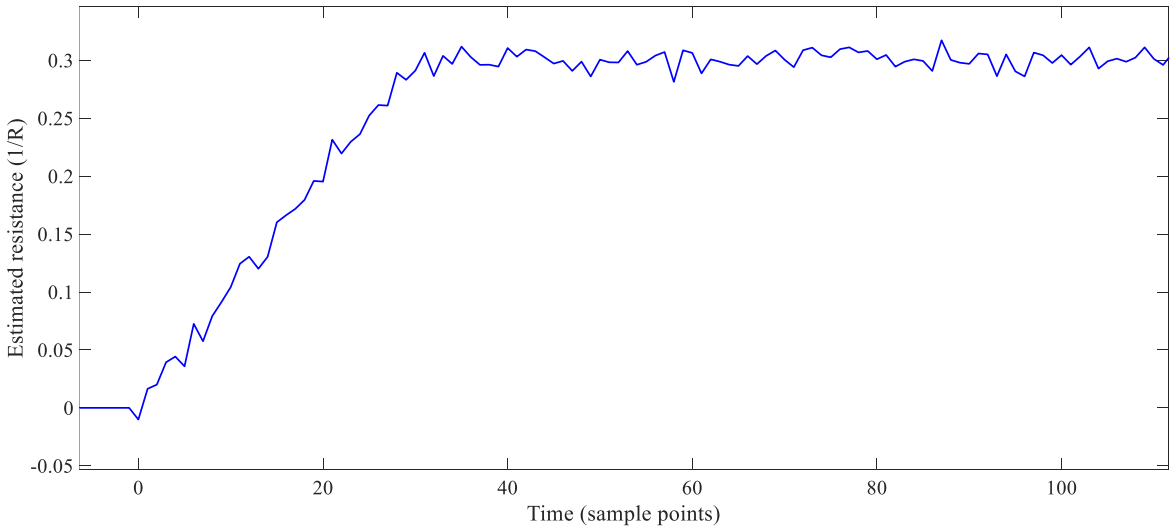

Figure 6.23 convergence curve of load resistance

The real time resistance estimation process is shown in Fig.6.24. Following Eq. 5.23 and Eq.5.24, two parameter convergence curves have been added together to obtain this resistance estimation result.

It is worth noting that the results are achieved with normal background system noise, and do not require PRBS injection. With this load resistance value, a constant ON/OFF control has been applied to improve the transient response.

The transient responses when using the proposed current balancing ON/OFF control method are shown in Fig.6.25 and Fig.6.26. It can be seen that the load voltage oscillation has been significantly reduced after applying the proposed adaptive control method. The overshoot is eliminated and the undershoot value is reduced from 2.56V to 1.64V. It takes 2.623ms for the load voltage to recover its steady state value; this is 5.05ms faster compared to the conventional fixed PID controller. The experimental results are consistent with the simulation results in chapter 5 (Fig.5.12 and Fig.5.13). This proves that the proposed current balancing ON/OFF control has

superior dynamic performance compared to the conventional PID control scheme, thus confirming the research hypothesis set out in this thesis.

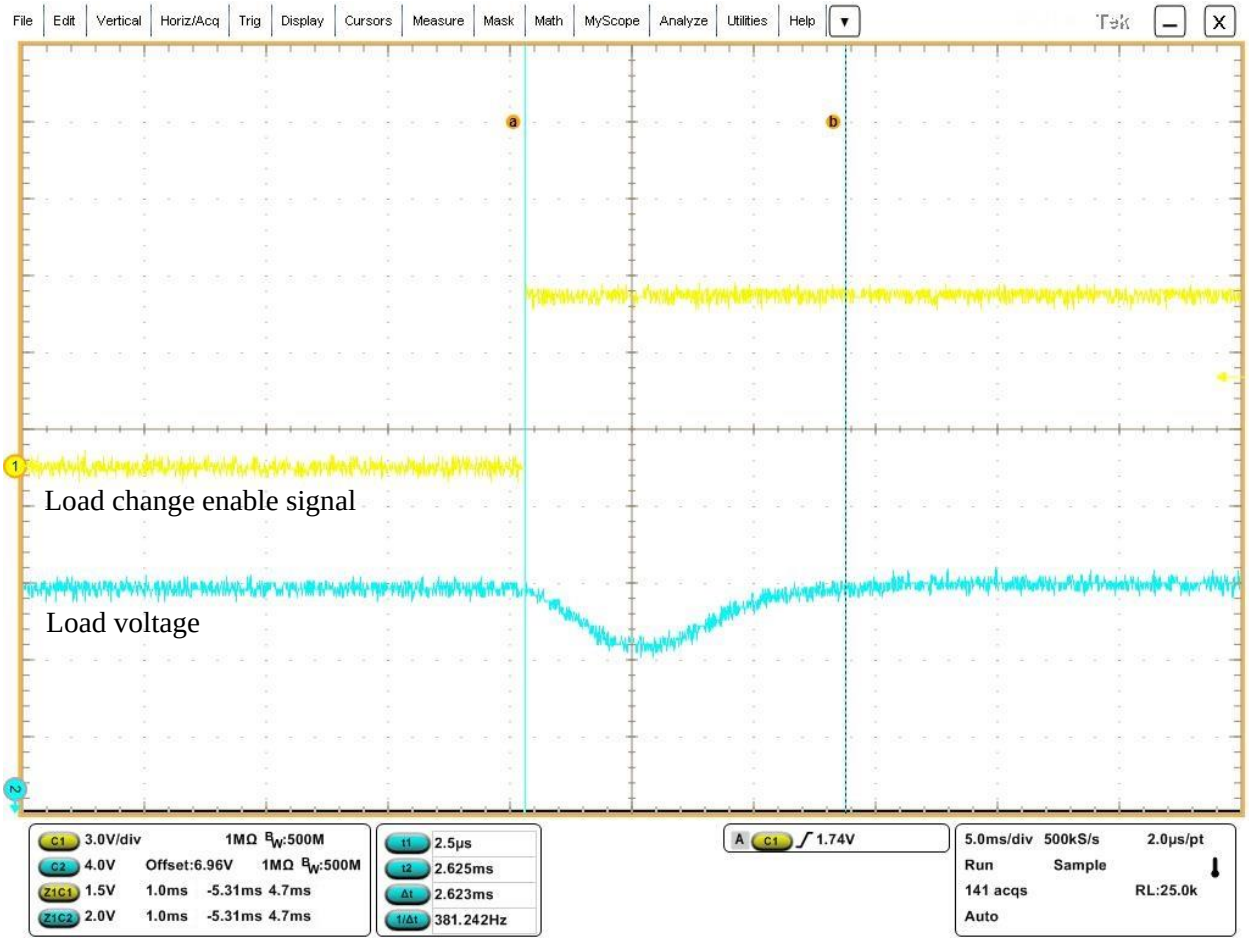

Figure 6.24 transient response of current balancing ON/OFF controller with abrupt load change from 18.4Ω to 3.4Ω, transient period measurement

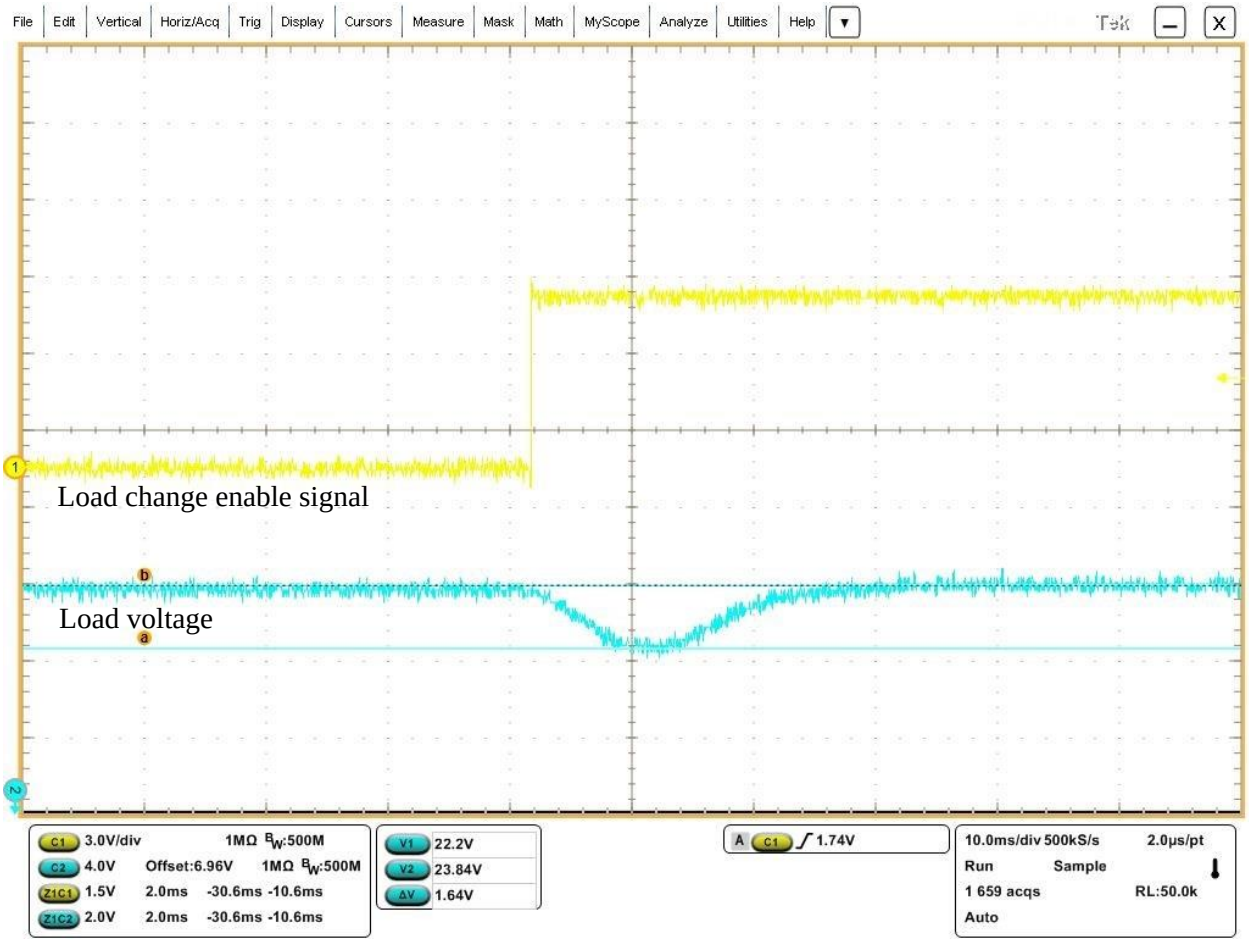

Figure 6.25 transient response of current balancing ON/OFF controller with abrupt load change from 18.4Ω to 3.4Ω, transient magnitude measurement

6.7 Chapter Summary

In this chapter, a dynamic performance and computational complexity comparison has been carried out for RLS and FAP algorithms, for the purposes of real-time system identification of a DC-DC synchronous buck converter system.

The results validate the superiority of the FAP in terms of parameter convergence speed, accuracy, and computational complexity provided the projection order is kept small. Overall, it proves the FAP algorithm is an excellent candidate approach for system identification of a DC-DC buck converter system. The experiment results show close agreement with the simulation result presented in previous chapters and demonstrate the viability of the proposed FAP algorithm for real-time applications. Further research has been carried out to fully investigate the effect of projection order on parameter estimation convergence speed and accuracy in real-time. The results show that whilst convergence speed can modestly be improved, there is little improvement in the resultant accuracy. Also, the computational burden significantly increases with projection order. Therefore, a low projection order is recommended (K = 2) for low complexity, low cost DC-DC buck converter systems. Finally, this chapter also confirms the experimental operation of a novel adaptive current balancing ON/OFF controller for DC-DC power converter control. Results show that the current balancing ON/OFF controller has superior performance compared to the conventional PID controller; the adaptive controller can virtually eliminate overshoot, significantly reduce the period of undershoot offset, and improve settling time.

Chapter 7 Conclusion and Future Work

7.1 Thesis conclusion

System identification technique is necessary for many advanced controllers which need a priori information about system parameter. To successfully identify the system parameters and effectively apply the parameter values for tuning the controller signal, the algorithm for system identification must has a decent estimation accuracy, a fast estimation speed and a low computational cost in digital control applications. Unfortunately, many system identification methods stay in an offline level or cannot implemented with subsequent control method due to the high complexity and slow estimation speed.

The RLS algorithm is a popular candidate algorithm for system identification. It provides acceptable noise immunity performance and good tracking ability. However, the RLS algorithm is far from an ideal solution for cost sensitive, yet high performance, power electronic applications; it only offers modest convergence speed and imposes a relatively high computational burden on the microprocessor platform. Literature shows that many novel system identification algorithms can be applied for power electronic systems; however, they typically set out to optimise one metric only; nominally computational complexity or speed of estimation.

For this reason, this thesis set out to develop a system identification algorithm capable of simultaneously reducing the computational cost and convergence speed.

The second contribution of this thesis is the research and development of a new adaptive control method to improve the transient response of a DC-DC buck converter system.

7.2 FAP algorithm for system identification of DC-DC buck converter system

In this thesis, a novel on-line system identification method is proposed to overcome the limitations of the classic RLS algorithms. This algorithm is developed from a stochastic gradient decent algorithm. In this research, it is adapted for system identification in DC-DC SMPC applications. The proposed FAP algorithm has superior computational efficiency compared to the conventional RLS algorithm. The FAP algorithm is shown to successfully identify the parameters of a DC-DC buck converter when using a discrete transfer function modelling approach. All four parameters of the discrete transfer function are estimated iteratively by superimposing an 11-bit PRBS signal onto the duty cycle signal and sampling the load voltage signal. The mathematical derivation and simulation results demonstrate the superiority convergence speed of the FAP algorithm compared to the RLS. A detailed computational cost analysis is presented for both RLS and FAP. It is clearly shown that the computational cost of implementing the FAP is much less than the RLS algorithm.

Experimental validation of the FAP algorithm is carried out using a prototype synchronous DC-DC buck converter. This converter is voltage controlled by a Texas Instruments TMS320F28335™ DSP. The experiment results are consistently compatible to the simulation results. As a conclusion, the results prove that the proposed FAP algorithm is an excellent candidate algorithm for online system identification of SMPC parameters; offering both improved computational efficiency and convergence speed.

The research on system identification has led to the following publications:

- **Chen Wang**; Armstrong, M.; Gadoue, S.; Missailidis, P., "System identification of a DC-DC converter system using a Fast Affine Projection algorithm," *7th IET International Conference on Power Electronics, Machines and Drives (PEMD 2014)*, vol., no., pp.1,6, 8-10 April 2014
- **Chen Wang**; Bing Ji; Xueguan Song; Pickert, V.; Wenping Cao, "IGBT condition monitoring with system identification methods," *Transportation Electrification Asia-Pacific (ITEC Asia-Pacific), 2014 IEEE Conference and Expo* , vol., no., pp.1,6, Aug. 31 2014-Sept. 3 2014
- **Chen Wang**; Armstrong, M.; Gadoue, S., "Dual feedback adaptive control for voltage regulation of cascade DC-DC converter systems," *8th IET International Conference on Power Electronics, Machines and Drives (PEMD 2016)*

7.3 Adaptive current balancing ON/OFF control in DC-DC buck converter

The second major contribution of this thesis is the adaptive control application in improving transient response of DC-DC buck converter system. In this case, this transient response is triggered by an abrupt load resistance change during the DC-DC converter operation. This transient response can be summarised as a power transmission through the power storage components in SMPC system. With voltage and current signal fluctuating, the electric energy is transmitting from one power storage component to another and finally consumed in load resistor. By analysing this energy transmission behind the converter operation. An optimal ON/OFF scheme is easily found. This control method eliminates all unnecessary power transmission actions when applying conventional duty cycle control. Instead of that, investigated an optimal constant switching ON and constant switching OFF method to minimise the transient period and reduce the dynamic oscillation during transient period. A detailed mathematical derivation has been done to prove the superiority of this current balancing ON/OFF control compared with conventional PID control. By combing with FAP algorithm, this constantly ON period and constantly OFF period can be easily determined based on the system parameters. The simulation result proves the validity of using this current balancing ON/OFF control in DC-DC buck converter system. Similarly, as system identification experiment test, all adaptive control validation is applied in a same synchronous DC-DC converter, and it is controlled by a Texas Instruments TMS320F28335™ DSP. An abrupt load change is controlled by switching a power MOSFET which connected parallel with a power resistor in the resistor load series. From the experiment and simulation result, the significant overshoot is eliminated when applying proposed current balancing ON/OFF control scheme. The undershoot oscillation is minimised as well. Totally, the transient period has been dramatically reduced and the transient response has been significantly improved compared with a transient response result by applying conventional PID controller under same load change condition.

The research on adaptive control has led to the following publications:

- **Chen Wang**; Armstrong, M.; Gadoue, S., "System identification and adaptive control of a DC-DC converter using a current balancing ON/OFF control technique for optimal transient performance," *in Power Electronics and Applications (EPE'15 ECCE-Europe), 2015 17th European Conference on* , vol., no., pp.1-10, 8-10 Sept. 2015

7.4 Limitations and future work

This work focuses on system identification of SMPCs and adaptive control of DC-DC buck converter. Some limitations are concluded here for potential research topics and future work.

- The proposed parameter estimation method FAP algorithm is simpler than RLS only applying for the system model as ARX model (see section 4.51). It might be more complicated than RLS if applying in a high order system or the format of system model is not ARX model.
- The proposed Current Balancing ON/OFF (CBOO) method is limited by determining the ON period and OFF period. It needs a prior knowledge of load change. If the load change is small, the proposed FAP algorithm may not have enough sampling data to estimate the changed load resistance. This means this CBOO method cannot applied in a one-off load change scenario if the load change is too small.

In terms of the suggestion of future work, researchers can focus on the potential topic as follows.

The system identification algorithm in this research applying RLS and FAP algorithm due to their superiority on convergence speed, computational cost and estimation accuracy. As illustrated in Chapter 4, this FAP algorithm is one variation of the classic AP algorithm. Many other variations of AP algorithm have been developed in the field of acoustic echo-cancellation, adaptive filtering etc. Those variation such as Affine Projection Sign Algorithm (APSA), Practical Variable Step-Size Adaptive Algorithms (PVSSA), variable step-size affine projection sign algorithm (VSS-APSA) and Modified variable step-size affine projection sign algorithm (MVSS-APSA) are all possibly to be implemented into system identification of SMPC system. Also, many variations of RLS have been developed, either overcome the high computational cost, or increase the convergence speed. Those variation include but not limited: Fast Transversal Recursive Least Squares algorithm (FTRLS), Memoryless Polynomial RLS (MLPRLS), Fast QR-decomposition Recursive Least Squares (FQRD-RLS) algorithms, Low-Complexity Variable Forgetting Factor Recursive Least Squares (LCVFFRLS). All these variation and possibility for system identification of SMPCs is needed to be investigated. Moreover, some other adaptive algorithms which belongs to stochastic gradient descent algorithm family are also possible for system identification of SMPCs. A replacing adaptive algorithm probably can be found in the future which has a better convergence speed and lower computational cost. It may have a better noise immunity ability as well. With assisting by this adaptive algorithm, a better system identification result can

be found in the future. Besides, the specific ARX model for SMPCs mathematical model is different with AR model in some adaptive filtering application. A deep investigation of system identification performance evaluation based on variable adaptive algorithms on AR model and ARX model can be done in future.

In the aspect of adaptive control, the proposed current balancing ON/OFF control need a certain ON period for system identification. This period could be very short if the physical coefficients are selected different. In that case, a faster convergence speed of adaptive algorithm is needed. By applying this control method, the inductor current increases very fast during the ON period, an overcurrent protection is necessary for the special SMPC application.

Besides of that, an optimal adaptive control scheme can be investigated in DC-DC boost converter. The different operation principle determines the boost converter cannot maintain constant ON in a long period—the inductor cannot charge in a long period without connecting a consumable component. The coil may overheat due to the rapid increased high current. In this case, the proposed constant ON/OFF control cannot be implemented in boost converter. Therefore, it is worth to investigate an adaptive algorithm to improving the transient response in boost converter.

In terms of mathematical model of SMPCs, a more suitable model is necessary to be investigated due to the limitation of transfer function model and averaging state space model. The nonlinear behaviour caused by the switching action is a main restriction point for implementing many adaptive algorithms serving for SMPC system. Some researchers have been working on linearize the switching action via a different mathematical method. For example, a Monodromy matrix is introduced in [9], this matrix can describe the operational performance during the switching action period. Researches can focus on using such mathematical model to do the system identification via an appropriate adaptive algorithm.

Another deep research can be carried out in PRBS signal. The amplitude and bits number much affect the estimation accuracy in RLS and FAP. How the PRBS works on improving estimation accuracy is a good research objective in further study. A detailed mathematical derivation about it can be investigated in the future.

Alternatively, the topologies of SMPCs are numerous, this research only focus on a simple DC-DC buck converter topology. Boost converter, buck-boost converter, interleaved buck/boost

converter are all widely used in industrial applications. Different adaptive algorithm are probably suitable for different topologies. A comparison study can be carried out to investigate same adaptive algorithm performance variation in different SMPC topologies.

Combination with existing advanced control scheme is also a good research topic. Many existing advanced control schemes such as model based predictive control, sliding mode control, nonlinear control is investigated in many years. If the combination between them and a proper adaptive algorithm can be built, those control schemes can be more easily to implement in industrial applications.

Appendix A Simulink model of system identification and adaptive control

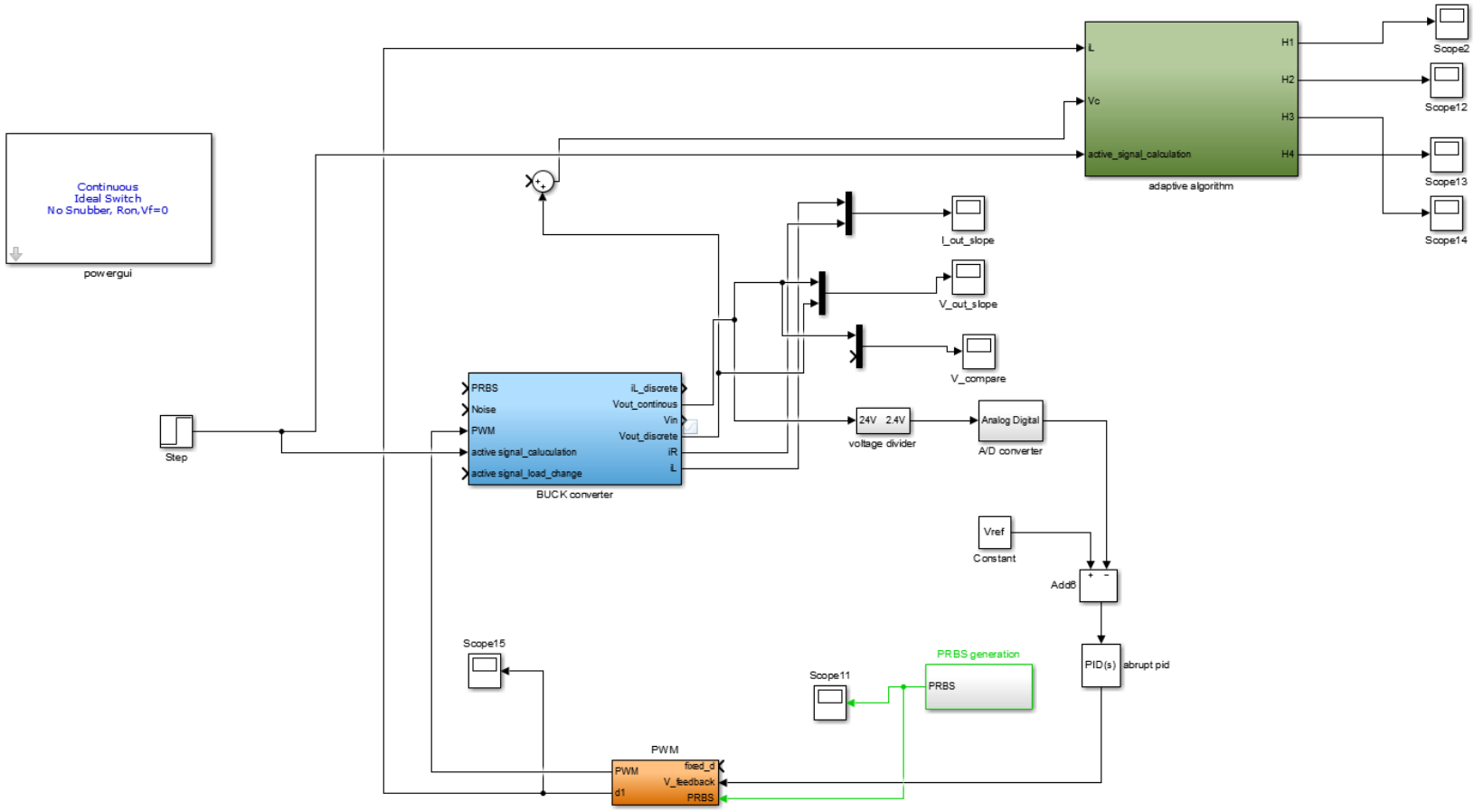

Figure A.1 simulation model of propose system identification method

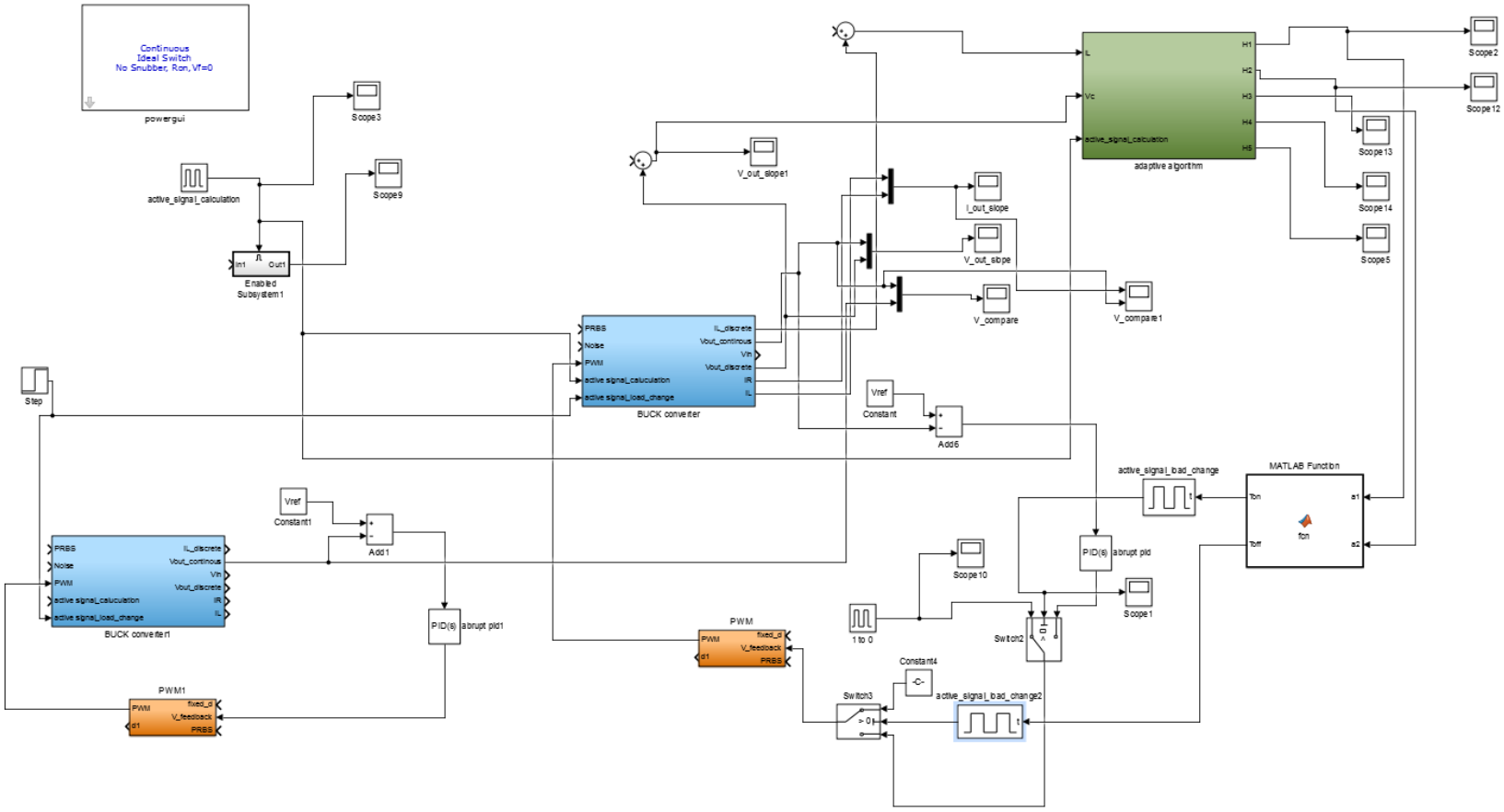

Figure A.2 simulation model of adaptive current balancing ON/OFF control

Appendix B schematic circuit of DC-DC buck converter system

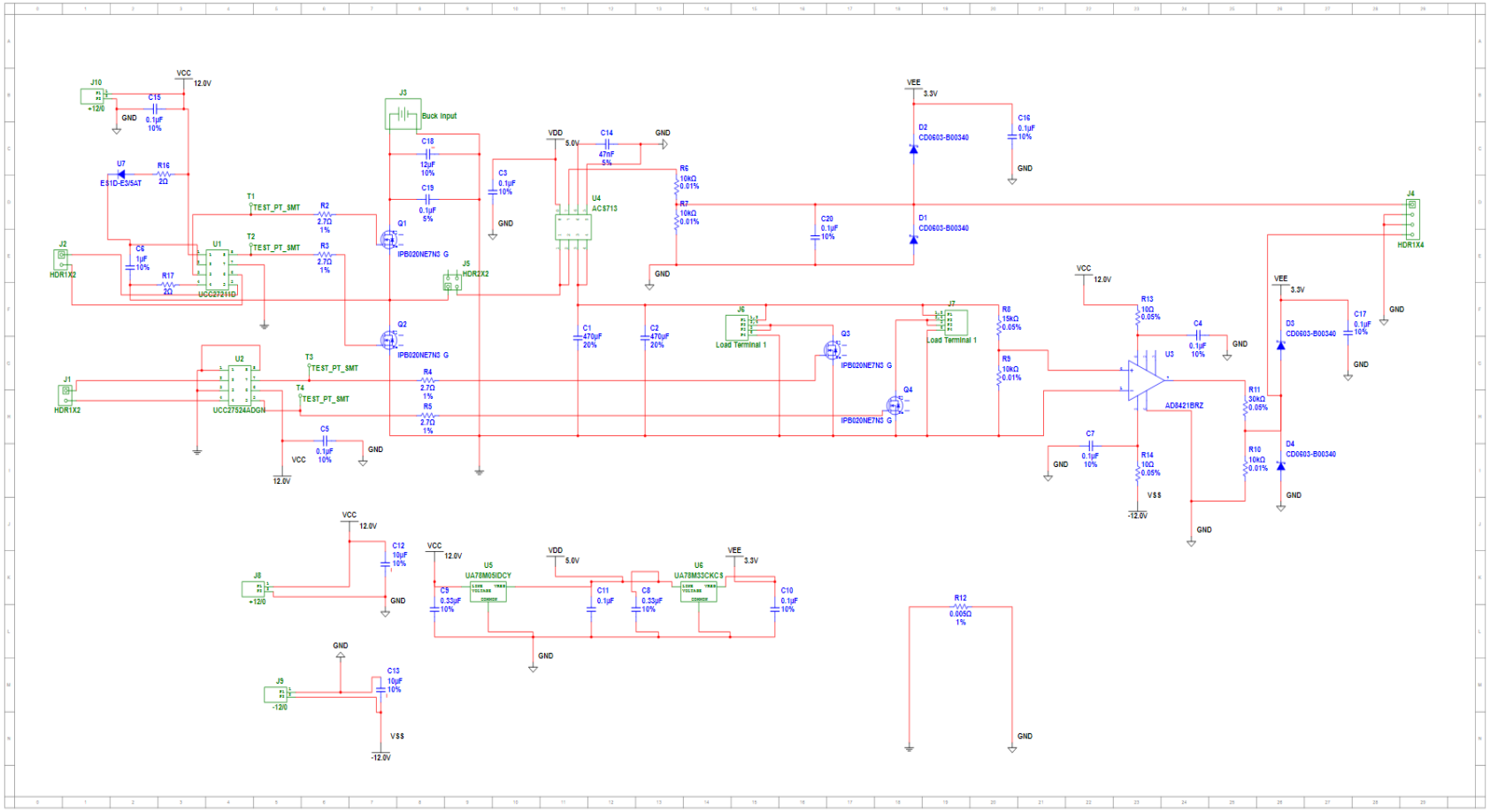

Figure B. 1 schematic circuit of DC-DC buck converter system

References

[1] Y. V. Zakharov, G. P. White and J. Liu, "Low-Complexity RLS Algorithms Using Dichotomous Coordinate Descent Iterations," in IEEE Transactions on Signal Processing, vol. 56, no. 7, pp. 3150-3161, July 2008.

[2] M. Algreer, M. Armstrong and D. Giaouris, "Active Online System Identification of Switch Mode DC–DC Power Converter Based on Efficient Recursive DCD-IIR Adaptive Filter," in IEEE Transactions on Power Electronics, vol. 27, no. 11, pp. 4425-4435, Nov. 2012.

[3] B. X. Li and K. S. Low, "Low Sampling Rate Online Parameters Monitoring of DC–DC Converters for Predictive-Maintenance Using Biogeography-Based Optimization," in IEEE Transactions on Power Electronics, vol. 31, no. 4, pp. 2870-2879, April 2016.

[4] M. Ahmeid, M. Armstrong, S. Gadoue, M. Al-Greer and P. Missailidis, "Real-Time Parameter Estimation of DC–DC Converters Using a Self-Tuned Kalman Filter," in IEEE Transactions on Power Electronics, vol. 32, no. 7, pp. 5666-5674, July 2017.

[5] M. Algreer, M. Armstrong and D. Giaouris, "Adaptive PD+I Control of a Switch-Mode DC–DC Power Converter Using a Recursive FIR Predictor," in IEEE Transactions on Industry Applications, vol. 47, no. 5, pp. 2135-2144, Sept.-Oct. 2011.

[6] W. Stefanutti, P. Mattavelli, S. Saggini, M. Ghioni, "Autotuning of digitally controlled buck converters based on relay feedback", IEEE Trans. Power Electron., vol. 22, no. 1, pp. 199-207, Jan. 2007.

[7] A. Hajizadeh, A. H. Shahirinia, N. Namjoo and D. C. Yu, "Self-tuning indirect adaptive control of non-inverting buck–boost converter," in IET Power Electronics, vol. 8, no. 11, pp. 2299-2306, 11 2015.

[8] P. Cortes, M. P. Kazmierkowski, R. M. Kennel, D. E. Quevedo and J. Rodriguez, "Predictive Control in Power Electronics and Drives," in IEEE Transactions on Industrial Electronics, vol. 55, no. 12, pp. 4312-4324, Dec. 2008.

[9] H. Wu, V. Pickert, D. Giaouris and B. Ji, "Nonlinear Analysis and Control of Interleaved Boost Converter Using Real-Time Cycle to Cycle Variable Slope Compensation," in IEEE Transactions on Power Electronics, vol. 32, no. 9, pp. 7256-7270, Sept. 2017.

[10] G. Feng, E. Meyer and Y. F. Liu, "A Digital Two-Switching-Cycle Compensation Algorithm for Input-Voltage Transients in DC–DC Converters," in IEEE Transactions on Power Electronics, vol. 24, no. 1, pp. 181-191, Jan. 2009.

[11] D. Giaouris, S. Banerjee, B. Zahawi and V. Pickert, "Stability Analysis of the Continuous-Conduction-Mode Buck Converter Via Filippov's Method," in IEEE Transactions on Circuits and Systems I: Regular Papers, vol. 55, no. 4, pp. 1084-1096, May 2008.

[12] E. Rodriguez, A. El Aroudi, F. Guinjoan and E. Alarcon, "A Ripple-Based Design-Oriented Approach for Predicting Fast-Scale Instability in DC–DC Switching Power Supplies," in IEEE Transactions on Circuits and Systems I: Regular Papers, vol. 59, no. 1, pp. 215-227, Jan. 2012.

[13] G. Feng, E. Meyer and Y. F. Liu, "A Digital Two-Switching-Cycle Compensation Algorithm for Input-Voltage Transients in DC–DC Converters," in IEEE Transactions on Power Electronics, vol. 24, no. 1, pp. 181-191, Jan. 2009.

[14] L. Wang, Q. H. Wu, Y. K. Tao and W. H. Tang, "Switching Control of Buck Converter Based on Energy Conservation Principle," in IEEE Transactions on Control Systems Technology, vol. 24, no. 5, pp. 1779-1787, Sept. 2016.

[15] M. A. Eleffendi and C. M. Johnson, "Application of Kalman Filter to Estimate Junction Temperature in IGBT Power Modules," in IEEE Transactions on Power Electronics, vol. 31, no. 2, pp. 1576-1587, Feb. 2016.

[16] S. Chattopadhyay and S. Das, "A Digital Current-Mode Control Technique for DC–DC Converters," in IEEE Transactions on Power Electronics, vol. 21, no. 6, pp. 1718-1726, Nov. 2006.

[17] K. Y. Cheng, F. Yu, F. C. Lee and P. Mattavelli, "Digital Enhanced V2-Type Constant On-Time Control Using Inductor Current Ramp Estimation for a Buck Converter With Low-ESR Capacitors," in IEEE Transactions on Power Electronics, vol. 28, no. 3, pp. 1241-1252, March 2013.

[18] S. Pan and P. K. Jain, "A Low-Complexity Dual-Voltage-Loop Digital Control Architecture With Dynamically Varying Voltage and Current References," in IEEE Transactions on Power Electronics, vol. 29, no. 4, pp. 2049-2060, April 2014.

[19] L.Ljung, System Identification: Theory for the User, 2nd ed.: Upper Saddle River, NJ: Prentice Hall, 1999.

[20] W. Greblicki, "Nonparametric identification of Wiener systems," in IEEE Transactions on Information Theory, vol. 38, no. 5, pp. 1487-1493, Sep 1992.

[21] B. Mu, W. X. Zheng and E. W. Bai, "Variable Selection and Identification of High-Dimensional Nonparametric Additive Nonlinear Systems," in IEEE Transactions on Automatic Control, vol. 62, no. 5, pp. 2254-2269, May 2017.

[22] A. Novak, B. Maillou, P. Lotton and L. Simon, "Nonparametric Identification of Nonlinear Systems in Series," in IEEE Transactions on Instrumentation and Measurement, vol. 63, no. 8, pp. 2044-2051, Aug. 2014.

[23] V. Valdivia, A. Barrado, A. LÁzaro, P. Zumel, C. Raga and C. FernÁndez, "Simple Modeling and Identification Procedures for “Black-Box” Behavioral Modeling of Power Converters Based on Transient Response Analysis," in IEEE Transactions on Power Electronics, vol. 24, no. 12, pp. 2776-2790, Dec. 2009.

[24] B. Miao, R. Zane, D. Maksimovic, "System identification of power converters with digital control through cross-correlation methods", IEEE Trans. Power Electron., vol. 20, no. 5, pp. 1093-1099, Sep. 2005.

[25] M. Shirazi, J. Morroni, A. Dolgov, R. Zane, D. Maksimovic, "Integration of frequency response measurement capabilities in digital controllers for DC-DC converters", IEEE Trans. Power Electron., vol. 23, no. 5, pp. 2524-2535, Sep. 2008.

[26] Chen Wang; Armstrong, M.; Gadoue, S.; Missailidis, P., "System identification of a DC-DC converter system using a Fast Affine Projection algorithm," Power Electronics, Machines and Drives (PEMD 2014), 7th IET International Conference on , vol., no., pp.1,6, 8-10 April 2014

[27] G.P. Rangaiah, P.R. Krishnaswamy, Estimating second-order dead time parameters from underdamped process transients, Chemical Engineering Science, Volume 51, Issue 7, 1996, Pages 1149-1155, ISSN 0009-2509,

[28] Lei Chen, Junhong Li, Ruifeng Ding, Identification for the second-order systems based on the step response, Mathematical and Computer Modelling, Volume 53, Issues 5–6, March 2011, Pages 1074-1083, ISSN 0895-7177

[29] Tao Liu, Furong Gao, A frequency domain step response identification method for continuous-time processes with time delay, Journal of Process Control, Volume 20, Issue 7, August 2010, Pages 800-809, ISSN 0959-1524

[30] H. Rake, Step response and frequency response methods, Automatica, Volume 16, Issue 5, 1980, Pages 519-526, ISSN 0005-1098

[31] J. Jin, Q. Qu and Y. Gu, "Robust zero-point attraction least mean square algorithm on near sparse system identification," in IET Signal Processing, vol. 7, no. 3, pp. 210-218, May 2013.

[32] Y. Zhang, S. Xiao, D. Huang, D. Sun, L. Liu and H. Cui, "l 0-norm penalised shrinkage linear and widely linear LMS algorithms for sparse system identification," in IET Signal Processing, vol. 11, no. 1, pp. 86-94, 2 2017.

[33] J. N. Lin and R. Unbehauen, "Bias-remedy least mean square equation error algorithm for IIR parameter recursive estimation," in IEEE Transactions on Signal Processing, vol. 40, no. 1, pp. 62-69, Jan 1992.

[34] R. Singer and R. Sea, "Increasing the computational efficiency of discrete Kalman filters," in IEEE Transactions on Automatic Control, vol. 16, no. 3, pp. 254-257, Jun 1971.

[35] Jiaxin Chen, Jianguo Zhu and Youguang Guo, "A unified hybrid model with two level networks for peak current mode controlled buck-boost converters operating in DCM and CCM," 2007 International Conference on Electrical Machines and Systems (ICEMS), Seoul, 2007, pp. 186-190.

[36] J. Poon, P. Jain, C. Spanos, S. K. Panda and S. R. Sanders, "Fault Prognosis for Power Electronics Systems Using Adaptive Parameter Identification," in IEEE Transactions on Industry Applications, vol. 53, no. 3, pp. 2862-2870, May-June 2017.

[37] Ó. Jiménez, Ó. Lucía, I. Urriza, L. A. Barragán and D. Navarro, "Analysis and Implementation of FPGA-Based Online Parametric Identification Algorithms for Resonant Power Converters," in IEEE Transactions on Industrial Informatics, vol. 10, no. 2, pp. 1144-1153, May 2014.

[38] Q. Tong, Q. Zhang, R. Min, X. Zou, Z. Liu and Z. Chen, "Sensorless Predictive Peak Current Control for Boost Converter Using Comprehensive Compensation Strategy," in IEEE Transactions on Industrial Electronics, vol. 61, no. 6, pp. 2754-2766, June 2014.

[39] A. Calle-Prado, S. Alepuz, J. Bordonau, J. Nicolas-Apruzzese, P. Cortés and J. Rodriguez, "Model Predictive Current Control of Grid-Connected Neutral-Point-Clamped Converters to Meet Low-Voltage Ride-Through Requirements," in IEEE Transactions on Industrial Electronics, vol. 62, no. 3, pp. 1503-1514, March 2015.

[40] Guang Feng; Meyer, E.; Yan-Fei Liu, "A New Digital Control Algorithm to Achieve Optimal Dynamic Performance in DC-to-DC Converters," IEEE Transactions on Power Electronics, vol.22, no.4, pp.1489,1498, July 2007

[41] R. Pintelon, J. Schoukens, W. Van Moer and Y. Rolain, "Identification of linear systems in the presence of nonlinear distortions," in IEEE Transactions on Instrumentation and Measurement, vol. 50, no. 4, pp. 855-863, Aug 2001.

[42] M. Badoni, A. Singh and B. Singh, "Comparative Performance of Wiener Filter and Adaptive Least Mean Square-Based Control for Power Quality Improvement," in IEEE Transactions on Industrial Electronics, vol. 63, no. 5, pp. 3028-3037, May 2016.

[43] N. Namjoo and A. Hajizadeh, "Adaptive control of non-inverting buck-boost converter," The 5th Annual International Power Electronics, Drive Systems and Technologies Conference (PEDSTC 2014), Tehran, 2014, pp. 211-216.

[44] Z. Zhao and A. Prodi¿, "Limit-Cycle Oscillations Based Auto-Tuning System for Digitally Controlled DC–DC Power Supplies," in IEEE Transactions on Power Electronics, vol. 22, no. 6, pp. 2211-2222, Nov. 2007.

[45] J. A. Abu Qahouq, L. Huang and D. Huard, "Efficiency-Based Auto-Tuning of Current Sensing and Sharing Loops in Multiphase Converters," in IEEE Transactions on Power Electronics, vol. 23, no. 2, pp. 1009-1013, March 2008.

[46] A. Costabeber, P. Mattavelli, S. Saggini and A. Bianco, "Digital Autotuning of DC–DC Converters Based on a Model Reference Impulse Response," in IEEE Transactions on Power Electronics, vol. 26, no. 10, pp. 2915-2924, Oct. 2011.

[47] J. A. Abu Qahouq and V. Arikatla, "Online Closed-Loop Autotuning Digital Controller for Switching Power Converters," in IEEE Transactions on Industrial Electronics, vol. 60, no. 5, pp. 1747-1758, May 2013.

[48] A. Barkley and E. Santi, "Improved Online Identification of a DC–DC Converter and Its Control Loop Gain Using Cross-Correlation Methods," in IEEE Transactions on Power Electronics, vol. 24, no. 8, pp. 2021-2031, Aug. 2009.

[49] Ren, Z., and Zhu, G. G., 2009, “Pseudo-Random Binary Sequence Closed Loop System Identification Error With Integration Control,” Proc. Inst. Mech. Eng., Part I: J. Syst. Control Eng., 223, pp. 877–884.

[50] T. Roinila, M. Vilkko and T. Suntio, "Frequency-Response Measurement of Switched-Mode Power Supplies in the Presence of Nonlinear Distortions," in IEEE Transactions on Power Electronics, vol. 25, no. 8, pp. 2179-2187, Aug. 2010.

[51] J. Morroni, R. Zane and D. Maksimovic, "An Online Stability Margin Monitor for Digitally Controlled Switched-Mode Power Supplies," in IEEE Transactions on Power Electronics, vol. 24, no. 11, pp. 2639-2648, Nov. 2009.

[52] M. Bhardwaj, S. Choudhury, R. Poley and B. Akin, "Online Frequency Response Analysis: A Powerful Plug-in Tool for Compensation Design and Health Assessment of Digitally Controlled Power Converters," in IEEE Transactions on Industry Applications, vol. 52, no. 3, pp. 2426-2435, May-June 2016.

[53] A. Costabeber, P. Mattavelli, S. Saggini and A. Bianco, "Digital Autotuning of DC–DC Converters Based on a Model Reference Impulse Response," in IEEE Transactions on Power Electronics, vol. 26, no. 10, pp. 2915-2924, Oct. 2011.

[54] M. M. Peretz and S. Ben-Yaakov, "Digital Control of Resonant Converters: Resolution Effects on Limit Cycles," in IEEE Transactions on Power Electronics, vol. 25, no. 6, pp. 1652-1661, June 2010.

[55] A. Kelly and K. Rinne, "A Self-Compensating Adaptive Digital Regulator for Switching Converters Based on Linear Prediction," in IEEE Applied Power Electronics Conference and Exposition (APEC 2006), 2006, p. 7 pp.

[56] C. Y. Chan, S. H. Chincholkar and W. Jiang, "Adaptive Current-Mode Control of a High Step-Up DC–DC Converter," in IEEE Transactions on Power Electronics, vol. 32, no. 9, pp. 7297-7305, Sept. 2017.

[57] P. Kshirsagar, D. Jiang and Z. Zhang, "Implementation and Evaluation of Online System Identification of Electromechanical Systems Using Adaptive Filters," in IEEE Transactions on Industry Applications, vol. 52, no. 3, pp. 2306-2314, May-June 2016.

[58] R. M. Milasi, A. F. Lynch and Y. W. Li, "Adaptive Control of a Voltage Source Converter for Power Factor Correction," in IEEE Transactions on Power Electronics, vol. 28, no. 10, pp. 4767-4779, Oct. 2013.

[59] R. J. Wai and L. C. Shih, "Adaptive Fuzzy-Neural-Network Design for Voltage Tracking Control of a DC–DC Boost Converter," in IEEE Transactions on Power Electronics, vol. 27, no. 4, pp. 2104-2115, April 2012.

[60] W. Al-Hoor, J. A. Abu-Qahouq, L. Huang, W. B. Mikhael and I. Batarseh, "Adaptive Digital Controller and Design Considerations for a Variable Switching Frequency Voltage Regulator," in IEEE Transactions on Power Electronics, vol. 24, no. 11, pp. 2589-2602, Nov. 2009.

[61] D. Maksimovic and R. Zane, "Small-Signal Discrete-Time Modeling of Digitally Controlled PWM Converters," in IEEE Transactions on Power Electronics, vol. 22, no. 6, pp. 2552-2556, Nov. 2007.

[62] R. W. Erickson and D. Maksimovi, Fundamentals of Power Electronics, 2nd ed. Norwell, Massachusetts, USA.: Kluwer Academic Publisher Group, 2001.

[63] A. R. Brown, "Sampled-data modeling of switching regulators," 1981 IEEE Power Electronics Specialists Conference, Boulder, Colorado, USA, 1981, pp. 349-369.

[64] M. Rodriguez, V. M. Lopez, F. J. Azcondo, J. Sebastian and D. Maksimovic, "Average Inductor Current Sensor for Digitally Controlled Switched-Mode Power Supplies," in IEEE Transactions on Power Electronics, vol. 27, no. 8, pp. 3795-3806, Aug. 2012.

[65] A. H. Sayed, Fundamentals of Adaptive Filtering. Hoboken, NJ: Wiley, 2003.

[66] Lee, D.-C.; Lee, K.-J.; Seok, J.-K.; Choi, J. -W, "Online capacitance estimation of DC-link electrolytic capacitors for three-phase AC/DC/AC PWM converters using recursive least squares method," IEE Proceedings - Electric Power Applications, vol.152, no.6, pp.1503,1508, 4 Nov. 2005

[67] X. S. Pu, T. H. Nguyen, D. C. Lee, K. B. Lee and J. M. Kim, "Fault Diagnosis of DC-Link Capacitors in Three-Phase AC/DC PWM Converters by Online Estimation of Equivalent Series Resistance," in IEEE Transactions on Industrial Electronics, vol. 60, no. 9, pp. 4118-4127, Sept. 2013.

[68] T. Souvignet, B. Allard and X. Lin-Shi, "Sampled-Data Modeling of Switched- Capacitor Voltage Regulator With Frequency-Modulation Control," in IEEE Transactions on Circuits and Systems I: Regular Papers, vol. 62, no. 4, pp. 957-966, April 2015.

[69] Poustie, A. J., Blow, K. J., Manning, R. J., & Kelly, A. E. (1999). All-optical pseudorandom number generator. Optics Communications, 159(4), 208-214.

[70] Shaoyong Yang; Bryant, A.; Mawby, P.; Dawei Xiang; Ran, L.; Tavner, P., "An Industry-Based Survey of Reliability in Power Electronic Converters," IEEE Transactions on Industry Applications, vol.47, no.3, pp.1441,1451, May-June 2011

[71] Shaoyong Yang; Dawei Xiang; Bryant, A.; Mawby, P.; Ran, L.; Tavner, P., "Condition Monitoring for Device Reliability in Power Electronic Converters: A Review," IEEE Transactions on Power Electronics, vol.25, no.11, pp.2734,2752, Nov. 2010

[72] Onuki, J.; Koizumi, M.; Suwa, Masateru, "Reliability of thick Al wire bonds in IGBT modules for traction motor drives," IEEE Transactions on Advanced Packaging, vol.23, no.1, pp.108,112, Feb 2000, doi: 10.1109/6040.826768

[73] Karamanakos, P.; Geyer, T.; Manias, S., "Direct Voltage Control of DC–DC Boost Converters Using Enumeration-Based Model Predictive Control," IEEE Transactions on Power Electronics, vol.29, no.2, pp.968,978, Feb. 2014

[74] Oucheriah, S.; Liping Guo, "PWM-Based Adaptive Sliding-Mode Control for Boost DC–DC Converters," IEEE Transactions on Industrial Electronics, vol.60, no.8, pp.3291,3294, Aug. 2013

[75] Chok-You Chan, "A Nonlinear Control for DC–DC Power Converters," IEEE Transactions on Power Electronics, vol.22, no.1, pp.216,222, Jan. 2007

[76] Texas Instruments. Data Manual (June 2007). TMS320F28335, TMS320F28334, TMS320F28332,TMS320F28235, TMS320F28234, TMS320F28232 Digital Signal Controllers (DSCs). [online]. Available: http://www.ti.com/lit/ds/symlink/tms320f28335.pdf.

[77] J. Ding, F. Ding, X. P. Liu and G. Liu, "Hierarchical Least Squares Identification for Linear SISO Systems With Dual-Rate Sampled-Data," in IEEE Transactions on Automatic Control, vol. 56, no. 11, pp. 2677-2683, Nov. 2011.

[78] M. Ned, T. M. Undeland, and W. P. Robbins, Power Electronics: Converters, Applications and Design, 3rd ed.: John Wiley & Sons, Inc., 2003.

[79] G. Zhou, J. Xu and J. Wang, "Constant-Frequency Peak-Ripple-Based Control of Buck Converter in CCM: Review, Unification, and Duality," in IEEE Transactions on Industrial Electronics, vol. 61, no. 3, pp. 1280-1291, March 2014.

[80] M. M. Peretz and S. Ben-Yaakov, "Time-Domain Design of Digital Compensators for PWM DC-DC Converters," IEEE Transactions on Power Electronics, vol. 27, pp. 284-293.

[81] H. Renaudineau, J. P. Martin, B. Nahid-Mobarakeh and S. Pierfederici, "DC–DC Converters Dynamic Modeling With State Observer-Based Parameter Estimation," in IEEE Transactions on Power Electronics, vol. 30, no. 6, pp. 3356-3363, June 2015.

[82] R. A. Dobre, V. A. Niţă, S. Ciochină and C. Paleologu, "New insights on the convergence analysis of the affine projection algorithm for system identification," 2015 International Symposium on Signals, Circuits and Systems (ISSCS), Iasi, 2015, pp. 1-4.

[83] Y. Cai and R. C. de Lamare, "Low-complexity variable forgetting factor mechanism for RLS algorithms in interference mitigation applications," 2012 International Symposium on Wireless Communication Systems (ISWCS), Paris, 2012, pp. 471-475.

[84] Y. Zakharov and F. Albu, "Coordinate descent iterations in fast affine projection algorithm," in IEEE Signal Processing Letters, vol. 12, no. 5, pp. 353-356, May 2005.

[85] M. Shoaib, S. Werner and J. A. Apolinario, "Multichannel Fast QR-Decomposition Algorithms: Weight Extraction Method and Its Applications," in IEEE Transactions on Signal Processing, vol. 58, no. 1, pp. 175-188, Jan. 2010.

[86] G. Zhou and J. Xu, "Digital Average Current Controlled Switching DC–DC Converters With Single-Edge Modulation," in IEEE Transactions on Power Electronics, vol. 25, no. 3, pp. 786-793, March 2010.

[87] Jingquan Chen, A. Prodic, R. W. Erickson and D. Maksimovic, "Predictive digital current programmed control," in IEEE Transactions on Power Electronics, vol. 18, no. 1, pp. 411-419, Jan 2003.

[88] L. Cao, K. H. Loo and Y. M. Lai, "Output-Impedance Shaping of Bidirectional DAB DC–DC Converter Using Double-Proportional-Integral Feedback for Near-Ripple-Free DC Bus Voltage Regulation in Renewable Energy Systems," in IEEE Transactions on Power Electronics, vol. 31, no. 3, pp. 2187-2199, March 2016.

[89] F. Xiong; J. Wu; Z. Liu; L. Hao, "Current Sensorless Control for Dual Active Bridge DC-DC Converter with Estimated Load-Current Feedforward," in IEEE Transactions on Power Electronics , vol.PP, no.99, pp.1-1

[90] V. Yousefzadeh and D. Maksimovic, "Sensorless optimization of dead times in dc–dc converters with synchronous rectifiers," in IEEE Transactions on Power Electronics, vol. 21, no. 4, pp. 994-1002, July 2006.

[91] J. Gordillo and C. Aguilar, "A Simple Sensorless Current Sharing Technique for Multiphase DC–DC Buck Converters," in IEEE Transactions on Power Electronics, vol. 32, no. 5, pp. 3480-3489, May 2017.

[92] J. Sun, J. Yang, W. X. Zheng and S. Li, "GPIO-Based Robust Control of Nonlinear Uncertain Systems Under Time-Varying Disturbance With Application to DC–DC Converter," in IEEE Transactions on Circuits and Systems II: Express Briefs, vol. 63, no. 11, pp. 1074-1078, Nov. 2016.

[93] V. Valdivia, A. Barrado, A. Lázaro, C. Fernández and P. Zumel, "Black-box modeling of DC-DC converters based on transient response analysis and parametric identification methods," 2010 Twenty-Fifth Annual IEEE Applied Power Electronics Conference and Exposition (APEC), Palm Springs, CA, 2010, pp. 1131-1138.

[94] S. Choi and M. Saeedifard, "An Educational Laboratory for Digital Control and Rapid Prototyping of Power Electronic Circuits," IEEE Transactions on Education, vol. 55, pp. 263-270, 2012.

[95] A. J. Fairweather, M. P. Foster, and D. A. Stone, "VRLA Battery Parameter Identification Using Pseudo Random Binary Sequences (PRBS)," in 5th IET International Conference on Power Electronics, Machines and Drives (PEMD 2010), 2010, pp. 1-6.

[96] D. S. Watkins and Ebooks Corporation., Fundamentals of Matrix Computations, 2nd ed. Hoboken: John Wiley & Sons Inc., 2002.

[97] A. V. Peterchev and S. R. Sanders, "Quantization Resolution and Limit Cycling in Digitally Controlled PWM Converters," IEEE Transactions on Power Electronics, vol. 18, pp. 301-308, 2003.

[98] Ljung, Lennart. "Perspectives on system identification." Annual Reviews in Control 34.1 (2010): 1-12.

[99] A. S. Nawaz, S. Pfeiffer, G. Lichtenberg and H. Schlarb, "Self-organzied critical control for the European XFEL using black box parameter identification for the quench detection system," 2016 3rd Conference on Control and Fault-Tolerant Systems (SysTol), Barcelona, 2016, pp. 196-201.

[100] G. Mercère, O. Prot and J. A. Ramos, "Identification of Parameterized Gray-Box State-Space Systems: From a Black-Box Linear Time-Invariant Representation to a Structured One," in IEEE Transactions on Automatic Control, vol. 59, no. 11, pp. 2873-2885, Nov. 2014.

[101] Ju-Yeop Choi, B. H. Cho, H. F. VanLandingham, Hyung-soo Mok and Joong-Ho Song, "System identification of power converters based on a black-box approach," in IEEE Transactions on Circuits and Systems I: Fundamental Theory and Applications, vol. 45, no. 11, pp. 1148-1158, Nov 1998.

[102] V. Serrano and K. Tsakalis, "A study on the on-line system identification and PID tuning of a buck converter," 2016 IEEE 13th International Conference on Networking, Sensing, and Control (ICNSC), Mexico City, 2016, pp. 1-5.

[103] S. Padhee, U. C. Pati and K. Mahapatra, "Modelling switched mode DC-DC converter using system identification techniques: A review," 2016 IEEE Students' Conference on Electrical, Electronics and Computer Science (SCEECS), Bhopal, 2016, pp. 1-6.

[104] T. Roinila, T. Helin, M. Vilkko, T. Suntio, H. Koivisto, "Circular correlation based identification of switching power converter with uncertainty analysis using fuzzy density approach", Simulation Modelling Practice and Theory, vol. 17, no. 6, pp. 1043-1058, 2009.

[105] M. Ahmeid, M. Armstrong, M. Al-Greer and S. Gadoue, "Computationally Efficient Self-Tuning Controller for DC-DC Switch Mode Power Converters Based on Partial Update Kalman Filter," in IEEE Transactions on Power Electronics. doi: 10.1109/TPEL.2017.2768618

[106] S. K. Kim and K. B. Lee, "Robust Feedback-Linearizing Output Voltage Regulator for DC/DC Boost Converter," in IEEE Transactions on Industrial Electronics, vol. 62, no. 11, pp. 7127-7135, Nov. 2015.

[107] M. V. Basin, C. B. Panathula, Y. B. Shtessel and P. C. R. Ramírez, "Continuous Finite-Time Higher Order Output Regulators for Systems With Unmatched Unbounded Disturbances," in IEEE Transactions on Industrial Electronics, vol. 63, no. 8, pp. 5036-5043, Aug. 2016.

[108] Y. F. Liu, E. Meyer and X. Liu, "Recent Developments in Digital Control Strategies for DC/DC Switching Power Converters," in IEEE Transactions on Power Electronics, vol. 24, no. 11, pp. 2567-2577, Nov. 2009.

[109] N. George, V. N. Panchalai and E. Sebastian, "Digital Feedback Control of a Full-Bridge DC-DC Converter with Input Voltage Based Gain Scheduling," 2014 Fourth International Conference on Advances in Computing and Communications, Cochin, 2014, pp. 347-351.

[110] W. R. Liou et al., "A Programmable Controller IC for DC/DC Converter and Power Factor Correction Applications," in IEEE Transactions on Industrial Informatics, vol. 9, no. 4, pp. 2105-2113, Nov. 2013.

[111] M. S. Manoharan, A. Ahmed and Joung-Hu Park, "Digital implementation of peak current mode control for single-phase H-Bridge inverter with slope compensation," 2013 International Conference on Electrical Machines and Systems (ICEMS), Busan, 2013, pp. 1502-1506.

[112] M. Hallworth and S. A. Shirsavar, "Microcontroller-Based Peak Current Mode Control Using Digital Slope Compensation," in IEEE Transactions on Power Electronics, vol. 27, no. 7, pp. 3340-3351, July 2012.

[113] J. J. Chen, Y. S. Hwang, J. F. Liou, Y. T. Ku and C. C. Yu, "A New Buck Converter With Optimum-Damping and Dynamic-Slope Compensation Techniques," in IEEE Transactions on Industrial Electronics, vol. 64, no. 3, pp. 2373-2381, March 2017.

[114] Q. Yu, R. Xiong, C. Lin, W. Shen and J. Deng, "Lithium-Ion Battery Parameters and State-of-Charge Joint Estimation Based on H-Infinity and Unscented Kalman Filters," in IEEE Transactions on Vehicular Technology, vol. 66, no. 10, pp. 8693-8701, Oct. 2017.

[115] M. M. Peretz and S. Ben-Yaakov, "Time-Domain Design of Digital Compensators for PWM DC-DC Converters," in IEEE Transactions on Power Electronics, vol. 27, no. 1, pp. 284-293, Jan. 2012.

[116] J. G. Truxal, Automatic Feedback Control Systems Synthesis. NewYork: McGraw-Hill, 1955.

[117] O. Garcia, A. de Castro, A. Soto, J. A. Oliver, J. A. Cobos, and J. Cezon, "Digital control for power supply of a transmitter with variable reference," in Proc. IEEE Appl. Power Electron. Conf., Dallas, TX, 2006, pp. 1411–1416.

[118] V. Yousefzadeh, W. Narisi, Z. Popovic, and D. Maksimovic, "A digitally controlled DC/DC converter for an RF power amplifier," IEEE Trans. Power Electron., vol. 21, no. 1, pp. 164–172, Jan. 2006.

[119] B. Miao, R. Zane, and D. Maksimovic, "Automated digital controller design for switching converters," in Proc. IEEE Power Electron. Spec. Conf., Recife, Brazil, 2005, pp. 2729–2735.

[120] V. Yousefzadeh, Narisi Wang, Z. Popovic and D. Maksimovic, "A digitally controlled DC/DC converter for an RF power amplifier," in IEEE Transactions on Power Electronics, vol. 21, no. 1, pp. 164-172, Jan. 2006.

[121] Z. Zhao, "Design and Practical Implementation of Digital Auto-Tuning and Fast-Response Controllers for Low-Power Switch-Mode Power Supplies," PhD Thesis, University of Toronto, 2008.